nagra.

Arbeitsbericht NAB 16-68

FEBEX-DP – Dismantling related supplementary documents

March 2017

F. Kober & N. van Meir (Editors)

National Cooperative
for the Disposal of
Radioactive Waste

Hardstrasse 73
P.O. Box 280
5430 Wettingen
Switzerland
Tel. +41 56 437 11 11

www.nagra.ch

nagra.

Arbeitsbericht NAB 16-68

FEBEX-DP – Dismantling related supplementary documents

March 2017

F. Kober[1] & N. van Meir[2] (Editors)[1)]

[1)] Nagra
[2)] NVM Consulting and Scientific Editing

KEYWORDS

FEBEX-DP, Dismantling, planning documents, forecast, laboratory intercomparison, corrosion, microbiology, hyperspectral scanning, thermal conductivity

National Cooperative
for the Disposal of
Radioactive Waste

Hardstrasse 73
P.O. Box 280
5430 Wettingen
Switzerland
Tel. +41 56 437 11 11

www.nagra.ch

Nagra Arbeitsberichte ("Working Reports") present the results of work in progress that have not necessarily been subject to a comprehensive review. They are intended to provide rapid dissemination of current information.

Contributions by
NAGRA: T. Sakaki, J.K. Becker, I. Gaus, N. Giroud
CHYN, Université de Neuchâtel: L. Fasnacht, P. Brunner, P. Renard
SKB: B. Kalinowski
Golder Associates Ltd.: D. Dixon

"Copyright © 2017 by Nagra, Wettingen (Switzerland) / All rights reserved.
All parts of this work are protected by copyright. Any utilisation outwith the remit of the copyright law is unlawful and liable to prosecution. This applies in particular to translations, storage and processing in electronic systems and programs, microfilms, reproductions, etc."

Table of Contents

Table of Contents I

List of Tables VI

List of Figures VII

1 General introduction 1
1.1 Scope of this report 1
1.2 FEBEX framework 1
1.3 Test configuration during FEBEX I 2
1.3 Dismantling of Heater #1 and test configuration afterwards (FEBEX II) 4
1.4 Concept of the dismantling of Heater #2 5

2 FEBEX-DP project planning 7
2.1 The dismantling phase: first planning schedule and objectives 7
2.2 Dismantling "status forecast" 7
2.3 Studying corrosion and microbial activity 7

3 Laboratory inter-comparison of methods and derived variability for key parameter values 9

4 On-site dismantling reports 13

5 Hyperspectral scanning 13

6 Thermal conductivity 13

7 References 15

App. A: Updated FEBEX-DP: Project Plan (Version 16/06/14) A-1
A.1 Introduction A-1
A.2 Dismantling objectives A-2
A.3 Main activities in the project A-3
A.3.1 Pre-dismantling modelling A-3
A.3.2 Field work related to the dismantling A-3
A.3.2 Laboratory program and analysis of the samples A-4
A.3.2.1 Expected status of the components to be sampled at the time of dismantling in 2015 ..... A-4
A.3.2.2 Types of analysis planned for different components A-6
A.3.2.3 Recalibration of the sensors A-9
A.3.3 Reporting A-9
A.4 Project organisation and resources A-9
A.5 Project milestones A-11
A.6 Delivrables A-12

A.7 Planning of activities, milestones and deliverables A-13

App. B: Forecast of anticipated status prior to dismantling the FEBEX "in situ" test – FEBEX-DP B-1
B.1 Introduction B-1
B.1.1 Purpose of the document B-1
B.1.2 Background B-2
B.1.2.1 Test configuration during FEBEX I (original test configuration) B-2
B.1.2.2 Test configuration after the first dismantling operation and current test configuration (FEBEXe) B-3
B.1.2.3 Objectives of the final dismantling B-4
B.2 Forecast of the anticipated status of the major components B-6
B.2.1 The service area and heated zone B-6
B.2.1.1 Initial properties prior to experiment emplacement and observations from the first excavation B-6
B.2.1.2 Expected status service area and heated zone B-6
B.2.2 Plug and plug interfaces B-7
B.2.2.1 Initial properties of the second shotcrete plug and observations from the first plug dismantling B-7
B.2.2.2 Expected status of the plug and plug interfaces B-8
B.2.3 The buffer: bentonite blocks B-9
B.2.3.1 Initial properties prior to experiment emplacement B-9
B.2.3.2 Observation from the first dismantling B-9
B.2.3.3 Expected status B-10
B.2.4 Instrumentation, corrosion of the sensors, coupons and tracers B-14
B.2.4.1 Initial status as emplaced B-14
B.2.4.2 Observation from the partial dismantling B-14
B.2.4.3 Expected status B-15
B.2.4.4 A special note on corrosion and microbiology B-16
B.2.5 Heater and liner B-17
B.2.5.1 Initial status as emplaced B-17
B.2.5.2 Observations from the first excavation B-18
B.2.5.3 Expected status B-18
B.3 Modelling B-18
B.4 Concluding Remarks B-19

App. C: FEBEX-DP – Objectives and strategy of the COMIC Group C-1
C.1 Introduction C-1
C.2 Objectives C-1
C.3 Metal corrosion and microbial processes C-2
C.3.1 Corrosion C-2
C.3.2 Microbial activity in bentonite buffers C-3

C.4 Samples' selection and sampling procedures C-4
C.4.1 Information gained from the partial dismantling C-4
C.4.2 Selection of samples C-4
C.4.3 Gas and water sampling prior to full dismantling C-5
C.4.4 Sampling during dismantling C-5
C.4.5 Corrosion C-5
C.4.6 Microbiology C-6
C.4.7 Final report C-9
C.5 Analytical techniques C-9
C.5.1 Task 1: Corrosion analyses (Tecnalia 2014) C-9
C.5.2 Task 2: bentonite analyses C-10
C.5.3 Task 3: Microbiology analyses C-10
C.5.4 Task 4: Chemical analyses of water and gases C-10
C.6 Organisation C-11

App. D: Assessing the variability of laboratory measurements on swelling clay (FEBEX) D-1
D.1 Letter accompanying the appendix D-1
D.2 Background to the round robin exercise D-2
D.3 Data Evaluation D-6
D.3.1 Material and batch records D-6
D.3.2 FEBEX mock-up and FEBEX: Clay block dry density D-7
D.3.2.1 FEBEX mock-up D-9
D.3.2.2 FEBEX density measurements D-12
D.3.3 Cation Exchange Capacity (CEC) D-15
D.3.4 Exchangeable Cation (EC) composition D-15
D.3.5 Hydraulic conductivity testing D-16
D.3.6 Mineralogical analyses D-19
D.3.7 Clay chemical composition D-19
D.3.8 Consolidation characteristics D-20
D.3.9 Gas permeability D-22
D.3.10 Thermal properties D-23
D.3.11 Swelling pressure D-24
D.3.12 Water retention curves D-27
D.4 Summary D-28

App. E: On-site extra reports during and after dismantling E-1
E.1 Plug dismantling and sampling Section 36 ..... E-1
E.2 Documenting the heater retrieval (04/06/2015) E-8
E.3 Documenting the disappearing gaps in bentonite Layer 45 (26/06/2015) E-24
E.4 Sampling bentonite with corrosion products in bentonite Layer 44 (26/06/2015) E-27

E.5 Retrieving metallic coupons (Rack A) in the FEBEX experiment at Grimsel (04/07/2015) E-32
E.5.1 Sample collection: Rack A3 and A4 (5 o'clock) E-34
E.5.2 Sample collection: Rack A1 and A2 (7 o'clock) E-36
E.5.3 Sample conditions E-38
E.5.4 Subsampling prospective E-39
E.6 Documenting the geological structures in the FEBEX-DP gallery after dismantling (23/09/2015) E-39
E.6.1 The granite wall during dismantling E-41
E.6.1.1 Section 37 ..... E-41
E.6.1.2 Section 39 ..... E-41
E.6.1.3 Section 41 ..... E-45
E.6.1.4 Section 43 ..... E-45
E.6.1.5 Section 45 ..... E-46
E.6.1.6 Section 46 ..... E-48
E.6.1.7 Section 47 ..... E-49
E.6.1.8 Section 47/48 ..... E-50
E.6.1.9 Section 49 ..... E-51
E.6.1.10 Section 50 ..... E-54
E.6.1.11 Section 52 ..... E-56
E.6.1.12 Section 53 ..... E-57
E.6.1.13 Section 59 ..... E-57
E.6.1.14 Section 62 ..... E-60
E.7 Sampling the plug-concrete/rock (C/R) interface by stabilised overcoring – sample splitting and distribution (05/10/2015) E-73
E.7.1 Status E-73
E.7.2 Location of boreholes (overview) E-73
E.7.3 Location of boreholes (detail) E-74
E.7.4 Drilling situation E-76
E.7.5 Sampling result E-77
E.8 Documenting the dummy-liner bentonite fillings E-83

App. F: GTS Phase VI – FEBEX-DP hyperspectral scanning for patterns of near-surface water content (August 2015) F-1
F.1 Abstract F-1
F.2 Scanned data and calibration F-2
F.2.1 Experimental setup and calibration process F-2
F.2.2 Calibration results F-3
F.2.3 Scans F-6
F.2.4 Preliminary analysis F-8
F.3 Laboratory experiment with bentonite F-8

F.4 Correlation of spectral measurements and water content F-11
F.5 Conclusion F-14
F.5.1 Achieved work F-14
F.5.2 Further work F-14

App. G: In-situ measurement of thermal conductivity of bentonite blocks during dismantling and a comparison with CIEMAT laboratory results G-1
G.1 Introduction G-1
G.2 Materials and methods G-4
G.2.1 KD2 Pro thermal analyzer G-4
G.3 Measurement sections G-6
G.4 In-situ thermal conductivity measurement results G-9
G.4.1 Section 46 ..... G-9
G.4.2 Section 53 ..... G-9
G.4.3 Section 58 ..... G-10
G.4.4 Section 61 ..... G-11
G.4.5 Summary of in-situ thermal conductivity measurements G-12
G.5 Comparison with laboratory-measured λ G-14
G.6 Water content and saturation (on-site sample results) G-16
G.7 Concluding remarks G-18
G.8 Acknowledgments G-19

App. H: References H-1

List of Tables

Tab. 1: Parameters initially considered for a laboratory inter-comparison. 9

Tab. 2: The nine remaining parameters and the source of the data..... 12

Tab. A-1: Currently planned analysis on samples taken from the components of the FEBEX in situ as part of FEBEX-DP. A-6

Tab. B-1: Temperature (in ºC) sensors in bentonite on 01.05.2014..... B-10

Tab. B-2: Pore pressure (in MPa) in the buffer till 01.05.2014. ..... B-11

Tab. B-3: Total pressure (in MPa) in the buffer till 01.05.2014. ..... B-12

Tab. C-1: Quantitative analyses of culturable heterotrophic aerobic bacteria (CHAB), SRB (SRB), autotrophic acetogens (AA) and iron-reducing bacteria (IRB) in the eleven ABM materials (from Svensson et al. 2011). C-3

Tab. C-2: Number of samples planned for corrosion and microbiology. C-7

Tab. D-1: Parameters initially targeted for inclusion in data collection and evaluation exercise. D-4

Tab. D-2: Summary of materials properties information evaluated. D-6

Tab. D-3: Statistical summary of density and moisture content measurements on FEBEX- Mock-up blocks. D-12

Tab. D-4: Exchangeable cation and cation exchange capacity of MX80 bentonite. D-16

Tab. D-5: Exchangeable cation and cation exchange capacity of FEBEX bentonite..... D-16

Tab. D-6: XRD analysis results for MX80 and FEBEX bentonites. D-21

Tab. D-7: Chemical composition of bentonites based on XRF and ICP analyses. D-21

Tab. E-1: Identification and composition of the 4 racks. E-33

Tab. E-2: Sampling results. E-77

Tab. G-1: Specifications of the thermal conductivity sensors..... G-5

Tab. G-2: Positions of the measuring points. G-7

Tab. G-3: Summary of the in-situ measurement results. G-12

List of Figures

Fig. 1: Overall layout of FEBEX "in-situ" test (left) and "mock-up" test (right). 2
Fig. 2: General layout of the FEBEX "in-situ" test (FEBEX I configuration). 3
Fig. 3: Status of the FEBEX "in-situ" test after the partial dismantling (FEBEX II configuration). 4
Fig. A-1: Current FEBEXe configuration. A-5
Fig. A-2: Organisational chart of FEBEXe. A-10
Fig. A-3: FEBEX-DP project timeline indicating milestones and deliverables. A-14
Fig. B-1: Original FEBEX (I) configuration (ENRESA 2006a) and indication of instrumented sections B-3
Fig. B-2: Current FEBEX-II configuration (ENRESA 2006a). B-4
Fig. B-3: Design of the Shotcrete plug for FEBEXe (ENRESA 2003). B-7
Fig. B-4: CIEMAT and AITEMIN gas pipes and sensors installed (ENRESA 2003) B-8
Fig. B-5: Appearance of a bentonite layer during construction (left) and after the first dismantling in 2002 (right) (ENRESA 2006a). B-10
Fig. B-6: Evolution of the volumetric water content measured by the Time Domain Reflectometers (TDR) showing the accelerated resaturation rate measured by the sensors close to the heater (Sakaki et al., in prep., NAB 16-21) B-13
Fig. B-7: Sensor status 01.05.2014 (Aitemin 2014b) B-15
Fig. B-8: Liner (left) and heater (right) as installed in 1996 (ENRESA 2003). B-17
Fig. C-1: Schematic view of the five sampling sections (white numbers) distributed longitudinally along the experiment. C-7
Fig. C-2: Location of the microbiology samples (BC/CS36-1 and -2) on Section 36, at the interface between the shotcrete plug and the bentonite buffer (source: AITEMIN 2014a). C-8
Fig. C-3: Cross-section of the samples to be taken in Section 48 (modified from: AITEMIN 2014a). C-8
Fig. D-1: Block shapes and locations used in FEBEX mock-up assembly. D-8
Fig. D-2: Block Assembly in FEBEX. D-8
Fig. D-3: Density and moisture content variability in intact FEBEX-type blocks. D-10
Fig. D-4: Comparison of density measured for intact blocks to subsamples cut from blocks manufactured using FEBEX clay for the FEBEX mock-up. D-11
Fig. D-5: Density measurements obtained for FEBEX 2002 outer-section decommissioning using different techniques. D-14
Fig. D-6: Hydraulic conductivity of MX80 and FEBEX bentonites. D-18
Fig. D-7: Gas permeability of FEBEX bentonite. D-23
Fig. D-8: Thermal conductivity of FEBEX bentonite (after Villar 2002). D-24
Fig. D-9: Dry density – swelling pressure relationships for FEBEX and MX80. ..... D-26

Fig. D-10: Suction – moisture relationships for FEBEX and MX80 bentonites. D-27
Fig. E-1: Cleaning of shotcrete between the heater car tracks. E-1
Fig. E-2: Robot leaving the gallery. E-1
Fig. E-3: Robot leaving the tunnel. E-2
Fig. E-4: The site after completion of the shotcrete dismantling exposing the dummy. E-2
Fig. E-5: Sampling B-B-36-7 to 9 before taking off the blocks. E-3
Fig. E-6: Samples B-B-36-1 to 3 after dismantling showing that blocks can be taken off intact at original block boundaries most of the times. E-3
Fig. E-7: Block B-B-36-1 (outer ring) with iodine paper on top (left) and at its original wall position. E-4
Fig. E-8: Block B-B-36-3 (inner ring) with positions where bentonite was squeezed into liner holes (left) and liner with bentonite filled liner holes at same position. E-5
Fig. E-9: Corrosion pattern at block B-B-36-6. ..... E-6
Fig. E-10: Preparation for sampling of block B-B-36-4 to 6 revealed quite wet bentonite in accordance with the observation during the overcoring of C-C-32-6OC. E-6
Fig. E-11: Final image after sampling Section 36. ..... E-7
Fig. E-12: The AITEMIN on site making long-shifts (Bárcena & Martin). E-7
Fig. E-13: Track extension preparation. E-8
Fig. E-14: Final site preparation. E-9
Fig. E-15: The tracks are ready for the heater car. E-10
Fig. E-16: The heater winch attached (screwed) and welded to the heater E-11
Fig. E-17: The heater car in place for pulling out the heater. E-12
Fig. E-18: The heater comes OUT at around 12.30 am on 04.06.2015 after 18 years of duty. E-12
Fig. E-19: The AITEMIN team relieved and happy (FLTR, Jose-Pedro Carvajal, Christina de la Rossa, Ignacio Bárcena, Antonio Martin). E-13
Fig. E-20: The heater more than halfway out. E-13
Fig. E-21: bentonite debris on top of the retrieved heater. E-14
Fig. E-22: bentonite still sticking at the front of the retrieved heater. E-14
Fig. E-23: The heater is completely out; front view (top picture) and view towards the back (lower picture). E-15
Fig. E-24: The first view into the now empty liner, showing bentonite protruded through the liner holes especially in the front and back part. E-16
Fig. E-25: The back side of the heater on the heater car on its way out of the gallery. E-17
Fig. E-26: The FEBEX-site with bentonite Layer 40 exposed and the now empty liner E-17
Fig. E-27: The heater car with its control unit approaching the entrance of the gallery. E-18
Fig. E-28: The heater at the FEBEX installation site E-18

Fig. E-29: The team on site yesterday (Ingo Blechschmidt missing). E-19
Fig. E-30: Empty experiment....E-19
Fig. E-31: The frontal view of the empty liner. E-20
Fig. E-32: Close-ups of the protruding bentonite inside the liner....E-21
Fig. E-33: A full liner view – at the end the block boundaries of bentonite Layer 23 are visible....E-22
Fig. E-34: More close-ups of the inside of the liner. E-23
Fig. E-35: bentonite Layer 45 "As built" in 1997. ....E-24
Fig. E-36: bentonite Layer 45 on 25.06.2015. ....E-24
Fig. E-37: Gap 1....E-25
Fig. E-38: Gap 2....E-25
Fig. E-39: Gap 1 & 2. ....E-26
Fig. E-40: Gap 3....E-26
Fig. E-41: Fisurometer similar to that installed in Section 43 – 45. ....E-27
Fig. E-42: Corrosion halo on Section 46 (Layer 45)....E-28
Fig. E-43: Fisurometer in bentonite Layer 44 (Section 47) and corrosion halo. E-29
Fig. E-44: Closer view at the fisurometer. E-29
Fig. E-45: Drilling a bentonite sample. E-30
Fig. E-46: Inserting a Shelby tube around the drilled core, to protect the sample. E-30
Fig. E-47: Inserting the Shelby tube with help of the drilling machine. E-31
Fig. E-48: Location of the samples around the fisurometer. E-31
Fig. E-49: Scheme of the sampling plan in Layer 48....E-32
Fig. E-50: Initial set up of corrosion specimens and emplacement in blocks. E-33
Fig. E-51: A single Ti coupon surfacing out the hole of the liner. E-34
Fig. E-52: Another single Ti coupon surfacing from the host block upon digging. E-35
Fig. E-53: Rack A4 (left) and retrieved pieces from block A3 (right)....E-35
Fig. E-54: Position of the tube related to the drilling operation which is suspected to have destroyed rack A3. ....E-36
Fig. E-55: Host block with the racks A1 (left) and A2 (right) lying upon it. E-36
Fig. E-56: Rack A2 with corrosion pit on the edges of the coupons and sort of corrosion spots in the bentonite. E-37
Fig. E-57: Top view of host block of rack A1/2 after removal of the racks. E-38
Fig. E-58: FEBEX-DP gallery E-40
Fig. E-59: Left: Gallery at ~ 3 o'clock, showing interface of granite/lamprophyre and contact to bentonite further to the left. Right: Gallery at ~ 9 o'clock showing the contact shown in further detail under "PART B, structure 5"....E-41

Fig. E-60: Galleries' left side, detail lamprophyre structure under "PART B, structure 5"....E-41
Fig. E-61: Detail of wall at ~ 3 o'clock.....E-42
Fig. E-62: Close-up of Fig. E-61. .....E-42
Fig. E-63: Close-up of Fig. E-62. .....E-43
Fig. E-64: Rock wall surface at ~ 1 o'clock. E-43
Fig. E-65: Close-up of Fig. E-64. .....E-44
Fig. E-66: Detail of rock wall surface at ~ 10 o'clock. E-44
Fig. E-67: Detail of rock wall surface at ~ 10 o'clock, to the far right the bentonite surface is visible. E-45
Fig. E-68: Detail of rock wall and extensometer fixation at ~ 2 o'clock. E-45
Fig. E-69: Detail of rock wall and extensometer fixation at ~ 1 o'clock. E-46
Fig. E-70: Detail of rock wall at ~ 9 – 11 o'clock.....E-46
Fig. E-71: Detail of rock wall at ~ 3 – 5 o'clock.....E-47
Fig. E-72: Detail of Fig. E-71, showing the darker band to the left, while plastic remnants can be seen between the dark band and the ruler (a plastic foil has been used for water protection measures during construction and remained in the experiment for 18 years) – see below. E-47
Fig. E-73: Photo taken during the installation showing the plastic foil used for bentonite protection from wet rock wall surfaces.....E-48
Fig. E-74: Photo of the granite wall at ~ 9 – 11 o'clock. E-48
Fig. E-75: Photo taken from the wall fixation of the fissurometer sensor. E-49
Fig. E-76: Photo taken from the wall fixation of the fissurometer sensor. E-49
Fig. E-77: Photo taken from the left wall, at about 7 – 11 o'clock, just after the fissurometer dismantling. E-50
Fig. E-78: Left: Photo taken from towards 2 – 3 o'clock, showing a thin layer of bentonite left at the centre above the cable duct. Such thin bentonite layers (covers) seem to have developed in the vicinity of non-granite interfaces, in this case concrete of a total-pressure cell recession. Right: Detail looking into the interface bentonite/granite/concrete.....E-51
Fig. E-79: Detail of Fig. E-78 after removing the thin bentonite layer.....E-51
Fig. E-80: Detail of Fig. E-79 with two more bentonite layers removed.....E-52
Fig. E-81: Same situation as Fig. E-80 but on opposite wall at 9 o'clock.....E-52
Fig. E-82: Same situation as Fig. E-81 but two more bentonite layers removed.....E-53
Fig. E-83: Photo of 10 o'clock situation near permanent measure tape, discoloration still related to fisurometer vicinity.....E-53
Fig. E-84: Photo at ~ 10 o'clock, greenish discoloration at bentonite border near iodine paper. E-54
Fig. E-85: Close-up of Fig. E-84. .....E-54
Fig. E-86: Rock wall at 1 – 5 o'clock.....E-55

Fig. E-87: Detail rock wall(pressure sensor/bentonite wall, back part of Fig. E-86. .....E-55
Fig. E-88: Photo towards 10 o'clock. E-56
Fig. E-89: Detail rock Fig. E-88, lower part. E-56
Fig. E-90: Left: Photo towards 9 – 11 o'clock, upper part. Right: photo towards 8 – 11 o'clock, lower part.....E-57
Fig. E-91: Rock wall taken at height of Section 51 at 3 o'clock. E-57
Fig. E-92: Rock wall at 9 o'clock, see also structure "1" in PART B. E-58
Fig. E-93: Rock wall at ~ 8 – 10 o'clock, see also structure "1" in PART B. E-59
Fig. E-94: Detail rock wall at 10 o'clock. E-59
Fig. E-95: Rock wall at ~ 10 o'clock, with the end of the gallery seen already. E-60
Fig. E-96: Detail of Fig. E-95. .....E-60
Fig. E-97: Rock wall at 2 o'clock. E-61
Fig. E-98: Rock wall at 3 o'clock. E-62
Fig. E-99: Detail of rock wall at 10 o'clock. E-63
Fig. E-100: Detail of rock wall at 12 o'clock. E-63
Fig. E-101: The last ~ 2 m of the gallery between 1 – 5 o'clock. E-64
Fig. E-102: Detail of Fig. E-101. .....E-64
Fig. E-103: Detail of Fig. E-102. .....E-65
Fig. E-104: Rock wall from 2-12-9 o'clock (top line, view towards entrance of gallery). E-65
Fig. E-105: Rock wall at 9 – 11 o'clock. E-66
Fig. E-106: Detail of Fig. E-105. .....E-66
Fig. E-107: Rock wall between 7 and 10 o'clock. E-67
Fig. E-108: Detail of rock wall at 11 o'clock. E-68
Fig. E-109: Detail of rock wall at 11 o'clock with all bentonite removed. E-68
Fig. E-110: Image of the central total pressure sensor at the conical end of the drift. E-69
Fig. E-111: Left total pressure cell at the gallery end at 9 o'clock. E-70
Fig. E-112: Oblique view to the left total pressure cell at the gallery end at 9 o'clock. E-71
Fig. E-113: Lower part of the left total pressure cell at the gallery end at 9 o'clock. E-72
Fig. E-114: Overview of borehole locations. E-73
Fig. E-115: Originally planned sampling procedure. E-76
Fig. E-116: Finally applied sampling procedure. E-76
Fig. E-117: The FEBEX-DP experiment with dummy (void of the first FEBEX heater) and the second heater. E-83
Fig. E-118: The constructional gap between the liner and the dummy (image: The FEBEX-DP experiment with dummy (void of the first FEBEX heater) and the second heater – Fig. 39: ENRESA2003-PT 09-2003-Dismantling of the heater 1 at the FEBEX in-situ test). E-84

Fig. E-119: The liner after removal of heater 2 for comparison. E-85
Fig. E-120: The dummy-liner during dismantling – front view. E-86
Fig. E-121: The dummy-liner during dismantling – top view. E-86
Fig. E-122: The dummy-liner during dismantling – front view. E-87
Fig. E-123: Perforated liner (from bottom) with bentonite filled holes and scrapped off bentonite (dark holes in front). E-87
Fig. E-124: Above: end of dummy (above) towards heater, right – end of dummy with one bentonite block layer. E-88
Fig. E-125: Right: end of dummy (above) towards heater, right – end of dummy with one bentonite block layer E-88
Fig. E-126: Frontal part of dummy. E-89
Fig. E-127: Detail of frontal part of dummy, the deformation at 2 o'clock must have been existing during the second phase as it is equally filled with bentonite, see Fig. E-128. ..... E-89
Fig. E-128: Detail of frontal part of dummy still in place in the experiment with bentonite infill as discussed in Fig. E-127. ..... E-90
Fig. E-129: Frontal part of dummy towards the "lifted" (due to cutting of the liner and stress release). E-90
Fig. E-130: Detail of Fig. E-129. ..... E-91
Fig. E-131: Back part of dummy. E-91
Fig. E-132: Close up of Fig. E-131. ..... E-92
Fig. E-133: Close up of Fig. E-131. ..... E-92
Fig. E-134: Dummy back part with liner cut before cleaning off bentonite. E-93
Fig. E-135: Dummy back part with liner cut after cleaning off bentonite and cutting fresh surfaces. E-93
Fig. E-136: Detail of Fig. E-135. ..... E-94
Fig. E-137: Detail of Fig. E-135. ..... E-94
Fig. E-138: Dummy top view towards 9 o'clock. E-95
Fig. E-139: Cut liner segment with discolored bentonite still adhered to the liner. E-95
Fig. E-140: Same as Fig. E-139. ..... E-96
Fig. E-141: Detail of Fig. E-139. ..... E-96
Fig. E-142: Detail of Fig. E-139. ..... E-97
Fig. E-143: Detail of Fig. E-139. ..... E-97
Fig. E-144: Dummy-liner towards 3 o'clock. E-98
Fig. E-145: Detail of Fig. E-144, showing a bentonite protrusion into the liner – dummy gap. E-98
Fig. E-146: Detail of Fig. E-144, showing a bentonite protrusion into the liner – dummy gap. E-98
Fig. E-147: Detail of Fig. E-146, after making a fresh cut. E-99

Fig. E-148: Detail of Fig. E-146, after making a fresh cut. E-99
Fig. E-150: Detail of Fig. E-149, Section A. E-100
Fig. E-151: Detail of Fig. E-149, Section B. E-101
Fig. E-152: Detail of Fig. E-151. ....E-101
Fig. E-153: Detail of Fig. E-149, Section C. E-102
Fig. E-154: Detail of Fig. E-149, Section D. E-102
Fig. E-155: Detail of Fig. E-149, Section D. E-103
Fig. E-156: Detail of Fig. E-154, with a fresh cut into the protrusion. E-103
Fig. E-157: Looking towards 9 o'clock on the surface that was at the dummy and was "lifted" after the tension relieve after liner cutting (thus gap artificial). E-104
Fig. E-158: Same as Fig. E-Fig. E-157. ....E-105
Fig. F-1: Image of the studied area. F-2
Fig. F-2: Raw data. F-3
Fig. F-3: Calibrated data. F-3
Fig. F-4: Calibrated data after applying the second calibration step. F-4
Fig. F-5: Variance in function of wavelength. F-5
Fig. F-6: The five scans that were taken are shown here. F-7
Fig. F-7: Scan 4 plotted as p(x,y). F-8
Fig. F-8: Experiment set-up. F-9
Fig. F-9: Some sample spectra F-9
Fig. F-10: Plots of function h1 (upper) and h2 (lower). F-10
Fig. F-12: Function h1 and h2 for scan 1 ....F-11
Fig. F-13: Calculated volumetric water content for scans 1-5. ....F-13
Fig. G-1: Position of sampling sections for the laboratory analyses (Villar et al., in prep., NAB 16-17). G-2
Fig. G-2: Position of sampling sections for the on-site analysis (Villar & Iglesias 2016, NAB 16-12). G-2
Fig. G-3: Position of blocks received at CIEMAT for THM and THG tests in sampling sections 36, 47, 53 and 59. ....G-3
Fig. G-4: The KD2 Pro thermal analyzer. G-4
Fig. G-5: The TR-1 (left) and RK-1 (right) Pro needle sensors. G-5
Fig. G-6: In-situ thermal conductivity measurement sections. G-8
Fig. G-7: In-situ thermal conductivity as a function of radial distance (Section 46). G-9
Fig. G-8: In-situ thermal conductivity as a function of radial distance (Section 53). G-10
Fig. G-9: In-situ thermal conductivity as a function of radial distance (Section 58, Layer 13) G-10

Fig. G-10: In-situ thermal conductivity as a function of radial distance (Section 58, Layer 9)..... G-11
Fig. G-11: In-situ thermal conductivity as a function of radial distance (Section 61). G-11
Fig. G-12: Comparison of in-situ thermal conductivity resuls in the hot and cold sections. G-13
Fig. G-13: Thermal conductivity versus degree of saturation. (Figure taken from ENRESA 2002) G-13
Fig. G-14: Laboratory thermal conductivity measurement using Kemtherm QTM-D3 system (Photo from Villar et al., in prep., NAB 16-17). G-14
Fig. G-15: Comparison of the in-situ and laboratory mesaured thermal conductivity results..... G-15
Fig. G-16: Dry density and saturation (S) as a function of radial distance. G-16
Fig. G-17: Dry density and saturation (S) as a function of radial distance. G-17
Fig. G-18: Dry density and saturation (S) as a function of radial distance. G-17
Fig. G-19: Dry density and saturation (S) as a function of radial distance. G-18

1 General introduction

1.1 Scope of this report

This report joins together different technical documents of the FEBEX-DP dismantling procedures. Most of the technical information is in the associated appendices whereas the report itself gives a short summary of the content, leading the reader quickly to the right information. It should be stressed that all information is given as it was gathered at the time of dismantling without further interpretation, synthesis or conclusions.

After introducing the general FEBEX project framework in Chapter 1, Chapter 2 summarises several reports on the preparatory work for the dismantling phase. The **project plan** is detailed in Section 2.1; Section 2.2 summarises the **FEBEX-DP status forecast** that allowed a better preparation of the dismantling. Section 2.3 gives a short overview of the preparations necessary for the sampling of **corrosion phenomena** and **microbial activities**. From Chapter 3 onward the technical documents relate to the actual dismantling. Chapter 3 describes the results of a **laboratory inter-comparison exercise**. The experiment looked at a number of typical parameters characterising swelling clay. It allowed to identify the accuracy and determined a general variability to be expected for this parameter. Chapter 4 retraces parts of the dismantling process as an ad-hoc diary (called **extra reports**) with notes and pictures taken with the purpose of keeping all FEBEX-DP partners up to date and informed as well as documenting phenomena visible only during the dismantling process. Chapter 5 clarifies the **hyperspectral scanning** experiment, and finally Chapter 6 details the in-situ **thermal conductivity measurements**.

1.2 FEBEX framework

FEBEX (Full-scale Engineered Barrier Experiment in Crystalline Host Rock) is a research and demonstration project that was initiated by ENRESA (Spain).

The aim of the project is to study the behaviour of near-field components in a repository for high-level radioactive waste in granite formations. The main objectives of the project can be grouped in two areas:

- Demonstration of the feasibility of constructing the engineered barrier system in a horizontal configuration according to the Spanish concept for deep geological storage (AGP), and analysis of the technical problems to be solved for this type of disposal method
- Better understanding of the thermo-hydro-mechanical (THM) and thermo-hydro-geochemical (THG) processes in the near field, and development and validation of the modelling tools required for interpretation and prediction of the evolution of such processes.

The project consists of two large-scale tests (see Fig. 1) – "in situ" and "mock-up" (the latter is managed by CIEMAT in Spain) –, a series of laboratory tests, and THM and THG modelling tasks.

The full-scale heating test ("in-situ" test), to which this document refers, was performed at the Grimsel underground laboratory in Switzerland, also known as Grimsel Test Site (GTS) or Felslabor Grimsel (FLG in German). A complete description of the FEBEX project objectives and test program can be found in the "FEBEX Full-scale Engineered Barriers Experiment in Crystalline Host Rock. PRE-OPERATIONAL STAGE SUMMARY REPORT" (Enresa 1998a).

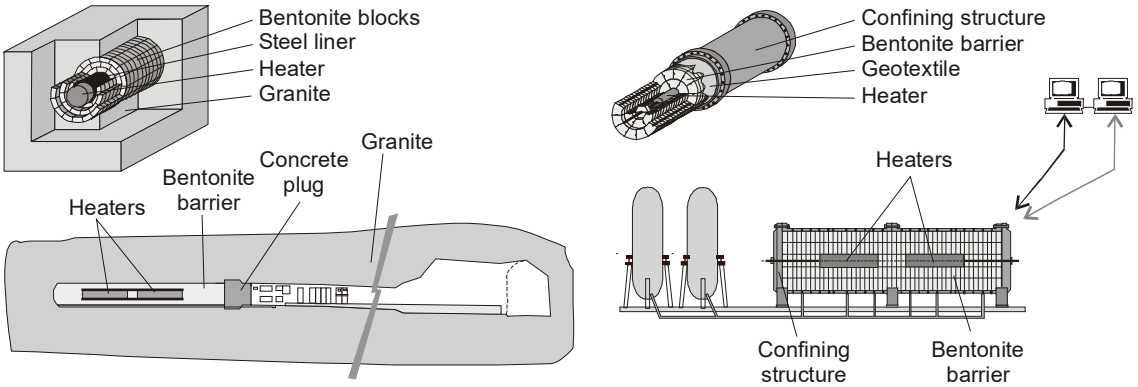


Fig. 1: Overall layout of FEBEX "in-situ" test (left) and "mock-up" test (right).

The project started in 1994, and has been supported by the European Commission through consecutive contracts, identified as FEBEX I (contract nº FI4W-CT-95-0006) for the period January 1996 to June 1999, and FEBEX II (contract nº FIKW-CT-2000-00016), from September 2000 to December 2004. Afterwards, NF-PRO covered the period from January 2005 to December 2007. And finally, in January 2008 the "in-situ" test was transferred from ENRESA to a consortium composed of SKB (Sweden), POSIVA (Finland), CIEMAT (Spain), Nagra (Switzerland) and more recently KAERI (South Korea), grouped in the FEBEXe Consortium, which supports it currently.

The in-situ experiment dismantling was carried out in 2015 and new partners, interested in taking part in the planned sampling and analysis operations, were incorporated into the Consortium (now called FEBEX-DP) for that purpose, namely US DOE (USA), OBAYASHI (Japan), RWM (UK), ANDRA (France), BGR (Germany) and SURAO (Check Republic).

1.3 Test configuration during FEBEX I

The installation of the "in-situ" test was carried out at the GTS. A horizontal drift with a diameter of 2.28 m was excavated in the Grimsel granodiorite especially for this experiment using a TBM (a tunnel boring machine). Two electrical heaters, of the same size and of a similar weight as the reference canisters, were placed in the axis of the drift. The gap between the heaters and the rock was backfilled with compacted bentonite blocks, up to a length of 17.40 m, requiring a total 115'716 kg of bentonite. The backfilled area was sealed with a plain concrete plug placed into a recess excavated in the rock and having a length of 2.70 m and a volume of 17.8 m^3. Fig. 2 shows the dimensions and layout of the test components schematically.

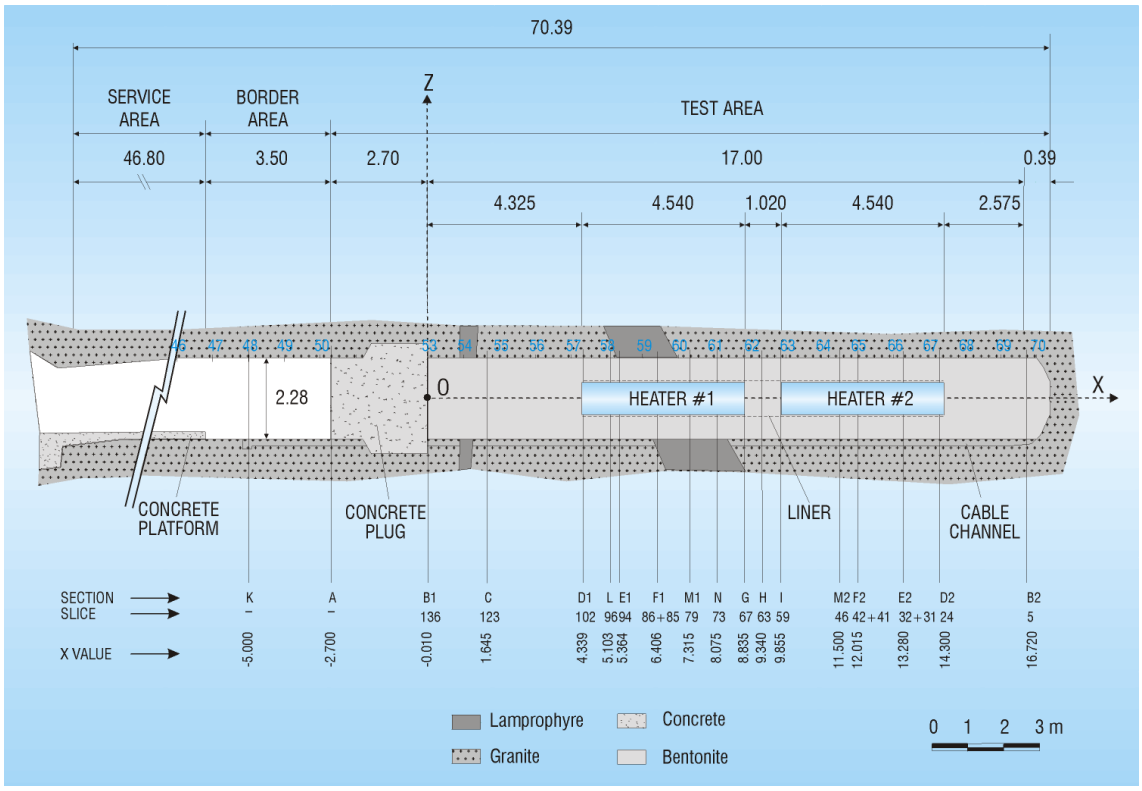


Fig. 2: General layout of the FEBEX "in-situ" test (FEBEX I configuration).

A total of 632 instruments were placed in the system along a number of instrumented sections, both in the bentonite buffer and in the host rock, to monitor relevant parameters such as temperature, humidity, total and pore pressure, displacements, ... etc. The instruments were of many different kinds and their characteristics and positions are fully described in the report titled "FEBEX Full-scale Engineered Barriers Experiment in Crystalline Host Rock. FINAL DESIGN AND INSTALLATION OF THE IN-SITU TEST AT GRIMSEL" (ENRESA 1998b).

A Data Acquisition and Control System (DACS) located in the service area of the FEBEX drift collected the data provided by the instruments. This system recorded and stored information from the sensors and also controlled the power applied to the electrical heaters, in order to maintain a constant temperature at the heaters/bentonite interface. The DACS allowed the experiment to be run automatically, with remote supervision from Madrid. Data stored at the local DACS were periodically downloaded in Madrid and used to build the experimental Master Data Base.

The construction of the concrete plug was completed in October 1996, and the heating operation started on 28.02.1997. A constant temperature of 100 °C was maintained at the heaters/bentonite interface, while the bentonite buffer was slowly hydrating with water from the surrounding rock. A complete report that includes both the installation of the test and the results gathered after two years of operation is given in "FEBEX full-scale engineered barriers experiment for a deep geological repository for high level radioactive waste in crystalline host rock FINAL REPORT" (Enresa 2000).

1.3 Dismantling of Heater #1 and test configuration afterwards (FEBEX II)

A partial dismantling of the FEBEX "in-situ" test was carried out during the summer of 2002, after 5 years of continuous heating. The operation included the demolition of the concrete plug, the removal of the section of the test corresponding to the first heater, and the sealing with a new shotcrete plug. A large number of samples from all types of materials were taken for analysis. A number of instruments were subsequently dismantled, and some new ones were installed. Accordingly, system design was adapted, and the physical layout was changed in order to ease the partial dismantling operation.

The buffer and all components were removed up to a distance of 2 metres from Heater #2 to minimise disturbance of the non-dismantled area. A dummy steel cylinder with a length of 1 m was inserted in the void left by Heater #1 in the centre of the buffer. Some new sensors were installed in that one additional metre of bentonite buffer.

Additional sensors were introduced in boreholes drilled in the buffer parallel to the drift. To simplify this operation, the new concrete plug was constructed in two phases: an initial temporary plug measuring just 1 m in length, which was built immediately after dismantling, and a second section to complete the plug length to the 3 m planned in the design of the experiment. Unlike FEBEX I, the new plug was a parallel plug, without a recess excavated in the rock, constructed by shotcreting.

The description of the partial dismantling operation is given by the report titled "Dismantling of the Heater #1 at the FEBEX "in-situ" test. Description of operations" (Enresa 2003). The configuration of the test, after completing the partial dismantling operation and construction of the full plug length, is shown in Fig. 3.

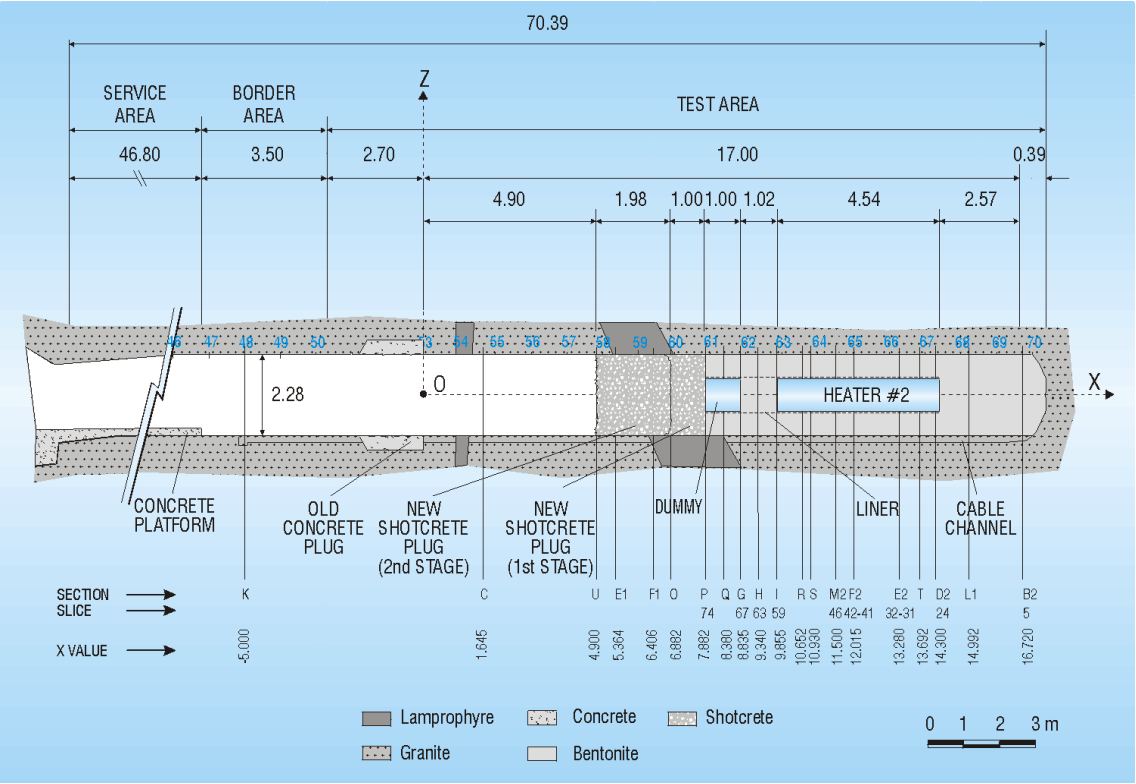


Fig. 3: Status of the FEBEX "in-situ" test after the partial dismantling (FEBEX II configuration).

A more complete report that describes the test from the conception up to two years of operation after the partial dismantling is given in the document titled "FEBEX Full-scale Engineered Barriers Experiment. UPDATED FINAL REPORT 1994 – 2004" (Enresa 2006).

1.4 Concept of the dismantling of Heater #2

The objective of the second dismantling operation, carried out throughout 2015, was to dismantle all the remaining parts of the "in-situ" test, including Heater #2. This operation includes carrying out a complete sampling of the bentonite, rock, relevant interfaces, sensors, metallic components and tracers to allow the analysis of the barriers' condition after 18 years of heating and natural hydration.

Analytical results will be compared with data obtained from the partial dismantling (Enresa 2006); the monitoring data (Rey et al. 2016) as well as with the results derived from modelling efforts (Lanyon & Gaus 2013). The results are expected to increase the current knowledge and confidence for the FEBEX-DP partners in bentonite performance with a focus on thermo-hydro-mechanical (THM) and thermo-hydro-chemical (THC) processes as well as on corrosion and microbial activity. The reporting of the laboratory analysis and dismantling *results is expected to be complete by mid of 2017 with a final integrated report issued in early 2017.*

All details about the planned dismantling operation and sampling program are given in the reference documents: "FEBEX-DP (GTS) Full Dismantling Test Plan" (Bárcena & García-Siñeriz 2015a), "FEBEX-DP (GTS) Full Dismantling Sampling Plan" (Bárcena & García-Siñeriz 2015a).

2 FEBEX-DP project planning

2.1 The dismantling phase: first planning schedule and objectives

Before actual dismantling started in 2015, a dismantling phase "project plan" was developed in several stages. A first version was published in June 2014[1] and is attached to this report as Appendix A. The project plan stated the objectives of the dismantling phase as well as the scheduled activities regarding fieldwork and modelling. It further specified the organisational chart of the project team and listed the responsibilities of each. Finally, it listed the expected milestones and deliverables along with a provisional planning schedule.

2.2 Dismantling "status forecast"

A detailed forecast of the expected status of the in-situ test is given in appendix B[2]. This status report was based on ongoing monitoring and measurements, modelling results as well as results from the FEBEX partial dismantling phase in 2002 (ENRESA 2006, PT 05-0-2006 – updated Final Report). The document reported in Appendix B thus identified the areas or major components of the experiment that are of interest for detailed examination and sampling in order to meet the objectives of the dismantling. They can be listed as

- The service area and heated zone
- Plug and plug interfaces
- Buffer
- Sensors and corrosion probes
- The heater and finally
- The liner

Based on this document a more detailed and overarching dismantling and sampling plan was established (Aitemin 2014)

2.3 Studying corrosion and microbial activity

Appendix C[3] gives the objectives and sampling strategy of the COMIC (COrrosion and MICrobiology) group during the dismantling phase. This group was set up after a broad interest in those fields was recognized. Given the primary experimental objectives and set-up of the experiment in 2002 (ENRESA 2006, PT 05-0-2006 – updated Final Report) it should be kept in mind that it was not specifically nor fully designed for this subject. Appendix C also lists the expected analysis methods to be used and the organisational chart. The COMIC group specifically targeted the investigation of microbial activities and corrosion to estimate how this could impact the safety of a high-level nuclear waste repository.

---

1 First published as AN 14-326

2 First published as AN 14-611

3 Originally published as AN 14-421

3 Laboratory inter-comparison of methods and derived variability for key parameter values

The data evaluation report in appendix D[4] is the final interpretation of a laboratory inter-comparison exercise for a number of analysis techniques to derive certain material characteristics of the FEBEX bentonite (Serrata Clay) supplemented occasionally by the more commonly used MX80 bentonite. Initially, twelve parameters (or properties) derived by different laboratories (sometimes with different analysis techniques) on the same material were compared. The analysis of the different sets of measurements and results were to give an idea about the general variability in parameter values and measurement methods between laboratories in order to compare these different laboratories' measurements results during the dismantling process. The twelve parameters are listed in Tab. 1 (and repeated in appendix D). However, for the parameters "batch information", "consolidation" and "water retention/suction", not enough datasets were available for a meaningful comparison. The remaining nine parameters were evaluated as listed in Tab. 2.

Tab. 1: Parameters initially considered for a laboratory inter-comparison.

Activity	Parameter	Notes and definitions
1	Batch information MX80 and FEBEX	Material source information. This includes manufacturer/supplier, year of receipt or production of material, manufacturer's batch #, transfer records between laboratories and any other information that clearly tracks the materials reported.
2	Bulk/dry density and gravimetric water content	Data should be limited to tests completed on initial, reference or as-placed FEBEX block materials only. Materials recovered from the previously completed FEBEX partial dismantling or laboratory prepared materials should not be included. • Gravimetric water content defined as mass of water/ mass of water-insoluble soil minerals • Dry density defined as mass of soil minerals/volume of specimen • Bulk density defined as total mass/volume of specimen These will be done during FEBEX-DP as per Technical Report CIEMAT/DMA/2G206/1/12 and also in FEBEX-DP: Project plan – Version 15/01/14.
3	Cation Exchange Capacity (CEC)	CEC values as per ENRESA2006-PT 05-1-2006 (Tab. VI, p 19). These tests are to be done during FEBEX-DP as per Technical Report CIEMAT/DMA/2G206/1/12 and also in FEBEX-DP: Project plan - Version 15/01/14.
4	Exchangeable Cations (EC)	EC values as per ENRESA2006-PT 05-1-2006 (Tab. VI, p 19) These tests are to be done during FEBEX-DP as per Technical Report CIEMAT/DMA/2G206/1/12 and are also in FEBEX-DP: Project plan - Version 15/01/14.

[4] Initially published as AN 15-126

Tab. 1: Cont.

Activity	Parameter	Notes and Definitions
5	Hydraulic conductivity tests (k)	Data only for fresh water or compositions close to that of FEBEX site. No treated, altered or otherwise changed material information to be included. Data of type reported in ENRESA2006-PT 05-1-2006 (Section 4.4.1.4) is needed. These tests are to be done during FEBEX-DP as per Technical Report CIEMAT/DMA/2G206/1/12 and in FEBEX-DP: Project plan - Version 15/01/14.
6	Mineralogical analyses	• Provide details of technique, e.g. CuKα; CoKα; ptw treated … • Information related to bulk mineralogy only. Not size fractionated specimens, chemically treated…. • Presented as % content of each mineral type as per ENRESA2006-PT 05-1-2006 (p 17, para 3). • Include amorphous mineral information also if available (see ENRESA2006-PT 05-1-2006 (p 17, Tab. I and II). These tests are to be done during FEBEX-DP as per Technical Report CIEMAT/DMA/2G206/1/12 which calls for a comprehensive mineralogical evaluation12 and included in FEBEX-DP: Project plan - Version 15/01/14.
7	Clay chemical composition	Technique and accuracy of results from analytical reports. Data as per ENRESA2006-PT 05-1-2006 (Tab. II, p 18). These tests are to be done during FEBEX-DP as per Technical Report CIEMAT/DMA/2G206/1/12 and also in FEBEX-DP: Project plan - Version 15/01/14.
8	Consolidation parameters, preconsolidation pressure; Coefficient of consolidation (Cc)	Method, specimen size and any modifications to materials. Test data as per ENRESA2006-PT 05-1-2006 (Section 4.4.1.6). Both parameters are derived from same test data. This type of testing is scheduled during FEBEX-DP as per Technical Report CIEMAT/DMA/2G206/1/12 and also in FEBEX-DP: Project plan - Vers 15/01/14.
9	Gas permeability (Kg)	Method, specimen size, gas type, degree of saturation and any modifications to materials to be documented. This data was not in ENRESA2006-PT 05-1-2006 but tests are proposed for conduct as part of FEBEX-DP as per Technical Report CIEMAT/DMA/2G206/1/12 and also in FEBEX-DP: Project plan - Version 15/01/14.

Tab. 1: Cont.

Activity	Parameter	Notes and Definitions
10	Thermal properties	Method, water content, density… results need to be included. This parameter is needed for later analysis of FEBEX THM. Data as per ENRESA2006-PT 05-1-2006 Section 4.4.1.7. This type of testing is scheduled during FEBEX-DP as per Technical Report CIEMAT/DMA/2G206/1/12 and also in FEBEX-DP: Project plan – Vers 15/01/14.
11	Swelling pressure	Data is limited to that collected using either fresh water or compositions close to that of FEBEX site. No treated, altered or otherwise changed material information. Data as per ENRESA2006-PT 05-1-2006 (Section 4.4.2.2). Note: this was not identified as a test to be done as part of testing scheduled during FEBEX-DP in CIEMAT/DMA/2G206/1/12. They are however included in FEBEX-DP: Project plan- Version 15/01/14.
12	Water retention (suction-moisture) Relative humidity-shrinkage	Suction-Moisture (Water-retention) curve. Data as per ENRESA2006-PT 05-1-2006 (p.20 Fig. 3). This type of testing is scheduled during FEBEX-DP as per Technical Report CIEMAT/DMA/2G206/1/12 and also in FEBEX-DP: Project plan - Version 15/01/14. Shrinkage. A measure of volume change of compacted specimen exposed to known relative humidity (suction) conditions.

Tab. 2: The nine remaining parameters and the source of the data.

Parameter #	**Description**	**Notes**	**Organizations providing data***
2	FEBEX Bulk & Dry Density	Substantial data provided and assessed	CIEMAT
3	Cation Exchange Capacity	Substantial data provided and assessed	CT, BT, BGR, CIEMAT
4	Exchangeable Cation Composition	Substantial data provided and assessed	CT, BT, BGR, CIEMAT
5	Hydraulic conductivity tests (k)	Substantial data provided and assessed	BT, CT, CIEMAT
6	Mineralogical analyses	Substantial data provided and assessed	CT, BT, BGR, CIEMAT
7	Clay chemical composition	Substantial data provided and assessed	CT, BT, BGR, CIEMAT
9	Gas permeability (K_g)	FEBEX Data provided and assessed	CIEMAT
10	Thermal properties	FEBEX Data provided and assessed	CIEMAT
11	Swelling pressure	Substantial data provided and assessed	BT, CT, CIEMAT

* Organizations supplyind data:
BGR: Federal Institute for Geosciences and Natural Resources (Bundesanstalt für Geowissenschaften und Rohstoffe) (Germany)
BT: B+Tech OY (Finland)
CIEMAT: Centro de Investigaciones Energéticas, Medioambientales y Tecnológicas (Spain)
CT: Clay Technology AB (Sweden)

4 On-site dismantling reports

A number of "extra reports" were issued during and after dismantling. These reports consist mostly of direct observations from the dismantling (e.g. corrosion features), detailed studies of specific objects (e.g. detailed liner and heater inspections) or activities (e.g. heater retrieval). They represent "ad hoc" impressions and interpretations and do not claim a thorough and balanced investigation and interpretation. Some observations of the overcoring methods and sampling are separately reported in Mäder et al. (2016). These documents are regrouped here as Appendix E.

5 Hyperspectral scanning

Appendix F documents the Short Wave InfraRed (SWIR) hyperspectral experiment that was carried out on the surface of a bentonite slice in August 2015. Before dismantling, some very novel or advanced techniques were tested to optimise bentonite sampling and in-situ/on-site characterisation. The goal was to avoid significant sampling or analysis artefacts and to facilitate spatially extensive and fast measurements (García-Siñeriz et al. 2016a, 2016b).

The idea was that the hyperspectral scanning of a freshly excavated bentonite surface could give a fast and efficient overview of near-surface water content patterns. Calibration of the measurements was obtained by comparing the scans to measured water content in bentonite samples (Villar et al. 2016) and by a laboratory experiment where a bentonite block was wetted, left to dry and then scanned. The experiment resulted in an empirical linear relationship linking shortwave infrared intensity to water content.

6 Thermal conductivity

In a similar effort as the hyperspectral scanning experiment, thermal conductivity was measured in situ on site in a section where blocks were also collected for laboratory thermal conductivity measurements (Villar et al., in prep., NAB 16-17). Results of these measurements can be found in appendix G[5] to this document. They showed that the thermal conductivity values measured in situ and in the laboratory were mostly consistent and that the combined effect of water saturation (increasing from the centre of to the rock wall) and dry density (decreasing from the centre to the rock wall) cancelled each other giving a constant thermal conductivity value in the radial direction.

[5] Originally published as AN 16-505

7 References

AITEMIN (2014): "Full Dismantling Test Plan (In Situ Experiment)".

Bárcena, I. & García-Siñeriz, J.L. (2015a): FEBEX-DP (GTS) Full Dismantling Test Plan R7. Nagra Arbeitsbericht NAB 15-14.

Bárcena, I. & García-Siñeriz, J.L. (2015b): FEBEX-DP (GTS) Full Dismantling Test Plan. Nagra Arbeitsbericht NAB 15-15.

Enresa (1998a): FEBEX Pre-Operational Stage Summary Report. Publicaciones Técnicas 01/98, Enresa, Madrid, Spain.

Enresa (1998b): FEBEX – Final design and installation of the "in situ" test at Grimsel. Enresa Report Publicaciones Técnicas 1998-12.

Enresa (2000): FEBEX Project. Full-scale Engineered Barriers Experiment for a Deep Geological Repository for High Level Radioactive Waste in Crystalline Host Rock. Final Report. Enresa Report 1/2000, Enresa, Madrid, Spain.

Enresa (2003): Dismantling of the Heater #1 at the FEBEX "in situ" test. Description of operations. Enresa Report PT 2003-09.

Enresa (2006): Full-scale Engineered Barriers Experiment. Updated Final Report 1994-2004. Enresa Report PT 2006-05-0.

García-Siñeriz, J.L., Abós, H., Martínez, L.V., De la Rosa, C., Mäder, U. & Kober, F. (2016b): FEBEX DP: Dismantling of Heater #2 at the FEBEX "in situ" test: Description of operations. Nagra Arbeitsbericht NAB 16-11.

García-Siñeriz, J.L., Martínez, L.V., Rey, M. & Abós, H. (2016a) : Results of laboratory investigations in preparation of the dismantling of the FEBEX-e/FEBEX-DP in-situ test and on-site experiments during the dismantling. Nagra Arbeitsbericht NAB 16-9.

Lanyon, W. & Gaus, I. (2013): Main outcomes and review of the FEBEX In Situ Test (GTS) and Mock-Up after 15 years of operation". Nagra Arbeitsbericht NAB 13-96.

Mäder U., Detzner, K., Kober, F., Abplanalp, H., Baer, T. & Cloet, V. (2016): FEBEX-DP – Plug Overcoring and Concrete-bentonite Interface Sampling prior to Dismantling. Nagra Arbeitsbericht NAB 16-10.

Martínez, L.V., Abós H. & García-Siñeriz, J.L. (2016): FEBEXe: Final Sensor Data Report (FEBEX "in situ" Experiment). Nagra Arbeitsbericht NAB 16-19.

Villar et al. (in prep.): FEBEX-DP Postmortem THM/THC Analysis Report. Nagra Arbeitsbericht NAB 16-17.

Villar, M.V., Iglesias, J.R., Abós, H., Martínez, L.V., de la Rosa, C. & Manchón, M.Á. (2016): FEBEX-DP on-site analyses report. Nagra Arbeitsbericht NAB 16-12.

Appendix A: Updated FEBEX-DP: Project Plan (Version 16/06/14)

A.1 Introduction

This document describes the project plan for the FEBEX-DP (Dismantling Phase) project which was initiated in 2014. The document refers to four supporting documents, of which the first is currently finalised:

- Review of the FEBEX in-situ experiment and the mock-up after 15 years of operation and monitoring (Lanyon & Gaus 2013)
- Forecast of the anticipated status prior to dismantling the FEBEX "in-situ" test in 2015 (see appendix B this document)
- Full Dismantling Test Plan (In-Situ Experiment), Aitemin (2014), and its Addenda (Martinez & García-Siñeriz 2015): describing the preparations and the field activities for the dismantling
- Full Dismantling Sampling Plan (In-Situ Experiment), Aitemin (2013): describing the location of the sampling sections and the samples to be taken – status June 2013
- CIEMAT (2012) Test Plan.

The FEBEX experiment at the Grimsel Test Site (GTS) consists of an in-situ full-scale engineered barrier system (EBS) test for the disposal of high level waste (HLW) performed under natural conditions. The experiment is based on the Spanish reference concept in crystalline rock in which the canisters are placed horizontally in drifts and surrounded by a clay barrier constructed of highly compacted bentonite blocks. It was initiated and led by Enresa in 1995 and has been one of the research subjects in three subsequent European projects. In 2008, a consortium consisting of SKB, Ciemat, Posiva and Nagra (and since 2013 also KAERI) undertook the continuation of the experiment under the project name FEBEXe.

Heating started in 1997 and since then a constant temperature of 100 °C has been maintained, while the bentonite buffer has been slowly hydrating in a natural way. A total of 632 sensors were installed in the clay barrier, the rock mass, the heaters and the service zone to measure the following variables: temperature, water saturation, humidity, total pressure, displacement, water pressure. A partial dismantling and sampling of the EBS was carried out during 2002 (ENRESA 2006a).

The long monitoring phase and the partial dismantling in 2002 show that the EBS has largely performed as expected and the major processes and coupled thermal-hydro-mechanical or (geo)chemical processes (shortened to THM or THC coupling for the remainder of the document) affecting the buffer saturation during the initial thermal period identified prior to the start of the experiment have been confirmed.

Much of the buffer is saturated and significant swelling pressures have developed close to the rock. The low permeability of the saturated bentonite close to the rock ensured a slow saturation and showed that inhomogeneity in rock properties have no influence on buffer saturation. In addition, the buffer inhomogeneity due to construction has played a smaller role than expected and a relatively uniform axisymmetric thermal, saturation and stress response controlled by the distance from the heater has been observed. Density gradients within the buffer have developed due to swelling from the hydration and drying and shrinkage near the heater. These density gradients were evident in the data from the partial dismantling in 2002 and they followed an

axisymmetric saturation pattern, which was reproduced in equivalent laboratory tests (Villar et al. 2012a) and was predicted by coupled models (Gens et al. 2009).

The role of 2nd order processes and couplings on saturation has become more important as the hydraulic gradients have reduced. Such processes/couplings include: i) thermal osmosis; ii) threshold gradients for flow within the bentonite; and iii) the influence of evolution of porosity structure of the bentonite.

A review of the in-situ and mock-up test as well as the interpretation of the data is given in Lanyon & Gaus (2013).

The FEBEX in-situ dismantling project (FEBEX-DP) will provide a unique opportunity for sampling an engineered barrier and its components that underwent continuous heating and natural resaturation for 18 years under partly aerobic conditions. Because of these conditions, the impact of chemical processes is expected to be significant and quantifiable.

A.2 Dismantling objectives

The main objective of the FEBEX project is to study the behaviour of the near-field components in a repository for high-level radioactive waste in granite formations, i.e. to better understand the thermo-hydro-mechanical (THM) and thermo-hydro-chemical (THC) processes and increase confidence in the models required for interpretation in the evolution of such processes.

Based on the overall FEBEX objectives, the **primary objective** of the FEBEX in-situ dismantling project is to further complete the understanding of the processes affecting the components of the in-situ test through integration of the results of the dismantling with earlier monitoring and dismantling results with a focus on:

- Characterisation of the key physical properties (density, water content) of the bentonite and their distribution
- Characterisation of corrosion processes on instruments and coupons under evolving redox conditions and saturation states
- Characterisation of mineralogical interactions at material interfaces and potential impacts on porosity

These primary objectives will be obtained by pursuing the following **secondary objectives** regarding the main elements of the experiment:

- Buffer and interfaces
  - Obtaining a 3D-insight in the water content and density distributions of the bentonite through extensive sampling
  - Obtaining insight in THM parameters and their evolution in time through comparison with the values of the first dismantling
  - Characterizing pore water changes, modifications in the absorbed cations in the clays and potential mineralogical alteration
  - Microbiological characterisation

  - Of particular interest will be characterising the interfaces with the liner, the heater, the embedded corrosion coupons and instrumentation and the identification of potential chemical interactions affecting the bentonite

- Instrumentation and metal coupons
  - Recalibrating and correcting the monitoring results if required, analyse their mechanical performance
  - Analyse corrosion products

- Plug and interfaces
  - Investigating the performance of the shotcrete at macro and micro level as well as the potential chemical changes occurring along the interfaces (for example for the concrete/bentonite, concrete/granite and concrete /lamprophyre)

- Granite host rock (service area and heated zone)
  - Investigating the rock properties of both zones, in particular, the performance of the granite and the interfaces granite/bentonite

- The heater and liner
  - Analyse potential corrosion, changes of position of the heater and deformations of the liner

A.3 Main activities in the project

The implementation of the FEBEX-DP project foresees the following activities.

A.3.1 Pre-dismantling modelling

Using existing THM models (e.g. Dupray et al. 2013) the impact of switching off the heaters on the pressure and relative water content in the EBS will be evaluated. In case this is significant an assessment on the potential geochemical consequences (dissolution, precipitation due to changing temperatures and water content) of the buffer might be needed and used as input in order to optimise the sampling plan. Several teams are invited to use their own codes to compare prior to dismantling.

A.3.2 Field work related to the dismantling

1. Pre-operation tests for optimised sampling techniques (by AITEMIN)

2. Operation preparation

3. Checking the status of the equipment used in the partial dismantling (crane, extraction car, tracks, side dump wagon, rope winch, etc.), evaluation of the need to procure new equipment, revision of documentation

4. Drilling through the plug to obtain interface samples

5. Switch-off Heater 2 one month before plug demolition. In order to obtain intact and undisturbed samples from the shotcrete/bentonite interface, novel sampling techniques (based on core stabilisation and overcoring), will be used. These have been tested successfully at the GTS and the Mont Terri URL lately.

6. Dismantling Operation

   The dismantling operation will be carried out according to the following sequence:

   - Removal of instrumentation and auxiliary systems, protection of acquisition cabinets
   - Completion of steel tracks up to plug
   - Shotcrete plug demolition (and sampling if required) thereby trying to avoid damage to cables and instruments. Fulfilment of the associated quality control documentation during the sampling (samples/instrumentation removal included)
   - Removal of "dummy canister"
   - Removal and sampling of bentonite and liner up to the front of Heater 2, and shipping of samples. Fulfilment of the associated quality control documentation during sampling
   - Analysis and extraction of Heater 2
   - Removal and sampling of the remaining bentonite and liner, and shipping of samples. Fulfilment of the associated quality control documentation during sampling
   - Removal of monitoring and control system

A.3.2 Laboratory program and analysis of the samples

A.3.2.1 Expected status of the components to be sampled at the time of dismantling in 2015

In the following paragraphs the expected state of the components of the FEBEX in situ is described. The anticipated state is based on the properties of the emplaced materials, the assessment of the impact of the ongoing process and the outcome of the partial dismantling in 2002.

The following components are considered in the sampling program (Fig. 1):

a) Service area and heated zone

b) Plug and plug interfaces

c) Buffer

d) Sensors

e) Heater

f) Liner

Shotcrete plug: the total pressure (hydraulic and gas) behind the plug is between 6 – 8 MPa. This pressure needs to be released locally by drilling through the entire plug before the sampling operation can start. The shotcrete bentonite interface is expected to show mineralogical interaction products accumulated over more than 10 years.

bentonite blocks: Drier blocks are expected in the inner ring (close to the heater) as well as in the centre of the non-heated zone, and more humid blocks in the outer ring. Blocks were put in place in 1996 and have reached swelling pressures between 6 – 8 MPa and relative humidity between 40 – 90 %. It is anticipated that the construction gaps will have disappeared completely. Some swelling and displacements of the buffer towards the drift entry due to stress release is expected. Tracers impregnated in filter paper, in sintered metal, compacted bentonite blocks, or glass ampoules have been emplaced and analysis of targeted bentonite samples are expected to illustrate diffusion behavior reflecting the 18 year long ongoing saturation.

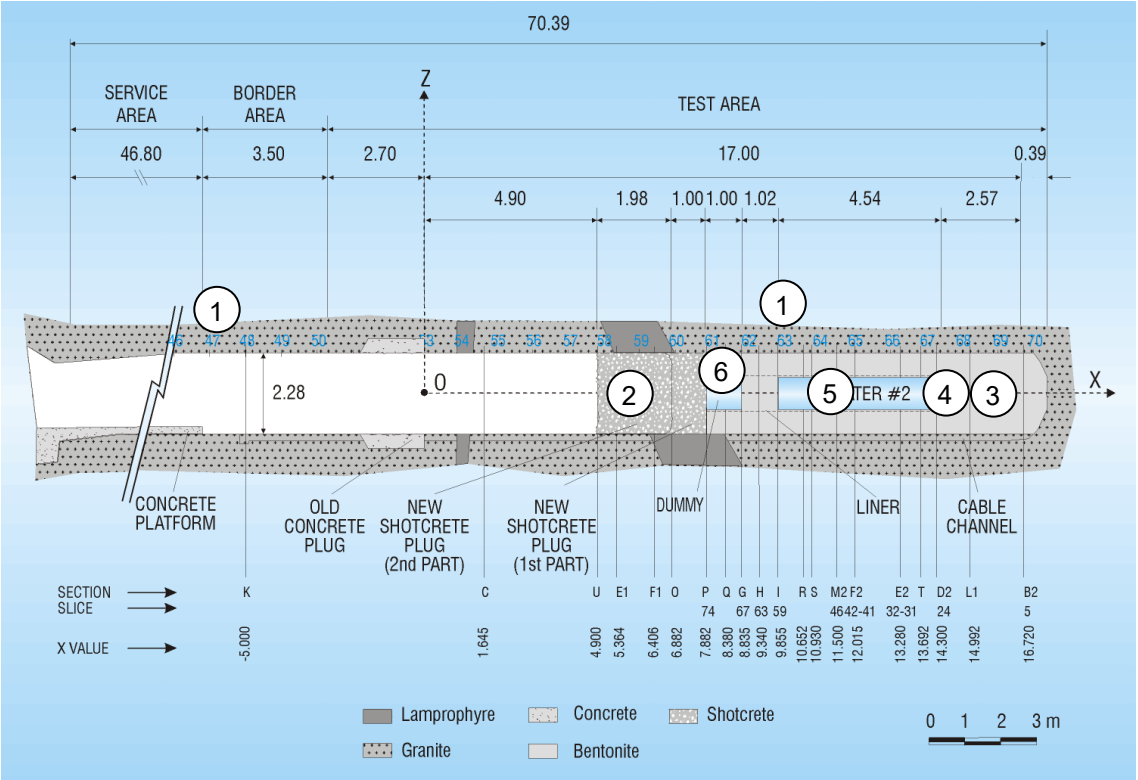


Fig. A-1: Current FEBEXe configuration.

Coupons: samples of different candidate metals for manufacturing of containers (coupons) have been inserted inside the buffer material and underwent corrosion during 18 years. The analysis in 2002 (after 5 years) showed no generalised and/or local corrosion on the stainless steel and titanium specimens, while the carbon steel coupons showed slight generalised corrosion, with corrosion rate values of 0.10 µm/year. No localised corrosion phenomena were detected. The copper coupons showed corrosion rates of 0.71 µm/year for the Cu-ETP, and 0.74 µm/year for the Cu10Ni alloy. The corrosion suffered by the Cu30Ni alloy was negligible (Enresa 2004).

Instrumentation: corrosion of the instrumentation under partly aerobic conditions is expected. The analysis during the dismantling in 2002 concluded that the high humidity, together with the presence of sulphate reducing bacteria in the bentonite were at the base of that. Sulphur rich corrosion products, as well as the morphology of the corrosion indicated localised corrosion phenomena induced by sulphate reducing bacteria. Cracking typical of stress corrosion induced by the presence of chlorides and/or products resulting from the metabolic activity of the

sulphate reducing bacteria was also observed. General corrosion was observed on the steel components in some cases leading to the destruction of the component.

Heater 2, liner and dummy canister: as the humidity in the inner part of the buffer is rather low, limited corrosion is expected for all three steel components. During the partial dismantling in 2002 slight uniform generalised corrosion over its whole surface, with oxide layers less than 20 microns thick. The liner corrosion was generalised and non-uniform, with maximum values of approximately 130 microns on the external surface and 200 microns on the internal surface.

Granite: the tunnel was excavated in 1995 using a tunnel-boring machine (TBM). The existence and time evolution of the excavation damaged zone (EDZ) can be assessed and compared for both the heated area and service area.

A.3.2.2 Types of analysis planned for different components

Based on the anticipated status of the components Tab. A-1 gives an overview of the analyses that are currently being planned. The final analysis scheme and the location of the samples will be described in the sampling book and might deviate from the one described here. Currently, an update due to budget constraints and new partner wishes will be prepared and issued in the summer of 2014. I will be discussed and finalised in a field meeting in September 2014.

Tab. A-1: Currently planned analysis on samples taken from the components of the FEBEX in situ as part of FEBEX-DP.

No.	Sampling location/ experiment component sampled	Type of sample	Type of analysis/method (organization who will be in charge)	Method
1	Service and heated area	Crack development	Visual and acoustic inspection, laser beam	
		Humidity and temperature		
2	Plug and plug interfaces (shortcrete)	Physico-geochemical/ mineralogical	Porosity	X-ray 3D computed microtomography, XRD, SEM-EDX, FTIR, TGDSC
	(Shortcrete)		Pore structure and distribution	SEM, FIB
			Mineralogy	Microxrd, XRD, SEM, SEM-EDX, TEM, thin sections, optical microsopy
			Swelling pressure	Oedometer
			Unconfined compression strength (Mechanical press)	Unconfined compression strength (Mechanical press)
			Shear strength (triaxial cell)	Shear strength (triaxial cell)
			Biological sampling	Biological sampling
			Isotopic signature of carbon and oxygen in carbonates both in the cement matrix (UAM)	

Tab. A-1: Cont.

No.	Sampling location/ experiment component sampled	Type of sample	Type of analysis/method (organization who will be in charge)	Method
			Pore water chemistry studies	
			Microbiology - Visual inspection	MPN, optical microscopy
3	Buffer material	Gas	Quantitative composition	DO probe, Raman
	(bentonite)	Porewater	Quantitative composition	Chemical analyses (major, trace and ultrace elements, Fe(II)/Fe(III), NPOC (non-purgable organic carbon), TC, TOC and TIC
		Mineralogy	Mineralogical/Crystallography composition in bulk and clay (density, grain size distriburion, porosity, pore size distrubution, surface area)	XRD, SEM-TEM, SEM-EDX, FTIR, TG-DSC (UAM)
			Elemental content in the bulk and in the clay fraction	Mineralogy (XRD, TG-DSC, FTIR, XPS, RMN, Mössbauer, SEM, HRTEM and TEM, STEM, XANES, EXAFS)
			CEC, cation and anion analyses in PW and clay	
			Layer charge (n-alkylammonium ion-exchange echnique)	
			Isoelectric and zero charge points (titration)	
			Aqueous leachates	
			Inorganic and organic C and S (carbon and sulfur analyzer)	
			Organic matter	
		THM	***Hydraulic properties***	Relative humidity (capacitive sensor)
				Suction/water
				Hydraulic conductivity
				Gas permeability
			Mechanical properties	Performance of the joints
				Strain at saturation under load
				Preconsolidation pressure under oedometric conditions
			Thermal properties	Thermal conductivity
			THGC	
			Thermo-hydro-geochemical tests	Pore water and redox fronts

Tab. A-1: Cont.

No.	Sampling location/ experiment component sampled	Type of sample	Type of analysis/method (organization who will be in charge)	Method
			Analysis of tracers distribution	X-Ray fluorescence, ICP-MS, NITIMS, IC, ISE
			Corrosion products, corrosion processes, corrosion rates and metallographic characterisation	XRD, Raman spectroscopy, SEM-EDS and optical microscopy
			Microbiology – Visual inspection	MPN, optical microscopy
4	Sensors	Sensors	All sensors status and calibration	
			Corrosion products, corrosion processes, corrosion rates and metallographic characterization	XRD, Raman spectroscopy, SEM-EDS and optical microscopy
			Microbiology – Visual inspection	MPN, optical microscopy
5	Heater		Interfaces iron-bentonite	
			Iron distribution, coordination and oxydation state	Mössbauer, XANES, EXAFS
			Pore structure and distribution	SEM, FIB
			Mineralogy	Microxrd, XRD, SEM, TEM, Mössbauer
			Swelling pressure	Oedometer
			Biological sampling	
			Corrosion products, corrosion processes, corrosion rates and metallographic characterization	XRD, Raman spectroscopy, SEM-EDS, optical microscopy
			Iron, salts and exchangeable cation distributions, changes in physical properties, geochemical evolution	FTIR, Mössbauer spectroscopy, SEM-EDS, TEM-SAED XRD, soluble extracts, CEC, exchangeable complex determinations
			Microbiology – Visual inspection	MPN, optical microscopy
6	Liner		Interfaces iron-bentonite	
			Iron distribution, coordination and oxydation state	Mössbauer, XANES, EXAFS
			Pore structure and distribution	SEM, FIB
			Mineralogy	Microxrd, XRD, SEM, TEM, Mössbauer
			Swelling pressure	Oedometer
			Biological sampling	
			Corrosion products, corrosion processes, corrosion rates and metallographic characterization	XRD, Raman spectroscopy, SEM-EDS and optical microscopy

Tab. A-1: Cont.

No.	Sampling location/ experiment component sampled	Type of sample	Type of analysis/method (organization who will be in charge)	Method
			Iron, salts and exchangeable cation distributions, changes in physical properties, geochemical evolution	FTIR, Mössbauer spectroscopy, SEM-EDS, TEM-SAED XRD, soluble extracts, CEC, exchangeable complex determinations
			Microbiology – Visual inspection	MPN, optical microscopy

A.3.2.3 Recalibration of the sensors

Sensors that have been recovered in good condition will be recalibrated and if required, monitoring data can be corrected.

A.3.3 Reporting

Planned activities prior to dismantling will be described in the following documents

- Dismantling plan
- Sampling plan and sampling book
- Analysis plan
- QA/QC plan

After completion of each activity, reporting of the activity will be completed by the contractor/laboratory that performed the activity according to their QA procedures. Integration of results will occur in summary reports, the Final Dismantling Report and Final FEBEX *in-situ* Report being the key documents. These reports will be coordinated by the consortium supported by contractors according to the Nagra QA procedures.

A.4 Project organisation and resources

The project organisation is shown in Fig. A-2 below. The organisation between the FEBEXe partners is described in the Experiment Agreements between the FEBEXe partners.

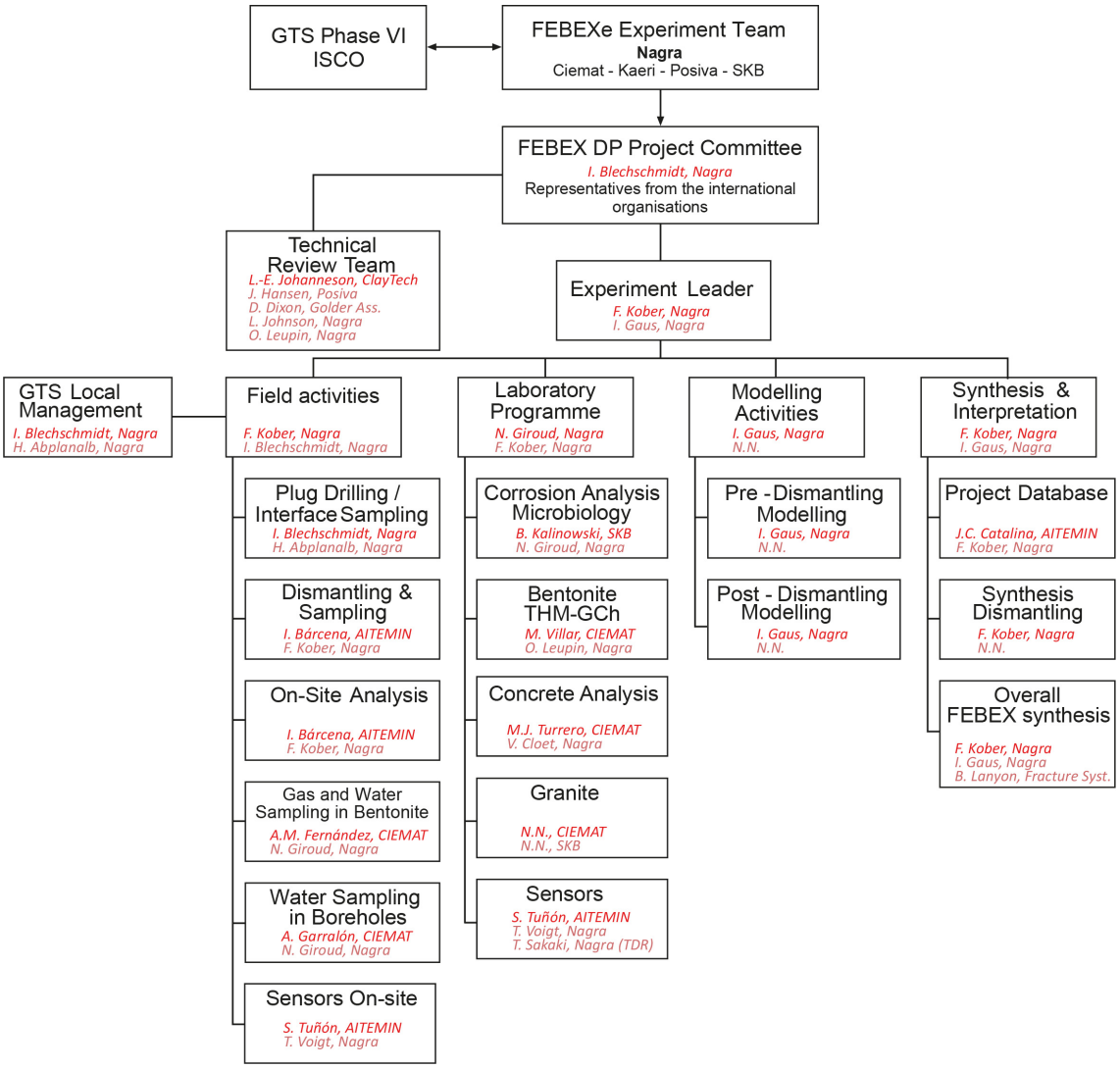


Fig. A-2: Organisational chart of FEBEXe.

The role of the Experiment Leader is

- Overall management of the Experiment
- Coordination of individual tasks
- Taking the overall financial responsibility for implementing the Experiment according to the guidelines defined by the Experiment Team. Organising bookkeeping for the Experiment and providing a settlement of accounts to the Experiment Partners
- Providing required information to the International Steering Committee GTS Phase VI (ISCO) on behalf of the Experiment Team
- Coordination of work at the GTS
- Awarding contracts on behalf of the Experiment Partners for the GTS field work, subject to prior decision by the Experiment Team.

The role of the Experiment Team is

- Plan the Experiment in detail
- Supervise the implementation of the necessary work (field work, laboratory programme, analysis)
- Ensure reporting as required
- Decide detailed working programs
- Decide the corresponding budget for the Experiment.

The Project Committee meets every 6 months. The Project Committee consists of the Chairman, the FEBEXe Experiment Team and the non-voting representatives of the international organisations. During the Project committee meetings one

- Decides on the Experiment concept
- Approves the global budget for the Experiment
- Approves the detailed budget for the forthcoming activities (normally on an annual basis)
- Reviews and settles the accounts of the previous year
- Takes go/no-go decisions at critical milestones of the Experiment
- Decides on the management responsibility of the tasks
- Reviews and approves the Deliverables

The technical review team reviews the deliverables of the project and makes recommendations for improvement.

Coordination meetings between the Experiment leader and the Task leaders and contractors are organised as needed.

A project platform will allow access to the project documentation including the meeting minutes and the reports. The project platform provides a link to the project database containing the results of the analysis.

The FEBEX in-situ dismantling requires a budget of approximately 1.3 Mio. CHF.

A.5 Project milestones

Past major milestones in the project were (Fig. A-3):

M1:	Pre Kick-off FEBEX-DP Meeting (FEBEXe partners)	23.04.2014
M2:	Kick-off of FEBEX-DP	10.06.2014

Major upcoming milestones in the project are:

M3:	Sampling/Dismantling plan finalised (field meeting)	09/2014
M4:	FEBEX-DP workshop	12/2014
M5:	Dismantling start at GTS	04/2015

M6:	FEBEX-DP partner meeting	07/2015
M7:	Dismantling at GTS finalised	09/2015
M8:	"As dismantled" report ready; FEBEX-DP partner meeting	01/2016
M9:	FEBEX-DP partner meeting	07/2016
M10:	Final FEBEX-DP partner meeting, Synthesis reports ready	12/2016

A.6 Delivrables

The following deliverables will be produced.

In the preparation phase:

DP1: Dismantling plan

DP2: Sampling plan and sampling book

DP3: Analysis plan

DP4: QA/QC plan

DP5: Setup and development of the project database

DP6: THMC modelling prior to dismantling

In the dismantling phase and analysis phase:

DA 1: "As dismantled" report (including on-site analysis)

DA 2.1 – DA2.x: Laboratory reports provided by contributing laboratories

DA 3: Compilation of all dismantling analyses – link to the sampling book

DA 4: Completed project database

In the interpretation phase:

DI 1: Integration of the bentonite analyses and conclusions

a) Description and interpretation of the findings regarding the bentonite analyses (THM, THC)

b) Interpretation in the light of recent literature

DI 2: Chemical interactions at interfaces – description and conclusions

a) Observations, measurements and interpretation at the bentonite/rock, and bentonite/cement interface

b) Interpretation in the light of recent literature and similar experiments

DI 3: Microbiological observations from the FEBEX in situ

a) Description of current analysis
b) Comparison with previous results

DI 4: Observed corrosion processes in the FEBEX in situ and their drivers

a) Corrosion observed
b) Microbiology linked to corrosion processes
c) Analysis from the gas sampling (if performed)
d) Geochemical impact on the adjacent bentonite

DI 5: Synthesis report on the FEBEX in situ dismantling

a) Host rock conditions
b) bentonite and interface reactions
c) Corrosion processes
d) Sensor recalibration
e) Post-excavation analysis of the pre-dismantling modelling
f) Post-dismantling modelling

DI 6: Synthesis report on the FEBEX in-situ experiment – major outcomes.

Participation in conferences and the submission of papers to peer-reviewed journals will be pursued and encouraged.

A.7 Planning of activities, milestones and deliverables

The projects consists of four phases (Fig. A-3):

1. Preparation phase
2. Dismantling phase (field activities)
3. Laboratory and analysis phase
4. Interpretation and synthesis phase

The project timeline, including the dates for the Milestones and the Deliverables is provided in Fig. A-3.

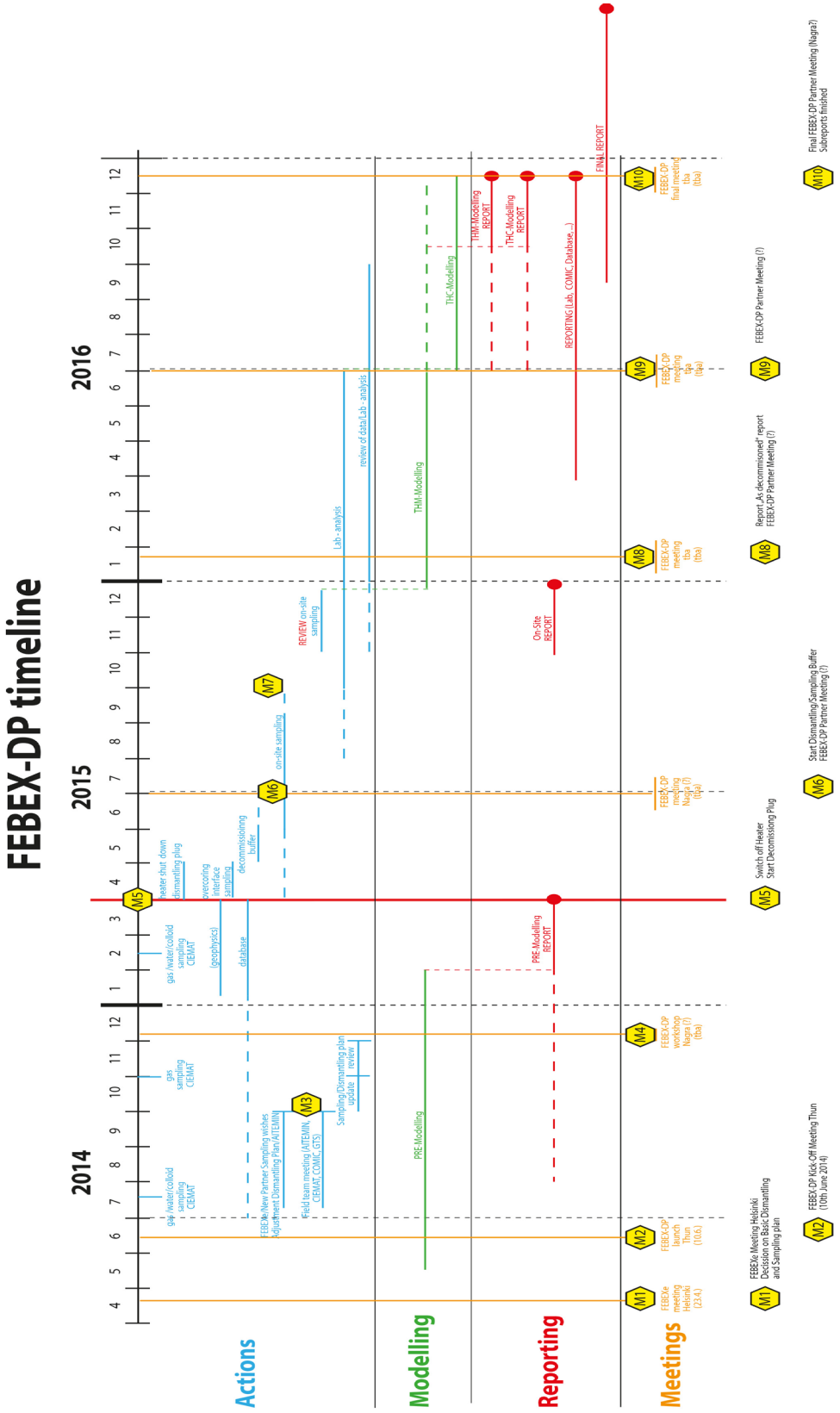


Fig. A-3: FEBEX-DP project timeline indicating milestones and deliverables.

Appendix B: Forecast of anticipated status prior to dismantling the FEBEX "in situ" test – FEBEX-DP

B.1 Introduction

The FEBEX ("Full-Scale Engineering Barrier EXperiment in Crystalline Host Rock") experiment at the Grimsel Test Site consists of an "in-situ" full-scale test performed under natural conditions. The experiment is based on a previous Spanish reference concept for the disposal of radioactive wastes in crystalline rock (AGP Granito) which considered that canisters enclosing the conditioned wastes are placed in horizontal drifts, surrounded by a clay barrier constructed of highly-compacted bentonite blocks. The experiment has already provided a unique insight into Engineered Barrier System (EBS) evolution at a 1:1 scale under natural conditions over a time frame covering a significant part of the early EBS evolution in a repository. Although initiated almost 20 years ago, FEBEX meets the current needs to demonstrate the functioning and performance of various repository components.

The FEBEXe consortium (Ciemat, KAERI, Nagra, Posiva and SKB) has initiated the final dismantling of the FEBEX "in-situ" test in 2015. This decision was based on the expectation that further changes of the state of the buffer will be very slow, and probably not provide significant new information. A full buffer saturation is also unlikely to be achieved under current operational conditions.

Following a call for new partners, the FEBEX consortium was joined by ANDRA, BGR, Obayashi, RWM, SURAO and US-DOE under the project name FEBEX-DP (DP – Dismantling Project) becoming effective in June 2014. First planning and preparations for the final dismantling started in 2012 with the drafting of a dismantling and sampling plan, which will become definitive by the end of 2014. In April 2015, the remaining heater will be switched off and excavation of the plug will start, preceded by a sampling program focusing on the cement plug and the cement-bentonite interface. After ca. 1 month of excavation and simultaneous cooling of the buffer, a buffer dismantling/sampling operation period of ca. 3 – 4 months is foreseen. During 2015 – 2016, an extensive cement and bentonite laboratory analysis program, including the calibration of retrieved sensors will be carried out. Analytical results will be compared to data obtained from the partial dismantling (ENRESA 2006a); the monitoring data (AITEMIN 2014) as well as to the results derived from modelling efforts (see Lanyon & Gaus 2013). The results are expected to increase the current knowledge and confidence for the FEBEX-DP partners in bentonite performance with a focus on thermo-hydro-mechanical (THM) and thermo-hydro-chemical (THC) processes as well as on corrosion and microbial activity. The reporting of the laboratory analyses and dismantling results is expected to be complete by the end of 2016 with a final integrated report issued in early 2017.

B.1.1 Purpose of the document

This document describes the anticipated status of the components of the FEBEXe "in-situ" test at the time of the start of the final dismantling. It is based on measuring and modelling activities completed in the course of the experiment and experience from the partial dismantling carried out during 2002 (ENRESA 2006a, Lanyon & Gaus 2013). The purpose is to identify the areas or major components of the experiment that are of interest for detailed examination in order to meet the objectives of the experiment dismantling.

The outcome of the dismantling is expected to be highly valuable since the components have undergone heating and natural re-saturation during 18 years. Furthermore, it will be possible to

make a comparison not only with the initial state, but also with the results from the partial dismantling during 2002. This will provide a valuable time-dependent characterisation of the near-field components under conditions similar to those in a repository for high-level radioactive waste. It will also be comparable to results obtained by similar projects, such as the SKB – Prototype Repository dismantling (Svemar et al. 2016).

It is highlighted here, that due to the specific configuration of FEBEX and its location, several conditions may not reflect final or future repository designs. It has to be considered, that:

- The Grimsel host-rock has no to very spatially limited EDZ.
- Shear zones and dykes are present in the emplacement gallery.
- Grimsel groundwater is characterised by low electrical conductivity, neutral to high pH (7 –10), low carbonate alkalinity and content and low dissolved oxygen.;
- The bentonite used was FEBEX (Serrata clay) in a block concept.
- Numerous sensors, cables and tracers were emplaced in the buffer and host rock.
- The temperature curve may not resemble real temperature behaviour after container emplacement.
- The composition of the initial cement plug and its overall design was not ideal because of leakage in order to establish redox and microbial indices under controlled conditions. The configuration of the second plug was optimised and less permeable in the light of characterising redox and microbial indices.

The document provides a starting point for the planning of the dismantling and sampling of the FEBEXe "in-situ" test. All sensor data mentioned are referring to the latest report including data up to 01.05.2014 (AITEMIN 2014b), with various data only reliable for specific time intervals during the experiment.

B.1.2 Background

B.1.2.1 Test configuration during FEBEX I (original test configuration)

The construction of this test was carried out in 1996 at the Grimsel Test Site – GTS, Switzerland. Two electrical heaters, of the same size and of a similar weight as the reference canisters, were placed in the axis of a horizontal drift excavated in the Grimsel granodiorite. The drift was constructed especially for this experiment using a Tunnel Boring Machine (TBM) with a diameter of 2.28 m. The gap between the heaters and the rock was backfilled with compacted bentonite blocks, up to a length of 17.40 m, requiring a total of 116 tons of FEBEX bentonite ("Serrrata" clay). The backfilled area was sealed with a plain concrete plug keyed into a recess excavated in the rock and having a length of 2.70 m and a volume of 17.8 m^3. Fig. B-1 shows the dimensions and layout of the test components schematically.

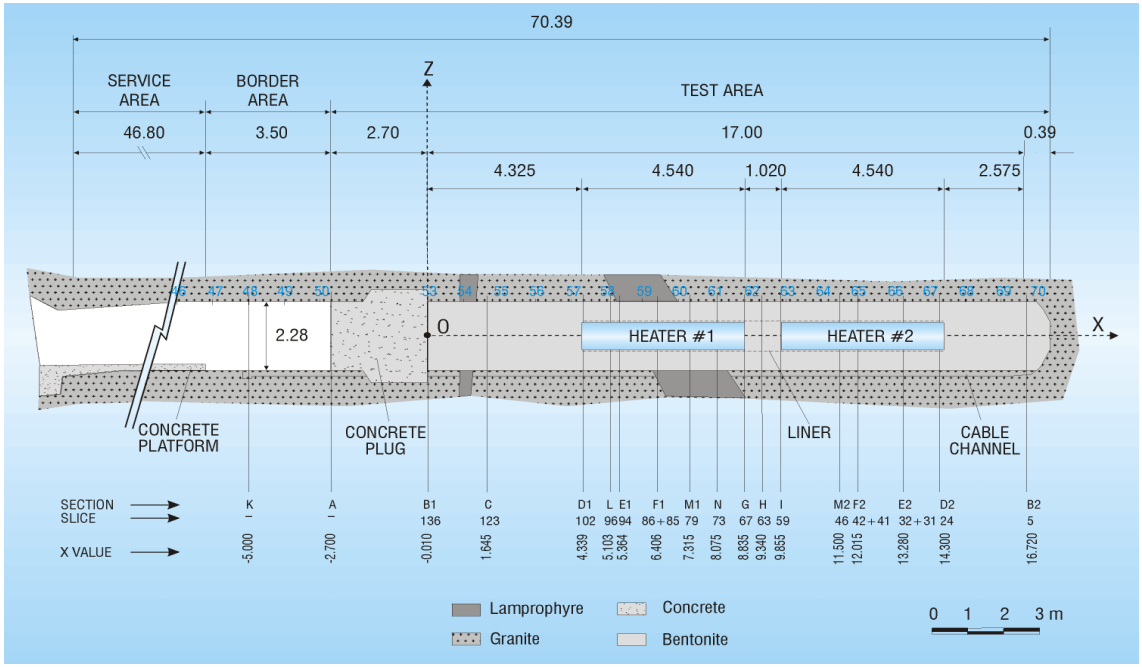


Fig. B-1: Original FEBEX (I) configuration (ENRESA 2006a) and indication of instrumented sections.

In order to monitor relevant parameters such as temperature, humidity, total and pore pressure, displacements, etc., a total of 632 instruments were placed in the system along a number of instrumented sections, both in the bentonite buffer and in the host rock, (ENRESA 1998a). The construction of the first concrete plug was completed in October 1996, and the heating operation started on 28.02.1997.

B.1.2.2 Test configuration after the first dismantling operation and current test configuration (FEBEXe)

In 2002, a partial dismantling of the "in-situ" test was conducted, consisting of removing one of the heaters and leaving the other in operation. The design and planning of the partial dismantling operation was conditioned by three basic objectives:

To carry out an intensive sampling program of the test components (bentonite, rock, metals, and instruments) located in the area of the first heater.

To perform a canister retrieval exercise in such a way that information be provided on the potential technological problems that may be found in an operation of this kind in the real case.

To re-construct the test, with the necessary amendments and improvements, in order to continue the heating and hydration phase with the second heater over a long timescale.

During the dismantling operation, a large number of samples from different materials (rock, concrete, bentonite, water, chemical tracers and metals) were taken for analysis (ENRESA 2006a, 2006b). The initial plan was to remove the buffer and all components up to a distance of 1 meter from Heater #2 (Section G in Fig. B-1). However, and in view of the risk of disturbing the non-dismantled area, it was finally decided to leave one additional meter of buffer, as a result of which the dismantling was carried out up to the longitudinal coordinate x = 7.882 (see

Fig. B-2). A dummy steel cylinder with a length of 1 m was inserted in the void left by Heater #1 in the center of the buffer. Some new sensors were installed in that one additional meter of bentonite buffer (ENRESA 2003) in order to increase the density of measurements in the buffer, and also to extend the life expectancy of the instrumentation system.

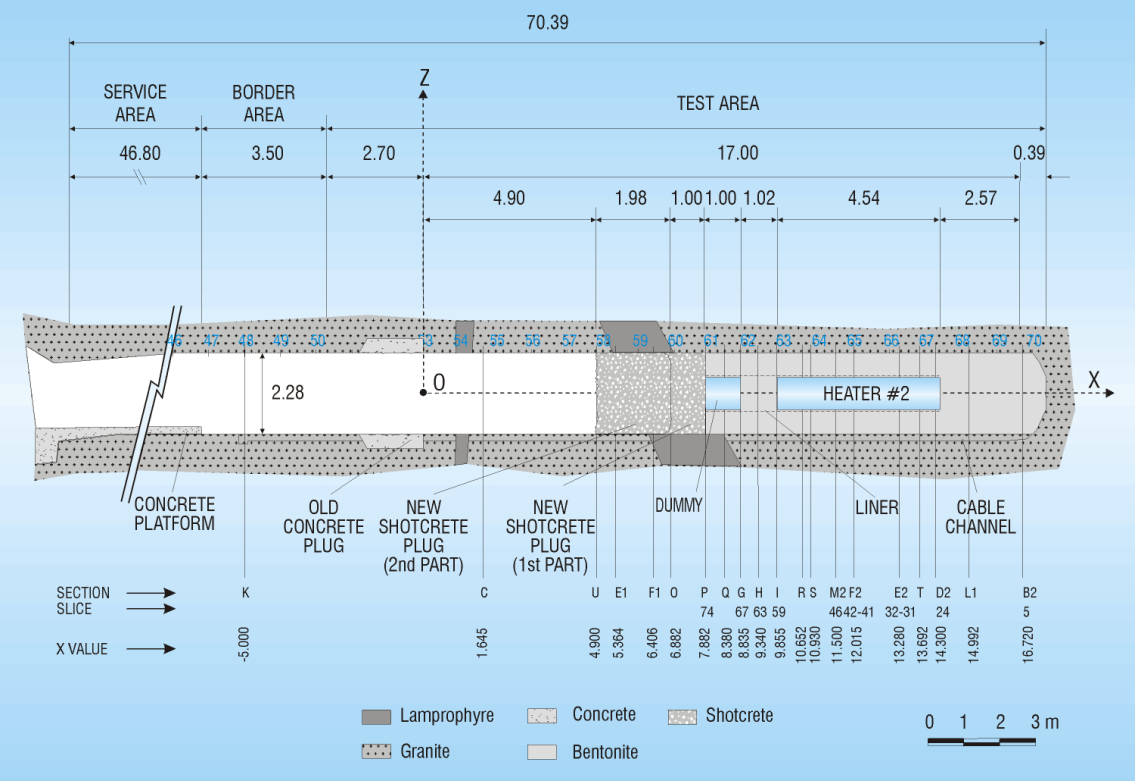


Fig. B-2: Current FEBEX-II configuration (ENRESA 2006a).

Explanation for numbers see Section B-2.

Also, sensors were introduced in boreholes drilled in the buffer parallel to the drift. To simplify this operation, a new concrete plug was constructed in two phases: an initial temporary plug measuring a length of 1 m, which was built immediately after dismantling, and a second section to complete the plug length to the 3 m planned in the design of the experiment. The configuration of the test, after completing the dismantling operation and construction of the full plug length, is shown in Fig. B-2.

B.1.2.3 Objectives of the final dismantling

The long-term objective of the FEBEX-project has been to study the behaviour of the near-field components in a repository for high-level radioactive waste in granite formations, i.e. to better understand the thermo-hydro-mechanical (THM) and thermo-hydro-chemical (THC) processes and to increase the confidence in modelling approaches required for interpretation and prediction of the evolution of such processes.

Based on this, the main objective of the final dismantling is to further develop the understanding of the processes affecting the components of the in-situ test through integration of the results of the dismantling with earlier results, monitoring and modelling data.

The following objectives are targeted:

- **Buffer:** A 3D-insight will be obtained for the water content and density distributions of the bentonite through extensive sampling. A full laboratory tests campaign will characterise the buffer status in terms of THM parameters. A comparison with the initial values and the values from the partial dismantling will allow a time-dependent characterisation of the buffer evolution. Chemical analysis will allow characterising pore water changes, modifications in the absorbed cations in the clays and potentially mineralogical alteration. The identification of potential chemical interactions for fluid or gas pathways will be pursued. THM and THC data will allow evaluating the predictive capability of the respective numerical codes.

- **Buffer Interfaces:** Of particular interest is the characterisation of the interfaces of the buffer with the liner, the heater (if existing), the embedded corrosion coupons and instrumentation. For obtaining perfectly intact and in-situ samples, novel sampling techniques (e.g. overcoring) will be used. Additional focus will be placed on the interfaces of bentonite blocks parallel or perpendicular to the drift orientation.

- **Microbiology:** Beside the corrosion on coupons and instruments, corrosion induced by microbes in situ, dependencies of microbial survival and the related effects of swelling pressure in clay barriers under certain redox conditions will be investigated. It is acknowledged that current known boundary condition necessary for constrained corrosion-microbiology related investigations were not fully met during installation of the FEBEX experiment in 1996.

- **Instrumentation:** The sensors/instrumentation will be extracted with great care for recalibrating and correcting the monitoring results. Analysing their mechanical performance and impact of corrosion on their performance are other objectives. Special attention will be given to the recalibration of TDRs.

- **Plug and interfaces:** The objective is to investigate the performance of the shotcrete at macro and micro level as well as the potential chemical changes occurring along the interfaces (concrete/bentonite, concrete/granite and concrete/lamprophyre).

- The **heater and liner** are subjected to high temperatures, humidity and pressures and therefore potential corrosion, changes in position of the heater and deformations of the liner are possible and characterisation will take place to assess this.

- **Granite host rock** (service area and heated zone): Although negligible changes were inferred from the partial dismantling it would be of special interest to investigate the rock mass properties of these two different zones, in particular the performance of the granite and the interfaces granite/bentonite after 18 year of continuous interface coupling.

B.2 Forecast of the anticipated status of the major components

The following areas/components are considered to be of major interest (as referred to in Fig. B-2):

- Service area and heated zone
- Plug and plug interfaces
- Buffer
- Sensors and corrosion probes
- Heater
- Liner

Other overarching status statements will be provided for COrrosion and MICrobiology (COMIC), gas-water measurements and modelling.

B.2.1 The service area and heated zone

B.2.1.1 Initial properties prior to experiment emplacement and observations from the first excavation

A rock sampling campaign was carried out in the service area to obtain "blank" samples for comparison with equivalent rock samples to be collected subsequently from the heated zone. After the partial dismantling of the "in-situ" test, sampling occurred in the first heated zone with the purpose of inspecting the mechanisms of a potential excavation damaged zone (EDZ) creation around the test drift after a period of more than five years of heating. Only minor changes in porosity were detected, with an increase in degree of porosity and depth (cm) of porosity occurring in the lamprophyres (ENRESA 2006b). This is supported by a gas permeability test with values around 1×10^{-19} m^2, pointing at the absence of a marked damage.

B.2.1.2 Expected status service area and heated zone

Due to the general absence of a significant EDZ in the Grimsel granite and the fact that only negligible effects of the drift were recorded after the partial dismantling (ENRESA 2006a), it is suspected that very little to no changes of the mechanical and hydraulic properties of the granite will have occurred between the partial and the final dismantling. This is also expected because of temperatures in the range of 30 – 40 °C at the buffer/granite interface (see Tab. A-1). The drift will be characterized and documented by a visual inspection. Independent of FEBEX-DP, water and colloid studies in boreholes within the FEBEX drift are investigated (Buil et al. 2010; Missana et al. 2011). The pore water analysis in boreholes parallel and radial to the drift indicates an increase in the Na+ and Cl- content over time by diffusional processes of the solutes transferred from the bentonite pore water towards the granite groundwater. Colloid studies in boreholes parallel to the drift show increased fractions of colloid particles due to the bentonite barrier, though with complex signatures due to artefacts from the drilling operations.

B.2.2 Plug and plug interfaces

B.2.2.1 Initial properties of the second shotcrete plug and observations from the first plug dismantling

The phase of installing the second shotcrete plug was preceded by installing further instruments (humidity and total pressure cells). The concrete plug used for the confinement of the remaining part of the FEBEX "in-situ" test was designed as a parallel plug, without keys or anchors in the rock, constructed by the shotcreting technique. The basic design of the plug is shown in Fig. B-3.

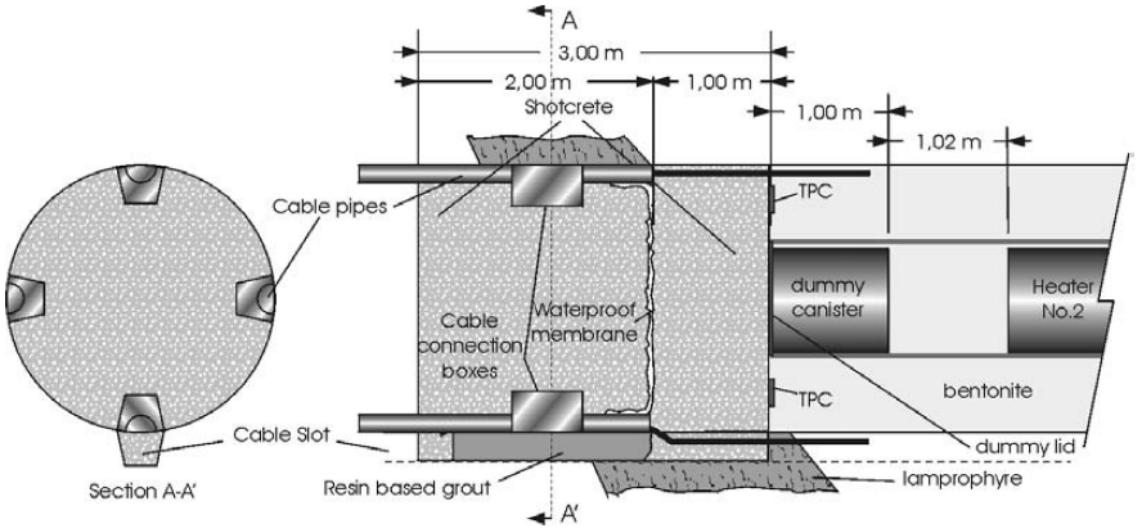


Fig. B-3: Design of the Shotcrete plug for FEBEXe (ENRESA 2003).

The plug was constructed in two stages: first a section with a thickness of 1 m, and at a later stage the remaining part up to the total length of 3.0 m. The first section of the plug was put in place in July 2002. Mechanical tests on plug cores showed an average compressive strength of 32 MPa. Drilled cores showed the presence of some voids and poor quality areas, but these irregularities were limited to a few localised zones. Hydraulic conductivity estimated on test cores is 1.10^{-11} m/s (ENRESA 2003). In August 2002, four linear displacement transducers were installed in contact with the shotcrete surface and removed in March 2003 with an outward displacement of about 1.5 mm mainly for the lower sensors.

Furthermore, additional pipes were installed in boreholes drilled across the existing temporary plug and the bentonite buffer before the construction of the rest of the plug. Three gas injection/collection pipes by GRS, six pipes with water sampling devices and humidity sensors by CIEMAT, and two pipes with total pressure sensors and thermocouples by AITEMIN (Fig. B-4, ENRESA 2003). The final 2 m of gunite shotcrete were injected in June 2003 with a higher compressive strength (mean 40 MPa) and a similar hydraulic conductivity as the first section. Four linear displacement transducers were installed.

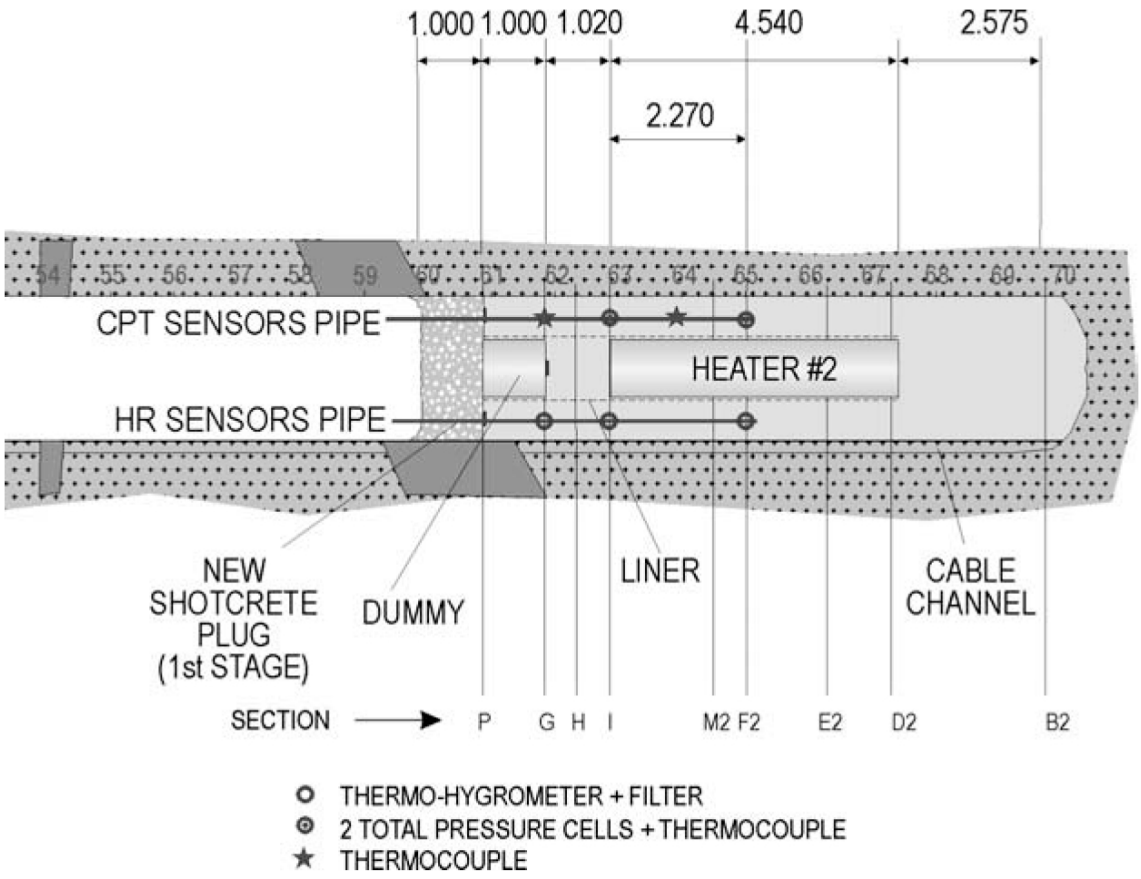


Fig. B-4: CIEMAT and AITEMIN gas pipes and sensors installed (ENRESA 2003).

B.2.2.2 Expected status of the plug and plug interfaces

The total pressure (hydraulic and gas) behind the plug is between 6 – 8 MPa with a total displacement at the plug front of less than 0.5 mm (AITEMIN 2014a). This pressure will be released locally by drilling through the entire plug in order to perform overcoring of the intact interface cement/bentonite. Besides the overcoring, three long cores obtained over the whole length in outer and inner parts of the plug will be cored to characterise longitudinal and radial trends in the cement. After this core sampling, the first 2 m of the shotcrete will be dismantled, followed by a further sampling campaign of 1 m cores in a radial pattern in the remaining part of the shotcrete.

Characterisation of the concrete properties and comparison with the initial properties is envisaged. Of great interest is the characterisation of ongoing chemical interactions at the interfaces with the bentonite (and potential knock-on effects on the physical properties). Compared to the partial dismantling, intact interfaces will be preserved due to the overcoring technique, allowing in situ analysis of changes across material boundaries. It is anticipated that intact cores comprising ~ 40 cm of shotcrete and at least ~ 30 cm of bentonite (at least equal to the width of 2 FEBEX-bentonite blocks) will be obtained by resin-stabilised overcoring.

The demolition operations of the remaining plug section should be performed in a controlled manner, by observing crack developments (visually or by acoustic emission sensors) and monitoring potential displacements (by laser beam) as soon as the concrete thickness decreases.

B.2.3 The buffer: bentonite blocks

B.2.3.1 Initial properties prior to experiment emplacement

The dry density specified in the design of the blocks (made of 100 % "Serrata" clay) was 1.70 g/cm^3. This density was determined taking into account the probable volume of the construction gaps and the need to have a barrier with an average dry density of 1.60 g/cm^3. For a dry density of 1.60 g/cm^3, the swelling pressure is of the order of 5 MPa. The initial water content of the blocks ranged between 12.5 and 15.5 %. The blocks were inserted manually (Fig. B-5, left).

B.2.3.2 Observation from the first dismantling

Drier blocks were observed in the inner ring (close to the heater) as well as in the centre of the non-heated zone, and more humid ones in the outer ring. Blocks partially reached the maximum swelling pressure and a relative humidity between 40 – 90 %. Mechanical integrity, completely closed gaps and displacement of the buffer towards the drift entry due to stress release were observed as expected (Fig. B-5, right). The gravimetric water content and dry density of bentonite samples taken during dismantling were determined on site and in the laboratory.

Partial dismantling provided observations of certain changes in buffer mineralogy and pore water chemistry related to the flux of water from the geosphere and redistribution of moisture within the buffer. An open issue is the existence of aerobic conditions within the buffer and its influence on corrosion and microbial processes (see below). The influence of the geosphere is characterised by the absence of very high inflow locations that might cause localised erosion or piping and the relatively high granite matrix conductivity (~ 10^{-11} m/s) has ensured that saturation is controlled by the bentonite. Similarly disturbances in the geosphere (drilling and opening of nearby boreholes) have had only very limited, if any, effect on the EBS.

Much of the buffer was saturated and significant swelling pressures developed throughout the outer part of the buffer. The low permeability of the saturated bentonite close to the rock ensures a slow saturation and inhomogeneity in rock properties have no influence on buffer saturation. Density gradients within the buffer have developed due to swelling on hydration and drying and shrinkage near the heater, characterised by an axisymmetric saturation pattern.

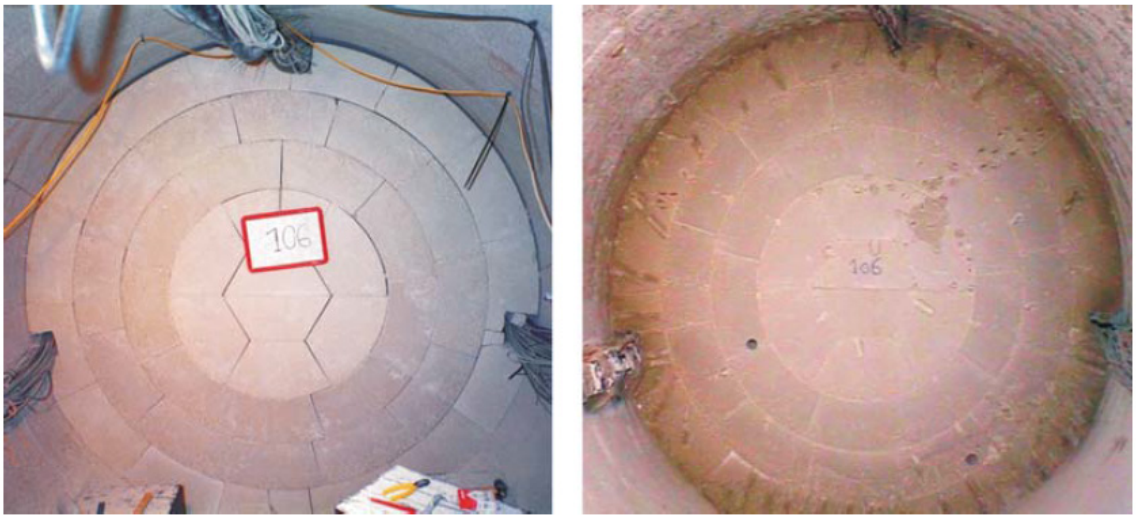


Fig. B-5: Appearance of a bentonite layer during construction (left) and after the first dismantling in 2002 (right) (ENRESA 2006a).

B.2.3.3 Expected status

Current temperatures around the heater's surface are between 112 – 136 °C and decrease radial-symmetrically in the buffer to ~ 35 °C at the bentonite/rock interface (Tab. B-1).

Tab. B-1: Temperature (in ºC) sensors in bentonite on 01.05.2014.

Average increases/decreases with regard to the last report are included in brackets (AITEMIN 2014a). Data per April 2014.

	Section G (1 m from heater)	**Section I** (heater front)	**Section S** (1 m into heater zone)	**Section F2** (middle of heater)	**Section D2** (heater rear end)	**Section B2** (gallery end)
Outer ring	30 – 34 (0)	37 – 39 (0)	--	--	36 – 37 (0)	22 (0)
Intermediate ring	34 – 39 (0)	53 – 63 (+ 0.5)	71 (1)	75 (0)	53 – 55 (0)	22 (0)
Inner ring	37 – 42 (0)	83 – 87 (0)	92 (0)	93 – 99 (- 0.5)	81 – 86 (- 1.5)	22 (0)

The hydration of the bentonite barrier continued, probably reaching full saturation in the outer and intermediate bentonite rings. Pore pressures (Tab. B-2) indicate suction close to the heater while the total pressures (Tab. B-3) have been increasing since the partial dismantling, exceeding the maximum expected swelling pressure and reaching up to 6 MPa at some points of the barrier. The highest pressure at any location (at the rock surface) was measured to be 6.36 MPa. The Time Domain Reflectometers (TDRs) close to the heater show an accelerated increase in water content during the last years (Fig. B-6, data up to March 2013). bentonite block displacements (in the centre near the heater) range between 2 mm to 4 mm with no long-term monitoring due to failure of sensors (AITEMIN 2014b).

Tab. B-2: Pore pressure (in MPa) in the buffer till 01.05.2014.

Average increases/decreases with regard to the last report are included in brackets (AITEMIN 2014a).

	Section H (0.5 m from heater)	**Section F2** (middle of heater)	**Section E2** (1 m from middle of heater)
Outer ring	0.16 – 0.23 (+ 0.01)	0.24 (+ 0.02)	0.18 – 0.39 (+ 0.05)
Intermediate ring	0.08 – 0.16 (- 0.01)	-0.06 – 0.00 (- 0.01)	- 0.03 – 0.05 (0)
Inner ring	0.03 – 0.05 (0)	--	--

Tab. B-3: Total pressure (in MPa) in the buffer till 01.05.2014.

Average increases/decreases with regard to the last report are included in brackets.

	Section E1 (contact rock – plug)	**Section P** (contact plug – bentonite)	**Section G** (1 m from heater zone)	**Section I** (heater front)	**Section F2** (middle of heater)	**Section E2** (1 m from heater rear end)	**Section B2** (gallery end)
Radial direction	Rock surface 0.42 – 0.97 (+ 0.02)	--	--	--	Rock surface 6.67 (+ 0.08)	Rock surface > 5	--
	--			--	Intermediate ring --	--	
	--			Inner ring 0 (0)	--		
Tangential direction	--	--	--	Intermediate ring 2.23 (- 0.16)	Intermediate ring 1.97 (+ 0.13)	--	--
				--	--		
Axial direction	--	Intermediate ring 5.71 – 6.23 (+ 0.02)	--	--	--	--	Intermediate ring 5.8 (+ 0.1)
		--	Centre of section 5.62 (+ 0.04)				--

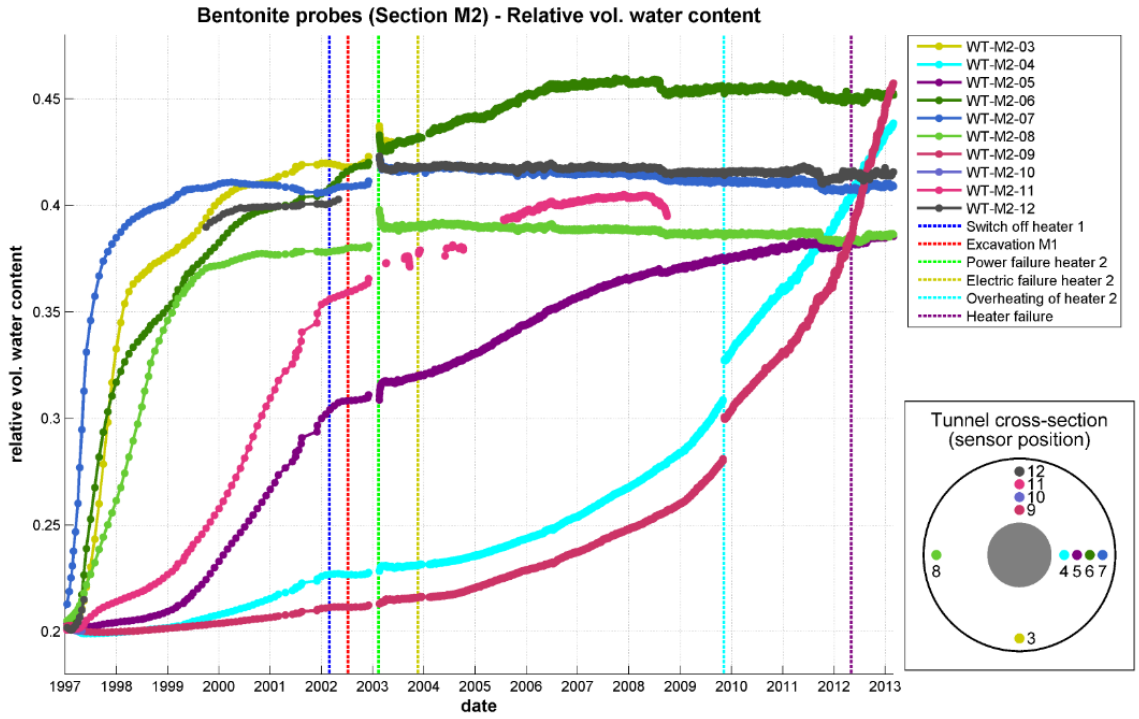


Fig. B-6: Evolution of the volumetric water content measured by the Time Domain Reflectometers (TDR) showing the accelerated resaturation rate measured by the sensors close to the heater (Sakaki et al., in prep., NAB 16-21).

The directly measured progress in saturation since the first excavation will allow verification of not only the monitoring results, but also of the modelled saturation pattern after the cooling-down phase. The post-mortem bentonite sampling program envisages taking buffer samples to characterise the solid and liquid phases, in order to confirm predictions and validate existing models of THM and THC processes. Samples will be taken from different parts of the buffer in order to:

- Analyse the physical, physico-chemical, mineralogical, chemical and textural changes that occurred in the clay by heating and hydration, taking also into account the effect of joints and interfaces (concrete, granite, metal components, corrosion products), and in relation to organic compounds. Mainly, the water contents and densities will be determined.
- Analyse the chemical evolution of the bentonite pore water as a function of:
  1. The hydration and temperature profiles
  2. The interaction with alkaline waters from the concrete plug
  3. The interaction with sensors, heater, organic compounds and corrosion products
- Study the flow paths of the different types of chemical tracers that were placed in the clay and the clay/rock contact during the installation phase
- Validate and check the capacity of the numerical codes (THM and THC) being developed to predict the bentonite behaviour in an engineered barrier, and the modifications experienced by the bentonite in a direct and representative way

The sampling will take place in vertical sections normal to the axis of the tunnel, and in each section several samples will be taken along different radii. To ensure redundancy, more samples than needed will be taken. A detailed sampling and dismantling plan will provide the guidelines for sampling (AITEMIN 2014a).

B.2.4 Instrumentation, corrosion of the sensors, coupons and tracers

B.2.4.1 Initial status as emplaced

A total of 670 sensors were installed in the bentonite barrier and had the requirement to withstand temperatures of up to 100 ºC, pressure of up to 5 MPa, and high corrosion rates. To analyse corrosion behaviour under close to actual repository conditions, specimens of different metallic materials were placed in the clay barrier. The specimens are of various types of steel (both carbon and stainless), titanium, and copper, as well as welds of the same materials. The specimens were located at points within the bentonite situated very close to the heaters.

Numerous chemical tracers have been installed in the test. The tracers selected are of both the conservative and non-conservative type. The tracers impregnated in filter paper have been installed in a uniform manner along certain surfaces of the bentonite barrier/rock interface, generally in zones of water entry, and are stapled to the bentonite blocks of the exterior crown of the barrier, whereas those in sintered metal, compacted bentonite blocks, or glass ampoules are located in pre-drilled holes in pre-determined blocks of bentonite (ENRESA 1998d).

B.2.4.2 Observation from the partial dismantling

During the partial dismantling 188 sensors were extracted and additional 52 sensors were installed in the buffer front after the first excavation (ENRESA 2003). The sensors and their cables were found to be in good contact with the bentonite and those close to the rock walls were highly pressed towards the rock. Some of them were found to be damaged due to the high pressure. No noticeable changes in sensor positions were found. Some of the sensors in the bentonite were found to be severely corroded, especially at the front end of Heater #1 (ENRESA 2006a).

Mechanical deformation of the probes and cable defects could be observed during the excavation phase. Calibration measurements in air and water were performed after excavation and compared to the calibration measurements before installation. In air no change of the TDR signal could be detected, but in water approx. a 10 % longer travel time was observed. bentonite probes in the vicinity of TDRs were analysed for water content and density for calibration.

A corrosion study (Aitemin & Inasmet 2003) of the extracted components showed the following:

- **Sensors**

  The high humidity, together with the presence of sulphate-reducing bacteria in the bentonite housing the sensors are the reasons behind the significant corrosion observed in these components. The sulphur rich corrosion products, as well as the morphology of the corrosion indicate localised corrosion phenomena induced by sulphate-reducing bacteria.

  Stress corrosion induced by the presence of chlorides and/or products resulting from the metabolic activity of the sulphate-reducing bacteria resulted in cracking.

With the carbon steel components, the corrosion observed was of the generalised type, with the almost complete destruction of the component being observed on occasions.

- **Corrosion coupons**

  Very little general only local corrosion was observed on the stainless steel and titanium specimens.

  The carbon steel coupons showed very slight generalised corrosion, with corrosion rate values of 0.10 µm/year. No localised corrosion phenomena were detected.

  The copper coupons showed corrosion rates of 0.71 µm/year for the Cu-ETP, and 0.74 µm/year for the Cu10Ni alloy. The corrosion suffered by the Cu30Ni alloy was negligible.

- **Tracers**

  Iodide was placed in filter papers at the outer part of the barrier, in contact with the granite, in the lamprophyre area, which was covered over a length of 3 meters with 120 iodide-doped papers on the lower right-hand part of the barrier. Laboratory tests showed that iodide concentration reflected the water front movement, with a sharp increase towards the middle part of the barrier.

B.2.4.3 Expected status

The status in May 2014 is shown in Fig. B-7.

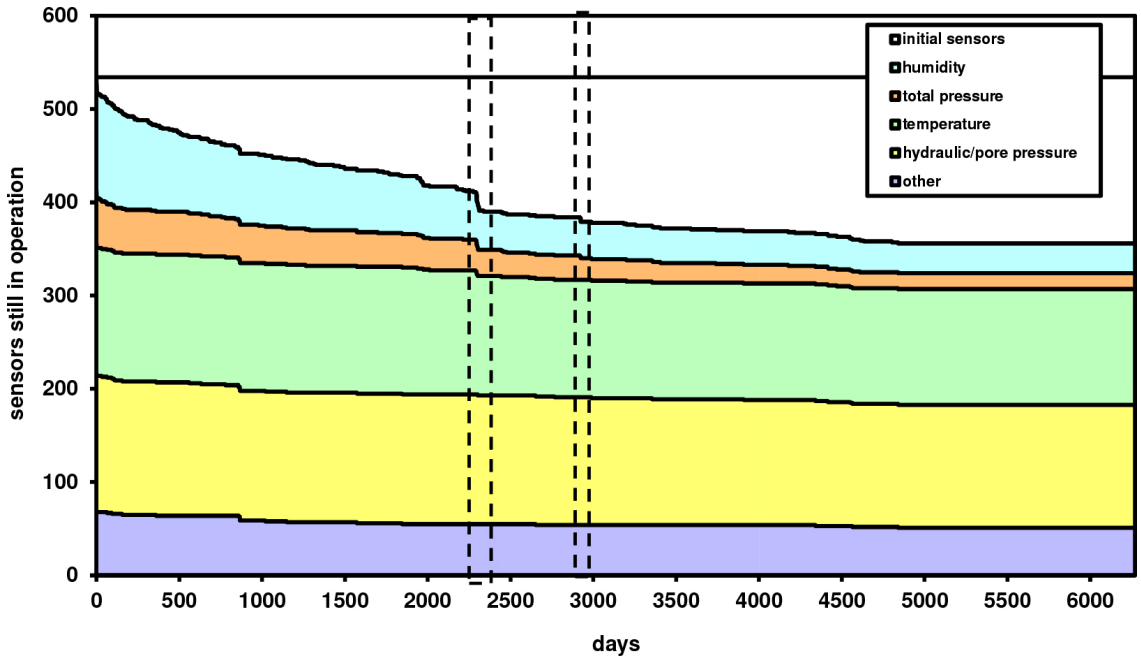


Fig. B-7: Sensor status 01.05.2014 (Aitemin 2014b).

The expected position of the coupons, instruments/cabling will be verified accurately before any demolition or sampling operation of each instrumented section. Damaged sensors might be due to corrosion, fractures or mechanical damage, flooded filters, cable damage, etc. Visual inspection, careful handling, signal and cable checking, recalibration will follow a dedicated procedure for data interpretation since most sensors were emplaced in 1996 and did not anticipate 18 years of operation.

As 13 years have passed since the last excavation it is expected that corrosion has further progressed and that the information related to the ongoing corrosion processes will be of high value. This is because of a potentially higher degree of reaction products, which will allow a better characterisation and identification of the mineral phases that have formed. The experience obtained during the partial dismantling concerning the tracers will improve the sampling and analysis techniques to be applied for the final dismantling. The sampling will provide for example information concerning the water front movement at different zones where filter papers with iodide were placed (a fractured area and a lamprophyre area), which can be compared with the water content of the bentonite buffer.

B.2.4.4 A special note on corrosion and microbiology

Evidence of significant corrosion and microbial activity after 5 years of heating and obtained during the partial dismantling is limited to one instrument section where conditions may have been aerobic and humidity influenced by the instrumentation. No macroscopic mineralogical changes and near-constant global chemistry suggested restricted activities (ENRESA 2006a). However, the degree of humidity and the presence of sulphate-reducing bacteria or chlorides and/or products are suggestive of conditions enhancing controlled (stress) corrosion processes.

From the Experimental Phase 1 prior to the partial dismantling, it can be asserted that oxygen levels decreased rapidly after the closure of the experiment. However, a measureable concentration of O_2 was observed. While the low measured concentrations can indicate the presence of O_2 in the experiment, they can also be the consequence of a small air contamination of the samples upon sampling or sample handling, and are therefore not considered conclusive. Furthermore, although the pore water is reducing (predominance of Fe^{2+} in the total iron), an increase of oxidized species is observed in the solid phase as compared to a reference sample of FEBEX bentonite. The combined study of the corrosion of metallic components and of the microbiological activity in the bentonite showed a strong influence, respectively presence, of SRB (anaerobic) in the parts of the experiment where substantial corrosion had been observed. However, in the same samples, aerobic microorganisms were also detected, in similar or even greater counts.

The gas analyses performed during the Experimental Phase 2 (2002 – 2014) revealed similar, low O_2 concentrations, even before the emplacement of the gas-tight membrane. However, the variability of the data during Phase 2 is even greater then observed in Phase 1 (Giroud 2014). This is likely attributable to air contamination before, during, or after sampling. Considering this information, special care has been taken to make the plug water- and gas-tight during Phase 2. However, the low concentrations of oxygen in the gas phase, together with the presence of anaerobic bacteria in some parts of the bentonite and a predominance of Fe^{2+} in the total iron of the pore water suggests that the FEBEX experiment tends towards an anoxic, reducing environment. Likely, there are heterogeneities in the redox state due to possible O_2 inflow through the plug, along the sensor cables and pipes, or possibly the EDZ. The difficulty in assessing the redox conditions in general is due to the very high sensitivity of the redox potential to atmospheric contamination.

It is expected that results from the final excavation in 2015, after 18 years of heating, saturation and chemical impacts, will provide more evidence regarding the corrosion and the chemical processes affecting the EBS. Before starting the dismantling, gas and water samples have been collected from the existing sampling tubes, and the gas pore pressure measured. Keeping anoxic conditions during air drilling (overcoring) is not currently within the scope of this project. However, the contamination of the solid samples by O_2 can be limited if the samples are packed under vacuum or in an inert gas phase immediately after sampling. The preservation of the in-situ redox conditions is critical for the study of corrosion products. Therefore, when possible, the bentonite blocks hosting the corrosion coupons should be extracted in one piece as much as possible and packed as described above. Nevertheless, the fact that the experiment was not designed to be gas-tight might reveal corrosion and microbial processes that are not representative for those expected in a repository after closure.

B.2.5 Heater and liner

B.2.5.1 Initial status as emplaced

The remaining heater (#2) within the steel liner has external dimensions of 4.54 m length, a diameter of 0.90 m, and a weight of almost 11 t. The material is carbon steel with thickness of 100 mm. A continuous steel liner was emplaced in the same drift (Fig. B-8). This steel liner consists of a perforated steel tube measuring 15 mm in thickness, providing the space into which the heater is inserted (Fig. B-8). The steel liner required for the test has a length of 10 m, corresponding to the length of the two heaters plus the 1 m separation between them. The material of the steel liner is conventional alloyed steel for boilers and pressure vessels. The inner diameter of the liner is 940 mm; thus a difference of 40 mm with respect to the outer diameter of the heaters to allow correct insertion of the heaters.

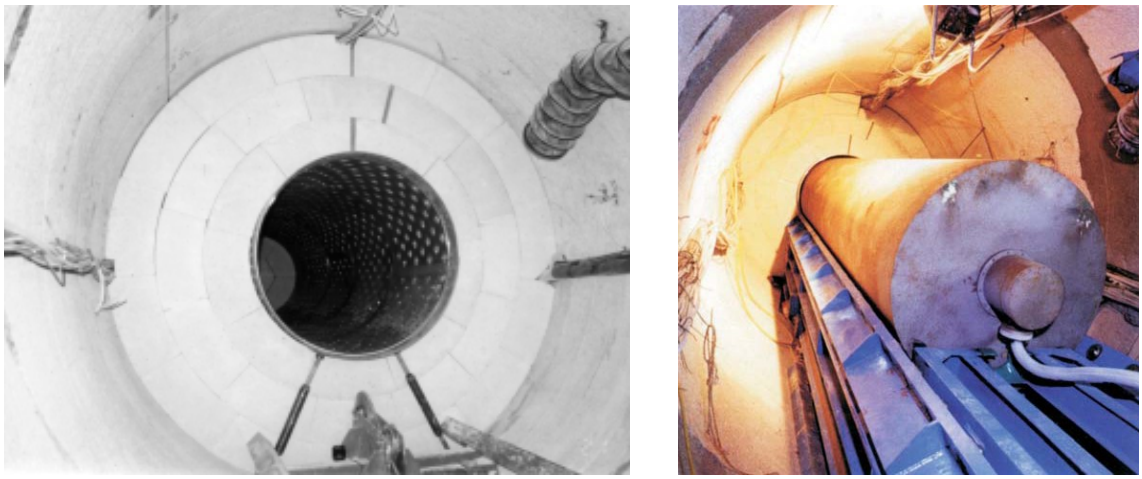


Fig. B-8: Liner (left) and heater (right) as installed in 1996 (ENRESA 2003).

B.2.5.2 Observations from the first excavation

The first heater extraction posed no problems and was performed smoothly. A corrosion study (Aitemin 2003) of the extracted components showed the following outcomes (see also Section B.2.4.4.):

- **Heater**

  It shows slight uniform general corrosion over its whole surface, with oxide layers less than 20 microns thick in all the cases examined.

  No localised corrosion phenomena were observed.

- **Liner**

  The nature of corrosion detected on the liner was non-uniform, with maximum values of penetration of the corrosion of approximately 130 microns on the external surface and 200 microns on the internal surface.

  No localised corrosion phenomena were observed.

B.2.5.3 Expected status

Displacement readings of the canister indicate movements in the range of -15 mm to 7 mm, however, due to sensor failure these measurements do not conclude the final dismantling state (AITEMIN 2014a). As the humidity in the inner part of the buffer is low, limited corrosion is expected for all steel components. Extraction will be done with the corresponding transport element (ad-hoc extraction car for heater, light low wagon for liner sections and extraction table for dummy) and samples of each component will be analysed in various laboratories. In case the extraction of the heater is not possible due to excessive deformations of the liner, sampling around the heater liner should be considered in a first stage. This operation will permit the release of stress and, consequently, permit extraction of the heater in a second stage. It is anticipated that due to the low humidity, a direct contact of heater and bentonite (pushed through the perforated liner) does not exist, unless bentonite has fallen onto the heater as observed during the partial dismantling. Therefore, the better preserved liner/bentonite interface will be the target for interface analysis and current studies target obtaining intact interfaces.

B.3 Modelling

THM modelling within FEBEX has demonstrated its capability with regard to the prediction of the evolution of such large-scale systems based on laboratory characterisation of the buffer. The very good prediction from CODE_BRIGHT analyses of the dismantling data after five years of heating is important evidence concerning the predictive capabilities of coupled THM analyses, at least in the short term.

The availability of a final dataset from the In-Situ Test, together with data from supporting laboratory programs provides an opportunity to make a synthesis regarding the capability of the "standard THM model" and its developments. The large-scale test dataset will also continue to be of great value in providing an opportunity to benchmark new THM approaches.

B.4 Concluding Remarks

The sampling and dismantling will be guided by an overarching plan currently being finalised (AITEMIN 2014a). The THM and THC analysis program will then follow through a baseline program led by CIEMAT (CIEMAT 2014) and is complemented by various in-kind contributions of the individual partners Additionally, a review of key FEBEX-bentonite (and partially MX80) THM/THC parameters obtained by the participating laboratories prior to the final dismantling will provide a baseline for inter-laboratory comparison of the data for the integration of the final results of FEBEX-DP.

Appendix C: FEBEX-DP – Objectives and strategy of the COMIC Group

C.1 Introduction

bentonite clay buffer and the metal canister with high level radioactive waste are part of the so-called engineered barrier system (EBS). The various elements forming this system are susceptible to deterioration processes. Microbial activity could impact the deterioration rate of each of these barrier elements and thus impact the safety by compromising a repository's isolation and containment functions

The presence of microbes may affect a radioactive waste repository environment in various ways. Biological processes include many reactions that are very slow or do not occur in sterile lifeless chemical systems such as sulphate reduction to sulphide (Goldstein & Aizenshtat 1994, Cross et al. 2004). This is because life has the ability to over-run activation energy barriers and other energetic circumstances that block many spontaneous chemical reactions. Life is possible from -20 °C up to above 113 °C (Burgess et al. 2008, Madigan et al. 2012). Life is also possible within a large pH range, from pH 1 up to at least pH 12 (Yumoto 2007, Pedersen et al. 2004). Furthermore, the phylum Deinococcus-Thermus contains species that can survive doses of radioactivity many times greater than the lethal dose for humans. *Deinococcus radiodurans*, a major species in this group, has the ability to reassemble its chromosome after being shattered by high levels of radiation (e.g. Madigan et al. 2012). However, when it comes to dependencies of microbial survival and activity on swelling pressure in clay barriers few studies have been done and the upper limits for survival and activity have not yet been established. Assessing the impact of microbial activity on EBS is fairly recent and the role of microbiology under repository-relevant conditions needs better framing.

Within the FEBEX-DP project, which consists of the dismantling of the FEBEX in-situ experiment at the Grimsel Test Site (GTS), a strong focus is set on the investigation of corrosion and microbiological activity. A dedicated group to COrrosion and MICrobiology (COMIC) ensures the coordination of the activities related to these particular topics under the leadership of SKB, in collaboration with Nagra and will involve various partners and laboratories (see Section C.6.

This document presents the objectives of the COMIC activities and how they will be addressed.

C.2 Objectives

The main goals of the COMIC group are summarised below:

- Confirm the prediction of long-term performance of radioactive waste canisters under deep-geological repository conditions by quantifying and characterizing the corrosion of the various metals present in the FEBEX experiment
- Understand the processes behind canister corrosion induced by microbes in situ
- Contribute to the characterisation of the impact of microbial activity on the long-term properties of the bentonite barrier, seals and plug systems in geological disposal concepts
- Gain systematic information on the effectiveness of the bentonite buffer to inhibit microbial activity by studying parameters such as density, pH, temperature, water saturation, and gas concentrations

- Provide additional, and if possible statistically meaningful, data to improve the calibration of numerical THM models, in order to improve the prediction capabilities of the long-term performance of a geological repository for spent nuclear fuel waste

C.3 Metal corrosion and microbial processes

C.3.1 Corrosion

High-level radioactive waste, mostly spent fuel and waste from reprocessed fuel will be encapsulated in iron or copper canisters. These canisters will in many cases be surrounded by an engineered barrier consisting of swelling clay in the host rock. The metal and the clay barriers are commonly denoted engineered barrier systems (EBS) and are susceptible to deterioration processes. The most challenging degradation processes are

a) Metal corrosion

b) Illitization of smectite and nontronite

c) Degradation of concrete

Corrosion will eventually cause the canister to breach, leading to radionuclide release. Illitization will compromise the clay buffer's swelling properties by reducing its barrier function, as a result of microbial dissolution of Fe(III) in the smectite structure either by reduction (Kim et al. 2004) or by complexation with microbial ligands (Perdrial et al. 2009). Concrete degradation may prematurely destabilize plugs and seal system.

Microbial activity could impact the rate of each of these deterioration processes and thus impact the safety case by compromising a repository's isolation and containment functions.

Steel canisters will corrode under anaerobic, wet conditions, generating H_2. Whether such processes are relevant for H_2 generation from copper too, is still under investigation at present (e.g. Bengtsson et al. 2013). Many microorganisms efficiently use H_2 as electron donor, among others for sulphide and acetate production. Some sulphate-reducing bacteria (SRB) are capable of electrical microbially influenced corrosion (EMIC) (Enning and Garrelfs 2014). Such EMIC have been reported to corrode steel at a rate of 900 μm per year or more (Enning and Garrelfs 2014). Microbial scavenging for H_2 or electrons directly from the metals is believed to accelerate anaerobic corrosion of iron and copper as was demonstrated during the MINICAN experiments at Äspö HRL (Smart et al. 2014). In addition, copper is sensitive for acetate, nitrite and ammonium which may generate stress corrosion cracking. In FEBEX extensive corrosion of the heater and the carbon steel liner around it is not expected as the conditions closest to the heater is likely to be too warm and too dry to favour microbial activity and/or chemical corrosion.

ISSUE/OBJECTIVE: What is the evolution of the corrosion on the various metals since the first dismantling, with additional time and increased saturation of the buffer?

To what extent are microorganisms that may accelerate corrosion of canisters in the near-field either by hydrogen/electron scavenging or by production of sulphide and/or gas present in the FEBEX bentonite buffer?

C.3.2 Microbial activity in bentonite buffers

The current state of knowledge regarding MX-80 is that microbial activity ceases when the wet density approaches 2.0 Mg/m^3 as a result of high swelling pressure and reduction in porosity (Pedersen 2010). Because swelling pressure increases exponentially with density, this inhibiting effect is quickly decreasing when the density decreases. Microbial activity is high at 1.75 Mg/m^3 if all other growth promoting variables are favourable. There are many different commercial bentonites that may give a different (higher or lower) mitigating effect at similar density.

Another important variable is water activity. Stroes-Gascoyne et al. (2013) noted that all samples analysed for microbes from the engineered buffer system had water activities > 0.96. Similar results were observed for both FEBEX and MX-80. Pore water in MX-80 can contain 0.1 M sulphate and there is often significant amounts of organic material in bentonites. However, the FEBEX bentonite contains about 7 times less sulphate compared to MX-80 and most of the carbon content is inorganic for both clays (Svensson et al. 2011). In addition, most commercial bentonites have been found to contain large numbers of cultivable microorganisms including iron-reducing and sulphide-producing bacteria (SPB) (Tab. C-1). The FEBEX clay contains both iron-reducing bacteria (IRB), SRB, autotrophic acetogens and to a larger extent culturable heterotrophic aerobic bacteria (Svensson et al. 2011, Stroes-Gascoyne et al. 2013).

ISSUES: How does the swelling pressure and water content affect the microbial activity in bentonite? How do the microbial activity and diversity vary in a cross section of the bentonite from the wetter parts closest to the rock wall inward toward the heated canister?

Tab. C-1: Quantitative analyses of culturable heterotrophic aerobic bacteria (CHAB), SRB (SRB), autotrophic acetogens (AA) and iron-reducing bacteria (IRB) in the eleven ABM materials (from Svensson et al. 2011).

Material	**CHAB[a] g^{-1}**	**MPN SRB[b] g^{-1}**	**MPN AA[b] g^{-1}**	**MPN IRB[b] g^{-1}**
Asha 505	84'400 ± 109'000	91 (38 – 409)	< 10	67 (13 – 170)
Calcigel	420 ± 490	56 (21 – 152)	< 9	110 (43 – 410)
Callovo Oxfordian	230 ± 400	< 10	< 11	114 (45 – 425)
Deponit CA-N	1'000 ± 570	9 (4 – 44)	< 10	77 (32 – 207)
FEBEX	68'600 ± 26'000	10 (5 – 50)	19 (5 – 79)	120 (47 – 448)
Friedland	1'750 ± 880	68 (26 – 198)	35 (13 – 106)	6'900 (2'590 – 22'800)
Ibeco Seal M-90	5'830 ± 4'860	61 (23 – 178)	63 (24 – 183)	7'920 (2'970 – 26'200)
Ikosorb	4'500 ± 4'590	< 10	< 10	117 (46 – 439)
Kunigel V1	0 ± 0	< 10	< 11	10 (5 – 56)
MX-80	6'600 ± 1'620	< 10	9 (5 – 46)	263 (105 – 895)
Rokle	200 ± 340	9 (5 – 46)	< 10	110 (45 – 280)

[a] ± Standard deviation
[b] Lower and upper 95 % confidence interval

Because of the risk of loss of density and swelling capacity due to buffer erosion and illitization, and the fact that some repository concepts use pellets which have lower emplacement density, a key issue is to document the lower density limit for microbial activity in bentonite buffer and host clays.

IRB have been shown to reduce ferric iron in nontronite to ferrous iron, thereby affecting the swelling properties of such clays (Kim et al. 2004). The presence of a similar process for smectite, i.e. microbial mineralogical alterations, is not well investigated. Attack of IRB on the ferric iron bearing minerals of bentonite buffers may reduce the swelling capacity of the clay, which would favour even further microbial activity inside the buffer. Another consequence of the reduced swelling capacity is to facilitate the diffusion of sulphide species towards the canister, enhancing corrosion.

ISSUES/OBJECTIVES: Are microorganisms able to accelerate degradation of bentonite based buffers? What microbes are active? How do the microbial activity and speciation vary with temperature and humidity in the buffer (i.e. from heater to rock wall)?

Many bacteria able to respire oxygen also have the ability to excrete compounds not favourable for a repository for high-level radioactive waste; examples of such compounds are organic acids and bioligands (chelators) that can mobilise radionuclides (e.g. Johnsson et al. 2009, Kalinowski et al. 2006).

ISSUE: To what extent do bioligands contribute to the mobilisation of radionuclides at repository-like conditions?

C.4 Samples' selection and sampling procedures

C.4.1 Information gained from the partial dismantling

Corrosion was investigated on the corrosion coupons excavated during the first dismantling, as well as on the heater, liner, and selected sensor housings (AITEMIN-INASMET 2003). A similar sampling and analytical plan will be performed during the final dismantling.

Very limited characterisation of microbial populations was performed during sampling of the FEBEX-bentonite in the previous excavation (ENRESA 2006a; Lanyon & Gaus 2013). Microbial-influenced corrosion associated with SRB was identified in one section around Heater 1 where the sensor configuration may have favoured humidity transport. The interpretation of the microbiological data was also limited by the suboptimal constraint of the experiment's redox conditions. Consequently, a strong focus is set during final dismantling on the characterisation of the redox conditions in the bentonite buffer and on the active microbiological population.

C.4.2 Selection of samples

Additional data from sections around Heater 2 after 18 years of saturation and heating would be valuable in evaluating the distribution of microbes and the importance of the potential preferential flow paths of the pipes and instrument cables. Various types of samples will be extracted from the FEBEX in-situ experiment as base material for the various interests of the COMIC group. The large categories are:

- Gas and water samples from the bentonite pore space
- Corrosion coupons
- Other metal components present in the experiment
- Interfaces between the bentonite and various materials (concrete, metal, rock)
- bentonite

C.4.3 Gas and water sampling prior to full dismantling

Gas and water compositions in the bentonite buffer have been monitored during the entire lifetime of the experiment. A last sampling campaign will take place just before the beginning of the dismantling activities. Sampling is performed by CIEMAT, and the samples are analysed for gases, water chemistry, and redox potential (Giroud 2014). Potentially, microbial activity may also be assessed by non-volatile organic carbon measurement.

As H_2 is consumed rapidly by e.g. SRB, low or non-detectable amounts of hydrogen are expected. The same applies for acetate. Little or no microbial activity is expected close to the heater as it is likely to be too warm and dry for them there. Low levels of nitrate are also expected as the nitrate-reducing bacteria are often found all over in a subsurface environment.

C.4.4 Sampling during dismantling

A description of the exact position of the samples is given in the Full Dismantling and Sampling Plan established by AITEMIN (2014a).

C.4.5 Corrosion

The analysis of the effects of corrosion and the corrosion products on the various metallic parts present in the experiment will be carried out by TECNALIA. An extensive description of the samples to be taken is given in the Full Dismantling Plan by AITEMIN (2014a):

- The heater consists of a carbon steel cylinder with welded lids having the following dimensions: 4.54 × 0.9 m. The thickness of the walls is 1000 mm. It is estimated to study a section taken from one of the vertical ends, consisting of the lid with its welded joints, and a 300 mm section of the cylindrical part.
- The liner consists of a perforated steel tube. It is planned to sample and analyse corrosion of a 1m long segment of the liner
- The corrosion coupons consist of carbon steel, AlSl 316 stainless steel, titanium alloys grade 2,7 and 12, copper ETP, cupro-nickel alloys 70/30 and 90/10 respectively. It is initially estimated to analyse at least 3 coupons for each alloy (2 for the corrosion rate estimation and the third one for the metallographic analysis)
- The sensors are contained in austenitic alloy housing in order to protect them from the surrounding conditions. The intension is to study corrosion on the housing of 4 sensors. Of particular interest are the extensometers, originally connecting the heater to the rock wall, which showed a distinct longitudinal corrosion gradient linked to the water content gradient in the bentonite.

The bentonite surrounding or adhered to the samples under examination will be also analysed.

C.4.6 Microbiology

The various samples will be taken in five different sections of the experiment, shown in Fig. C-1. Section 36 represents the interface between the shotcrete plug and the bentonite buffer; Sections 42, 48 and 54 represent bentonite sections around the heater; Section 60 represents a bentonite-only section behind the heater. In addition to the FEBEX-DP project focussing on corrosion and microbiology, a project proposal has been submitted to Horizon 2020 to study the impact of microbial activity on the long-term performance of engineered barriers. The total number of samples amounts to 108, with 63 and 36 samples for FEBEX-DP and MIND, respectively, as well as 9 samples for University of Manchester (Tab. C-2).

The interface between the shotcrete plug and the bentonite will be sampled as two separate samples, in two different locations of Section 36 (Fig. C-2). In the sections around the heater (42, 48 and 54), the samples for microbiology will comprise bentonite samples and the interface between the rock and the bentonite (Section 48 shown in Fig. C-3). For the latter case, it is recommended to scrape the rock surface manually with e.g. a scalpel in order to collect microbiological material. The other suggested option of overcoring the rock together with a piece of bentonite protected by resin may result in problems in removing the microbes from the resin. The resin may also be toxic to the microbes. One should keep in mind, however, that scraping is a time consuming procedure that need to be performed on site by a trained specialist. Although the collected material may not prove sufficient with this method, it can potentially provide the best results. Sampling of Section 42 will provide an insight of the amount of material that can be collected by scraping, and allow adapting the sampling procedure for the following sections.

bentonite samples for microbiology will cover cross sections from the clay that is in contact with the rock wall toward the canister, i.e. from the outermost, water saturated parts inward toward the canister where conditions are warmer and drier in order to be able to study gradient effects (Fig. C-3). Microbial sample plugs with clay should be wrapped in Al-bags with N_2 or Ar in order to remain anaerobic until arrival at the laboratory.

As many microbes prefer growing attached to surfaces, attempts to sample biofilms should also be done from canister, liner, and coupons. In order to be able to study both corrosion products and biofilms only part of the coupons should be scraped as the surface might be scratched. If possible attempts to extract microbes from clay particles should be done. Such sampling was done successfully during the dismantling of the Prototype repository at Äspö HRL (Arlinger et al. 2013).

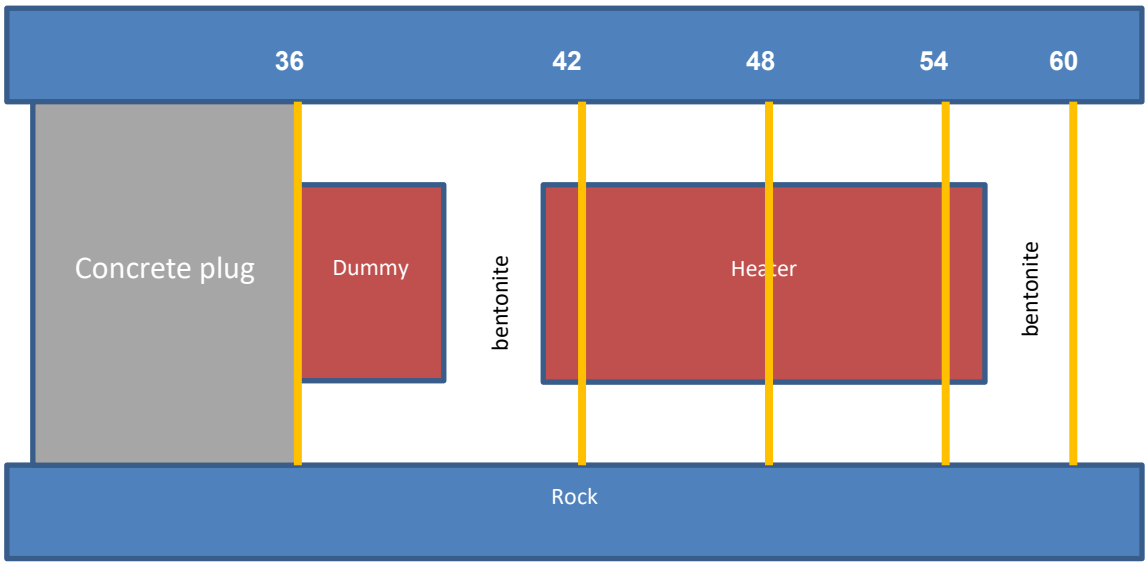


Fig. C-1: Schematic view of the five sampling sections (white numbers) distributed longitudinally along the experiment.

The number of samples in each section is shown in Tab. C-2.

Tab. C-2: Number of samples planned for corrosion and microbiology.

FEBEX-DP refers to this project and MIND refers to samples stored for the Horizon 2020 MIND project.

Section	**Type of sample**	**FEBEX-DP**	**MIND**	**University Manchester**	**Total**
36	Shotcrete-bentonite interface	1			1
42	bentonite	9	12		21
42	bentonite-rock interface	2			2
48	bentonite	9	12	9	30
48	bentonite-rock interface	2			2
54	bentonite	9	12		21
54	bentonite-rock interface	2	12		2
60	bentonite	13			13
60	bentonite-rock interface	2			2
Various	Metal-bentonite (corrosion+microbiology)	14			14
Total		63	48	9	120

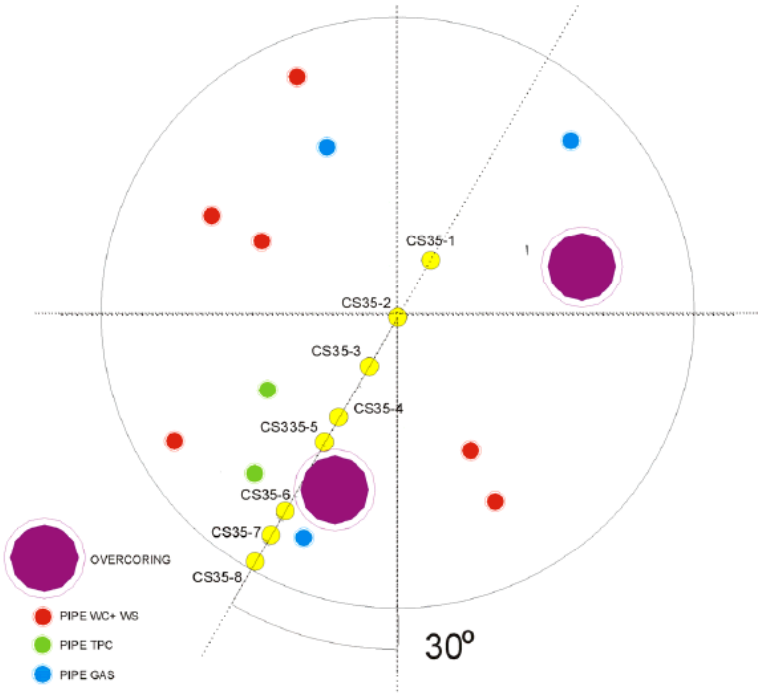


Fig. C-2: Location of the microbiology samples (BC/CS36-1 and -2) on Section 36, at the interface between the shotcrete plug and the bentonite buffer (source: AITEMIN 2014a).

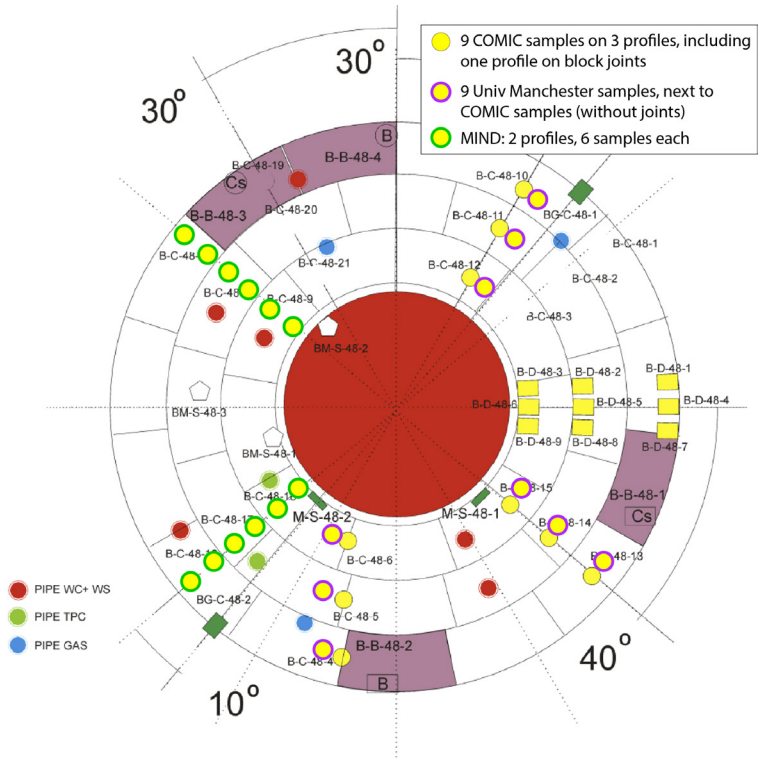


Fig. C-3: Cross-section of the samples to be taken in Section 48 (modified from: AITEMIN 2014a).

The analytical programme of the FEBEX-DP project also comprises chemical analyses of the bentonite through leaching. The leachate will be analysed by titration and ion chromatography in order to determine the concentration of Cl^-, Na^+, SO_4^{2-}, S^{2-} and HCO_3^-. The pH and the conductivity of the bentonite will be also measured. Total carbon and organic carbon (TOC/DOC), as well as iron content and degree of reduction should also be analysed. The ratio of ferrous and ferric iron can be determined using titration and or Mössbauer spectroscopy on the solid material.

C.4.7 Final report

The final report will collect all the results and conclusions of the corrosion study performed on the FEBEX-DP components.

C.5 Analytical techniques

C.5.1 Task 1: Corrosion analyses (Tecnalia 2014)

Test pieces will be cut and examined

The extent and morphology of the corrosion suffered by the components will be evaluated. Cuts to be done on the components for later analysis will be decided on.

Initially, it is estimated to cut the heater lid, its welded joint and a section of the body some 300 mm long. However, the possibility to cut another slice is not excluded in case a significant corrosion in other sections of the heater is observed.

Cutting of small pieces, second cutting of heater, liner, coupons and sensors will be carried out.

Metallographic study

Metallographic sections from tested components will be prepared by embedding them in resin and polishing. These metallographic probes will be further studied by optical microscopy and SEM (scanning electron microscopy) in order to study the morphology and extension of the corrosion damage.

It is estimated that around 30 metallographic probes will be prepared.

Estimation of the corrosion rate of corrosion coupons

The average generalised corrosion rate of corrosion coupons will be calculated according to ASTM G1 standard. Where possible, at least 3 coupons should be supplied for each (base) alloy: two for corrosion rate evaluation and the third one for metallographic examination.

Chemical characterisation of the corrosion products and deposits

Semi-quantitative analyses will be conducted with Energy Dispersive X-ray Spectroscopy (EDX). The stoichiometric characterisation of these corrosion products will be carried out by RAMAN and /or XRD (X Ray Diffraction) spectroscopies.

C.5.2 Task 2: bentonite analyses

Analysis of bentonite, while relevant for the interpretation of microbiological and corrosion data, is not directly a task of the COMIC group. The main techniques put forward are visual inspection, optical and scanning electron microscopy, XRD, μ-Raman and Mössbauer-spectroscopy. A complete programme is presented in CIEMAT (2014).

C.5.3 Task 3: Microbiology analyses

Most Probable Number (MPN) analyses: IRB (reduces ferric iron to ferrous, which destroys the swelling properties of the buffer) SRB (produces corrosive sulphide). Nitrate reducing bacteria produce nitrite and possibly other compounds that could cause stress corrosion on the Cu). MPN is the preferred method for microbes in clay. Polymerase Chain Reaction (PCR), cloning, possibly Fish or Card-Fish will be used, if possible as the amount of DNA might be too small for these methods.

ATP-measurements to determine the number of active microorganisms and TNC (total number of cells) will also be determined. TNC will be determined using acridine orange or SYBRgold direct count.

MPN of culturable heterotrophic aerobic bacteria (respire oxygen and produce organic acids and chelators) may be added to the original tender from Microbial Analytics Sweden AB as their activity in the buffer will have an impact on the water chemistry during open repository phase and also if intrusion of oxygenated surface water would occur.

University of Manchester, additionally to quantitative culturing techniques (MPN), will also attempt to extract DNA from the bentonite samples.

C.5.4 Task 4: Chemical analyses of water and gases

The following analytical techniques are to be used for the determination of the various parameters of the bentonite pore water and gas:

- Gas composition: gas chromatography (GC) and various detectors (GC-TDR, GC-FYD)
- pH is measured when possible in an anoxic glove box.
- Cations (Na^+, K^+, Ca^{2+}, Mg^{2+}, Li^+, Sr^{2+}, Ba^{2+}): ion chromatography or ICP-AES
- Anions (Cl^-, SO_4^{2-}, NO_3^-, PO_4^{2-}, F^-, Br^-, I^-, $S_2O_3^-$, acetate, formate): ion chromatography
- Alkalinity at pH 4.3 and pH 8.2: potentiometric titration
- DOC, TOC, TIC: according to the standard method DIN EN 1484-H3
- Trace elements (Ag, Al, As, B, Cd, Co, Cr, Cu, Hg, Mo, Nb, Pb, Rb, Se, Si, Sn, Th, U, V, Zn, Zr): ICP-MS and/or ICP-AES
- Fe(II)/Fe(III): UV-Vis spectrophotometry with the ferrozine method on selected samples

C.6 Organisation

- Leaders of the COMIC group: Birgitta Kalinowski (SKB) and Niels Giroud (Nagra)
- Petra Christensten (SKB)
- Tiina Lamminmäki (Posiva)
- Corrosion analyses: Tecnalia, SKB (Johannes Johansson)
- Microbial analyses: Microbial Analytics Sweden AB
- Analyses of the buffer: CIEMAT and SKB (Daniel Svensson)
- Gas/water sampling, geochemical analyses: CIEMAT (Ana María Fernàndez-Diaz)
- Review board/ advisors: Rizlan Bernier-Latmani, (EPFL), Simca Stroes-Gascoyne (AECL)
- European Project MIND, WP2 – if granted

Appendix D: Assessing the variability of laboratory measurements on swelling clay (FEBEX)

D.1 Letter accompanying the appendix

Based on the comments provided on 27.01.2015, please find attached Revision 2 of the technical memorandum describing the results of the data collection and comparison exercise completed in support of the FEBEX decommissioning preparations. Notes on how the supplied comments were addressed will be sent as a separate email.

As discussed during the preparations for this work, this memorandum contains the results of examinations of supplied data related to the characterisation of the Spanish bentonite used in the FEBEX installation as well as the more commonly used MX80 bentonite.

Where sufficient data was obtained from the contributors to this activity, a brief evaluation of the consistency of the data and what degree of variability might be reasonably encountered in the conduct of the FEBEX materials recovered during decommissioning planned for 2015. From these evaluations, an attempt has been made to identify key factors that might lead to inconsistent measurements and how this might complicate the interpretation of the measurements made in the course of FEBEX decommissioning. Where possible, suggestions are provided that might assist in reducing possible sources of inconsistency during testing. It should be noted that one of the reviewers of draft identified some of the data provided as being average values with standard deviation value for several tests. I have reviewed this new information and revised the text accordingly, with no substantive change in conclusions arising. However, based on the lack of the individual test information regarding mineralogy from the source data, each of the submissions that were averages of non-available data were treated as individual tests when statistical evaluation was undertaken.

I also note that most of the data regarding block density actually refers to the FEBEX Mockup blocks, which were of different size and shape. Perhaps some production QC information is available that can be used to assess the as-produced variability of the blocks but none was included in materials supplied for inclusion in this memo.

It was an interesting exercise to complete this limited evaluation and although not all the parameters could be assessed, several were able to be examined and the results will assist in planning for future testing. In particular the definition of "normal" variability in values will be helpful when assessing trends that will certainly be present in the materials recovered as part of the FEBEX-DP. Let me know if any of the information contained in the attachment requires any further clarification or elaboration and I will address your concerns as quickly as possible.

Please also find attached to this email submission, a copy of the spreadsheet of revised data files generated as a result of reviewer comments. These represent a revised compilation of the information provided by the participants. There were a few minor changes to these files but they do not substantially alter the results presented in the original draft.

Best Regards

David Dixon
Senior Geoscientist

D.2 Background to the round robin exercise

As part of the preparations for the decommissioning of the FEBEX installation at Nagra's Grimsel site (**F**ull-scale **E**ngineered **B**arrier **E**xperiment – **D**ismantling **P**roject (FEBEX-DP)), an exercise to determine what variability in material characterisation parameter values for clays could be expected to be encountered as a result of analytical limitations or methodology. This involves, where possible, examination of supplied data to look for patterns that might be attributable to the testing method used. From these it may be possible to identify specific methodologies that would be subject to less variability and determine a reasonable range for the key index values for these materials. These parameters have been identified as being important for determining changes that have occurred in the FEBEX installation over its operation period. The statistical evaluations intend to identify a baseline, so as to determine if measurements made in the course of the dismantling project deviate from established statistical variability.

The study began with the identification of 12 properties (or sets of measurements) that would be measured as part of the materials testing program during dismantling and assessment of FEBEX. These parameters are listed in Tab. D-1 and data submissions from the FEBEX participants were requested. It was recognized that not all the FEBEX participants would have their own sets of material properties measurements but it was hoped that enough could be gathered to make the comparison of results from different laboratories (and sometimes using different analytical methods) possible. It was also recognized that some of the materials information on the Spanish Serrata clay used in FEBEX may be limited in terms of repetitions for many of the parameters of interest. Hence, it was decided to include the widely used and better characterized MX80 bentonite in this exercise to provide a larger body of data for some of the parameters of interest. From this it was hoped that generic material properties variation as the result of methodology could be separated from those associated with normal material variation or statistical scatter. This again will allow for clearer identification of FEBEX-DP properties changes rather than material- or method-induced variations.

As part of the first stages of collecting the characterization information there was a need to ensure that the contributors were all working from the same set of material properties definitions. The range of data to be included also needed to be clearly established as considerable data exists in the literature for boundary conditions (e.g. temperature, pore fluid composition and chemically altered) that were not relevant to establishing a properties baseline.

The basic material properties baseline definition and definitions are also provided in Tab. D-1. Also in Tab. D-1 are the linkages of these parameters to what is to be measured during FEBEX decommissioning.

The FEBEX partners were all requested to supply whatever data they might have available on the parameters in Tab. D-1. It is important to note that the scope of this study was limited to the use of information provided by the FEBEX partners and did not allow for searching literature or references for additional data. A more exhaustive search of literature might have provided a larger database for use in developing more tightly defined statistical limits for the parameters examined but was beyond the scope of this study. For the purposes of the FEBEX-DP and identification of key parameters that are particularly subject to method-induced variability, the study completed in this document provides a good baseline. It should also be noted that the references to FEBEX-DP documents provided in Tab. D-1 are provided for internal project reference purposes. The measurement of these parameters is included in the decommissioning plans and so determining the limits of their accuracy or source(s) of uncertainty is of direct importance to this project.

In Tab. D-2 a summary of the data types that were ultimately collected as well as the providers is presented along with a brief discussion of each data set. From the contributions received it was clear that three of the parameters of interest listed in Tab. D-1 (Batch information, Consolidation and Water retention/suction), did not have enough information available to allow for a meaningful evaluation of the influences of technique and inherent materials variability. The remaining 9 parameters did have sufficient information collected for at least an initial assessment to be done. The data provided is presented and a brief discussion on each set is provided in Section D-2.

Tab. D-1: Parameters initially targeted for inclusion in data collection and evaluation exercise.

Activity	Parameter	Notes and definitions
1	Batch information MX80 and FEBEX	Material source information. This includes manufacturer/supplier, year of receipt or production of material, manufacturer's batch #, transfer records between laboratories and any other information that clearly tracks the materials reported.
2	Bulk/dry density and gravimetric water content	Data should be limited to tests completed on initial, reference or as-placed FEBEX block materials only. Materials recovered from the previously completed FEBEX partial dismantling or laboratory prepared materials should not be included. • Gravimetric water content defined as mass of water/mass of water-insoluble soil minerals • Dry density defined as mass of soil minerals/volume of specimen • Bulk density defined as total mass/volume of specimen These will be done during FEBEX-DP as per Technical Report CIEMAT/DMA/2G206/1/12 and also in FEBEX-DP: Project plan – Version 15/01/14
3	Cation Exchange Capacity (CEC)	CEC values as per ENRESA2006-PT 05-1-2006 (Tab. VI, p 19) These tests are to be done during FEBEX-DP as per Technical Report CIEMAT/DMA/2G206/1/12 and also in FEBEX-DP: Project plan - Version 15/01/14
4	Exchangeable Cations (EC)	EC values as per ENRESA2006-PT 05-1-2006 (Tab. VI, p 19) These tests are to be done during FEBEX-DP as per Technical Report CIEMAT/DMA/2G206/1/12 and are also in FEBEX-DP: Project plan - Version 15/01/14
5	Hydraulic conductivity tests (k)	Data only for fresh water or compositions close to that of FEBEX site. No treated, altered or otherwise changed material information to be included. Data of type reported in ENRESA2006-PT 05-1-2006 (Section 4.4.1.4) is needed. These tests are to be done during FEBEX-DP as per Technical Report CIEMAT/DMA/2G206/1/12 and in FEBEX-DP: Project plan - Version 15/01/14
6	Mineralogical analyses	• Provide details of technique, e.g. CuKα; CoKα; ptw treated … • Information related to bulk mineralogy only. Not size fractionated specimens, chemically treated ... • Presented as % content of each mineral type as per ENRESA2006-PT 05-1-2006 (p 17, para 3) • Include amorphous mineral information also if available (see ENRESA2006-PT 05-1-2006 (p 17, Tab. I and II) These tests are to be done during FEBEX-DP as per Technical Report CIEMAT/DMA/2G206/1/12 which calls for a comprehensive mineralogical evaluation12 and included in FEBEX-DP: Project plan - Version 15/01/14.

Tab. D-1: Cont.

Activity	Parameter	Notes and definitions
7	Clay chemical composition	Technique and accuracy of results from analytical reports Data as per ENRESA2006-PT 05-1-2006 (Tab. II, p 18) These tests are to be done during FEBEX-DP as per Technical Report CIEMAT/DMA/2G206/1/12 and also in FEBEX-DP: Project plan – Version 15/01/14
8	Consolidation parameters, preconsolidation pressure; Coefficient of consolidation (Cc)	Method, specimen size and any modifications to materials Test data as per ENRESA2006-PT 05-1-2006 (Section 4.4.1.6). Both parameters are derived from same test data This type of testing is scheduled during FEBEX-DP as per Technical Report CIEMAT/DMA/2G206/1/12 and also in FEBEX-DP: Project plan – Version 15/01/14.
9	Gas permeability (K_g)	Method, specimen size, gas type, degree of saturation and any modifications to materials to be documented This data was not in ENRESA2006-PT 05-1-2006 but tests are proposed for conduct as part of FEBEX-DP as per Technical Report CIEMAT/DMA/2G206/1/12 and also in FEBEX-DP: Project plan – Version 15/01/14
10	Thermal properties	Method, water content, density … results need to be included. This parameter is needed for later analysis of FEBEX THM. Data as per ENRESA2006-PT 05-1-2006 Section 4.4.1.7 This type of testing is scheduled during FEBEX-DP as per Technical Report CIEMAT/DMA/2G206/1/12 and also in FEBEX-DP: Project plan – Version 15/01/14
11	Swelling Pressure	Data is limited to that collected using either fresh water or compositions close to that of FEBEX site No treated, altered or otherwise changed material information Data as per ENRESA2006-PT 05-1-2006 (Section 4.4.2.2). NOTE: This was not identified as a test to be done as part of testing scheduled during FEBEX-DP in CIEMAT/DMA/2G206/1/12. They are however included in FEBEX-DP: Project plan – Version 15/01/14.
12	Water retention (suction-moisture) Relative humidity - shrinkage	Suction-moisture (water-retention) curve. Data as per ENRESA2006-PT 05-1-2006 (p.20 Fig. 3) This type of testing is scheduled during FEBEX-DP as per Technical Report CIEMAT/DMA/2G206/1/12 and also in FEBEX-DP: Project plan – Version 15/01/14. Shrinkage. A measure of volume change of compacted specimen exposed to known relative humidity (suction) conditions

Tab. D-2: Summary of materials properties information evaluated.

Parameter #	Description	Notes	Organizations providing data*
2	FEBEX Bulk & Dry Density	Substantial data provided and assessed	CIEMAT
3	Cation Exchange Capacity	Substantial data provided and assessed	CT, BT, BGR, CIEMAT
4	Exchangeable Cation composition	Substantial data provided and assessed	CT, BT, BGR, CIEMAT
5	Hydraulic conductivity tests (k)	Substantial data provided and assessed	BT, CT, CIEMAT
6	Mineralogical analyses	Substantial data provided and assessed	CT, BT, BGR, CIEMAT
7	Clay chemical composition	Substantial data provided and assessed	CT, BT, BGR, CIEMAT
9	Gas permeability (K_g)	FEBEX Data provided and assessed	CIEMAT
10	Thermal properties	FEBEX Data provided and assessed	CIEMAT
11	Swelling Pressure	Substantial data provided and assessed	BT, CT, CIEMAT

* Organizations supplyind data:
BGR: Federal Institute for Geosciences and Natural Resources (Bundesanstalt für Geowissenschaften und Rohstoffe) (Germany)
BT: B+Tech OY (Finland)
CIEMAT: Centro de Investigaciones Energéticas, Medioambientales y Tecnológicas (Spain)
CT: Clay Technology AB (Sweden)

D.3 Data Evaluation

From the data contributions provided by the organizations involved in FEBEX, nine parameters were judged to have sufficient information available to allow for initial evaluation of parameter variability and the effects of testing technique on the results obtained.

The data requested were substantial for some parameters and some of the clays examined (MX80 and FEBEX) contained several dozen (or hundreds) of relevant data values. Other parameters were very limited in terms of data base size. Hence, as each of the parameters is examined, a discussion is made with reference to the particular parameter and material(s) provided.

D.3.1 Material and batch records

A major issue with the data provided for this study is the poor traceability of the material sources and their date of production (receipt). This is particularly the case with the MX80 bentonite that has been the subject of more than 30 years of study by many organizations and consists of many production runs. In many cases materials were transferred between

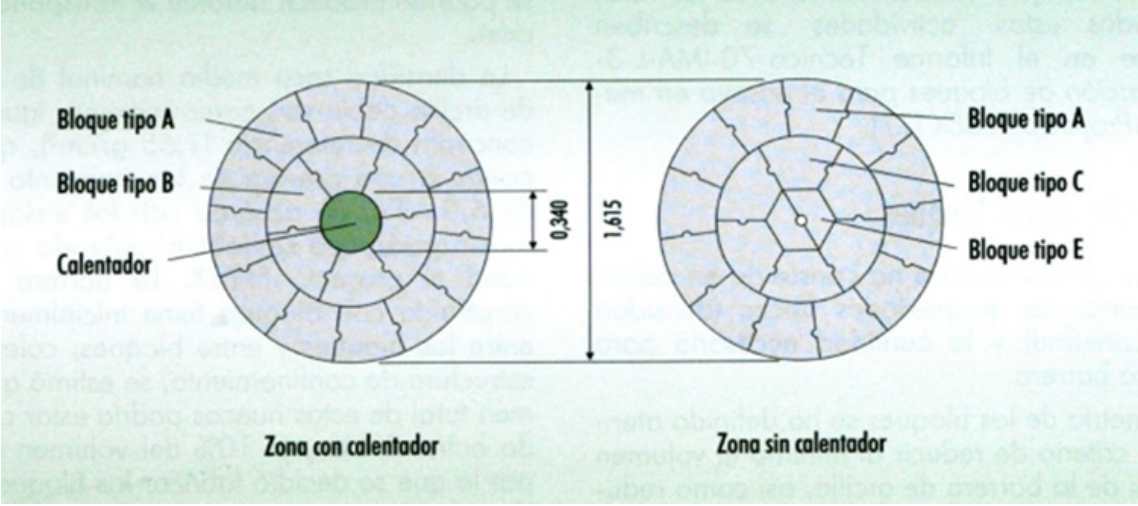
laboratories without traceable records being kept that would allow for linkage of results from different laboratories to exactly the same material batch. As a result it is difficult to separate the influence of batch variations from laboratory-produced variations. As with any natural mineral product, the quality will vary within the ore body, especially over many years of production. Hence, conclusions regarding intrinsic variability in test results must be carefully linked with the best knowledge of the actual material batch used, which will not be an issue for the FEBEX bentonite since it is a single source batch.

The FEBEX bentonite, while containing a much smaller data set for most parameters, has the advantage of representing only one shipment of material. As a result, variations in the results of characterization tests done on this material are far less susceptible to product variability and can be more closely linked to technique (and operator) factors.

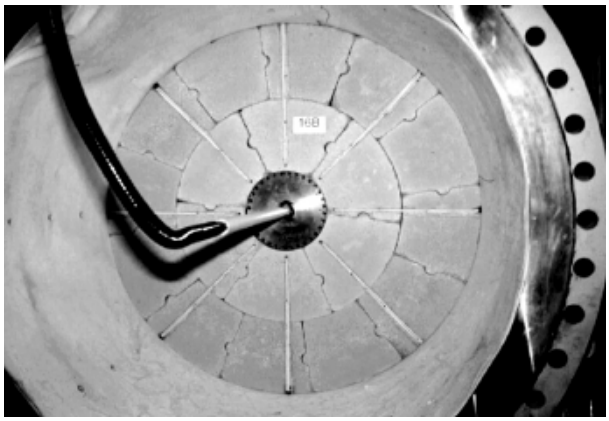
Based on the factors listed above, it was determined that the only effective way to try and compare many of the measured parameters for the MX80 and FEBEX materials was to simply lump MX80 results together and see what patterns might be observed. The FEBEX clay was assumed to represent a single batch.

D.3.2 FEBEX mock-up and FEBEX: Clay block dry density

The FEBEX clay (Serrata bentonite) was used to manufacture a large number of compacted blocks for subsequent use in both the FEBEX mock-up in Spain as well as the FEBEX installation at Grimsel. Figures showing the layout of these assemblies are provided as Fig. D-1 and Fig. D-2.



FEBEX mock-up (ENRESA 1998b)



FEBEX mock-up Construction (Martin 1999)

Fig. D-1: Block shapes and locations used in FEBEX mock-up assembly.

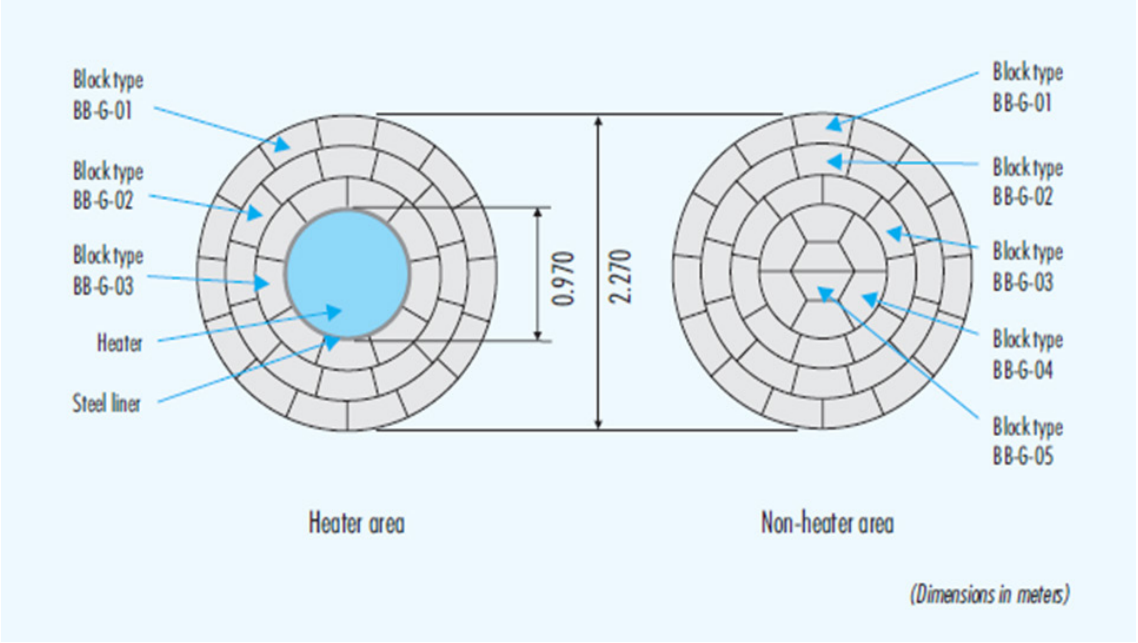


Fig. D-2: Block Assembly in FEBEX.

D.3.2.1 FEBEX mock-up

A key part of the decommissioning and sampling in FEBEX-DP will involve determining the end-of-test density and moisture conditions, so understanding what may cause variability in measurements is important. In order to investigate the variability that may be encountered during block manufacturing and consequently in the as-placed block assembly a study was undertaken using blocks manufactured for the FEBEX mock-up and the results are reviewed below.

The blocks used in the FEBEX mock-up were produced in three basic shapes (A, B, D) and a further 2 shapes (C, E) were subsequently cut/machined from them to provide the materials needed for the Mock-up experiment (see Fig. D-1) (Villar 1997, ENRESA 1998a). Ciemat provided a very large body of block density and moisture information, including the results of subsequently conducted subsampling of the blocks to determine any internal variations remaining from the manufacturing process.

It is noted that the measurement of the intact blocks in the Mock-up evaluation was based on physical measurement of the block dimensions, block mass and the moisture content of the feed material. In the subsample blocks, there will have been some cutting disturbance associated with sampling.

It should also be recognized that the data provided above in Tab. D-3 and in Fig. D-3 and D-4 were not for the blocks actually used in FEBEX, but for those used in the FEBEX-Mock-up. The actual FEBEX blocks were manufactured in a different location and were of different dimensions than the Mock-up blocks. The FEBEX blocks were slightly less dense that those used in the Mock-up. As a result internal and block-to-block dry density variability for FEBEX may be different than the 5 – 8 % observed for the Mock-up blocks. The as-built FEBEX installation was also of slightly lower average density (~ 1.60 t/m^3) as compared to the FEBEX mock-up (~ 1.65 t/m^3), which could also affect density distributions encountered during FEBEX-DP. There should therefore be an effort to evaluate any available as-built FEBEX block density data to see how it compares to the Mock-up blocks. The results from study of the Mock-up blocks do, however, provide a good means of evaluating the magnitude of variability that might be present in the FEBEX blocks.

The entire body of data provided on the FEBEX mock-up's as-built blocks is available in an electronic spreadsheet file that can be requested. Additionally, a statistical and graphical re-analysis was undertaken as part of this study to determine what degree of variability might be attributable to the as-manufactured block properties. From this it should be possible to clearly delineate what changes in density and water content in the actual FEBEX installation can be attributed to changes in the system and what is the result of the sampling or analytical method. Unfortunately there was no data available on the density and water content of the actual FEBEX blocks

The data was plotted in order to try and separate out any intrinsic patterns that might be of importance when sampling is done during FEBEX decommissioning. Fig. D-3 shows the results obtained from intact blocks for the various shapes manufactured for the FEBEX mock-up. Fig. D-4 then compares the results obtained on subsamples recovered during quality testing and study of block uniformity.

Fig. D-3 illustrates both the variability in the measured intact blocks of FEBEX-type material. The block data shows the notable difference in the density and moisture content for similarly shaped FEBEX blocks as well as for the different block shapes. Ideally the results should be nearly identical for a single production run (moisture content) block shape and compaction load.

The density variations within each block shape (ranging from approximately ± 30 kg/m^3 for the "A" and "B" type blocks to ± 45 kg/m^3 for the "D" blocks are unlikely to be entirely the result of inherent manufacturing variability since they were all manufactured using the same technique (uniaxial compression), compaction equipment and uniform batches of clay. There was a higher compaction load used to compact the type "D" blocks in an effort to increase their density. From the data presented in Fig. D-4 this higher compaction pressure would seem to have had limited success and resulted in a more density-variable material.

As can be seen in Fig. D-3, each of the block shapes was produced using several water contents. These differences were the result of slightly different water contents being identified in the materials used in the compaction activity. The results were presented on the assumption that the water content for a particular batch was uniform, although it is recognized that some unquantified variability was actually present. This would infer that the variability observed is a combination of manufacturing variability and measurement-methodology. Within each intact block type, there is a relatively narrow range of achieved density and measured moisture content for each manufacturing cycle (water content in Fig. D-3 and Fig. D-4), providing a measure that could be used as bounding values for evaluating subsequent changes. Of greater concern is the clearly greater degree of measured variation in the subsamples (Fig. D-4). These subsamples tend towards discernibly lower (2 – 4 %) density and a considerable scatter in the water contents measured. The range in measured density values is also higher (± 40 – 50 kg/m^3), than for the intact specimens. This pattern of measurement difference is common when larger specimens are cut and trimmed to provide more easily handled samples and likely will not be avoidable during FEBEX-DP. The results of the Mock-up block sampling study does highlight the need to use well-defined and consistent methodologies during sampling so as to ensure a limited variability (or at least consistent). The recovered blocks will also need to be packaged in such a manner that their interaction with the atmosphere is limited (moisture transfer and subsequent volume changes in samples).

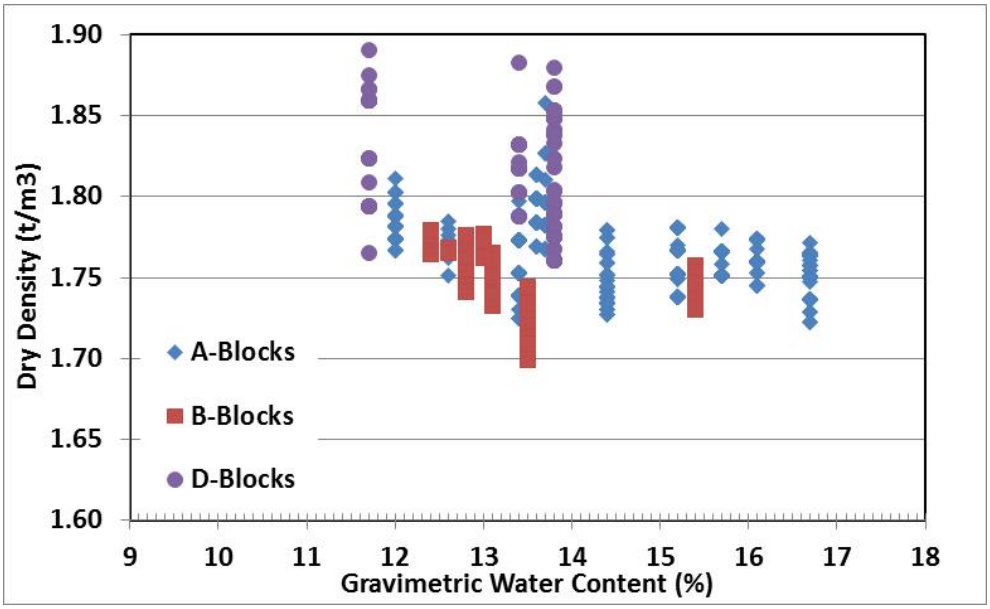


Fig. D-3: Density and moisture content variability in intact FEBEX-type blocks.

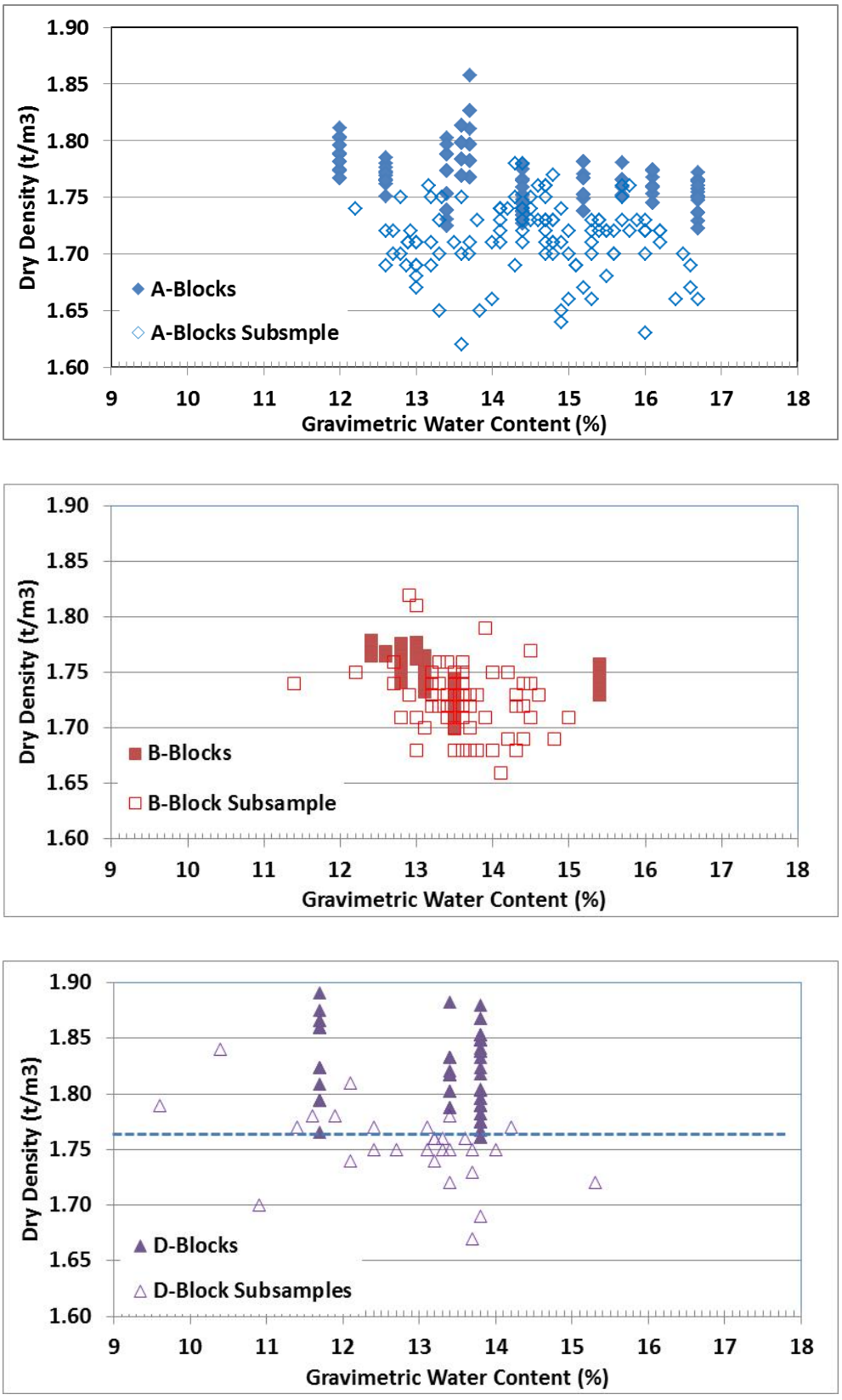


Fig. D-4: Comparison of density measured for intact blocks to subsamples cut from blocks manufactured using FEBEX clay for the FEBEX mock-up.

Using the data summary provided in Tab. D-3, the confidence limits for the density and moisture content for the as-placed blocks can be estimated. If this degree of scatter is also present in the as-manufactured FEBEX blocks then data falling outside this range could be judged as being a discernible change in the density state. Where data is not outside this range, care should be taken in concluding that there has been a discernible change unless it is supported by a consistent pattern of measurements.

Tab. D-3: Statistical summary of density and moisture content measurements on FEBEX-Mock-up blocks.

	Block Group A	**A Subsample**	**Block Group B**	**B Subsample**	**Block Group D**	**D Subsample**
Density						
Avg	1.77	1.71	1.76	1.72	1.82	1.75
Median	1.77	1.72	1.76	1.73	1.82	1.75
Stdev	0.02	0.08	0.02	0.03	0.04	0.03
n	623	118	323	71	91	28
Moisture						
Avg	14.21	14.53	13.19	13.63	13.13	12.83
Median	13.70	14.70	12.80	13.60	13.80	13.20
Stdev	1.43	1.12	0.92	0.60	0.91	1.19
n	623	118	323	71.0	91	28

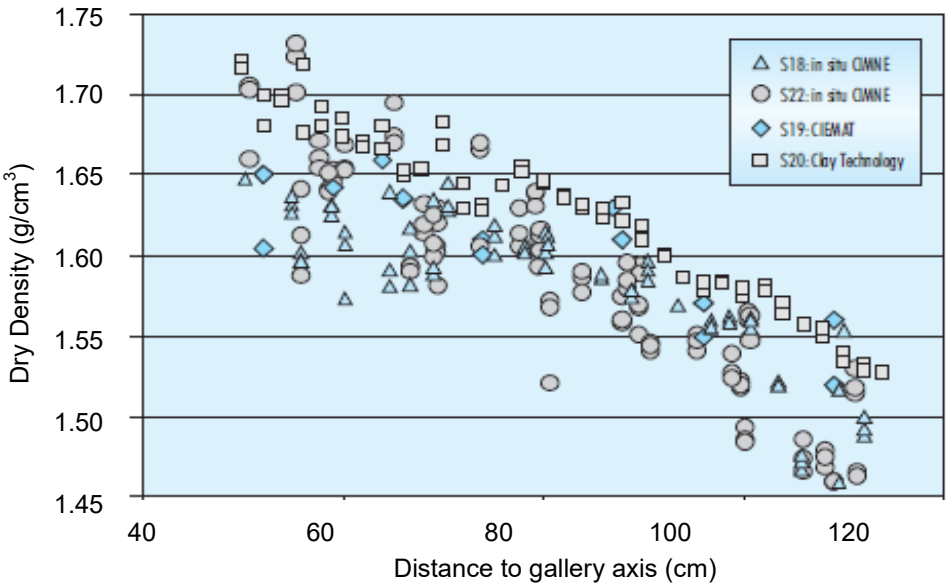
D.3.2.2 FEBEX Density measurements

As part of the decommissioning of the outer section of FEBEX in 2002 there was an extensive comparative testing program that involved 3 laboratories and three methods of density determination for blocks recovered during this decommissioning. These tests involved use of wax coating, mercury displacement and paraffin oil displacement to determine the density of recovered samples. The results of density measurements done in 3 adjacent sections are shown in Fig. D-5.

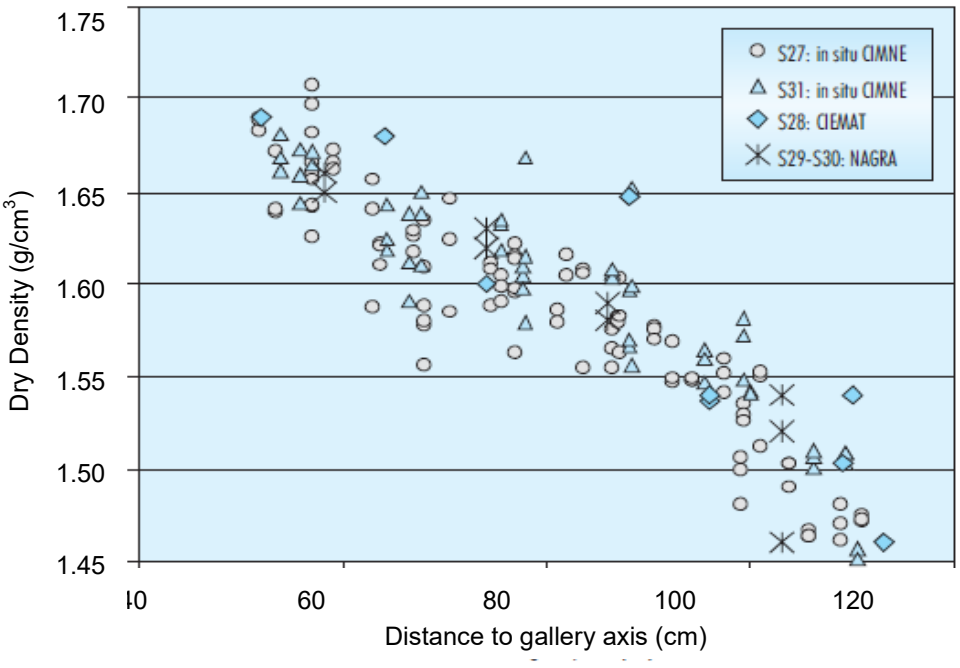
The density measurements compared the density results from samples recovered and tested on-site to those measured subsequently in the laboratory. Data from the field (CIMNE) used wax coating method while laboratories used mercury displacement technique (CIEMAT and Nagra) or paraffin oil emersion (Clay Technology). Evaluation of the effect of technique and timing on consistency of results was reported by Villar (2006), who concluded that the results obtained by mercury and paraffin emersion techniques were quite consistent with those obtained using the wax coating method. It was noted that the data produced by paraffin emersion tended to produce higher densities but this was attributed to possible desiccation of the specimens between recovery and testing rather than methodologically-induced.

The test data provided in Fig. D-5 provides some confidence in the consistency of the results between the various methods (data range typically 100 t/m^3 for a given location), but did not provide a comparison of results for the same method between laboratories. Therefore, it might be useful to conduct a series of controlled comparative tests in order to determine exactly what

measurement variability is the result of the testing method and what is operator-induced (different laboratories using the same method). If only one laboratory is used then internal variation and alternative methods could be evaluated. If more than one laboratory contributes, then the variability induced by "operator" could be added to the comparison. This would more clearly define intrinsic and operator-induced variations in the results, providing a better-defined degree of uncertainty in values measured.



Comparison of dry densities measured in situ (CIMNE) and in laboratory (CIEMAT and Clay Technology) in outer sections of FEBEX recovered in 2002. (Villar et al. 2006, Figure 151)



Comparison of dry densities measured in situ (CIMNE) and in laboratory (CIEMAT and NAGRA) in FEBEX outer sections recovered in 2002 (Villar et al. 2006, Figure 152)

Fig. D-5: Density measurements obtained for FEBEX 2002 outer-section decommissioning using different techniques.

D.3.3 Cation Exchange Capacity (CEC)

CEC is a key measure of the surface charge and changes in its value is often a good indicator that there has been a change in the chemical conditions (or mineralogy) of the clay. A second indicator of changing chemical conditions within the clay mass is the exchangeable cation composition (EC), listed as item 4 in Tab. D-1 and D-2. As the CEC and EC are linked to one-another, the CEC is discussed together with the EC in Section D.3.4

D.3.4 Exchangeable Cation (EC) composition

EC provides a measure of the initial ionic distribution within the clay minerals (and hence an indication of conditions within the surrounding pore fluid). The cation composition will affect parameters such as swelling capacity, swelling pressure and hydraulic conductivity. It will also influence how (or if) other ions can be transported through the clay mass under the combined influences of chemistry, temperature and hydraulic gradient. By knowing the initial state, and what degree of variability can be reasonably expected to be encountered in these measurements, changes induced by THM processes active in FEBEX can be assessed.

The data provided by four different laboratories on the CEC and EC properties of FEBEX and MX80 bentonites can be requested[1], and represent already published information (Olsson et al. 2013, Kumpulainen & Kiviranta 2010, ENRESA 1998a, 2000, 2006a, Gómez-Espina & Villar 2010, 2013, Villar 2006, Fernàndez et al. 2004) and unpublished data (BGR 2014). A reasonably large database was collected on both materials and a range of methodologies were included in the analytical methods used. From these data it would seem that measurement method affects the results obtained, but there were several different methodologies used, making separation of technique and material effects problematic. The CEC and EC values for MX80 and FEBEX materials are clearly different, which also allows for evaluating just what degree of generic variability might be expected.

Tab. D-4 provides the statistical summary of the MX80 bentonite and Tab. D-5 the same information for the FEBEX bentonite. For MX80 there were four contributing organizations (4 labs) and for FEBEX there were only two. However there is a substantial database available (29 and 14 respectively), providing the means to develop a measure of the variability of measurements on similar materials. Identification of data consistency for each method is however problematic and would require further study involving repetitive analyses using well-defined methods.

The two bentonites examined above show very different exchangeable ion compositions, as expected given their differing geological sources. The results in these tables do not show any consistent pattern of variation in results for the different methodologies used to conduct the analyses. Care should however be taken to ensure that the same methodology is used in the analysis of the FEBEX decommissioning samples to avoid any potential for criticism regarding the results obtained. Given that each laboratory uses slight variations to the same basic technique for analysis, ensuring methodological consistency could prove challenging.

The MX80 is, as expected, a clearly Na^{+}-dominated material with Ca^{+2} as its secondary cation and only minor Mg^{+2} present. The FEBEX material is very different in cation composition with Ca^{+2} and Mg^{+2} dominating and Na^{+} as a lesser (but still substantial) component. The FEBEX material has a discernibly higher total CEC than the MX80, which is consistent with its higher smectite content (see Section D.3.6). As a note regarding the analytical technique, the data provided included using a 1M NH_4AcO pH7 solution in the exchange process, which has been identified as likely providing high Ca exchange values due to calcite dissolution. However, for

the purposes of this study these values were included so as to obtain a conservative estimate for analysis variability.

The data in Tab. D-4 shows the Na-Ca cation content variability in the MX80 material, which provides some bounds on what could be interpreted as natural and alteration in post-experiment measurements. Tab. D-5 provides a similar bounding on the natural FEBEX material's variability with respect to its Ca-Mg-Na ratio. These variations are another key item to take as reference when post-decommissioning analyses are undertaken.

Tab. D-4: Exchangeable cation and cation exchange capacity of MX80 bentonite.

	Na^+	**K^+**	**Ca^{+2}**	**Mg^{+2}**	**Others**	**Total CEC**
MX80	(meq/100g)	(meq/100g)	(meq/100g)	(meq/100g)	(meq/100g)	(meq/100g)
Average	56.3	1.7	22.8	7.3	0.3	84.8
median	56.1	2.0	22.2	7.2	0.2	85.0
STDEV	4.6	0.5	5.1	1.4	0.3	6.6
N	29	29	29	29	6	51
Range	46 – 65	1.5 – 2.8	14.6 – 35	5 – 9.1		63 – 94

Tab. D-5: Exchangeable cation and cation exchange capacity of FEBEX bentonite.

	Na^+	**K^+**	**Ca^{+2}**	**Mg^{+2}**	**Others**	**Total CEC**
FEBEX	(meq/100g)	(meq/100g)	(meq/100g)	(meq/100g)	(meq/100g)	(meq/100g)
Average	26	3	39	34	0.4	101
Median	26	2.5	38	34.8	0.38	100
STDEV	2.6	0.3	6	2.5	0.0	7.1
N	11	11	11	11	2	11
Range	22 – 30	2.1 – 3	31 – 48	31-38		92 – 113

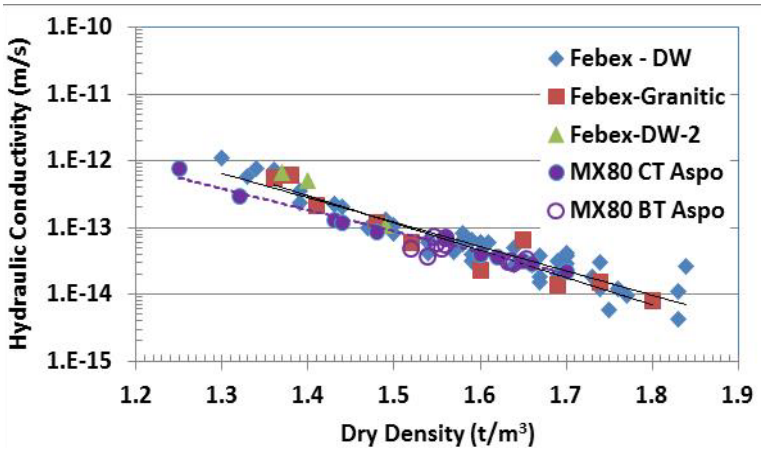
D.3.5 Hydraulic conductivity testing

The data provided for the two clays were tabulated and can be obtained upon request[1]. The relationship between dry density and hydraulic conductivity are provided in Fig. D-6. The data includes tests completed using freshwater as well as low salinity groundwater compositions, both of which should provide similar results.

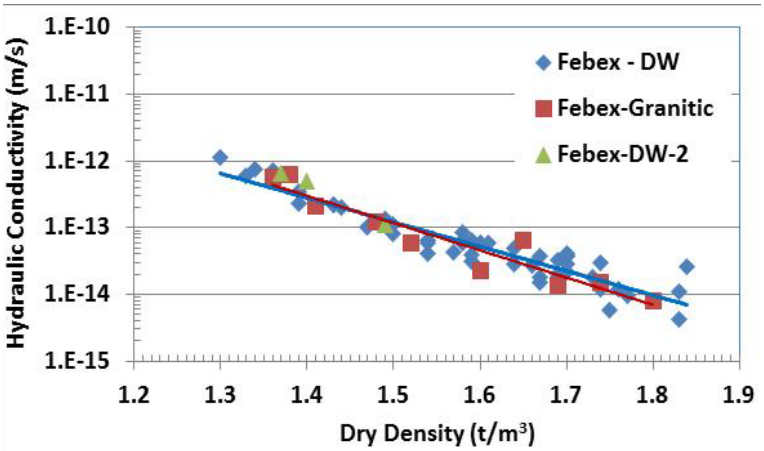
Data for MX80 was provided by two laboratories and follow the trends established in literature for this material (Kumpulainen & Kiviranta 2010; Kiviranta & Kumpulainen 2011 and Olsson et al. 2013). The FEBEX bentonite data were provided by a single laboratory (Villar 2002, Villar and Gómez-Espina 2009). The two materials show very similar trends in terms of change of hydraulic conductivity (k), with change in dry density, with the MX80 showing a slightly lower k than the FEBEX, particularly at lower density. This is generally attributed to the

difference in exchangeable cation composition for these two materials (FEBEX is a Ca-Mg dominated bentonite and MX80 is a Na-Ca dominated bentonite). The differences are, however, quite small, particularly at the densities of interest for FEBEX (> 1.6 t/m^3). The scatter in the data for FEBEX bentonite indicates that a range of ± one half order of magnitude (5x) in the k measured for a particular density is about the limit of accuracy in measurements done for this type of very low permeability material, particularly for systems having a low salinity. Although the data shown for the MX80 would seem to indicate a smaller range of data scatter, it is based on a very small data set. Inclusion of additional data from literature would be expected to generate a degree of scatter similar to that observed for the FEBEX bentonite.

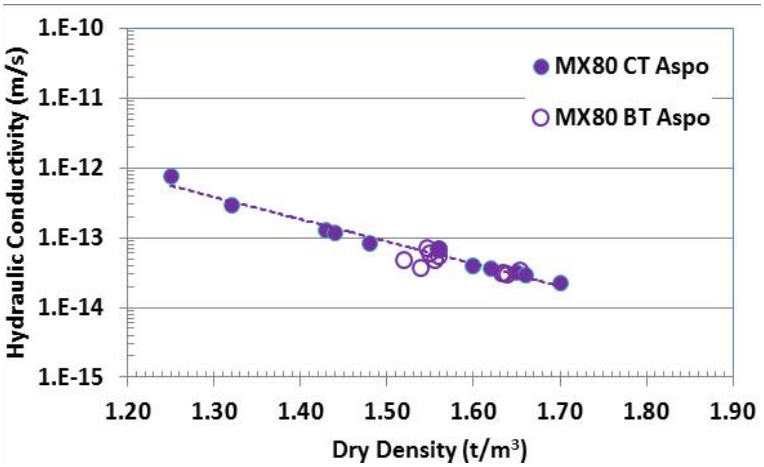
It should also be noted that the specimens tested and included in the plots shown in Fig. D-6 were for fresh material that was compacted directly into the test chamber. Testing of materials recovered from FEBEX will in all likelihood be disturbed and re-compacting may not be appropriate since it would disrupt any environmentally-induced changes in structure and hydraulic behaviour (e.g. cementation). It will therefore be necessary to carefully assess the methodology to use for testing the recovered FEBEX samples. It is also generally acknowledged that recovered or trimmed specimens are more prone to variability in their measured hydraulic properties, hence, care needs to be taken to try and separate sampling effects from actual behavioural changes. One way of doing this might be to use archived FEBEX blocks and extract samples from them in the same manner as will be used in the field and then test them. From this, it may be possible to establish a more representative set of density-k values for comparing with recovered material.



a) FEBEX and MX80 Data Compilation



b) FEBEX Data



c) MX80 Data

Fig. D-6: Hydraulic conductivity of MX80 and FEBEX bentonites.

D.3.6 Mineralogical analyses

An important set of measurements associated with the analysis of changes to the FEBEX bentonite will be the mineralogical and overall chemical composition of the system. Quantitative mineralogy is a challenging task and susceptible to interpretive bias depending on the software used to identify the mineral phases and the post-processing of recovered materials (e.g. fines separation, random versus oriented particles, sample washing, ion-exchange, glycolation, chemical treatment …). It is not uncommon for large differences to be reported for analyses of identical bentonite samples submitted to different laboratories, even when the same analysis is requested. The internal variability in results is typically not high within a single laboratory as their internal processes are consistent. As a result it will be important to ensure that the materials recovered from FEBEX are all treated the same and analysed using exactly the same analytical method. In this manner, while the absolute values obtained may vary, changes in composition will be identified which is the primary goal of mineralogical analyses here.

Tab. D-6 presents x-ray diffraction (XRD) data supplied for MX80 (3 laboratories, 21 analyses (Kiviranta & Kumpulainen 2011, Åkesson et al. 2012)) and FEBEX bentonite (1 laboratory, 2 analyses, ENRESA 1998a). The data for MX80 shows the type of variation that can be encountered in the analysis of bentonite mineralogy when very similar methodologies are used by analytical laboratories familiar with bentonite. Although the data provided for FEBEX was identified as being the average of multiple analyses, there was insufficient information provided on the number of tests this represents; the source data was not available, hence, determining the normal variability FEBEX bentonite was not possible.

The variation observed in the MX80 material is a result of a combination of factors including: natural variability of the material and the analytical influences described above. Hence, if mineralogical change is to be assessed it will be important to have a clearly characterised reference material and a single, agreed-upon analytical methodology to be used, especially if more than one laboratory is involved. This method specification should be defined before beginning any post-dismantling analyses and each laboratory should have a very clear understanding (written procedures) of every step of the analytical process. In this manner, a baseline can be established that will be directly comparable to the results of analyses conducted on the recovered materials. Care will also be needed in determining the degree of "accuracy" these results represent and how "minor" (e.g. a few percent in montmorillonite) changes in the values obtained can be interpreted. If different laboratories are involved, it might be helpful if they run triplicate samples to provide an internal measure of analytical variability.

D.3.7 Clay chemical composition

Another way of assessing changes to the overall composition of a bentonite sample is through total cation analysis. These data can be obtained by several methodologies, including X-ray Fluorescence (XRF) and total acid digestion (ICP). A considerable body of analytical data was available for MX80 (26 analyses), while the FEBEX has only 6, however the data available for the FEBEX clay shows limited scatter.

The analytical results provided for the MX80 and FEBEX bentonites are summarized in Tab. D-7 and the entire database is available upon request[1]. The data is a combination of published (e.g. Kiviranta & Kumpulainen 2011, ENRESA 1998a, 2000, 2006a) and unpublished data provided by other FEBEX partners (e.g. BGR 2014). Although some of the data provided for the FEBEX bentonite was identified as representing averaged values of several tests, the source data was not supplied and hence for statistical purposes where an average value was provided it was taken as a single measurement. The FEBEX clay analyses represent samples

recovered from the same production batch of material and are exactly the same material used in the Grimsel installation. This provides confidence in the representative nature of the values provided for use in subsequent decommissioning comparisons.

The MX80 material typically showed a greater range in measured composition, possibly a reflection of batch-to-batch variability of the material. These two clay types (MX80 and FEBEX) also differ noticeably in their natural Na, Ca and Mg contents, with the FEBEX bentonite having substantially more Ca and Mg present (consistent with their exchangeable cation compositions). Although chemical composition analyses are of limited use with respect to determining the location of cations in the system, they provide a measure of relative depletion (or enrichment) of the system as the result of cation redistribution over the course of the test.

D.3.8 Consolidation characteristics

Although requested as part of the data review, there was insufficient data provided for comparison of measured consolidation characteristics for the FEBEX or MX80 bentonite. The data provided for the FEBEX bentonite comes from the work of Villar (2002) and Villar & Lloret (2004).

Tab. D-6: XRD analysis results for MX80 and FEBEX bentonites.

MX80	Mont.	Illite	Muscovite	Illite + Muscovite	Mixed S/I	Chlorite	Kaolinite	Quartz	All SiO_2	Total Feldspars	Calcite	Siderite changed	Gypsum	Pyrite changed	Total Others
Average	85.5	0.4	1.3	1.7	0.0	0.1	0.0	4.0	4.9	4.7	0.6	0.7	0.9	0.5	1.1
Median	86.0	0.4		0.4				4.0	4.3	3.9	0.5	0.7	0.9	0.5	1.2
Standard Deviation	3.6	0.5	2.6	2.7		0.2		0.5	1.6	2.4	0.7	0.7	0.6	0.4	0.6
n	21	21	21	21	21	21	21	21	21	21	21	21	21	21	21
Range Reported	77.5-90.6	<2	0-8.3	0-8.9	NR	0-1.1	NR	2.9-5	2.9-8.3	1.5-9.8	0-3.1	<1.3	<1.7	<1.5	<1.9
FEBEX															
S2 and Febex					92*			2	4	3	1		trace		
S2 and Febex					94*	trace	trace?	2	2	1	2		trace		
* Reported as mixed Smectite/Illite with 11% Illite interlayers															

S2 = Serrata bentonite, source material for FEBEX bentonite
FEBEX = Processed Serrata bentonite, used in FEBEX and FEBEX mock-up experiments

Tab. D-7: Chemical composition of bentonites based on XRF and ICP analyses.

MX80	Si02	Al_2O_3	Fe_2O_3	Mg0	Ca0	Na_2O	K_2O	TiO_2	P_2O_5	Mn0	LOI	C (org)	CO_2	TOT/C	TOT/S
Average	60.9	19.7	3.7	2.4	1.3	2.2	0.6	0.1	Tr	Tr	8.6	0.2	0.2	0.3	0.3
Median	61.2	19.9	3.7	2.4	1.3	2.1	0.6	0.2			7.0	0.2	0.2	0.3	0.3
Standard Deviation	2.4	0.9	0.3	0.1	0.1	0.2	0.1	0.0			2.9	0.1	0.2	0.1	0.1
n	26	26	26	26	26	26	26	26	26	26	26	26	26	26	26
range	55.6-65.4	18.1-21.4	3.3-4.2	2.2-2.8	1.1-1.5	1.9-2.9	0.5-0.6	<0.17	Tr	Tr	5.4-15.7	<0.2	<0.2	0.1-0.7	<0.35

FEBEX	SiO_2	Al_2O_3	Fe_2O_3	Mg0	Ca0	Na_2O	K_2O	TiO_2	P_2O_5	Mn0	LOI	C (org)	CO_2	TOT/C	TOT/S
Average	58.2	18.5	3.4	4.7	2.1	1.7	1.1	0.1	0.0	0.0	7.6	0.4	0.2	0.5	0.1
Median	58.4	18.4	3.5	4.5	2.0	1.7	1.1	0.2	0.0	0.0	6.2	0.4	0.2	0.7	0.0
Standard Deviation	1.6	0.9	0.4	0.6	0.5	0.5	0.2	0.1	0.0	0.0	4.6	0.3	0.1	0.3	0.1
n	6	6	6	6	6	6	6	6	6	6	6	6	6	6	6
range	57-60	18-19.6	2.9-3.9	4.2-5.8	1.9-2.9	1.4-2.3	0.7-1.4	<0.3	TR	TR	4.7-6.8	<0.7	<0.3	<0.7	<0.2

D.3.9 Gas permeability

The gas permeability (and gas breakthrough) behaviour of compacted sealing materials is a potentially significant parameter in repository evolution. There are at least three potential processes that could lead to the build-up of gas pressures within a repository and this build-up could result either in breaching the engineered barriers when it reaches pressures sufficient to dewater them or else apply pressures to the exterior of the canisters. The magnitude and likelihood of these processes occurring in a repository are not discussed in this document, it is simply assumed that they may occur and hence the ability of the engineered barriers (e.g. bentonite) to transmit or resist gas movement through them is of importance and needs to be measured.

The processes that could lead to gas generation and/or pressure build-up within the repository include:

1. Compression of air initially present as the result of water inflow
2. Microbial-generated gas as a by-product of cell respiration
3. Hydrogen gas generation as the result of corrosion processes involving the canister

Gas permeability is a very challenging parameter to measure and is sensitive to minor changes in the bounding conditions present during testing.

There was only one set of data provided for gas permeability and gas breakthrough and these data are provided electronically upon request[1]. A plot showing the gas permeability data for FEBEX bentonite is presented as Fig. D-7 and taken from the work by Villar et al. (2013) and Gutiérrez-Rodrigo et al. (2014). These data show the trend of decreasing gas permeability with both increasing density and increasing degree of water saturation. In particular, in Fig. D-7 the data would appear to show that gas permeability decreases rapidly once water saturation exceeds approximately 80 %, indicative of the establishment of a discontinuous gas flow pathway. The trend lines provided in this figure are for illustrative purposes only and a more stringent analytical analysis was provided in the source documents. The data also show the considerable degree of scatter in the results available, which will make pre- and post-test FEBEX data comparison challenging unless there is a very substantial change in the values measured. An additional complicating factor will be to compare results of custom-built, intact specimens (current database) to the results obtained from trimmed samples probably disturbed during recovery.

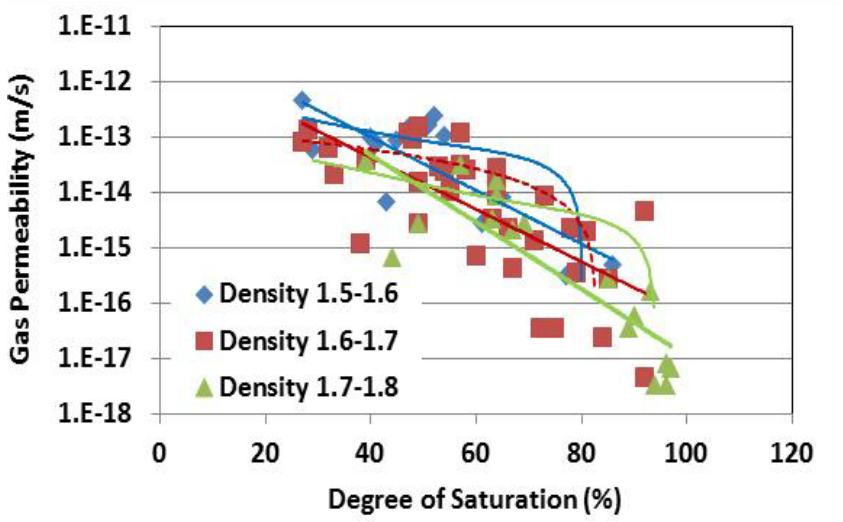


Fig. D-7: Gas permeability of FEBEX bentonite.

D.3.10 Thermal properties

As with the gas permeability data, the only information provided with respect to the thermal conductivity behaviour of bentonite was for the FEBEX material. Information generated by and reported in Villar (2002) is provided electronically upon request[1], a summary plot is shown in Fig. D-8. The data provided were re-evaluated based on the assumption that saturation values reported as > 100 % were actually 100 %. Alternative explanations for these values were provided by Villar (2002) but for the purposes of this summary, the assumption provided above was adopted.

The datas in Fig. D-8 shows the expected pattern of increasing thermal conductivity with increasing density and also with increasing degree of saturation. These data also illustrate the considerable degree of scatter in the values measured, in some cases as much as a 25 % difference in value is observed for the same conditions. This provides some bounding indicators to the values of thermal conductivity that can then be used in post-decommissioning thermal analyses done using as-measured density and moisture conditions in FEBEX.

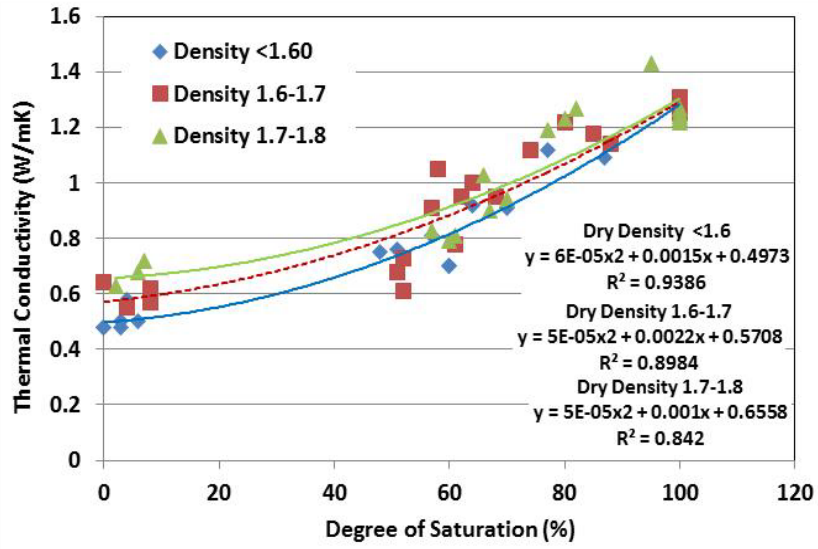


Fig. D-8: Thermal conductivity of FEBEX bentonite (after Villar 2002).

D.3.11 Swelling pressure

Swelling pressure (pressure measured at the contact between a rigidly-confined specimen and its confinement) is one of the most commonly measured (and important) parameters in the assessment of bentonite-based sealing materials. This parameter is affected by a range of variables (e.g. smectite content, smectite type, external cation composition and concentration, temperature, presence of cementitious materials…). As a result, a change in swelling pressure is often used as a key indicator to changes in system conditions.

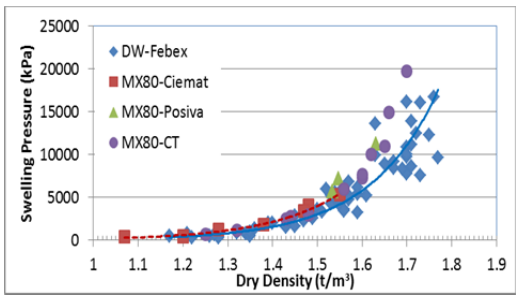
For the MX80 bentonite, as the result of more than 30 years of study by many laboratories, a very large database exists. In this study, data from 3 laboratories were received and included in the summary below. The MX80 data consisted of 34 measurements made on materials tested using either deionized or low salinity (< 10 g/L) pore fluids (see Appendix[1] for data details). These data (plotted in Fig. D-9), are drawn from several documents (Kumpulainen & Kiviranta 2010, Kiviranta & Kumpulainen 2011, Olsson et al 2013, Villar 2002, 2005, Villar & Lloret 2008, Villar et al. 2012b), and represent materials from several production batches of this material, adding a potential uncertainty regarding the mineralogical and chemical uniformity of these materials. The MX80 data presented in Fig. D-9 comes from several sources and so is identified separately on these plots in order to identify if there were any substantial differences in the results obtained by different labs. From the data presented it would appear that swelling pressure can be measured consistently and is not particularly sensitive to the operator.

The FEBEX bentonite, as noted previously, represents only a single batch of material and a substantial swelling pressure database (64 measurements) was presented in reports by Villar (2002) and Villar et al. (2012b). These data are presented In Fig. D-9 as FEBEX since there is only one source of data.

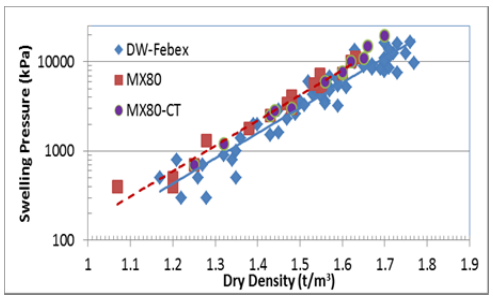
Swelling pressure data are typically plotted in one of two formats, either as a linear plot of density versus swelling pressure, or as a log swelling pressure – density. For ease of reader reference, both formats are provided in Fig. D-9. The lines shown in the plots provided

represent the best-fit trend lines for the data. In Fig.s D-9a and D-9b two lines are shown, one for the FEBEX bentonite database (solid) and one for the MX80 database (dashed).

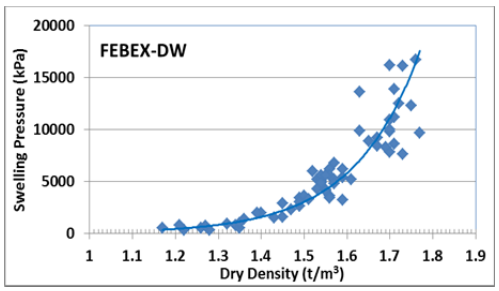
The data presented in Fig. D-9 (a-b) show that the two bentonites follow the same general trend of increasing swelling pressure with increasing dry density, but also that the two data series are not identical with FEBEX trending to a lower magnitude of measurement for the same dry density. This may be the result of the differences in the two materials, with FEBEX bentonite having a substantial smectite-illite interlaying. The FEBEX measurements also show a higher degree of scatter than those for the MX80. This scatter in measured swelling pressure is most noticeable at higher density (in the range of interest to FEBEX), with an approximately 30 – 40 % variability in measured values being observed, even when done by the same laboratory using the same methodology. This seems to be the general limit of the measurement accuracy, for which no definitive explanation has been developed. Consequently, there will need to be a very careful use of any swelling pressure data before concluding that there were changes to the materials in the course of the experiment's operation. Additionally, care will need to be taken to ensure that all tests are done in the same manner, thereby limiting any potential operator-induced effects. It should also be noted that tests done using materials recovered from FEBEX decommissioning will be disturbed and results might not be entirely indicative of the material's field properties.



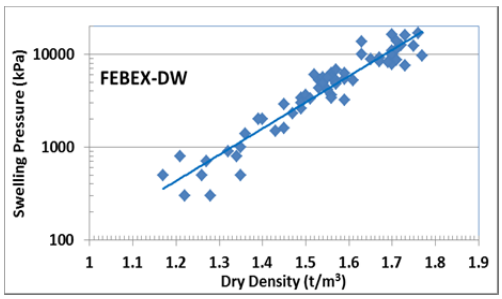
FEBEX and MX80 (linear plot)



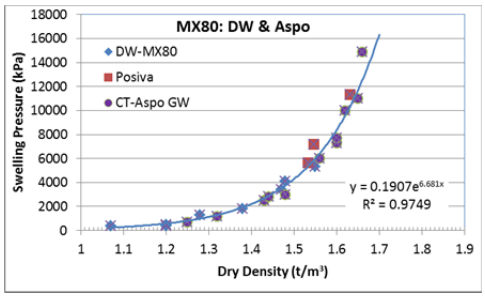
FEBEX and MX80 (log-linear plot)



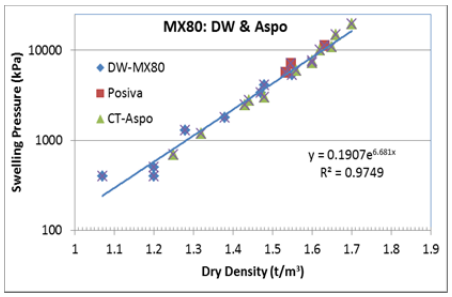
FEBEX bentonite (linear plot)



FEBEX bentonite (log-linear plot)



MX80 bentonite (linear plot)



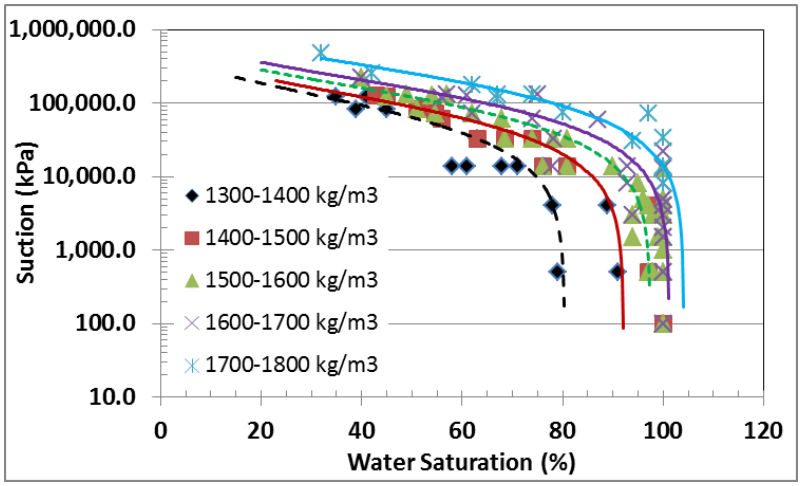
MX80 bentonite (log-linear plot)

Fig. D-9: Dry Density – swelling pressure relationships for FEBEX and MX80.

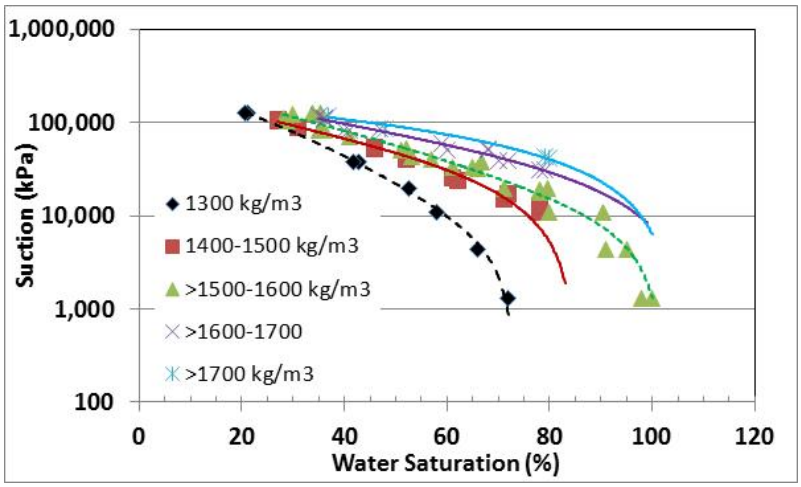
D.3.12 Water retention curves

The water retention (also known as suction-moisture) properties of compacted bentonite are an important parameter for modelling water uptake and redistribution in a bentonite mass. Data for FEBEX bentonite (Villar 2002, Villar & Gomez-Espina 2009) and MX80 (Villar 2005) were only supplied by one laboratory. They used the methodology described by Villar (2002) and are presented in Fig. D-10, with the data supplied electronically upon request[1].

The water retention curves for both FEBEX and MX80 bentonites show the expected trend of increasing suction with increasing density and decreasing degree of water saturation. The trend lines shown in Fig. D-10 are for illustration purposes only and should not be used without further statistical analysis.



a) Suction-Moisture Relationships for FEBEX bentonite



b) Suction-Moisture Relationships for MX80 bentonite

Fig. D-10: Suction – moisture relationships for FEBEX and MX80 bentonites.

D.4 Summary

This memorandum has compiled data supplied by various organizations associated with the FEBEX decommissioning and represents an initial attempt to identify the degree of uncertainty in the reference values for parameter values of particular importance in the interpretation of the decommissioning materials testing data.

The parameters of interest with respect to materials' properties can be broken into two general groupings:

- Geotechnical
- Geochemical/Mineralogical (mineralogy, mineral chemistry, CEC, EC)

Within the bounds of conditions present in FEBEX, the Geotechnical parameters are predominantly influenced by the parameters of density and water content, although geochemical properties and conditions will also affect them. Hence it will be extremely important to ensure that the methods used to recover samples (and measure these parameters) are done in an internally consistent manner and subject to minimal procedure-induced variability. Additional care will need to be taken to cause as little disturbance as possible to samples recovered for conduct of tests such as swelling pressure, hydraulic conductivity and gas permeability.

Within the Geochemical and Mineralogical parameters evaluation group, the characterisation tests need to be completed in a manner that minimises introduced variation in measurement results. Additionally, given the degree of scatter/uncertainty observed for several of these parameters, care is needed during interpretation to ensure that any interpreted changes in parameter values are clearly outside the range of normal variation in the baseline data.

Unless additional representative data can be found, there will also need to be some additional testing done on archive materials in order to improve the degree of confidence in some of the baseline values. In particular, data regarding the initial density of the blocks used in the actual FEBEX installation needs to be reviewed since determination of changes that may have occurred will be important. The conduct of several additional quantitative analyses of mineralogy and chemical composition on archive samples of the FEBEX clay using exactly the same method(s) proposed for use in characterisation of recovered materials should be undertaken at the same time as the recovered materials are analyzed. As part of the decommissioning planning, the laboratories involved in the mineralogical analyses should also establish a well-defined common methodology for doing these analyses. This process of including archived specimens in the conduct of all post-dismantling tests is a means by which relative changes can be identified rather than relying on the results of tests done using slightly different methodologies and different operators.

Appendix E: On-site extra reports during and after dismantling

E.1 Plug dismantling and sampling Section 36



Fig. E-1: Cleaning of shotcrete between the heater car tracks.



Fig. E-2: Robot leaving the gallery.



Fig. E-3: Robot leaving the tunnel.



Fig. E-4: The site after completion of the shotcrete dismantling exposing the dummy.



Fig. E-5: Sampling B-B-36-7 to 9 before taking off the blocks.



Fig. E-6: Samples B-B-36-1 to 3 after dismantling showing that blocks can be taken off intact at original block boundaries most of the times.





Fig. E-7: Block B-B-36-1 (outer ring) with iodine paper on top (left) and at its original wall position.



Fig. E-8: Block B-B-36-3 (inner ring) with positions where bentonite was squeezed into liner holes (left) and liner with bentonite filled liner holes at same position.



Fig. E-9: Corrosion pattern at block B-B-36-6.



Fig. E-10: Preparation for sampling of block B-B-36-4 to 6 revealed quite wet bentonite in accordance with the observation during the overcoring of C-C-32-6OC.

It was not possible to take individual blocks intact.



Fig. E-11: Final image after sampling Section 36.



Fig. E-12: The AITEMIN on site making long-shifts (Bárcena & Martin).

E.2 Documenting the heater retrieval (04/06/2015)

All annotations to the pictures are first field impressions by Dr. Florian Kober (Nagra) and can be interpreted differently by others.



Fig. E-13: Track extension preparation.



Fig. E-14: Final site preparation.



Fig. E-15: The tracks are ready for the heater car.



Fig. E-16: The heater winch attached (screwed) and welded to the heater.



Fig. E-17: The heater car in place for pulling out the heater.



Fig. E-18: The heater comes OUT at around 12.30 am on 04.06.2015 after 18 years of duty.



Fig. E-19: The AITEMIN team relieved and happy (FLTR, Jose-Pedro Carvajal, Christina de la Rossa, Ignacio Bárcena, Antonio Martin).



Fig. E-20: The heater more than halfway out.



Fig. E-21: bentonite debris on top of the retrieved heater.



Fig. E-22: bentonite still sticking at the front of the retrieved heater.



The heater is completely out … front view …



Fig. E-23: The heater is completely out; front view (top picture) and view towards the back (lower picture).

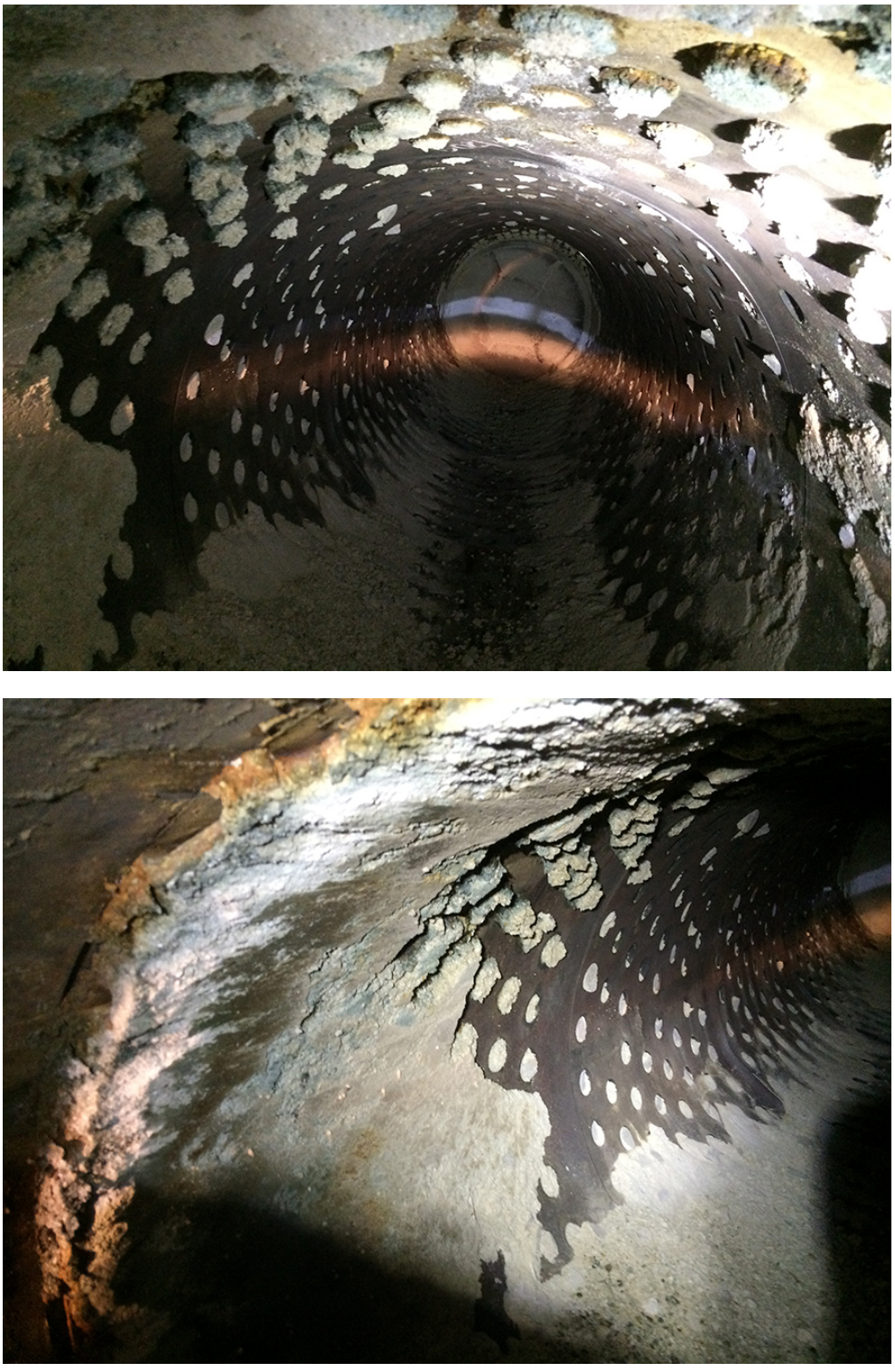


Fig. E-24: The first view into the now empty liner, showing bentonite protruded through the liner holes especially in the front and back part.

Below: The front-left part of the liner with a 1 – 2 cm crust of bentonite with oxidation signs going over into bentonite protruded through the liner holes, these protruded parts (if existing) were cut of in the lower half.



Fig. E-25: The back side of the heater on the heater car on its way out of the gallery.

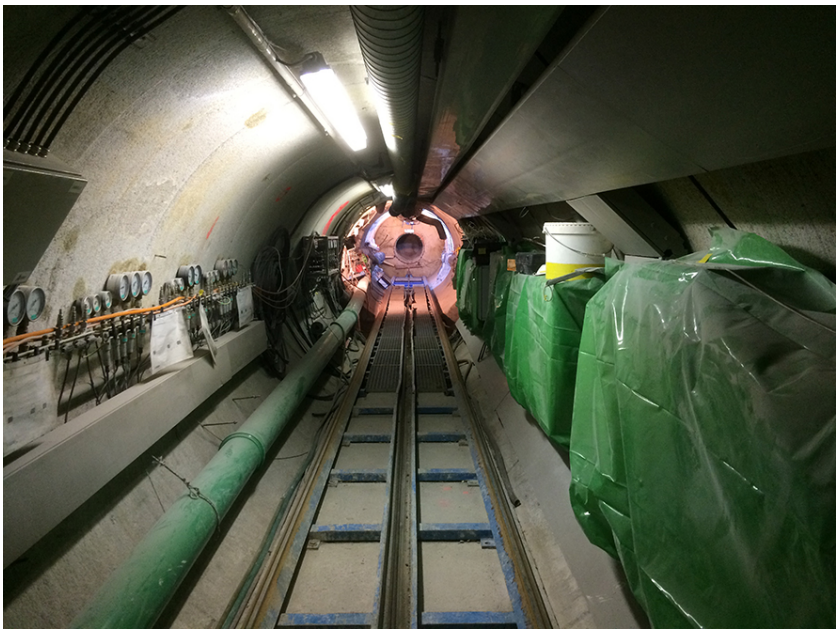


Fig. E-26: The FEBEX-site with bentonite Layer 40 exposed and the now empty liner.



Fig. E-27: The heater car with its control unit approaching the entrance of the gallery.



Fig. E-28: The heater at the FEBEX installation site.



Fig. E-29: The team on site yesterday (Ingo Blechschmidt missing).



Fig. E-30: Empty experiment.



Fig. E-31: The frontal view of the empty liner.

This figure shows bentonite entering through the liner perforation into the void between the liner and the heater, over an extensive surface. With depth into the liner these protrusions diminish and single protrusions are visible. These features become less distinct and disappear towards the middle of the heater before re-appearing again more abundantly at the end of the heater.

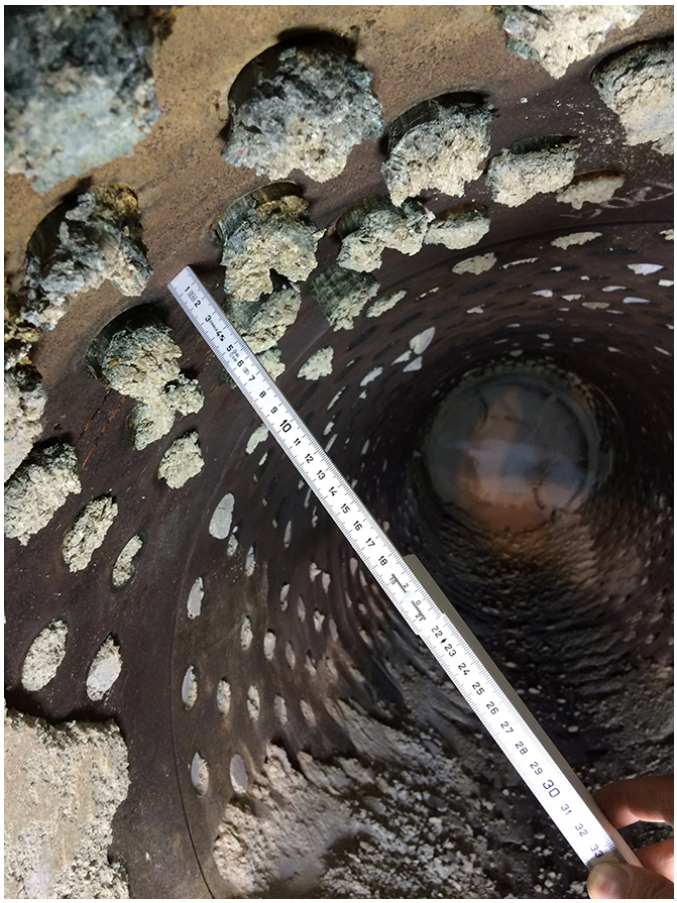




Fig. E-32: Close-ups of the protruding bentonite inside the liner.

(Upper) A close-up view of the frontal protruding bentonite being very porous and dry; it disintegrated on attempts to sample as one piece.

(Lower) Towards the start of the heater the protrusions were characterized by a higher degree of oxidized rings.



Fig. E-33: A full liner view – at the end the block boundaries of bentonite Layer 23 are visible.



Fig. E-34: More close-ups of the inside of the liner.

(Upper) A close-up view form the lower left frontal liner where bentonite protrusion were cut from the heater removal.

(Lower) Some other protrusion being less distinct and with oxidation rinds/rings

E.3 Documenting the disappearing gaps in bentonite Layer 45 (26/06/2015)

This report highlights the effects of bentonite swelling over 18 years in areas where initial construction gaps between blocks disappeared. Shown is bentonite Layer 45 (in between sampling Section 46 and 47) in 1997 and on 25.06. 2015.

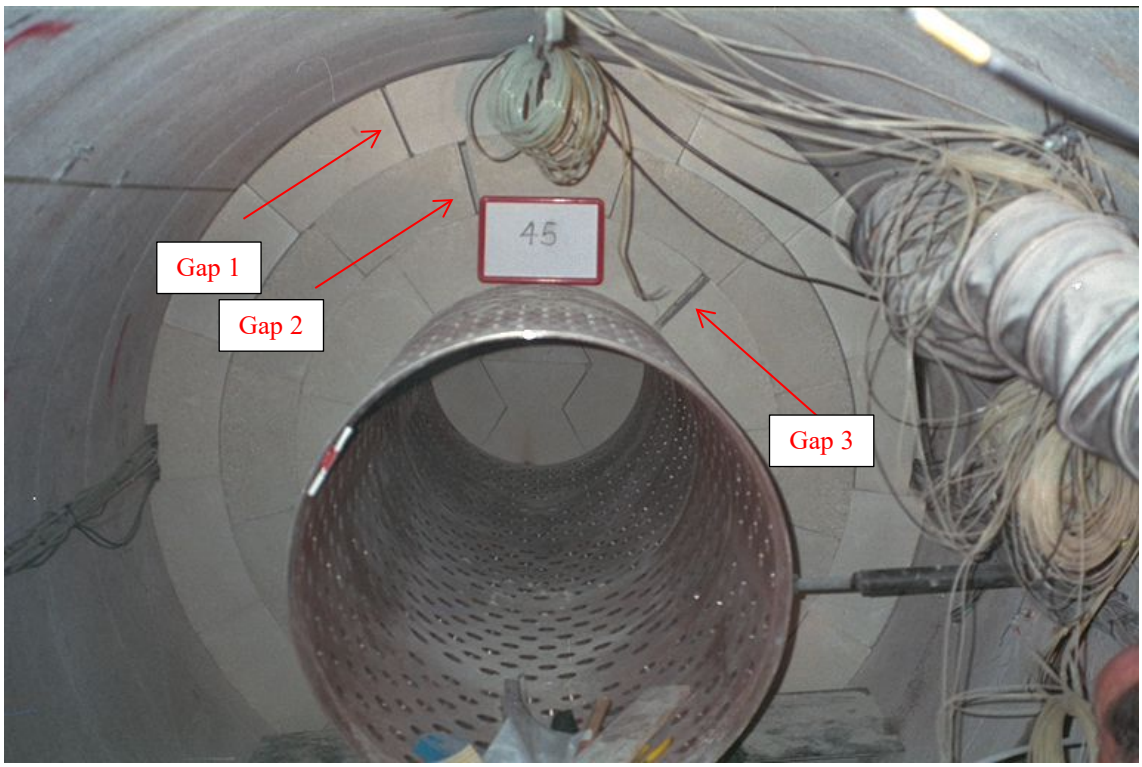


Fig. E-35: bentonite Layer 45 "As built" in 1997.

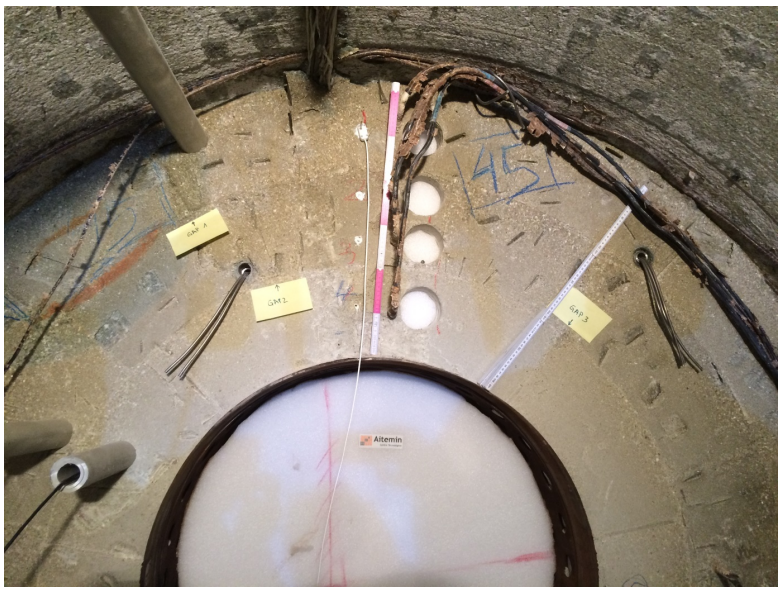


Fig. E-36: bentonite Layer 45 on 25.06.2015.

After completion of Layer 46 (in front of Layer 45 and already excavated on these images), holes were drilled and the TDR seen at 12 o'clock were emplaced. Additionally, a fisurometer, which was emplaced in Layer 44 causes the colour changes in the outer ring at 20 o'clock in figure E-33. In 2002, gas/water pipes were installed (at 10 and 11.30 o'clock). The yellow stickers mark the position of the gaps shown in Fig. E-37, and are enlarged in Fig. E-37 – 40. Note that the images were taken after Layer 45 had been exposed for one day.



Fig. E-37: Gap 1.



Fig. E-38: Gap 2.



Fig. E-39: Gap 1 & 2.

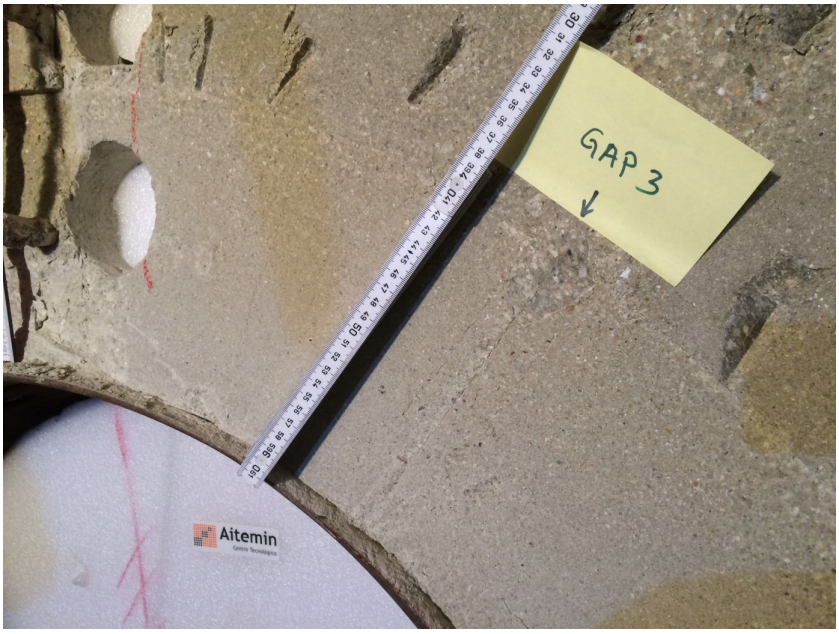


Fig. E-40: Gap 3.

E.4 Sampling bentonite with corrosion products in bentonite Layer 44 (26/06/2015)

This report describes the extra bentonite samples taken in an area strongly affected by the corrosion products of a sensor.

Sensor

The sensor is a fisurometer located in Section 47 (bentonite Layers 45 – 43). Fig. E- shows the type of sensor (the one on the picture is from another layer).

The characteristics of the sensor are:

- Housing made of E24 steel (French code)
- Support plate (same material as housing)
- 3 extensometers (SS316)
- Electronic box
- Stainless steel screws



Fig. E-41: Fisurometer similar to that installed in Section 43 – 45.

Bentonite sampling

On bentonite Layer 46 and 45, a blueish/greenish halo was visible at the location of the sensor, with some brown patches. Fig. E-42 shows the halo at the surface of bentonite Layer 45. The sensor, which is thicker than one bentonite layer, is located about 10 cm from this layer surface.

After seeing this section, it was decided to perform some additional bentonite sampling in the affected zones, for THG, microbiology and corrosion product analyses. The bentonite blocks in this area were sampled separately for both Layers 46 and 45 and vacuum packed.

Fig. E-43 shows the sensor after bentonite Layer 45 was removed. The visible layer is therefore Layer 44, corresponding to sampling Section 47.

At one corner of the fisurometer, some water inflow is visible (Fig. E-44), affecting the surrounding bentonite. The samples from this area will be dedicated to microbial analysis.

Fig.s E-45 through E-48 show the sampling procedure and final location of the 6 extra bentonite samples. The Shelby tubes were cleaned beforehand with ethanol and subsequently inserted in aluminum bags, flushed with Ar and vacuum packed.



Fig. E-42: Corrosion halo on Section 46 (Layer 45).



Fig. E-43: Fisurometer in bentonite Layer 44 (Section 47) and corrosion halo.



Fig. E-44: Closer view at the fisurometer.
At the top left corner, some water inflow is visible.



Fig. E-45: Drilling a bentonite sample.



Fig. E-46: Inserting a Shelby tube around the drilled core, to protect the sample.



Fig. E-47: Inserting the Shelby tube with help of the drilling machine.



Fig. E-48: Location of the samples around the fisurometer.

E.5 Retrieving metallic coupons (Rack A) in the FEBEX experiment at Grimsel (04/07/2015)

This short note by J. Hadi and P. Wersin (Uni Bern, Rock Water Interaction Group) describes how the four racks A of metallic coupons where retrieved from the experiment on July 1, 2015, and in which conditions they are upon examination. Note that there was about one month in between the heater retrieval (and thus air exposure of the inner liner and the bentonite exposed in the holes) and the excavation of the coupons. The empty liner was closed by a cap and the inner atmosphere monitored for temperature and humidity during this time.

The next scheme indicates where those samples were located in Layer 48 (sample M-S-48-1/2/3/4, i.e. the green squares circled in blue, Fig. E-49):

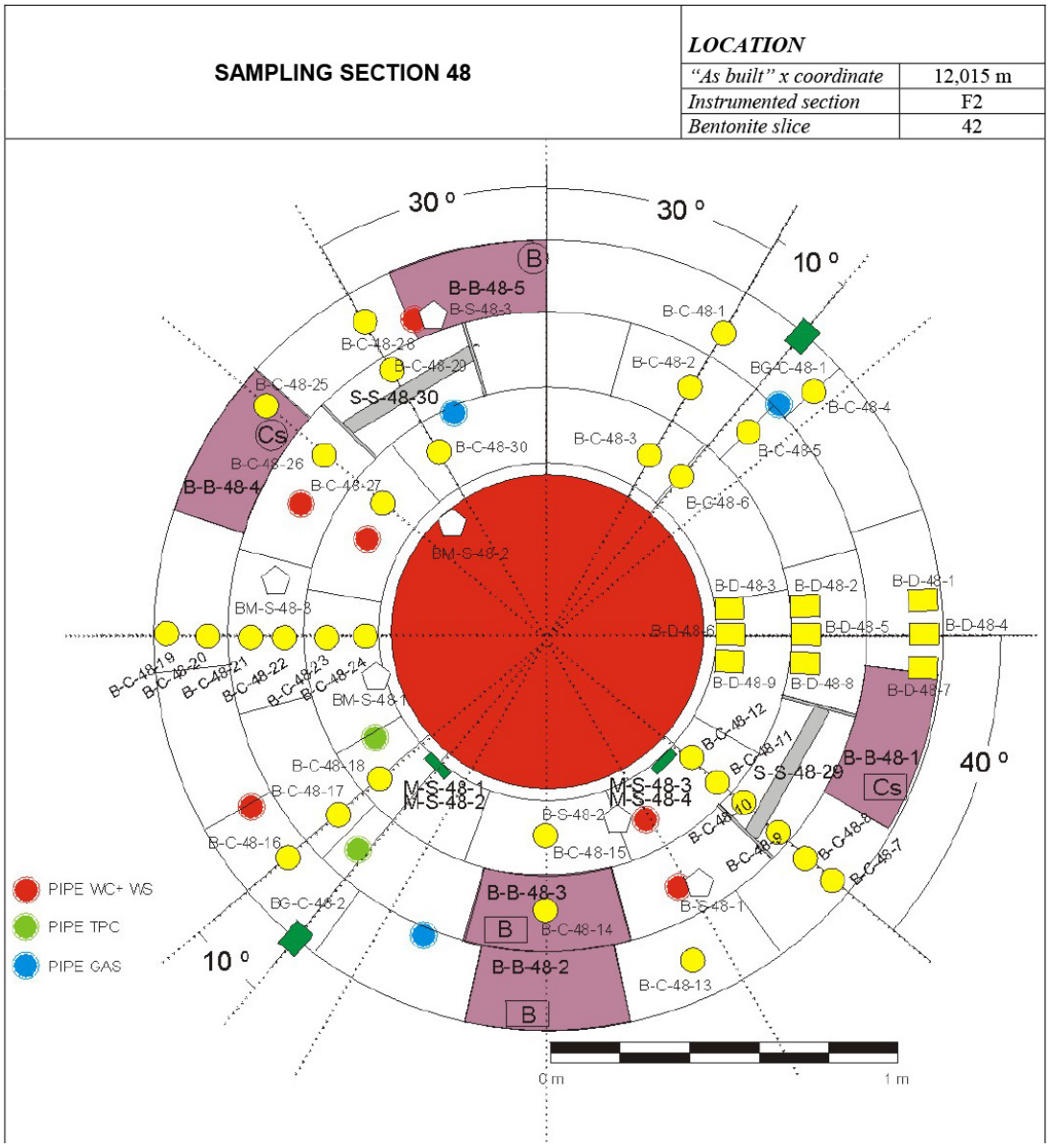


Fig. E-49: Scheme of the sampling plan in Layer 48.

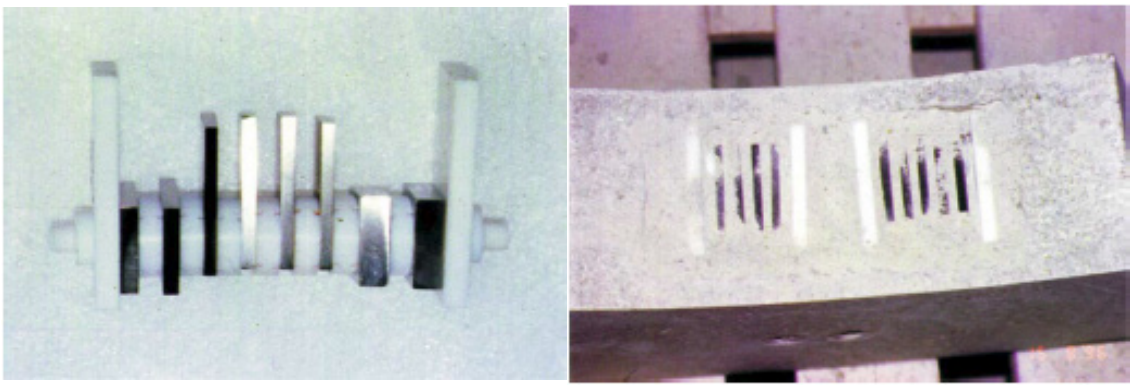


Fig. E-50: Initial set up of corrosion specimens and emplacement in blocks.

The 4 racks were divided in two groups (1A/2A and 3A/4A), which were embedded in two blocks, in the vicinity of the liner. It seems that a rectangular hole was carved in the inner face of each block (in contact with the liner), that the racks were placed in those holes, and that the holes were then filled with powdered bentonite (Fig 1B, ENRESA, PT 12/1998c). Further details can be found in the installation report (ENRESA PT12/1998c). Tab. E-1 indicates what type of material is in each rack:

Tab. E-1: Identification and composition of the 4 racks.

Rack	**Material**	**Type of coupon (and quantity)**						**Total quantity**
1A	Carbon steel TStE355	Base (2)	EBW (1)	PAW (1)	MAG (1)			5
2A	Stainless steel 316L	Base (2)	EBW (1)	FCAW (1)				4
3A	Titanium	Tigr2 (1)	Tigr7 (2)	Tigr12 (2)	Ti2EBW (1)	Ti7EBW (1)	Ti7PAW (1)	8
4A	Copper	Cu 99 % (2)	Cu10Ni (2)	Cu30Ni (1)				5

Carbon steel TStE355 is equivalent to UNE F6215; stainless steel 316L is equivalent to austenitic stainless material with code UNS S31603. EBW stands for Electron Beam Welding, PAW for Plasma Arc Welding, MAG for Metal Active Gas Welding, FCAW for Flux Cored Arc Welding. TiGr2,7 and 12 stands for titanium alloys grade 2 (UNS R50400), 7 (UNS R52400) and 12 (UNS R53400). Copper was either pure (UNS C11000), or a cupronickel alloy 90/10 (UNS C70600) or 70/30 (UNS C71500). All welding was done by INASMET.

E.5.1 Sample collection: Rack A3 and A4 (5 o'clock)

It should be noted that during the dismantling step the bentonite blocks in contact with the liner were relatively dry and could easily fall off as small chunks or even as powder. This made the dismantling more difficult.

Before trying to retrieve the first set of racks (A3 and A4), it was observed that rack A3 with the titanium coupons had been displaced and even damaged, as a single Ti coupon could be observed surfacing out from one hole of the liner into the liner, as shown in the next picture (Fig. E-51).



Fig. E-51: A single Ti coupon surfacing out the hole of the liner.

The operators from Aitemin tried to recover these first two samples by directly drilling into the host block with a pneumatic driller, which, however, fell into small pieces as they were progressing inside it. At some point, pieces of the rack A3 began to appear at the surface and were individually retrieved (Fig. E-52). Rack A3 could only be partially recovered. Two Titanium coupons, two Teflon screws and 1 of the two Teflon outer plates could not be found in the area. Three of the collected Ti coupons were even slightly bent. Fig. E-53 shows what could be recovered from the host block.



Fig. E-52: Another single Ti coupon surfacing from the host block upon digging.
Behind, two single Teflon screws can also be observed.

Ultimately, rack A4 could be retrieved in one piece, only showing minor damage on 1 outer Teflon plate. Although quite dry, some bentonite was still remaining between the Copper coupons.



Fig. E-53: Rack A4 (left) and retrieved pieces from block A3 (right).

It seems that the observed damages are related to a drilling operation back in 2002, where a tube was then placed. Drilling may have affected the racks' position. Rack A4 was slightly pushed to the side, while the driller went through rack A3 and destroyed it, moving all the pieces around.

It seems that the unrecovered parts may have been pushed further into the borehole and may appear upon dismantling further layers. The next picture (Fig. E-54) shows the approximate position of the tube that was further put in the drilled hole.



Fig. E-54: Position of the tube related to the drilling operation which is suspected to have destroyed rack A3.

E.5.2 Sample collection: Rack A1 and A2 (7 o'clock)

The two remaining racks were collected in a more convenient way. The entire host block together with the two racks was extracted, as shown in the next picture (Fig. E-55):



Fig. E-55: Host block with the racks A1 (left) and A2 (right) lying upon it.

As those two racks were loosely lying on the block, they were picked up by hand individually and packed separately. Doing so, the dry layers of clay sticking to the bottom of both racks fell apart as powder. Rack A2 with stainless steel coupons was still quite well surrounded by clay. The next picture (Fig. E-56) shows a bottom view of the rack A2. Only few corrosion pits were observed on the edge of the coupon, and corresponding "rust spots" could be observed in the surrounding clay and on the underlying host block. Concerning Rack A1, a rusty powder fell from the bottom upon picking and was lost in the tunnel (a very small amount, few hundreds of mg).



Fig. E-56: Rack A2 with corrosion pit on the edges of the coupons and sort of corrosion spots in the bentonite.

The host block was collected and packed separately (Fig. E-57). Once the two racks were removed, the underlying block surface did not show any significant impact related to their presence.



Fig. E-57: Top view of host block of rack A1/2 after removal of the racks.

E.5.3 Sample conditions

Rack A1: As shown on figure 6, steel coupons were completely covered with rust. Clay is still present between the coupons, but the underlying (which was quite rusty) and overlying clay was lost.

Rack A2: Stainless steel coupons show some minor corrosion pits on their edges (figure E-56). Clay is still present between the coupons and on top of it (figure E-55). The underlying clay part, showing minor corrosion spots, was lost.

Rack A3: This rack was destroyed and only partially recovered (figure E-53). Two Ti coupons are missing, and may be still present in deeper layers. Three of the recovered Ti coupons were bent. Apart from that, the titanium coupons seem "untouched", no corrosion has been observed visually.

Rack A4: This rack was retrieved in rather good conditions (figure E-53). Clay is still present between the coupons. Concerning corrosion, two groups of coupons can be distinguished: the thick one with dark corrosion products, and a thin one with green corrosion products.

Host block of rack A1 and A2: this sample has been collected and packed. However, it is not of great interest as no visible impact of the presence of the two racks can be observed.

E.5.4 Subsampling prospective

The problem only concerns rack A3: it is already "dismantled", resulting in separate coupons with barely any clay around it. Picking up one of those coupons for any kind of further analysis is not a problem.

For the other three still intact racks, things are more complicated. One has to know in advance what type of analysis is envisioned, especially regarding subsampling. As the clay material is quite dry, it appears difficult to partially dismantle each rack without losing the intercalated clay material, and thus each individual coupon-bentonite interface.

One safe way to maintain the integrity of those racks would be to embed them entirely in epoxy, allowing finer further subsampling. But this would also limit the further analysis to a range of spectroscopic characterizing techniques.

One other way, could be to isolate first a part of the rack with tape, allowing subsampling of the uncovered part without embedding it. This seems, however, much more difficult, as those sample have to be handled with extreme care, and inside a glove box, which further complicates the operation. Also one cannot envision cutting such thick coupons without damaging the rest of the sample.

E.6 Documenting the geological structures in the FEBEX-DP gallery after dismantling (23/09/2015)[6]

This short note illustrates the gallery's granite wall and geological structures (lamprophyres, fractures, veins) within the FEBEX-DP gallery during or shortly after the bentonite buffer dismantling. Thus, it reports only field observation and qualitative impressions. For orientation, the geological structures ("B") are indicated on a geological map produced prior to installation, serving as guidance for location of individual structures. Note that the structure labelled "3" has been covered by plastic in order to avoid "contamination" for any later sampling if requested and the plastic cover has not been taken away for the purpose of this documentation.

Generally, the contact between the bentonite buffer and the granite wall was little developed and the bentonite blocks were removed rather easily. The granite wall appeared in most cases "fresh". Occasionally, remnants of this bentonite layer indicating slicken slides (Harnische) occurred. More details are outlined in individual pictures in "A".

Note also, that grooves – as a result of the TBM drilling of the drift - have not been "filled" by the bentonite or hardly produced a negative in the bentonite blocks despite the high pressures.

The rock wall was not treated by any means since bentonite dismantling. The document does not aim to provide any interpretation.

---

[6] Authored by F. Kober (Nagra) with support from V. Martínez & H. Abóz (Aitemin) and B. Lanyon (Fracture Systems)

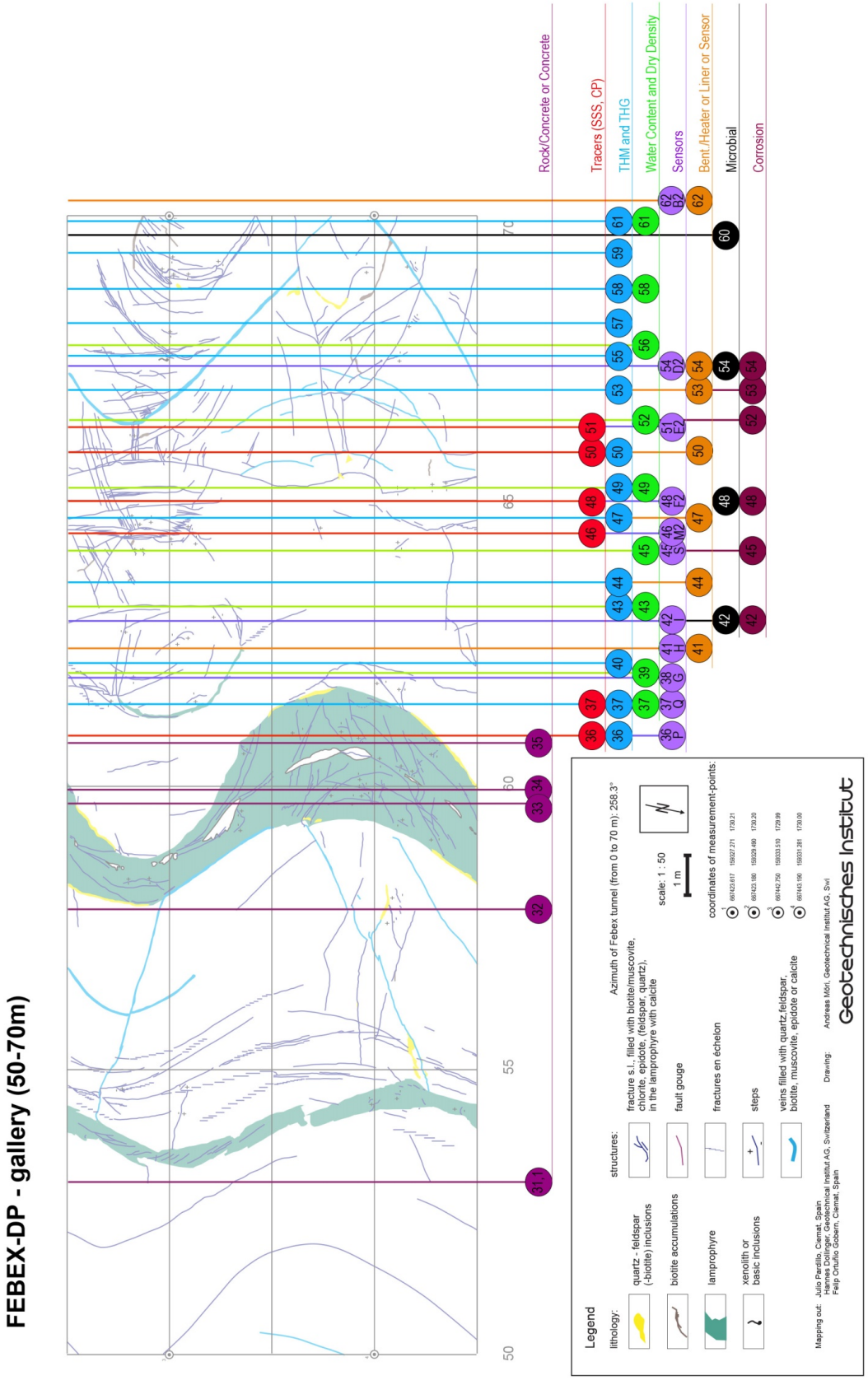


Fig. E-58: FEBEX-DP gallery.

E.6.1 The granite wall during dismantling

E.6.1.1 Section 37



Fig. E-59: Left: Gallery at ~ 3 o'clock, showing interface of granite/lamprophyre and contact to bentonite further to the left. Right: Gallery at ~ 9 o'clock showing the contact shown in further detail under "PART B, structure 5".

E.6.1.2 Section 39



Fig. E-60: Galleries' left side, detail lamprophyre structure under "PART B, structure 5".



Fig. E-61: Detail of wall at ~ 3 o'clock.



Fig. E-62: Close-up of Fig. E-61.



Fig. E-63: Close-up of Fig. E-62.



Fig. E-64: Rock wall surface at ~ 1 o'clock.



Fig. E-65: Close-up of Fig. E-64.



Fig. E-66: Detail of rock wall surface at ~ 10 o'clock.

E.6.1.3 Section 41



Fig. E-67: Detail of rock wall surface at ~ 10 o'clock, to the far right the bentonite surface is visible.

E.6.1.4 Section 43



Fig. E-68: Detail of rock wall and extensometer fixation at ~ 2 o'clock.



Fig. E-69: Detail of rock wall and extensometer fixation at ~ 1 o'clock.

E.6.1.5 Section 45



Fig. E-70: Detail of rock wall at ~ 9 – 11 o'clock.



Fig. E-71: Detail of rock wall at ~ 3 – 5 o'clock.

Note the darker (bentonite block wide – 12.5 cm) band of the just taken off bentonite layer (turning into pale grey after a few hours.



Fig. E-72: Detail of Fig. E-71, showing the darker band to the left, while plastic remnants can be seen between the dark band and the ruler (a plastic foil has been used for water protection measures during construction and remained in the experiment for 18 years) – see below.

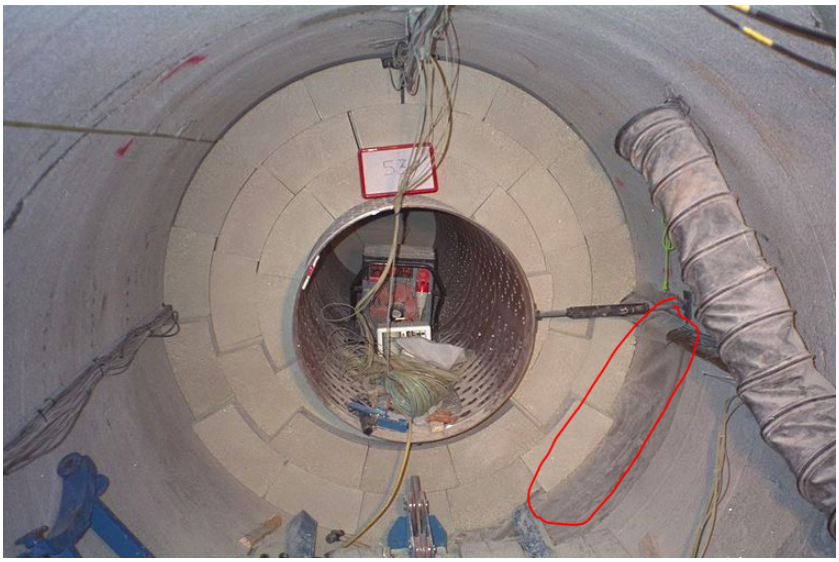


Fig. E-73: Photo taken during the installation showing the plastic foil used for bentonite protection from wet rock wall surfaces.

E.6.1.6 Section 46



Fig. E-74: Photo of the granite wall at ~ 9 – 11 o'clock.

Darker stripes at the granite wall near bentonite Layer 46 are not clear, effects of chiselling or possibly due to the upcoming fissurometer. Also seen are the blueish/greenish colour changes in the bentonite due to the effects of the interactions of the fissurometer with the bentonite

E.6.1.7 Section 47



Fig. E-75: Photo taken from the wall fixation of the fissurometer sensor.



Fig. E-76: Photo taken from the wall fixation of the fissurometer sensor.

E.6.1.8 Section 47/48



Fig. E-77: Photo taken from the left wall, at about 7 – 11 o'clock, just after the fissurometer dismantling.

Also seen are the blueish/greenish colour changes in the bentonite due to the effects of the interactions of the fisurometer with the bentonite.

E.6.1.9 Section 49



Fig. E-78: Left: Photo taken from towards 2 – 3 o'clock, showing a thin layer of bentonite left at the centre above the cable duct. Such thin bentonite layers (covers) seem to have developed in the vicinity of non-granite interfaces, in this case concrete of a total-pressure cell recession. Right: Detail looking into the interface bentonite/granite/ concrete.



Fig. E-79: Detail of Fig. E-78 after removing the thin bentonite layer.



Fig. E-80: Detail of Fig. E-79 with two more bentonite layers removed.

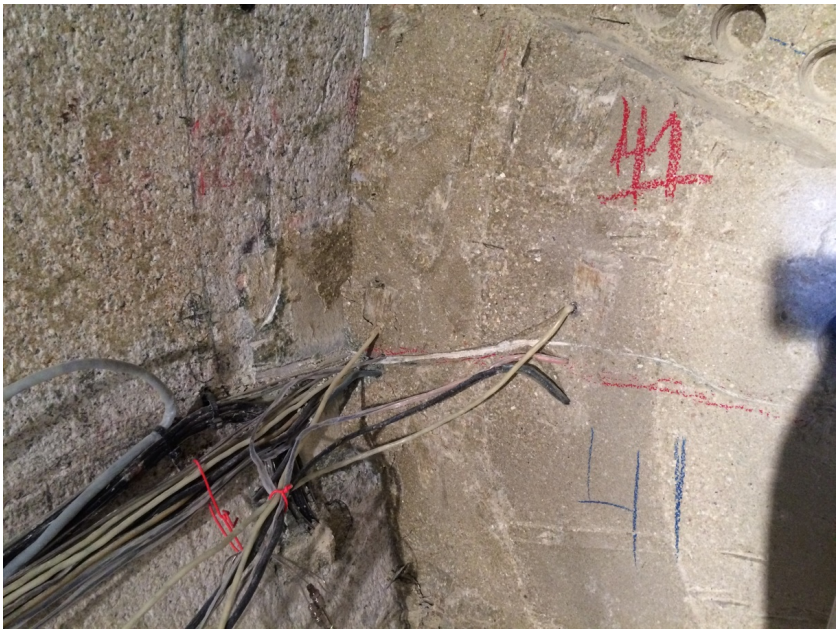


Fig. E-81: Same situation as Fig. E-80 but on opposite wall at 9 o'clock.



Fig. E-82: Same situation as Fig. E-81 but two more bentonite layers removed.



Fig. E-83: Photo of 10 o'clock situation near permanent measure tape, discoloration still related to fisurometer vicinity.

E.6.1.10 Section 50



Fig. E-84: Photo at ~ 10 o'clock, greenish discoloration at bentonite border near iodine paper.



Fig. E-85: Close-up of Fig. E-84.



Fig. E-86: Rock wall at 1 – 5 o'clock.



Fig. E-87: Detail rock wall(pressure sensor/bentonite wall, back part of Fig. E-86.

E.6.1.11 Section 52



Fig. E-88: Photo towards 10 o'clock.

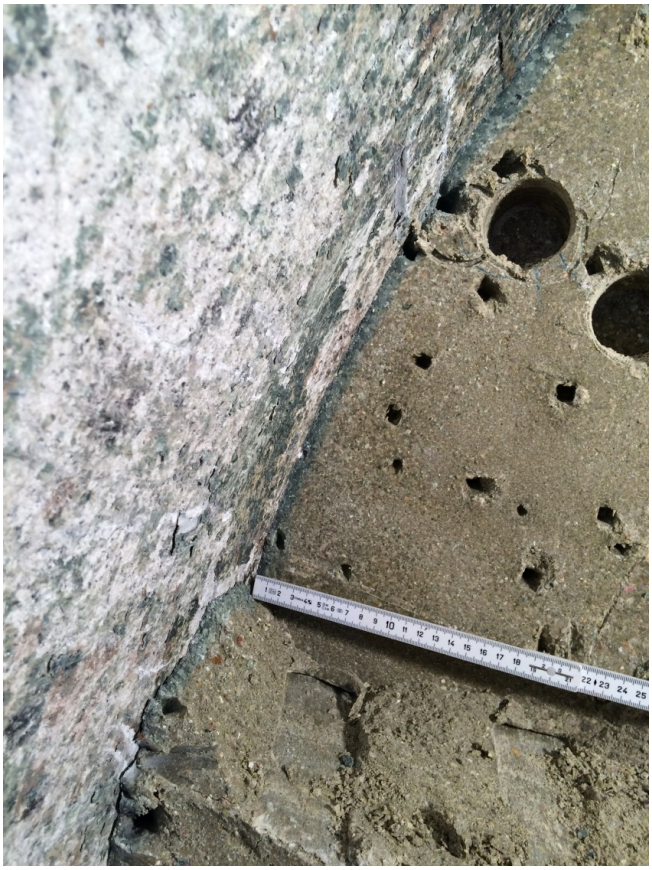


Fig. E-89: Detail rock Fig. E-88, lower part.

E.6.1.12 Section 53



Fig. E-90: Left: Photo towards 9 – 11 o'clock, upper part. Right: photo towards 8 – 11 o'clock, lower part.

E.6.1.13 Section 59



Fig. E-91: Rock wall taken at height of Section 51 at 3 o'clock.



Fig. E-92: Rock wall at 9 o'clock, see also structure "1" in PART B.



Fig. E-93: Rock wall at ~ 8 – 10 o'clock, see also structure "1" in PART B.



Fig. E-94: Detail rock wall at 10 o'clock.

E.6.1.14 Section 62



Fig. E-95: Rock wall at ~ 10 o'clock, with the end of the gallery seen already.



Fig. E-96: Detail of Fig. E-95.



Fig. E-97: Rock wall at 2 o'clock.



Fig. E-98: Rock wall at 3 o'clock.
Dark discolorations likely due to cable fixations.



Fig. E-99: Detail of rock wall at 10 o'clock.



Fig. E-100: Detail of rock wall at 12 o'clock.



Fig. E-101: The last ~ 2 m of the gallery between 1 – 5 o'clock.
Stripes on the wall represent bentonite block width.

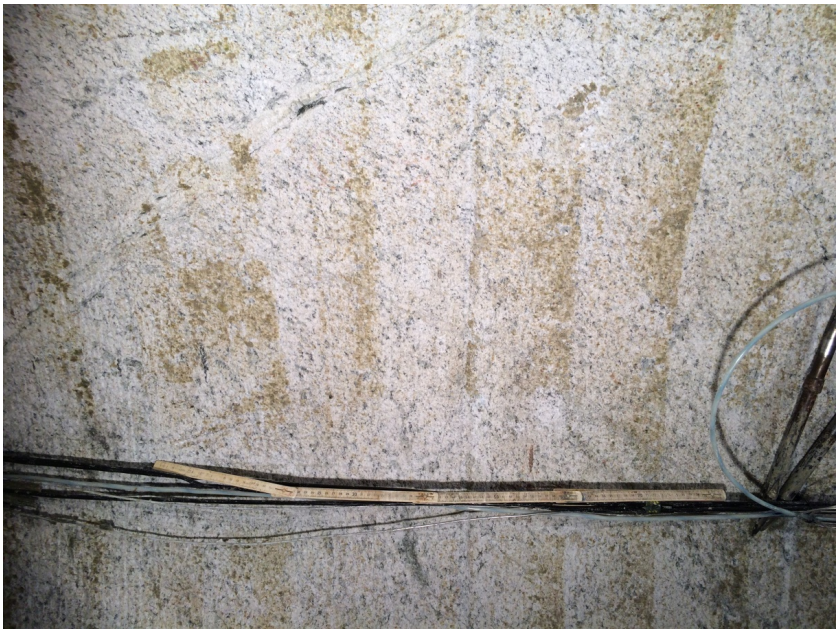


Fig. E-102: Detail of Fig. E-101.



Fig. E-103: Detail of Fig. E-102.



Fig. E-104: Rock wall from 2-12-9 o'clock (top line, view towards entrance of gallery).



Fig. E-105: Rock wall at 9 – 11 o'clock.



Fig. E-106: Detail of Fig. E-105.



Fig. E-107: Rock wall between 7 and 10 o'clock.
The structure to the left is equal to structure "1" in PART B.



Fig. E-108: Detail of rock wall at 11 o'clock.



Fig. E-109: Detail of rock wall at 11 o'clock with all bentonite removed.



Fig. E-110: Image of the central total pressure sensor at the conical end of the drift.



Fig. E-111: Left total pressure cell at the gallery end at 9 o'clock.



Fig. E-112: Oblique view to the left total pressure cell at the gallery end at 9 o'clock. This showed some constant water flux.



Fig. E-113: Lower part of the left total pressure cell at the gallery end at 9 o'clock. This showed some constant water flux.

E.7 Sampling the plug-concrete/rock (C/R) interface by stabilised overcoring – sample splitting and distribution (05/10/2015)[7]

E.7.1 Status

We, Obayashi, performed simple overcore sampling for recovering of C/R interfaces at the FEBEX area in GTS from 21 – 23.09.2015. The recovered cores are currently being processed at the Obayashi R&D by CT-XRD.

E.7.2 Location of boreholes (overview)

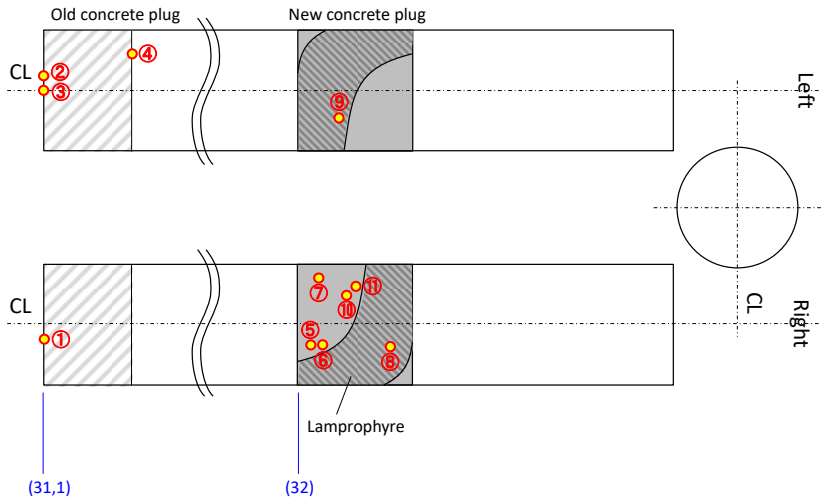


Fig. E-114: Overview of borehole locations.

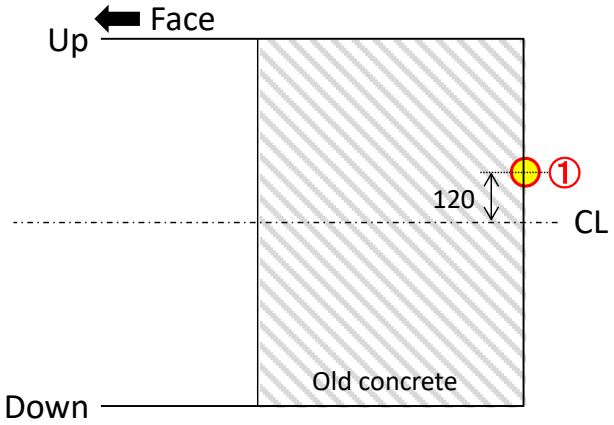
[7] Authored by Masao Uyama, Takashi Hitomi, Obayashi Co.

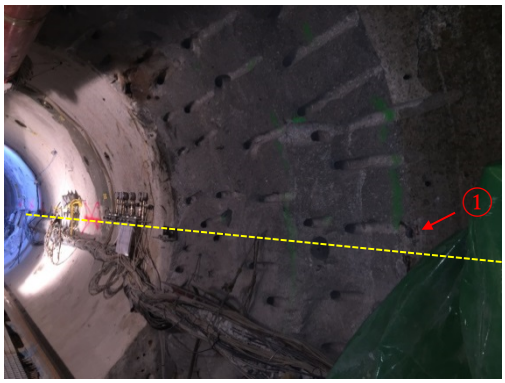
E.7.3 Location of boreholes (detail)

(1) Old Concrete Area

- **Drilling No.①**

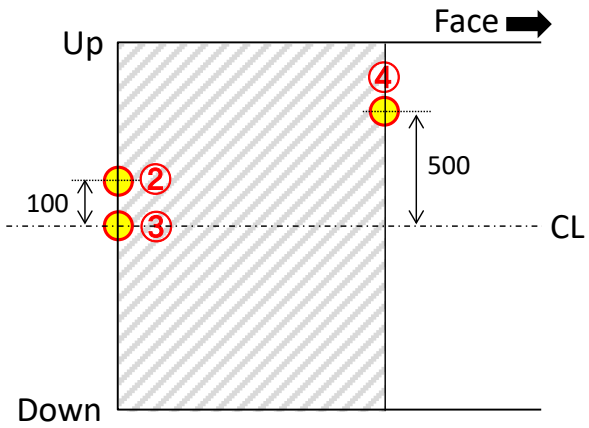
〔Right Side〕

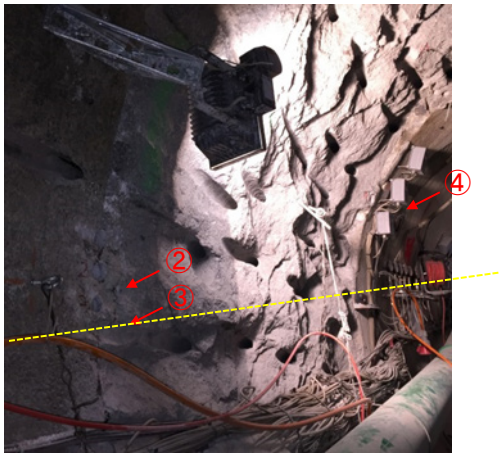




- **Drilling No.②③④**

〔Left Side〕

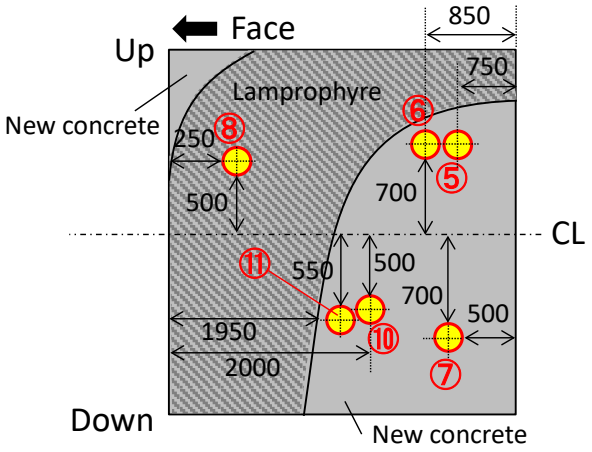


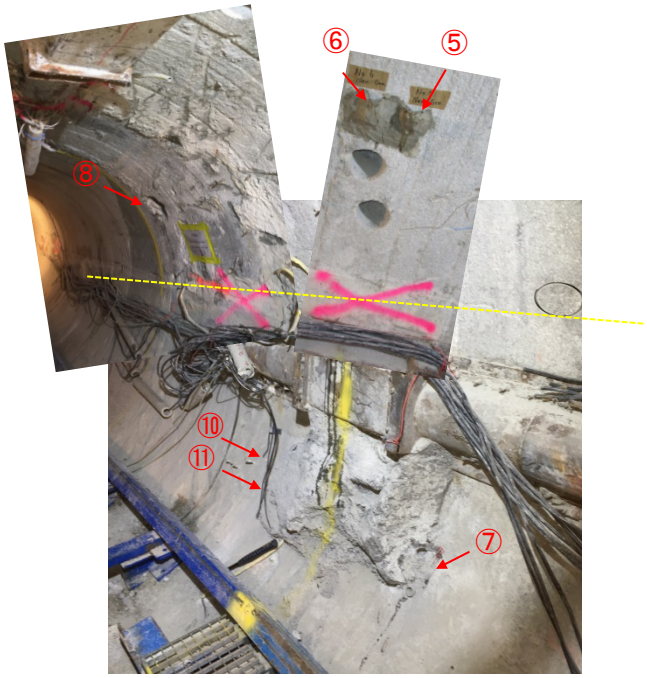


(2) New Concrete Area

- **Drilling No.⑤⑥⑦⑧ & ⑩⑪**

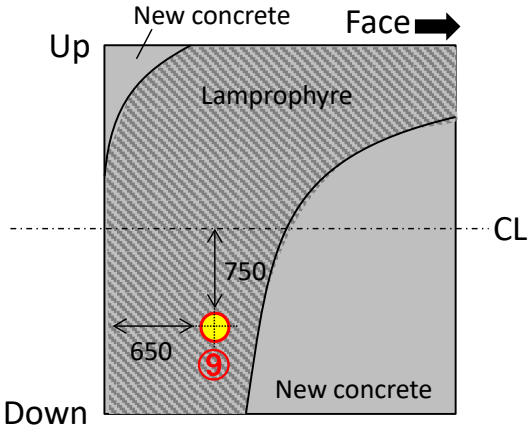
〔Right Side〕





- **Drilling No.⑨**

〔Left Side〕





E.7.4 Drilling situation

Originally, it was planned to drill a guiding hole of 20 mm in diameter, stabilising it with resin and overcoring it later by drilling a 25 mm-hole with a hand drilling machine. However, this original plan was abandoned, since the test cores/samples were recovered in unfavourable conditions. This is due to the fact that the concrete plug was exposed to dry condition for a longer time after dismantling (?), but also due to the dismantling activities that created many cracks by chipping and hammering. Therefore, the coring plan was changed to using only the 25 mm drill bit, filling the gap produced from the drill bit with resin (Sika) and overcoring the C/R interface after hardening the next day with the same diameter. The resin stabilized the sample sufficiently despite using the same drill bit diameter.

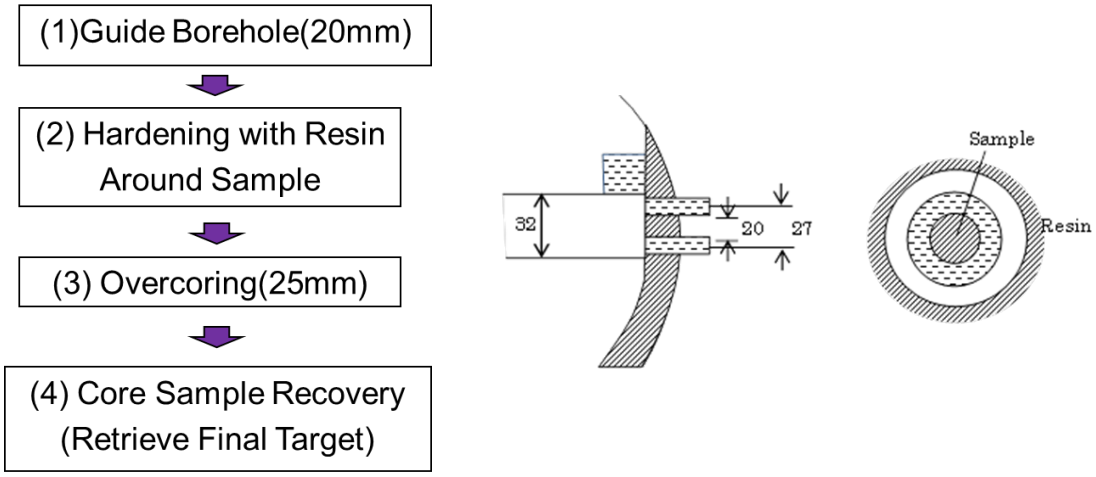


Fig. E-115: Originally planned sampling procedure.

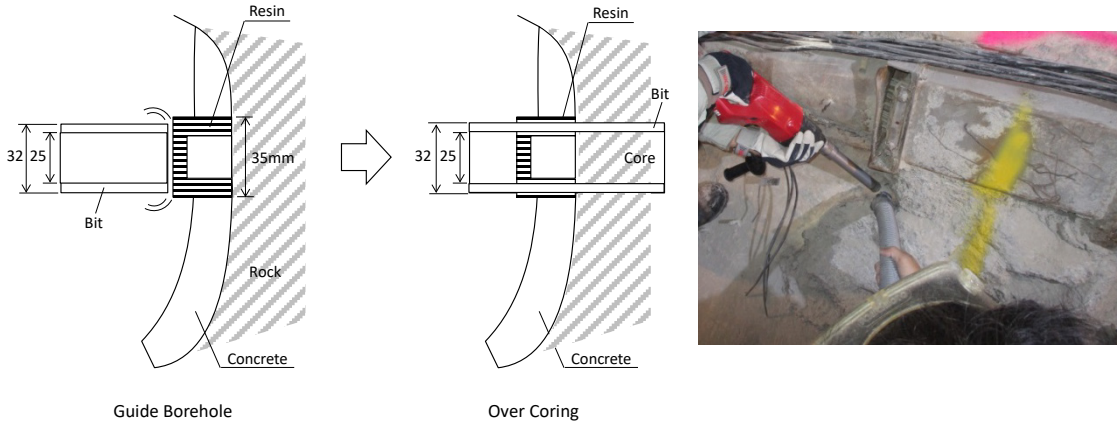


Fig. E-116: Finally applied sampling procedure.

E.7.5 Sampling result

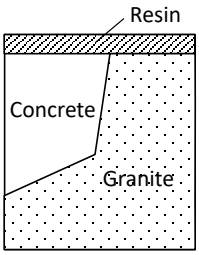
The result of sample recovery is shown in Tab. E-2 and the images below. While the area of an intact C/R interface is rather small, the obtained samples are considered suitable for CT-XRD analysis since the required size is only about "3.5 × 3.5 mm, L = 5 mm".

Tab. E-2: Sampling results.

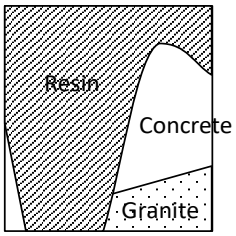
Drilling No.	Sample No.	Result	Remarks
①	CG-C-31,1-OB1	○	OLD concrete
②	CG-C-31,1-OB2	○	
③	CG-C-31,1-OB3	○	
④	CG-C-31,1-OB4	○	
⑤	CG-C-32-OB5	○	NEW concrete (Granite)
⑥	CG-C-32-OB6	×	
⑦	CG-C-32-OB7	×	
⑧	CL-C-32-OB8	○	NEW concrete (Lamprophyre)
⑨	CL-C-32-OB9	○	
⑩	CG-C-32-OB10	×	NEW concrete (Granite)
⑪	CG-C-32-OB11	○	

＜Drilling No.①（CG-C-31,1-OB1）＞

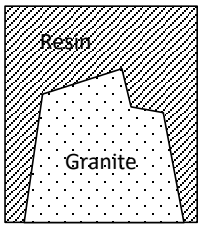




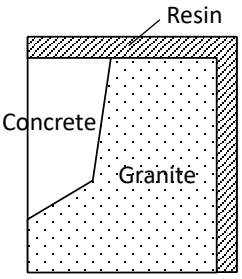






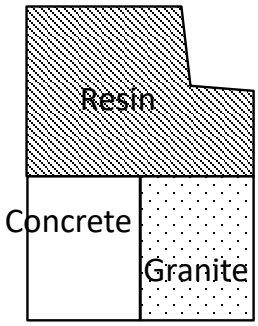






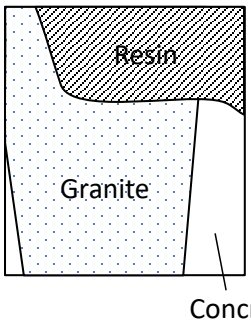
＜Drilling No.②（CG-C-31,1-OB2）＞





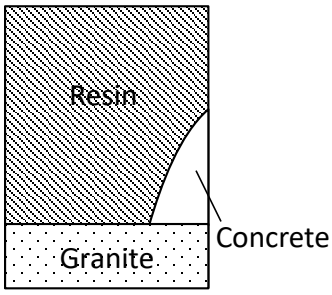
＜Drilling No.③（CG-C-31,1-OB3）＞





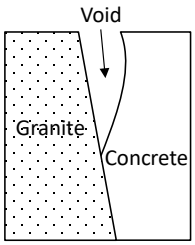
＜Drilling No.④（CG-C-31,1-OB4）＞



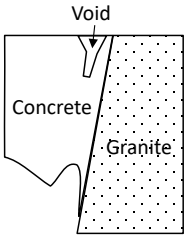


＜Drilling No.⑤（CG-C-32-OB5）＞



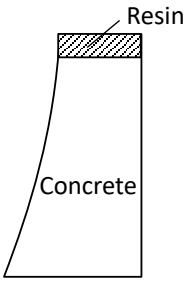






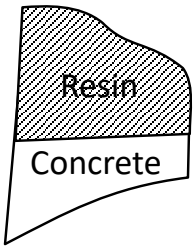
＜Drilling No.⑥（CG-C-32-OB6）＞





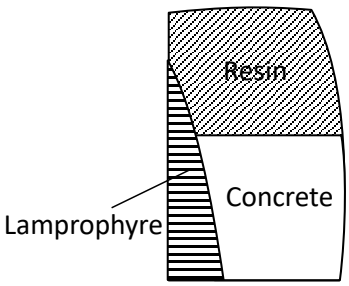
＜Drilling No.⑦（CG-C-32-OB7）＞





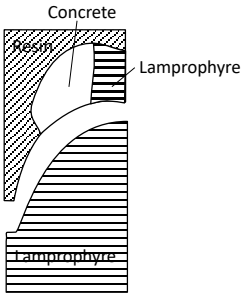
＜Drilling No.⑧（CL-C-32-OB8）＞



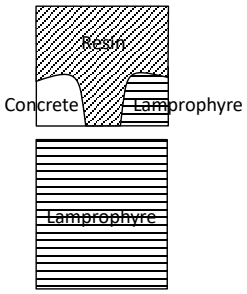


＜Drilling No.⑨（CL-C-32-OB9）＞



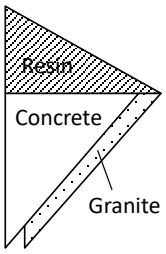




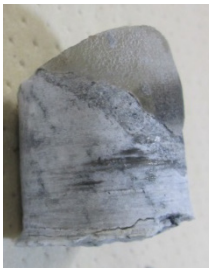


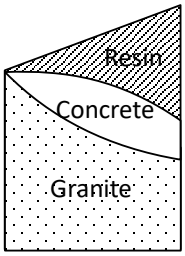
＜Drilling No.⑩（CG-C-32-OB10）＞

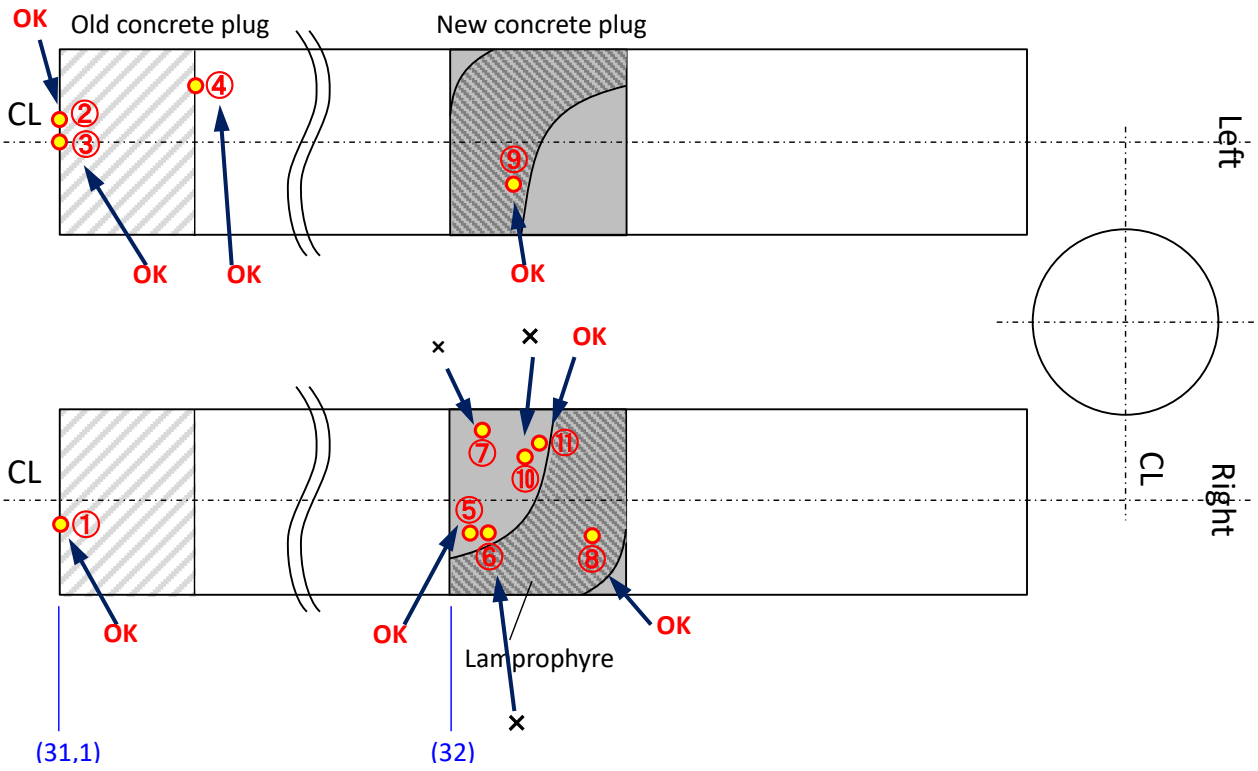




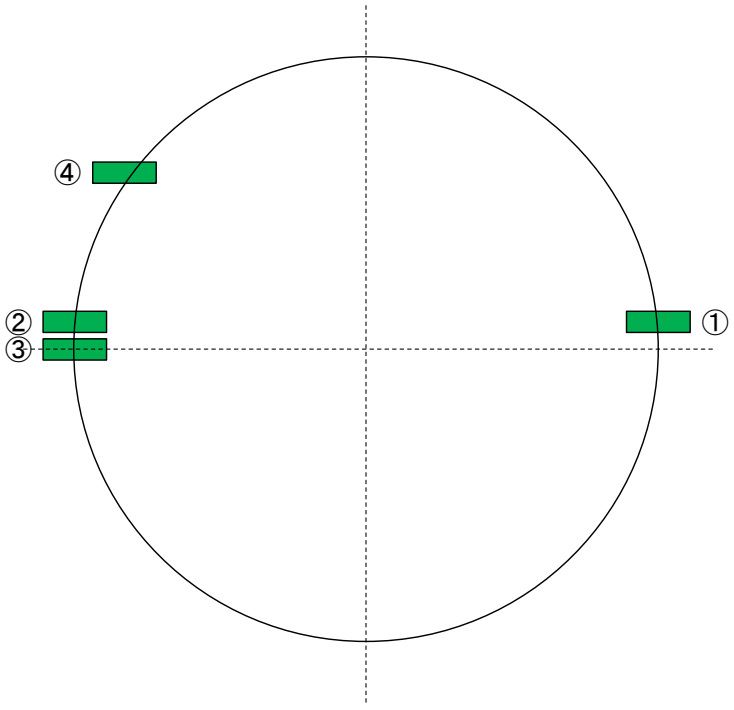
＜Drilling No.⑪（CG-C-32-OB11）＞



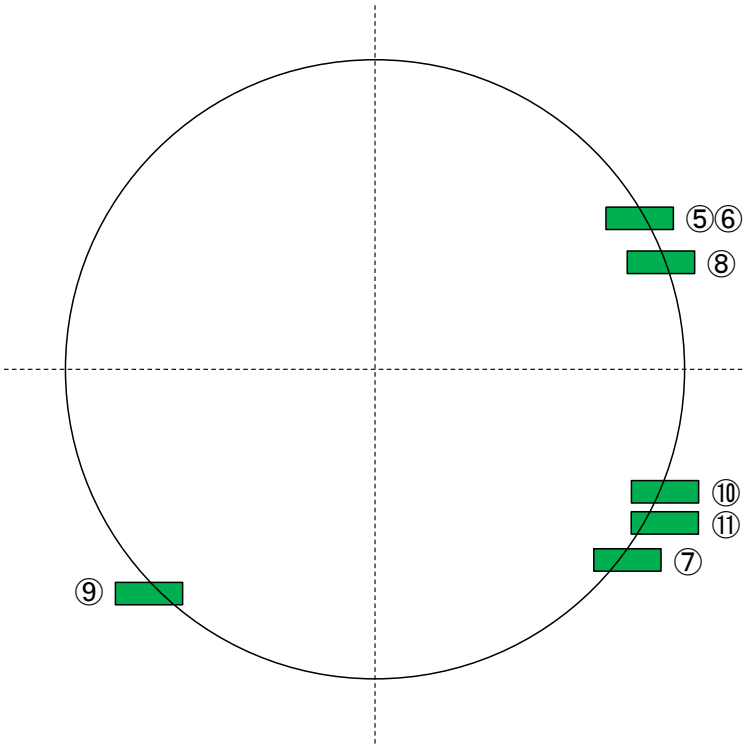




Sampling Section 32



Sampling Section 31,1



Sampling Section 32

E.8 Documenting the dummy-liner bentonite fillings

This short note illustrates the appearance of the dummy-liner-bentonite fillings. This is in addition to the documents that can be found for Section 39, which reported the dummy removal (www.grimsel.com → FEBEX-DP members' area, Section 39).

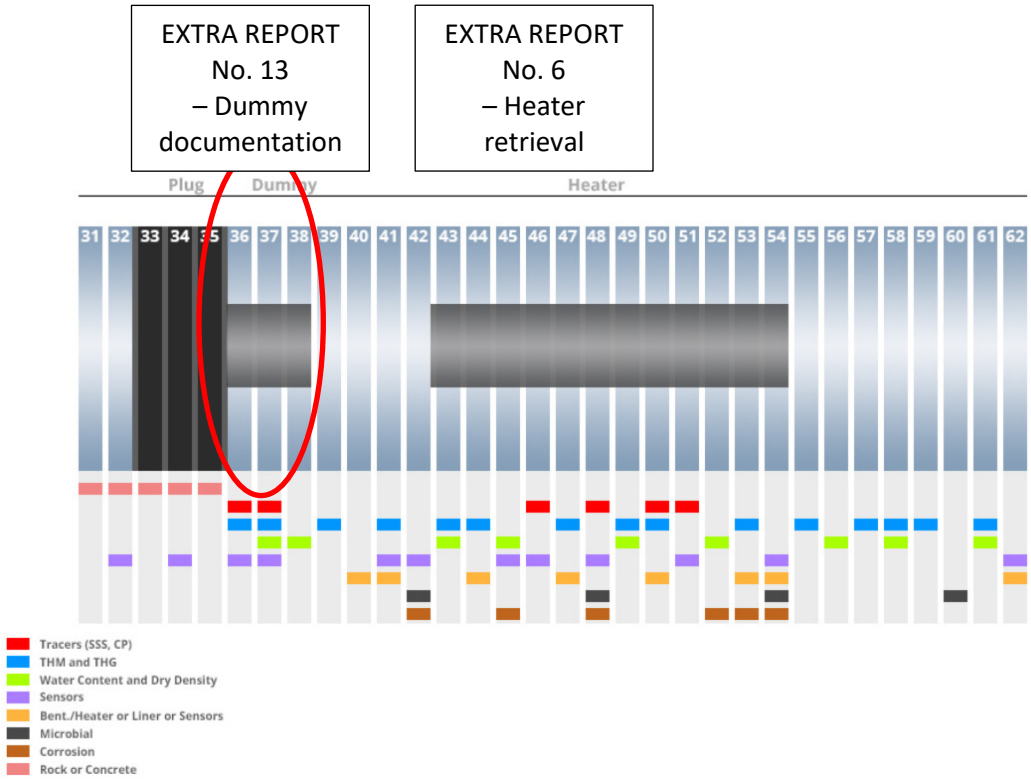


Fig. E-117: The FEBEX-DP experiment with dummy (void of the first FEBEX heater) and the second heater.

The dummy, a 1m long steel drum which filled the void left from the first FEBEX heater, was emplaced in 2002. The history of the buffer region in the dummy section (see Fig. E-114) is threefold:

- 1997 – 2002 **heating** to 100 °C-
- Subsequent **cooling** of the area in 2002, removal of heater 1, emplacement of dummy and closing of the experiment
- During the **remaining time between 2002-2015 the area was at temperatures of 30 – 40 °C** (see sensor report "AN 14 363 Sensors Data Report no 8 FEBEX in situ", this document can be downloaded at www.grimsel.com → FEBEX-DP members' area).

A constructional gap between the liner and the dummy existed after Heater 1 removal and emplacement of the dummy (Fig. E-115). An inspection of this part after the FEBEX-DP dismantling was performed and revealed that the gap was completely filled with bentonite (Fig. E-118. Note that between the dummy-liner removal (as one block) on May 26th, 2015, and the inspection on October 21st, 2015, several months passed by in which the dummy-liner was only simply covered by a plastic foil and stored in the main GTS access tunnel.

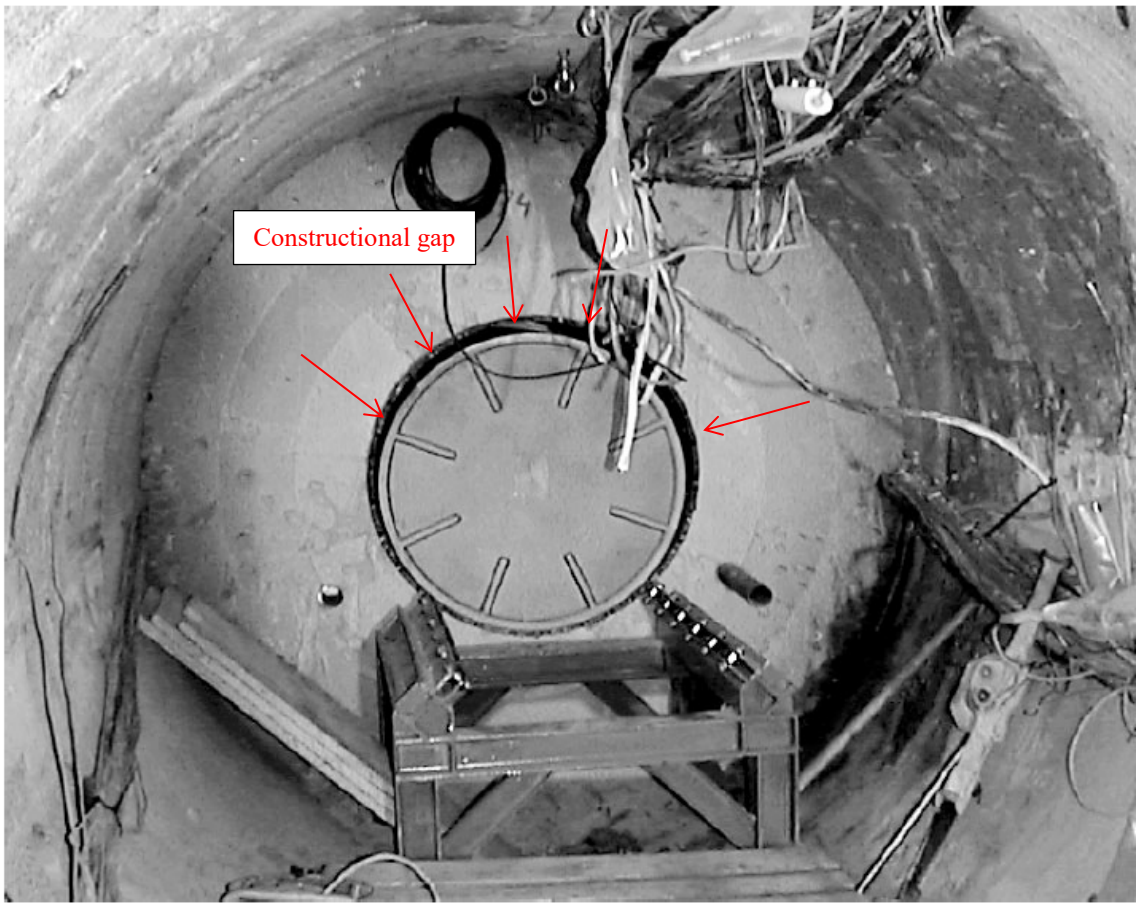


Fig. E-118: The constructional gap between the liner and the dummy (image: The FEBEX-DP experiment with dummy (void of the first FEBEX heater) and the second heater – Fig. 39: ENRESA2003-PT 09-2003-Dismantling of the heater 1 at the FEBEX in-situ test).

From observations, this bentonite must have derived from the bentonite blocks surrounding the dummy by swelling into the perforated liner and the space in between. The bentonite in the gap is rather dense and still "wet", compared to the bentonite that was swelling into the gap between the liner and heater 2 (Fig. E-119; and see also Section E.2 – Documenting the heater retrieval)

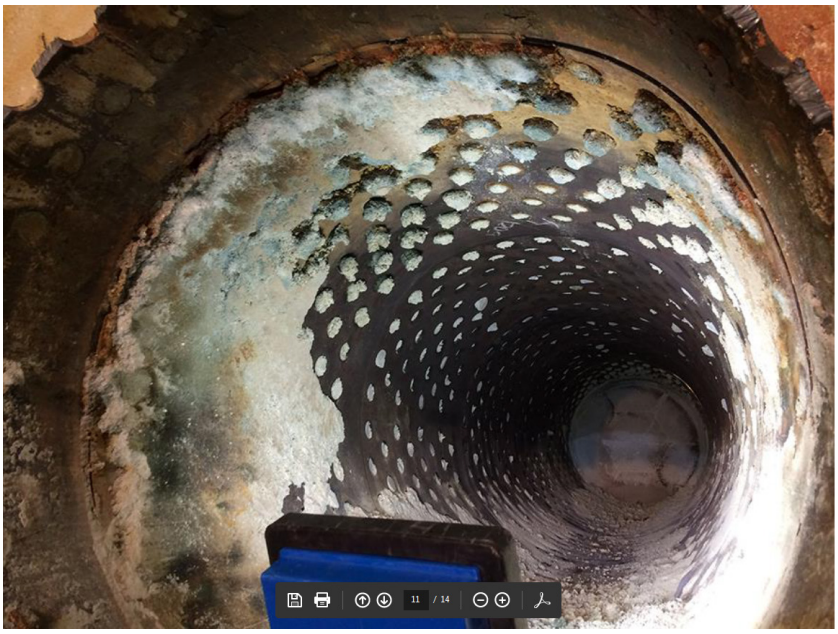


Fig. E-119: The liner after removal of heater 2 for comparison.

Note the bentonite protrusion (2 – 4 cm) into the liner, a spatially extensive bentonite cover in the frontal part (~ 2 cm thickness) with a similar extensive layer (~ 30 – 50 cm in length) of bentonite was found at the end of the heater. Towards the centre a transition to disconnected protrusions was formed. After ~ 1 m into the liner of the heater section almost no bentonite protrusions were observed (see Section E.2).

Some remarks:

- Note that when the liner was cut for inspection and documentation, the tension relieve of the liner caused a new gap, visible in photographs (e.g. Fig. E-151), which is not real with respect to bentonite filling discussed here.
- This documentation repeats some images from the dismantling of the relevant sections in May 2015 (details in www.grimsel.com → FEBEX-DP members' area).
- The document does not aim to provide any interpretation.



Fig. E-120: The dummy-liner during dismantling – front view.



Fig. E-121: The dummy-liner during dismantling – top view.



Fig. E-122: The dummy-liner during dismantling – front view.



Fig. E-123: Perforated liner (from bottom) with bentonite filled holes and scrapped off bentonite (dark holes in front).



Fig. E-124: Above: end of dummy (above) towards heater, right – end of dummy with one bentonite block layer.



Fig. E-125: Right: end of dummy (above) towards heater, right – end of dummy with one bentonite block layer .



Fig. E-126: Frontal part of dummy.



Fig. E-127: Detail of frontal part of dummy, the deformation at 2 o'clock must have been existing during the second phase as it is equally filled with bentonite, see Fig. E-128.



Fig. E-128: Detail of frontal part of dummy still in place in the experiment with bentonite infill as discussed in Fig. E-127.



Fig. E-129: Frontal part of dummy towards the "lifted" (due to cutting of the liner and stress release).



Fig. E-130: Detail of Fig. E-129.



Fig. E-131: Back part of dummy.



Fig. E-132: Close up of Fig. E-131.



Fig. E-133: Close up of Fig. E-131.



Fig. E-134: Dummy back part with liner cut before cleaning off bentonite.
Blackish parts in front are from plasma cutting.



Fig. E-135: Dummy back part with liner cut after cleaning off bentonite and cutting fresh surfaces.



Fig. E-136: Detail of Fig. E-135.



Fig. E-137: Detail of Fig. E-135.



Fig. E-138: Dummy top view towards 9 o'clock.



Fig. E-139: Cut liner segment with discolored bentonite still adhered to the liner.



Fig. E-140: Same as Fig. E-139.



Fig. E-141: Detail of Fig. E-139.



Fig. E-142: Detail of Fig. E-139.



Fig. E-143: Detail of Fig. E-139.

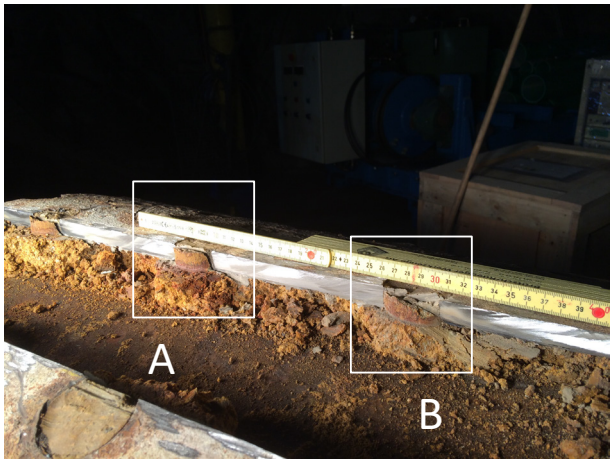


Fig. E-144: Dummy-liner towards 3 o'clock.



Fig. E-145: Detail of Fig. E-144, showing a bentonite protrusion into the liner – dummy gap.



Fig. E-146: Detail of Fig. E-144, showing a bentonite protrusion into the liner – dummy gap.



Fig. E-147: Detail of Fig. E-146, after making a fresh cut.

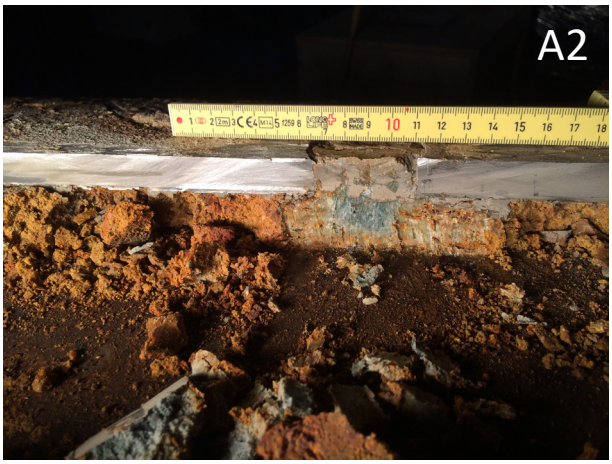


Fig. E-148: Detail of Fig. E-146, after making a fresh cut.

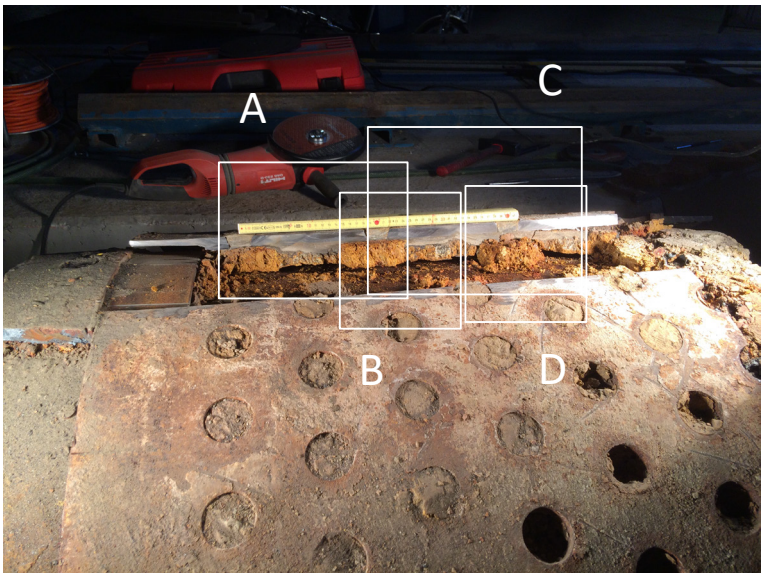


Fig. E-149: Dummy-liner towards 9 o'clock.



Fig. E-150: Detail of Fig. E-149, Section A.



Fig. E-151: Detail of Fig. E-149, Section B.



Fig. E-152: Detail of Fig. E-151.



Fig. E-153: Detail of Fig. E-149, Section C.



Fig. E-154: Detail of Fig. E-149, Section D.



Fig. E-155: Detail of Fig. E-149, Section D.



Fig. E-156: Detail of Fig. E-154, with a fresh cut into the protrusion.



Fig. E-157: Looking towards 9 o'clock on the surface that was at the dummy and was "lifted" after the tension relieve after liner cutting (thus gap artificial).

Near "A" in Fig. E-149.

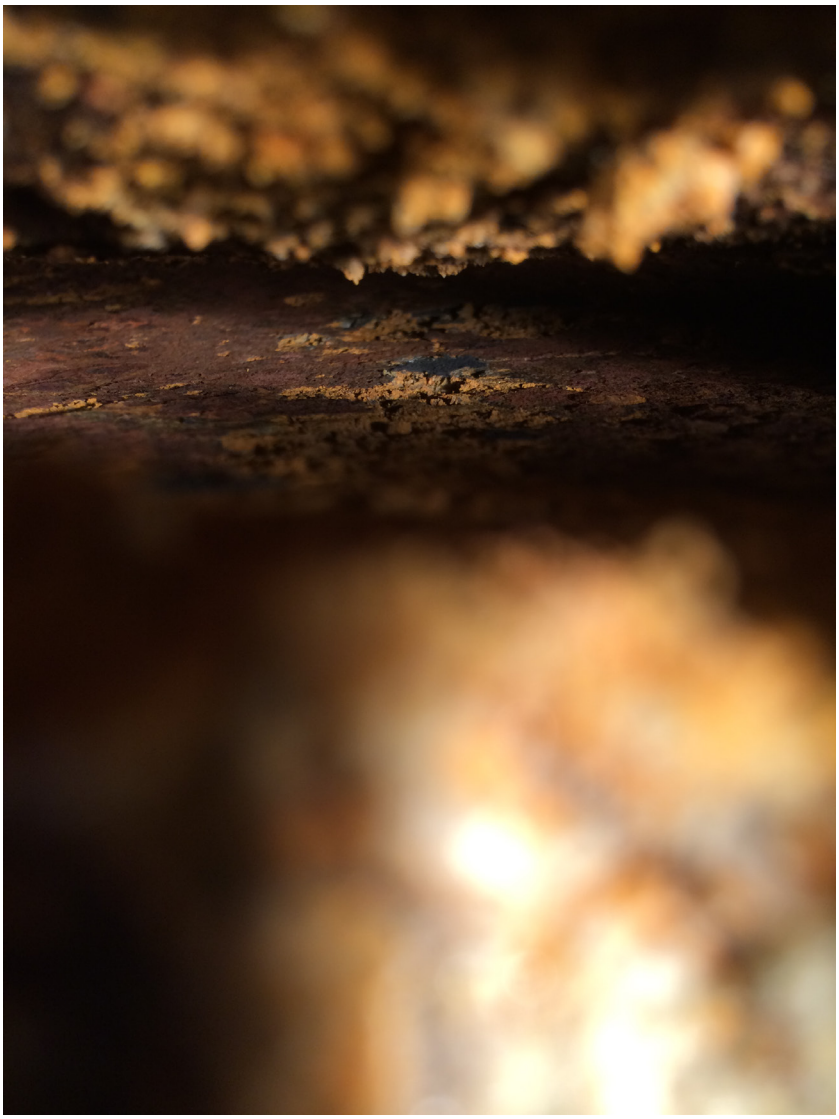


Fig. E-158: Same as Fig. E-Fig. E-157.

Appendix F: GTS Phase VI – FEBEX-DP hyperspectral scanning for patterns of near-surface water content (August 2015)[8]

F.1 Abstract

This report studies the feasibility of using a SWIR (Short Wave InfraRed) hyperspectral camera to measure the near-surface water content of bentonite.

We show that this technology is indeed suitable, and give a formula to estimate the volumetric water content given the spectrum of a pixel.

This report is structured in the following way:

- Part F.2 shows the scanned data, and evaluates the quality of the calibration.
- Part F.3 describes a small laboratory measurement using a sample of bentonite, which suggests a method of identifying the water content of bentonite.
- Part F.4 shows the results on the scans shown in part F.3 obtained using this method.
- Part F.5 concludes.

Throughout this document, we will use the following notations:

- x, y position (in pixel)
- λ wavelength (in nanometers)
- t time (in second)
- $m(x,y,\lambda)$ is the calibrated intensity at position (x,y) at wavelength λ
- For any function, the parameter is omitted when it does not vary (i.e. we do not write x when we work on a vertical line).
- If a parameter varies, and is omitted, we instead mean the value evaluated at all omitted parameters values. For example: $m(x,y)$ is the whole spectrum at the point (x,y) (which can be seen as a function $s(\lambda)=m(x,y,\lambda)$, with x,y fixed).

[8] Authored by Laurent Fasnacht, Philip Brunner, Philippe Renard – CHYN, Université de Neuchâtel.
Jens K. Becker – Nagra



Fig. F-1: Image of the studied area.

F.2 Scanned data and calibration

First, the results of the calibration process will be presented, then the scans, and finally a quick analysis will be made.

F.2.1 Experimental setup and calibration process

We use a SPECIM SWIR hyperspectral camera, which is able to measure 256 wavelengths, from 937.06 – 2'539.77nm, on a vertical line of 320 pixels. A mirror scanner, controlled by a stepper motor, is attached to the camera in order to be able to do 2D scans.

The scene is illuminated using two halogen lamps, connected through a Variac, which enable us to vary the light intensity.

As the non-uniformity correction provided by the manufacturer is not satisfactory (quality is not good enough, and it's not suitable for long integration times), we use our own novel calibration process, which is targeted at improving the smoothness of the output picture.

Unfortunately, since the temperature was quite low in the underground laboratory, the calibration step was not precise enough, we had to apply a second step, which basically consists of adding an offset to each pixels in order to smooth the pictures, and also masking some invalid data.

F.2.2 Calibration results

To evaluate the calibration process, the fifth scan will be used, at 10ms integration time. The calibration of the camera was done on the 15th of August 2015, very early in the morning, in order to have similar temperature conditions.

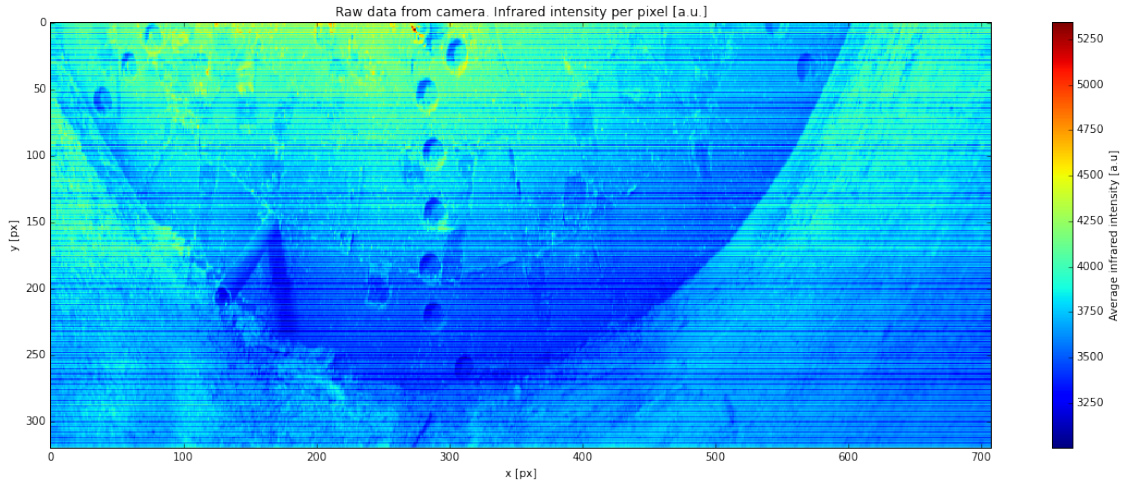


Fig. F-2: Raw data.

As we can see, the result is not usable. After calibration, the results are significantly improved:

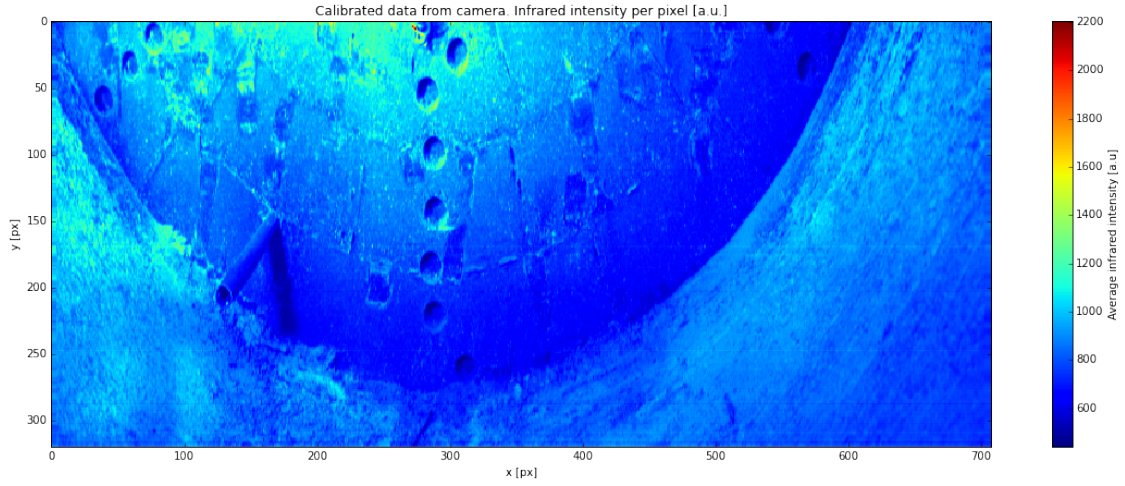


Fig. F-3: Calibrated data.

The results are already a lot more uniform. However, there are still horizontal lines. A causal analysis has shown that:

1. The temperature of the camera has a big impact on the sensor, and should be taken into account.
2. There are bad pixels (which can be interpolated by using the pixels above and below).

3. There are issues with the calibration at some wavelengths:
    - At 962 nm
    - Between 1'167 nm and 1'218 nm
    - Above 2'410 nm

A second step was applied, in order to fix these issues. This improves the quality of the results a lot, as we can see below (Fig. F-4). Note that there are no lines left on the full picture.

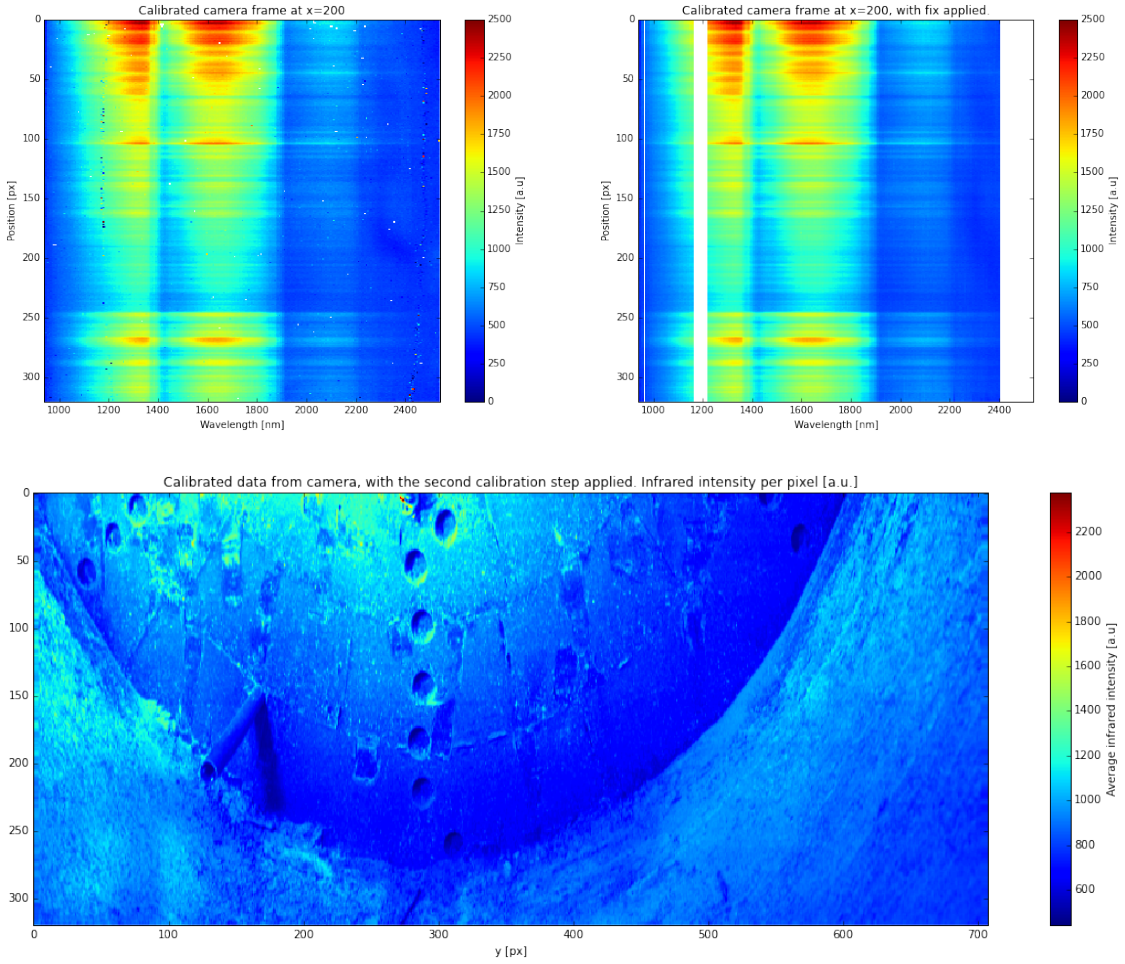


Fig. F-4: Calibrated data after applying the second calibration step.

The following plot (Fig. F-5) shows that the calibration reduced the variance for each wavelength. It could either be because we lost some information, or because the noise (bad pixels, bad calibration) is smaller. In this case, it is very likely that it is only the noise that was removed, mainly because we do not have huge peaks anymore, but still have the general shape.

This plot also suggests that the interesting regions are likely to be around the maximums at 1'300 nm and 1'600 nm.

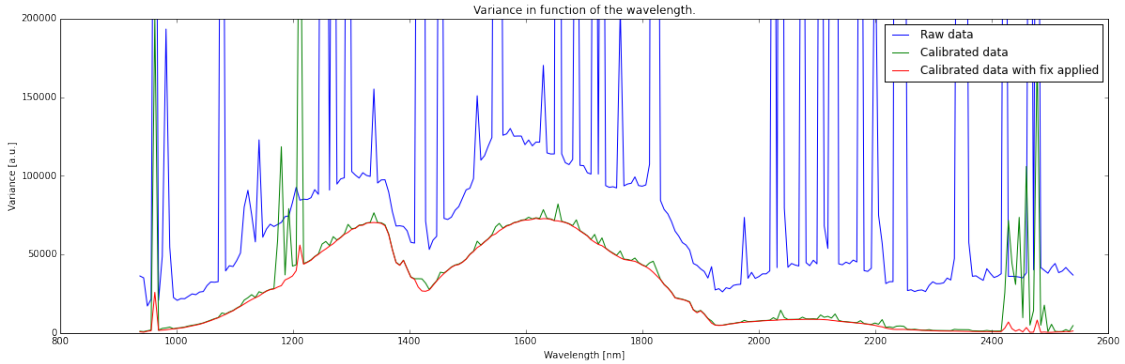


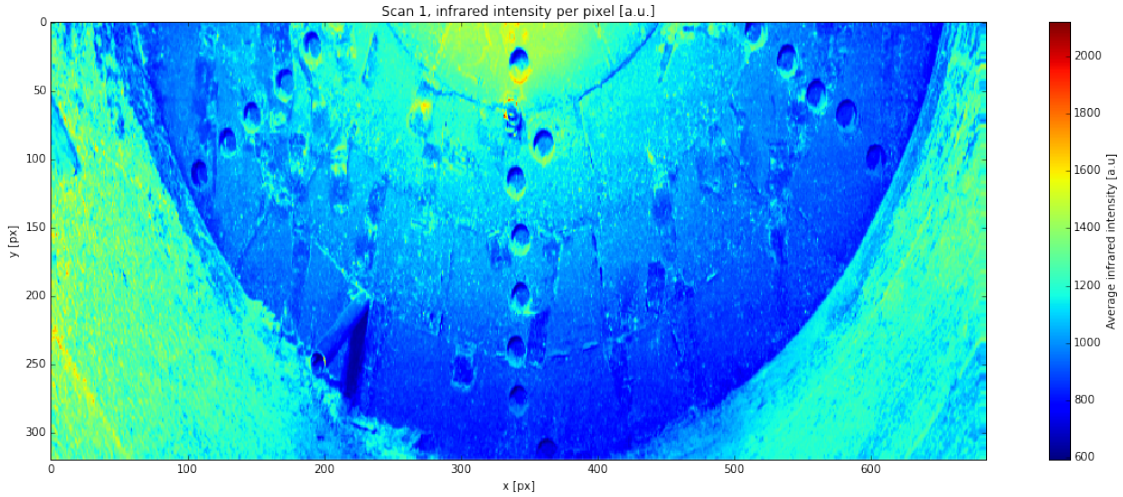
Fig. F-5: Variance in function of wavelength.

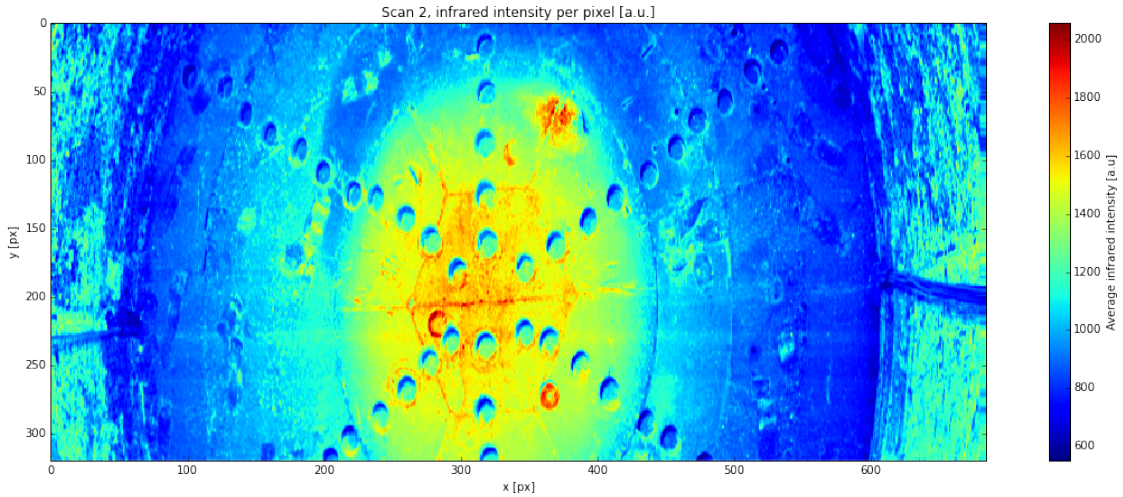
F.2.3 Scans

Five different scans were made:

- Scan 1 – 3 were made with low illumination.
- Scan 4 and 5 were made with higher illumination.

The average pixel intensity of the calibrated image of all these scans is shown hereafter.





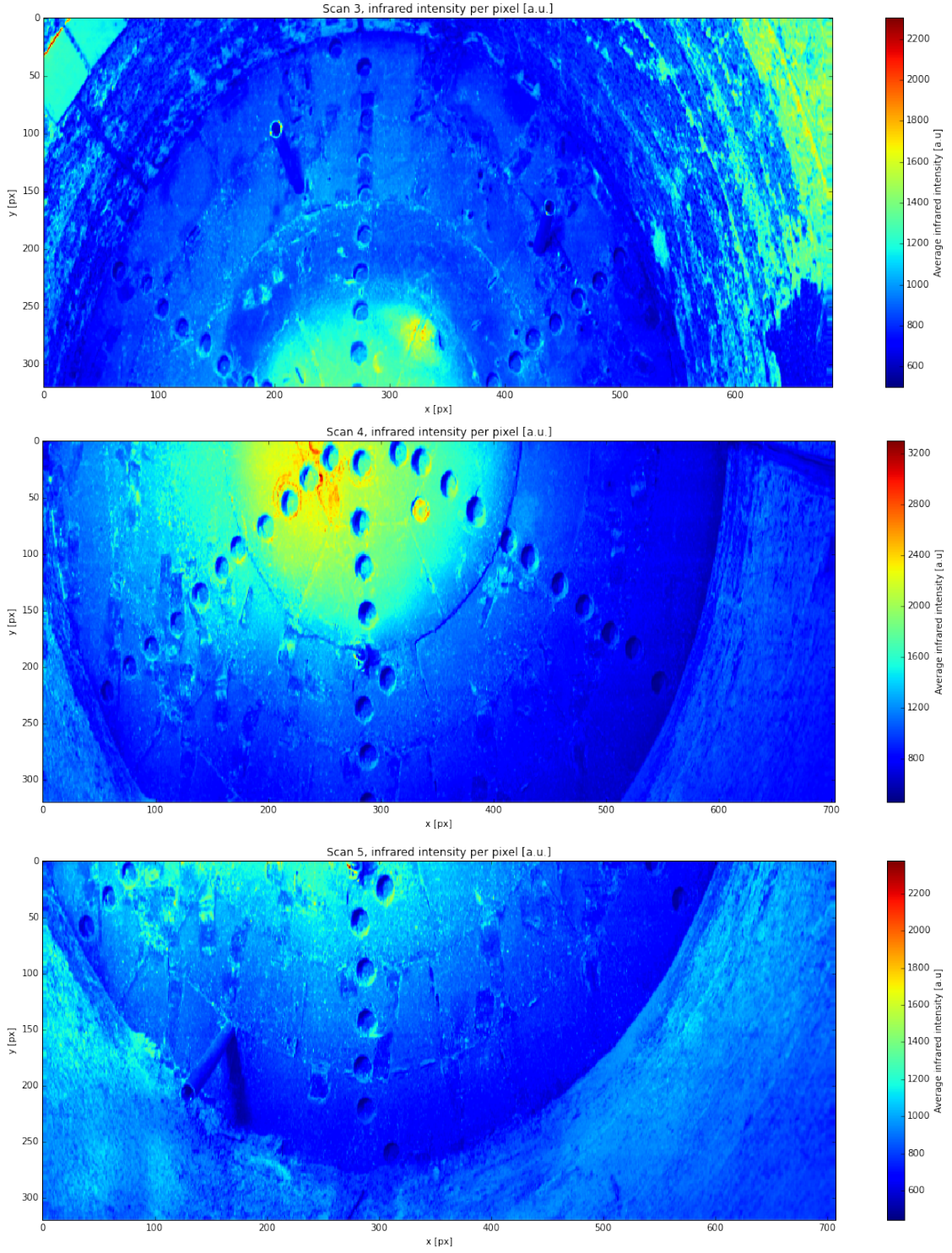


Fig. F-6: The five scans that were taken are shown here.

F.2.4 Preliminary analysis

Minimum noise fraction transformation did not give very interesting results, which is likely mainly because of the non-optimal calibration, and the continuous nature of the water content.

However, the plot about variance suggest that modifications of surface reflectance occurs at wavelengths near 1'300 nm and 1'600 nm.

For instance, the following plot shows:

$$p(x,y) = \frac{\int_{1573.2nm}^{1629.97nm} m(x,y,\lambda)\, d\lambda}{\int_{937.06nm}^{2539.77nm} m(x,y,\lambda)\, d\lambda}$$

where $m(x,y,\lambda)$ is the calibrated value. It strongly suggests that these wavelengths are related to the water content, therefore an additional experiment was made in the lab, which will be explained in Part F.3.

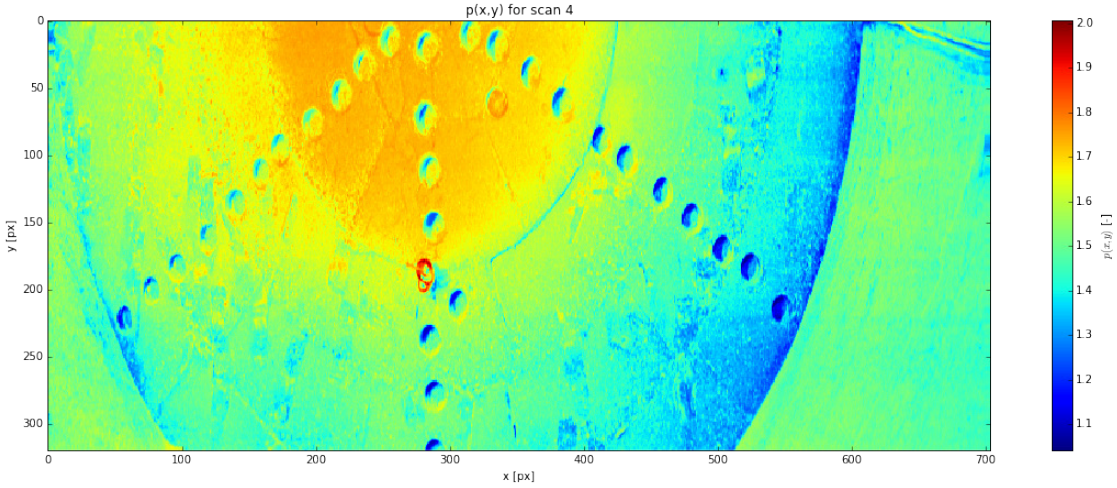


Fig. F-7: Scan 4 plotted as p(x,y).

F.3 Laboratory experiment with bentonite

In order to understand the behaviour of the spectrum of bentonite, a sample was put in front of the camera in the lab, using halogen lamps both for lightning and heating. Then, at t = 60 s, water was added. The idea was to have a large part of the sample soaked, but not all of it (in order to have control values).

Then a hyperspectral image was taken every 6s for 4 hours (the sample was drying during this time). Figures below show the set-up (Fig. F-8) and some sample spectra (Fig. F-9).

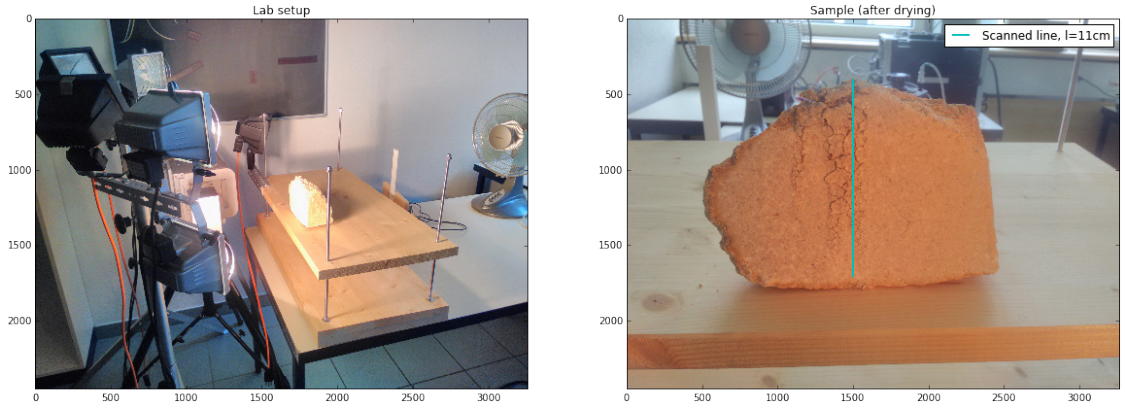


Fig. F-8: Experiment set-up.

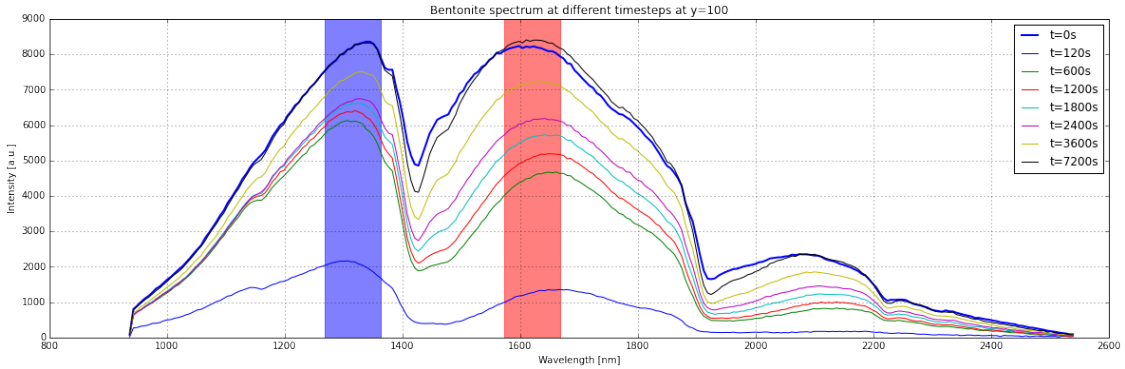


Fig. F-9: Some sample spectra.

As we can see, the difference of the spectrum due to near-surface water content is prominent in the red (between 1'573 and 1'668 nm) and in the blue (1'269 – 1'364 nm) areas.

The goal is to find a function f linking the measured spectrum $m(x,y)$ to the volumetric water content $v(x,y)$. To keep things simple, we'll write f as a composition of two functions, $f=g\circ h$, where h is a function mapping the spectrum to a scalar, which is empirically defined, and g is fitted according to the measured water content of the cores. Two different models were evaluated:

$$h_1 = \frac{\int_{1563nm}^{1668nm} m(x,y,\lambda)\, d\lambda}{\int_{1269nm}^{1364nm} m(x,y,\lambda)\, d\lambda}$$

(integral over the red area divided by the integral over the blue area)

$$h_2 = \frac{\int_{1269nm}^{1364nm} m(x,y,\lambda)\, d\lambda}{\int_{937.06nm}^{2539.77nm} m(x,y,\lambda)\, d\lambda}$$

(integral over the blue area divided by the integral over the whole spectrum)

The following plots show these two function for the lab experiment:

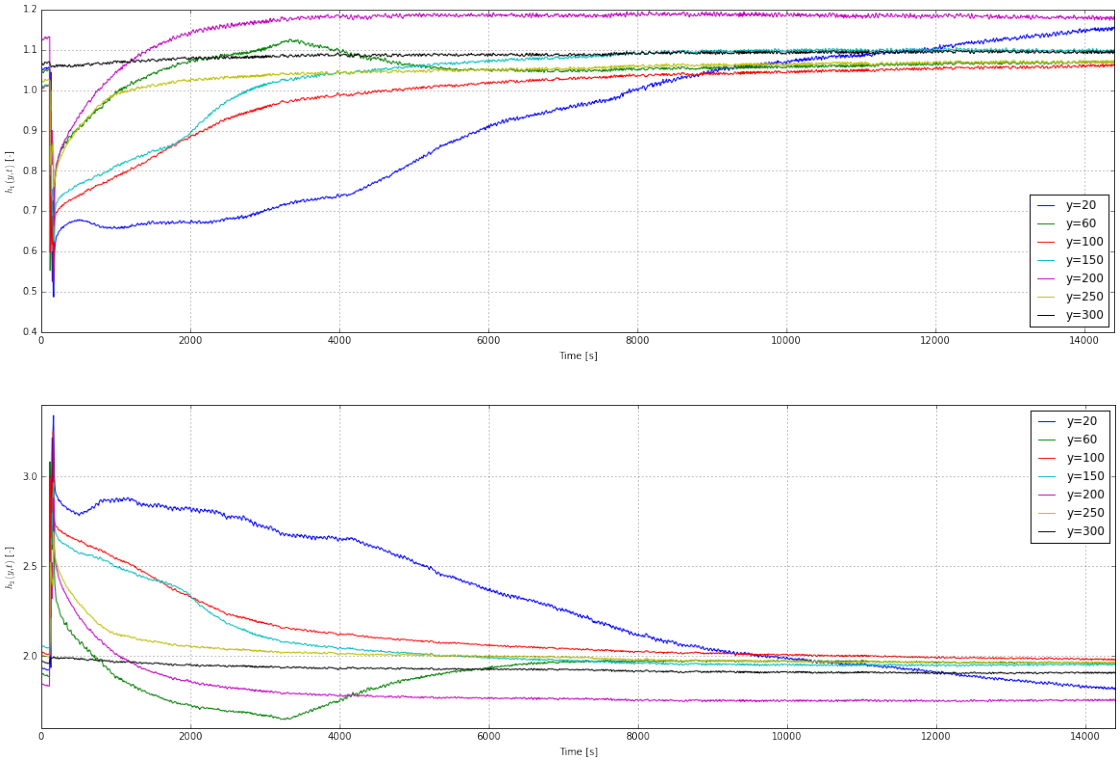


Fig. F-10: Plots of function h1 (upper) and h2 (lower).

As we can see, both capture the information about the drying of the bentonite pretty well in the lab experiment. Note however than h_2 is less sensitive to noise than h_1, since the divisor is taken over a wider spectral range.

In the next section, we'll see how these functions correlate with the measured water content.

F.4 Correlation of spectral measurements and water content

Since we know the water content of the bentonite cores, we can use this data to find g, and subsequently f.

Square patches were marked in the images in the centre of the boreholes, which should have approximatively the same water content as the samples analysed.

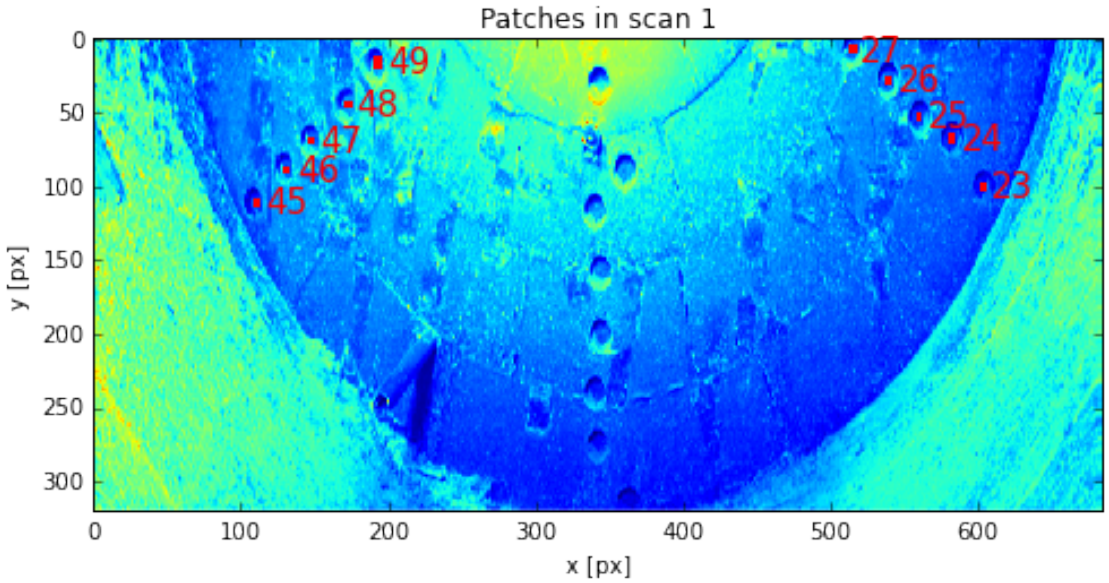


Fig. F-11: Location of the patches in scan1.

Then, once all patches are done, we can compare the results of $t_1(m(x,y))$ and $t_2(m(x,y))$ with the water content of the cores:

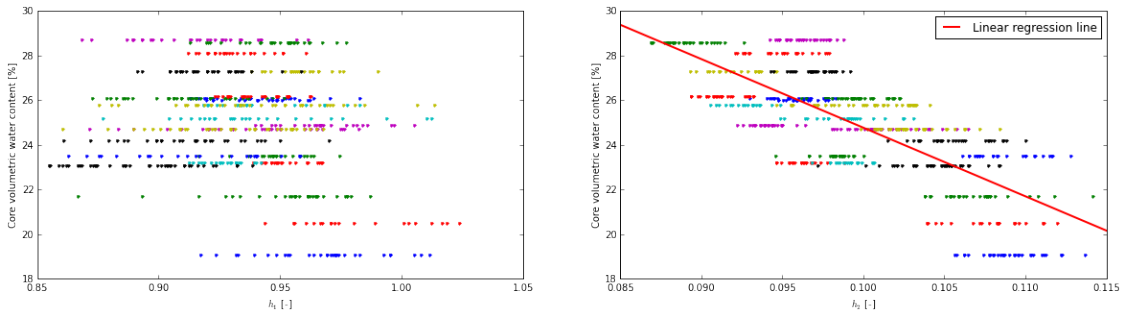


Fig. F-12: Function h1 and h2 for scan 1.

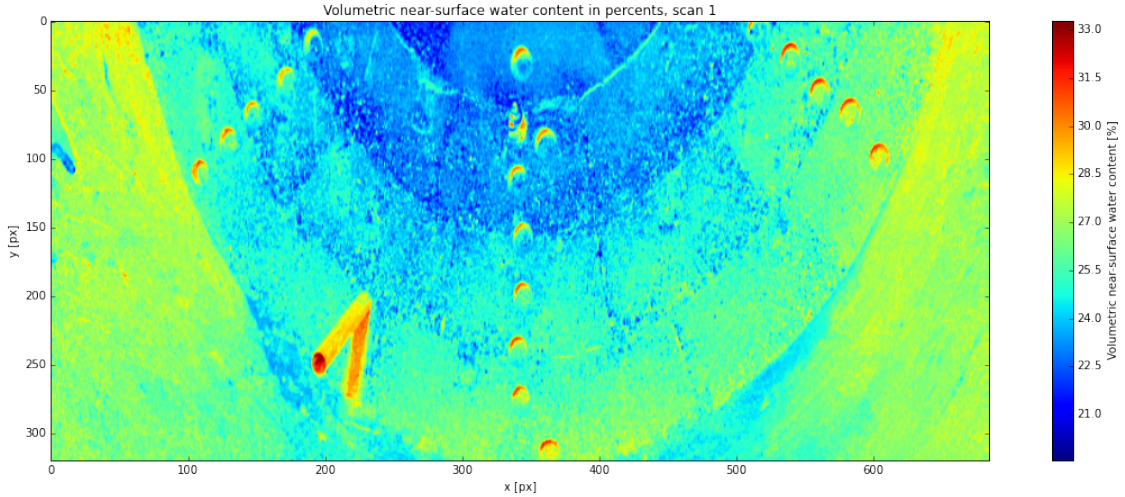
As we can see, h_1 doesn't give an interesting correlation (it is probably too sensitive to noise, as previously stated), whereas h_2 seems clearly related to the volumetric water content.

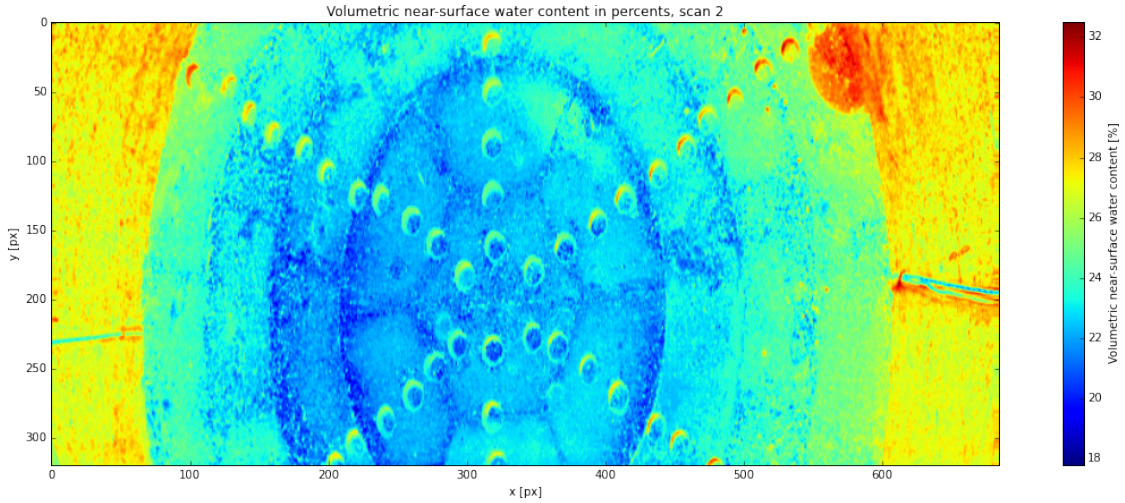
Since we do not have a lot of data points, it does not make too much sense to try and fit a complex function, therefore, a linear fit was made. We get the following:

$$v(x,y) = -307.14 \cdot h_2 = \frac{\int_{1269nm}^{1364nm} m(x,y,\lambda)\, d\lambda}{\int_{937.06nm}^{2539.77nm} m(x,y,\lambda)\, d\lambda} + 55.48$$

Given the data used for calibration, this estimate is likely to be valid only for $v \in [21,27]$, and is not very precise (looks like around $\pm$ 2 %). The next figure F-13 shows the previous relation applied to the scans. Keep in mind that the value make no sense for non-bentonite pixels, and for values outside the validity range.

This relationship is also only valid with the halogen lamps we're using, since it considers the light source as having a constant spectrum. Therefore it's also not valid in the part of the scan which is shades.





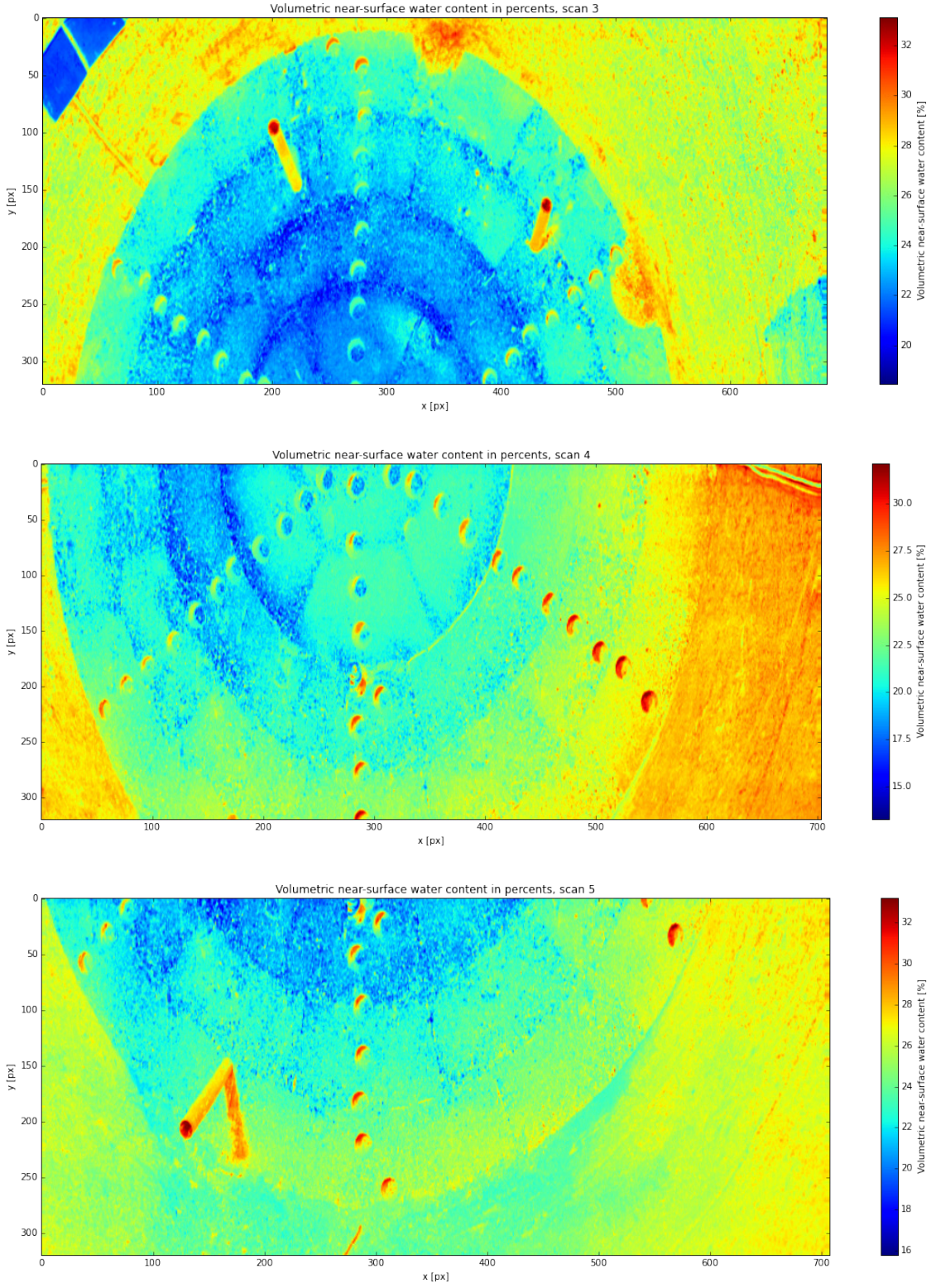


Fig. F-13: Calculated volumetric water content for scans 1-5.

F.5 Conclusion

F.5.1 Achieved work

This report shows that hyperspectral imaging is suitable to determine near-surface water content of bentonite.

A rough estimation of the relation between the spectrum and the water content was computed:

$$v(x,y) = -307.14 \cdot h_2 = \frac{\int_{1269nm}^{1364nm} m(x,y,\lambda)\, d\lambda}{\int_{937.06nm}^{2539.77nm} m(x,y,\lambda)\, d\lambda} + 55.48$$

Five hyperspectral scans were made. Despite the calibration issues due to temperature, high quality data were obtained.

F.5.2 Further work

The relationship between the bentonite water content and its spectrum should be studied in more details. In particular, the formula should be extended in order to take into account the spectrum of the light source, or equivalently to work using the reflectance of the sample instead of using the spectrum of the light emitted back. Also, samples with known water content should be scanned in optimal conditions, in order to have less measurement noise than in the underground lab.

Moreover, this would allow:

- An increase of the validity range of the formula
- A higher order fit
- A better precision in the values, since the formula would be calibrated on low noise data

On the engineering side, influence of the temperature on the measurement should be better characterized, to avoid the extra post-calibration fix, which is not as rigorous as the calibration process.

Appendix G: In-situ measurement of thermal conductivity of bentonite blocks during dismantling and a comparison with CIEMAT laboratory results[9]

G.1 Introduction

The aim of FEBEX (Full-scale Engineered Barriers Experiment) at the Grimsel Test Site was to study the behaviour of components in the near-field for a high-level radioactive waste (HLW) repository in crystalline rock under realistic conditions at the full scale (ENRESA 2000, 2006a). The repository concept is based on the Spanish reference concept (ENRESA, 1995). The thermal effect of the waste was simulated by means of two heaters placed horizontally in a clay barrier comprising of compacted bentonite blocks.

The first half of the FEBEX experiment was dismantled and heater No. 1 was retrieved in 2002 after five years of operation. The dismantling of the other half (FEBEX-DP project) was carried out between February and August 2015, after 18 years of continuous heating during which the temperature at the heater/bentonite contact was maintained at 100 °C.

The dismantling operations included the demolition of the concrete plug and the removal of all the bentonite in front of, surrounding the heater and at the back of it. Heater No. 2 was switched off on April 24, 2015 after demolishing the concrete plug, as the temperature in the area affected by the dismantling should be reduced to a level compatible with manual works (25 – 30 °C). In particular the dismantling of the bentonite barrier started in May 2015. A large number of concrete, bentonite, and metal samples from all types of materials were collected at sections shown in Fig. G-1 (Barcena & Garcia-Siñeriz 2015, NAB 15-14, García-Siñeriz et al. 2016, NAB 16-11). The collected bentonite blocks were sent to CIEMAT for analysis including measurements of density, water content, and thermal conductivity and the results are summarised in Villar et al. (in prep., NAB 16-17).

[9] Originally published as AN16-505.

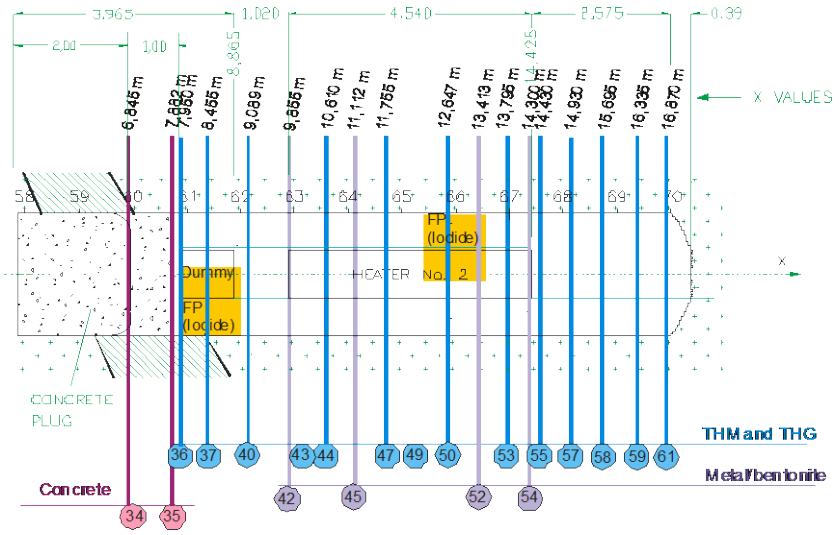


Fig. G-1: Position of sampling sections for the laboratory analyses (Villar et al., in prep., NAB 16-17).

Tunnel length 70 m, tunnel diameter 2.28 m, heater diameter 90 cm, liner inner diameter 94 cm, liner outer diameter 97 cm.

In addition to the sample analyses in the laboratory mentioned above, additional bentonite samples were collected from the sections shown in Fig. G-2 and their water content and dry density were analysed on site by AITEMIN. The procedures and results are summarised in García-Siñeriz et al. (2016, NAB 16-11) and Villar & Iglesias (2016, NAB 16-12).

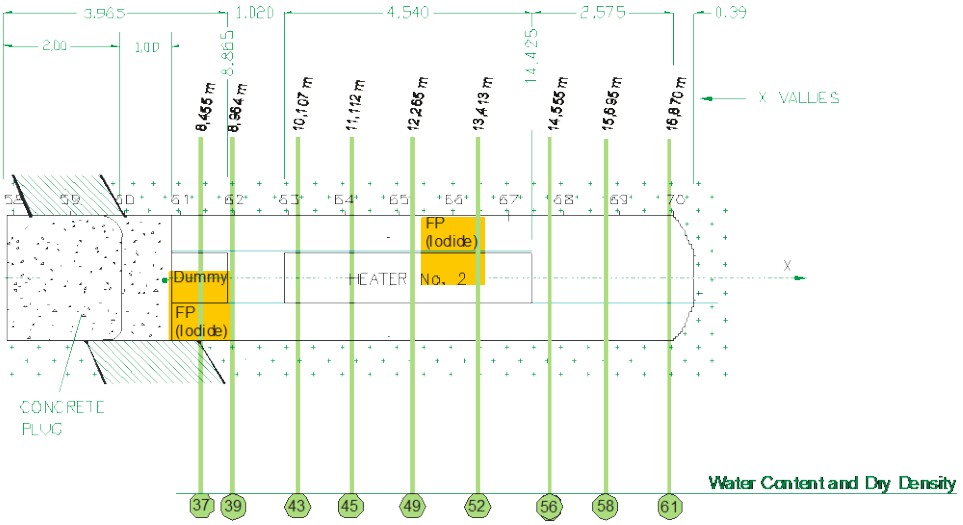


Fig. G-2: Position of sampling sections for the on-site analysis (Villar & Iglesias 2016, NAB 16-12).

Dry density and water content were measured outside the FEBEX tunnel.

Performing the measurements at the site significantly reduces time between sample collection and measurements. The on-site measurements were performed immediately after the samples were collected whereas the laboratory measurements were conducted 74-189 days after. Comparing the on-site and laboratory measurement results gives insight into the reliability of the laboratory results and may indicate whether or not there were any changes in the sample conditions (see Section G.5 for results).

In the above-mentioned on-site measurement campaign (García-Siñeriz et al. 2016, NAB 16-11 and Villar & Iglesias 2016, NAB 16-12), thermal conductivity measurements were not included. A series of *in-situ* thermal conductivity measurements was, thus, performed using a hand-held thermal analyser at various sections. By using a term "*in situ*", it is intended to note that the thermal conductivity measurements were performed *directly on the section surface in the FEBEX tunnel* as soon as the surface became available (i.e., the disturbance to the material was kept as little as possible). The *on-site* density and water content measurements were, on the other hand, performed outside of the FEBEX tunnel after the bentonite samples were collected.

This report summarises the in-situ thermal conductivity measurement activities and results. The obtained in-situ thermal conductivity was then compared with those from the laboratory measurements (Villar et al., in prep., NAB 16-17) using the blocks collected at the locations shown in Fig. G-3.

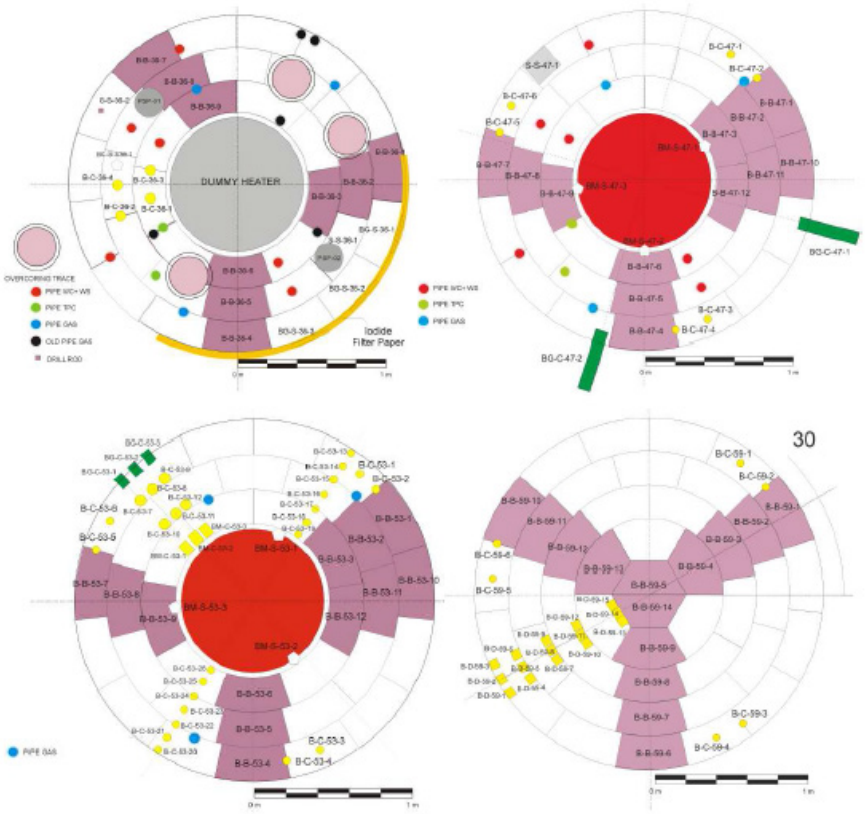


Fig. G-3: Position of blocks received at CIEMAT for THM and THG tests in sampling sections 36, 47, 53 and 59.

The position of blocks BB-36-7 and BB36-9 is interchanged (Barcena and Garcia-Siñeriz, 2015).

The results of the dry density and water content from the corresponding and/or adjacent sections are provided in Section G.6. This supplemental information should help interpreting the measured thermal conductivity results as the thermal conductivity of bentonite blocks is known to depend on the dry density, water content, and consequently on the degree of saturation.

G.2 Materials and methods

G.2.1 KD2 Pro thermal analyzer

The tool used for the in-situ measurement of thermal conductivity of the FEBEX bentonite blocks is the KD2 Pro thermal analyser (Decagon Devices Inc., USA, Fig. G-4). It consists of a handheld controller and sensor that is to be inserted into the medium of interest.

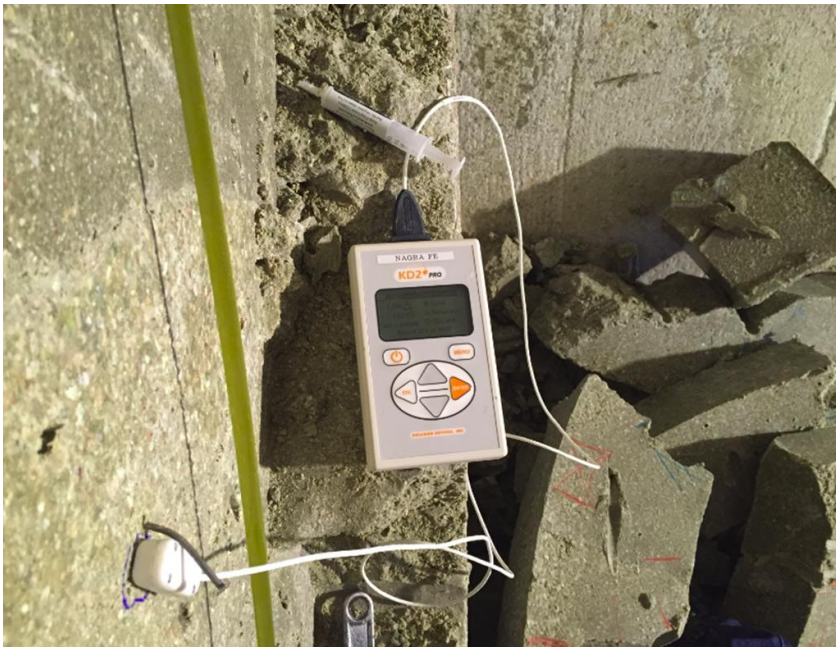


Fig. G-4: The KD2 Pro thermal analyzer.

The TR-1 needle sensor is inserted into the bentonite block (lower left). The syringe is the thermal grease.

For the KD2 Pro thermal analyser, four types of sensors are currently available for different applications. In this set of measurements, TR-1 and RK-1 single needle sensors (Fig. G-5) were selected which are more suited for solids (Decagon Devices, 2011).

The TR-1 sensor is designed primarily for soils, concrete, rocks, and other granular or solid materials. The relatively large diameter and typically longer heating time of the TR-1 sensor minimise errors from contact resistance in granular samples or solid samples with pilot holes. The RK-1 is designed more specifically for applications in solid materials such as rocks. Selected specifications and characteristics of the TR-1 and RK-1 sensors are shown in Tab. G-1.

Tab. G-1: Specifications of the thermal conductivity sensors.

	TR-1	**RK-1**
Needle size	10 cm length, 2.4 mm diameter	6 cm length, 3.9 mm diameter
Range	0.1 – 4.0 W/mK	0.1 – 6.0 W/mK
Accuracy	10 % for 0.2 – 4.0 W/mK ± 0.02 W/mK for 0.1 – 0.2 W/mK	10 % for 0.2 – 6.0 W/mK ± 0.02 W/mK for 0.01 – 0.2 W/mK
Read time*	5 min	10 min
Sample size**	~ 2 cm radius	~ 2 cm radius
Cable length (customized)	180 cm	180 cm

* Used in the measurement.
** At λ = 0.5 W/mK and depends on λ.

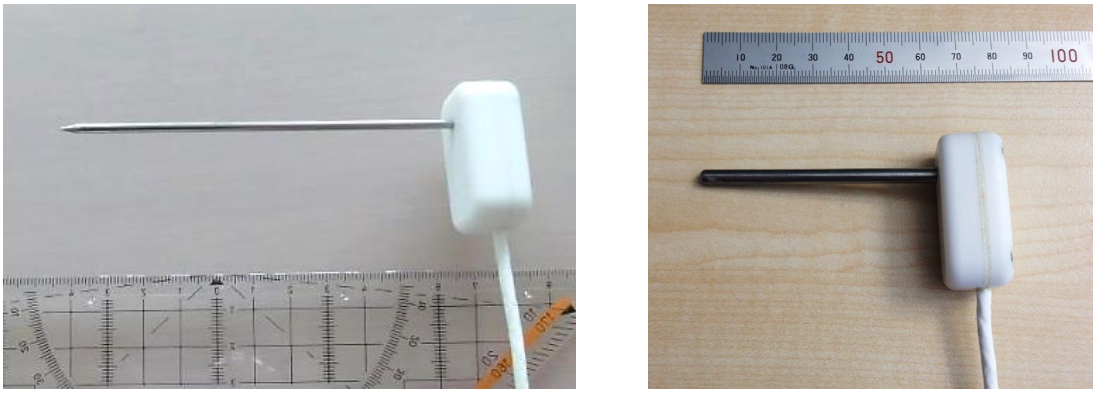


Fig. G-5: The TR-1 (left) and RK-1 (right) Pro needle sensors.

Both types of the sensors consist of a needle with a heating source along the entire length and a temperature sensor at the midpoint. A current is applied to generate heat and the transient temperature change is monitored. According to Decagon Devices (2011), the KD2 Pro calculates a thermal conductivity using algorithms based, e.g. on the line heat source analysis by Carslaw & Jaeger (1959) and Kluitenberg et al. (1993).

The *read time* is the time during which the measurement is performed. Heat is applied for half of the time (heating period), followed by a cooling period. The transient temperature is monitored over both heating and cooling periods and λ is calculated. The longer read time helps to prevent errors caused by effects of the large diameter needle and contact resistance between the sensor and the sample in granular and solid materials (Decagon Devices, 2009).

In solid materials where a pilot hole has been drilled and contact resistance can be significant, using thermal grease and extending the read time to the 10 minutes (maximum setting) will produce the most accurate results.

The needle sensors were installed following the procedures suggested by the manufacturer (Decagon Devices, 2011). A pilot hole was drilled using a drill bit with a diameter of either 2.40

mm (for TR-1) or 3.97 mm (RK-1). The depth of the pilot holes was made a few mm deeper than the length of the needle.

The accuracy of the measurement is highly dependent on the contact conditions between the needle and the bentonite block. ASTM D-5334-14 (ASTM 2014) suggests use of thermal grease with a thermal conductivity greater than 4 W/mK to minimize contact resistance errors. We used Arctic Silver Premium Silver Polysynthetic Compound, silver-filled thermal grease with a thermal conductivity of 8 W/mK from Arctic Silver, Visalia, CA (www.arcticsilver.com). A sufficient amount of the grease was pushed into the hole and the needle sensor was installed. While installing it, the needle was twisted to spread the grease inside the pilot hole. Air inside the pilot hole was finally compressed enough to push the needle back out, thus, the sensor head was fixed with a nail onto the block surface (also seen in Fig. G-4). This implies that the gaps between the needle and bentonite block was completely eliminated.

G.3 Measurement sections

Although this in-situ thermal conductivity measurement was not included in the original dismantling plan, the measurements were performed at four sections and five layers (Tab. G-2 and Fig. G-6). The measurement sections are well distributed both within the hot and cold sections; Sections 46 and 53 include the heater, sections 58 is at the rear part of the gallery, and Section 61 is at the end of the gallery. Details on the measurement positions within each section/layer are summarized in Tab. G-2.

It has to be noted here that a set of bentonite samples were collected from these or adjacent sections for on-site (Villar & Iglesias, 2016, NAB 16-12) and lab analysis (Villar et al., in prep., NAB 16-17).

Tab. G-2: Positions of the measuring points.

Section	Layer	point no.	with heater?	distance from center (cm)	distance from liner (cm)	Sensor type
46	45	1	Yes	101.5	53	RK-1 *
		2		85.5	37	
		3		75.5	27	
		4		60.5	12	
		5		104.5	56	
		6		87.5	39	
		7		75.5	27	
		8		58.5	10	
53	29	1	Yes	60.5	12	TR-1
		2		81.5	33	
		3		102.5	54	
58	13	1	No	15.7		TR-1
		2		35.2		
		3		59.2		
		4		80.7		
		5		102.6		
58	9	1	No	0.2		TR-1
		2		34.5		
		3		59.5		
		4		81.3		
		5		103.4		
		6		60.1		
		7		81.6		
		8		103.5		
		8		103.5		
61	4	1	No	34.5		TR-1
		2		59.5		
		3		81.3		
		4		103.4		

* RK-1 was switched to TR-1 as the needle was bent

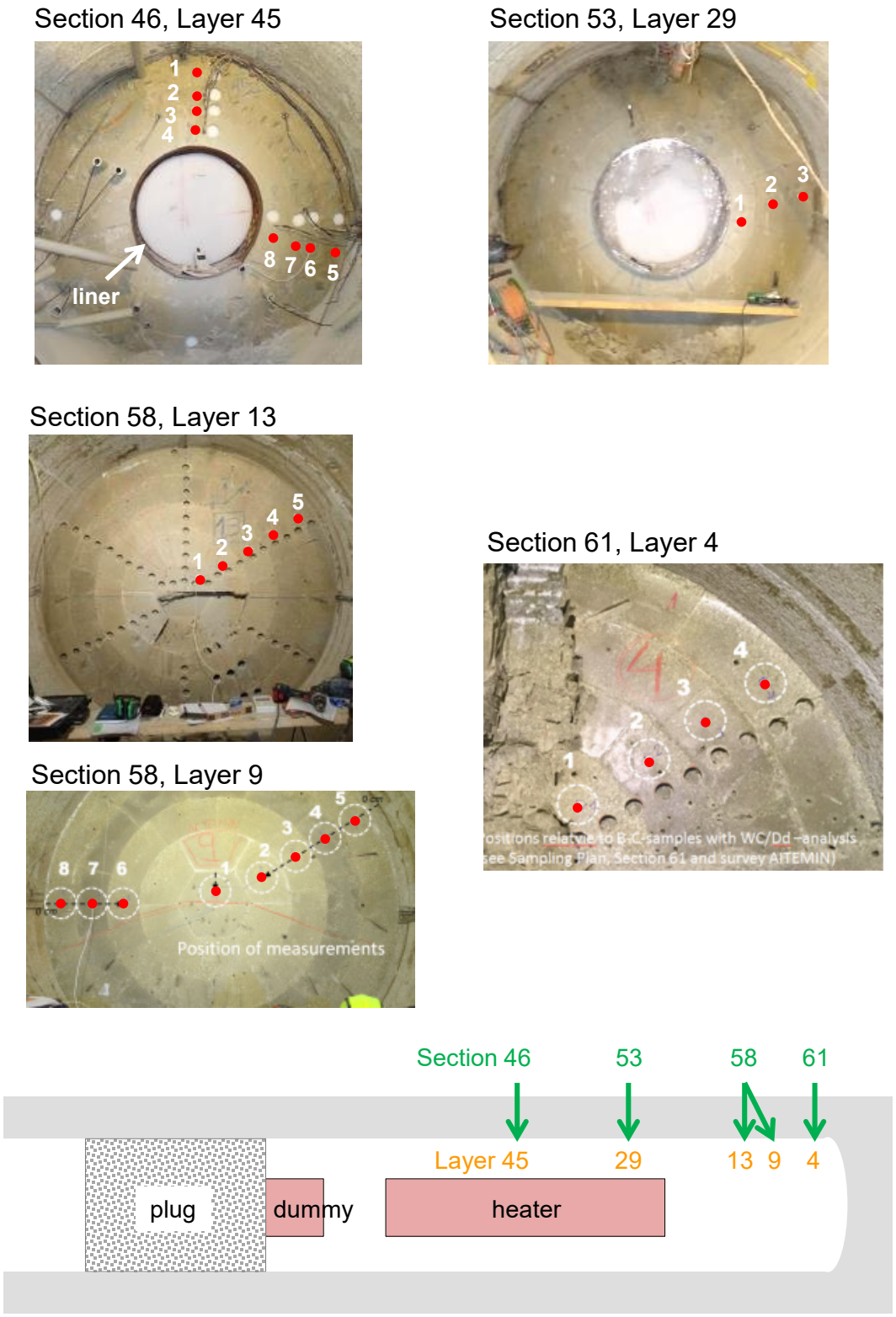


Fig. G-6: In-situ thermal conductivity measurement sections.

Each section generally comprises several slices of blocks. The Section 58 measurements were done for two slices.

G.4 In-situ thermal conductivity measurement results

In the following sections, the in-situ measured thermal conductivity λ results are presented for each measurement section. The measurement was done with the RK-1 sensor for Section 46 but the needle got bent during the installation. Therefore, from Section 53 on, we switched to the TR-1 sensor.

G.4.1 Section 46

The measurement of λ in this section was performed at eight locations. The measured λ values are plotted in Fig. G-7 as a function of radial distance from the tunnel centre. The λ values ranged from 1.18 – 1.32 W/mK. Three measurements (No. 4, 7 and 8) out of eight yielded λ values with high measurement errors (calculated by the thermal analyser), thus, the results are discarded (Decagon Devices, 2011). These occurred for the measurements near the heater where the bentonite blocks seemed harder and less wet. The conditions of the pilot holes might not have been good enough to achieve a perfect contact between the needle and bentonite. The measurements could not be repeated due to the time constraint at the site. The exact cause for the high errors remains unknown.

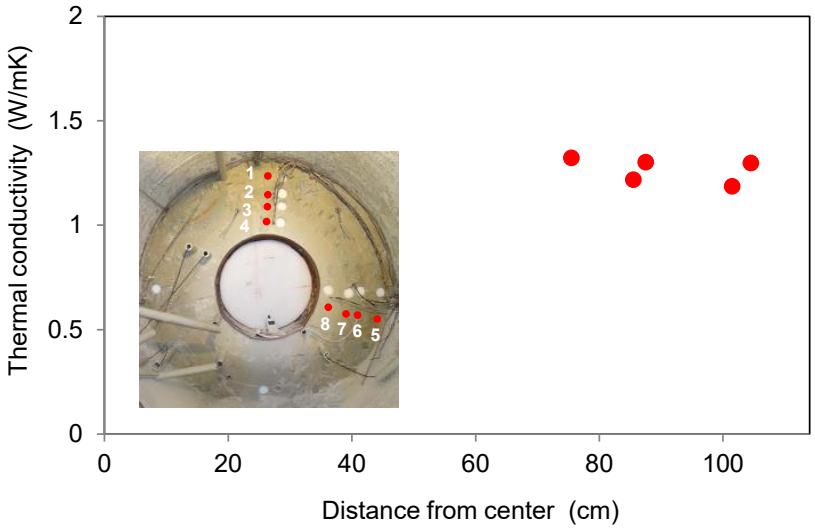


Fig. G-7: In-situ thermal conductivity as a function of radial distance (Section 46).
Measurements at No. 4, 7 and 8 failed.

G.4.2 Section 53

The measurements in this section were performed at three locations. From this section on, a different sensor (TR-1, 10 cm long) was used. The measured λ values ranged from 1.23 – 1.26 W/mK as shown in Fig. G-8. Although one of the measurements (No. 3) yielded a λ value with a high measurement error (as will be seen in Tab. G-3), the TR-1 sensor yielded a higher success rate. The λ value with a high measurement error was discarded (Decagon Devices, 2011).

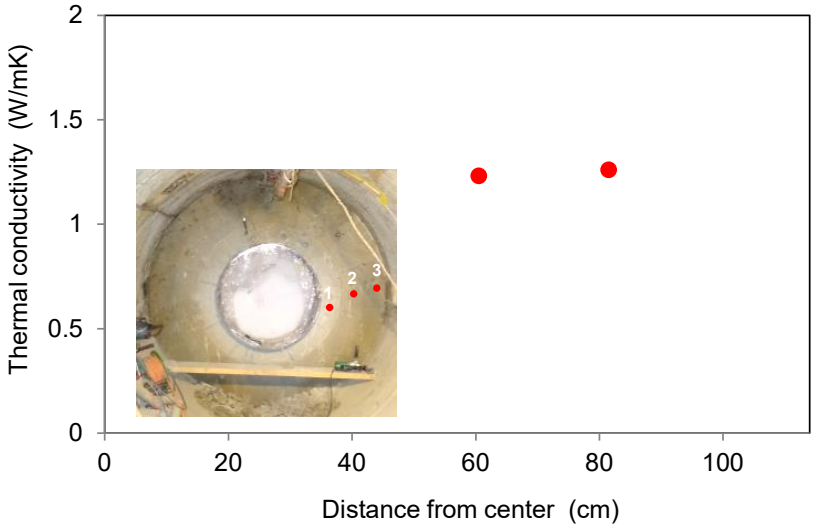


Fig. G-8: In-situ thermal conductivity as a function of radial distance (Section 53).
Measurement at No. 3 failed.

G.4.3 Section 58

The measurements in this section were performed at five and eight locations in Layers 13 and 9, respectively. The measured λ values ranged from 1.24 – 1.38 W/mK as shown in Fig. G-9 and G-10. All measurements in Layer 13 resulted in λ values with an acceptable error whereas one in Layer 9 (No. 4) yielded a high measurement error.

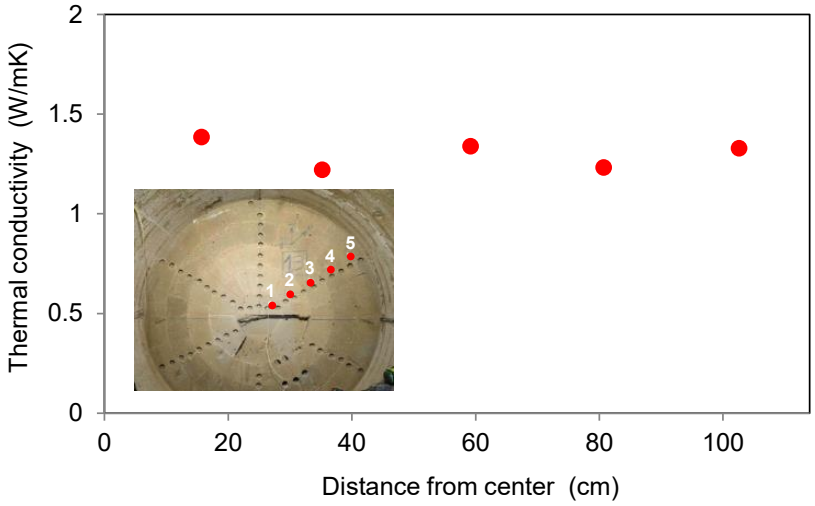


Fig. G-9: In-situ thermal conductivity as a function of radial distance (Section 58, Layer 13).
No measurement failure.

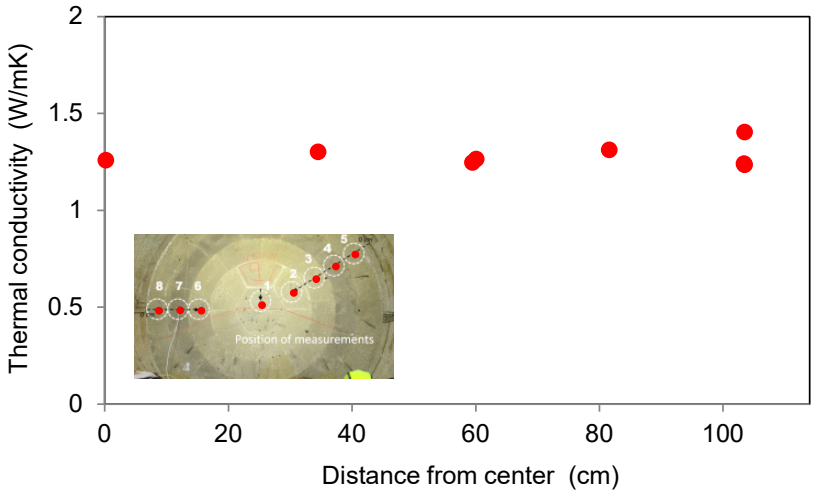


Fig. G-10: In-situ thermal conductivity as a function of radial distance (Section 58, Layer 9).
Measurement at No. 4 failed.

G.4.4 Section 61

The measurements in this section were performed at four locations. The measured λ values ranged from 1.20 – 1.30 W/mK as shown in Fig. G-11. None of the measurements yielded a high measurement error.

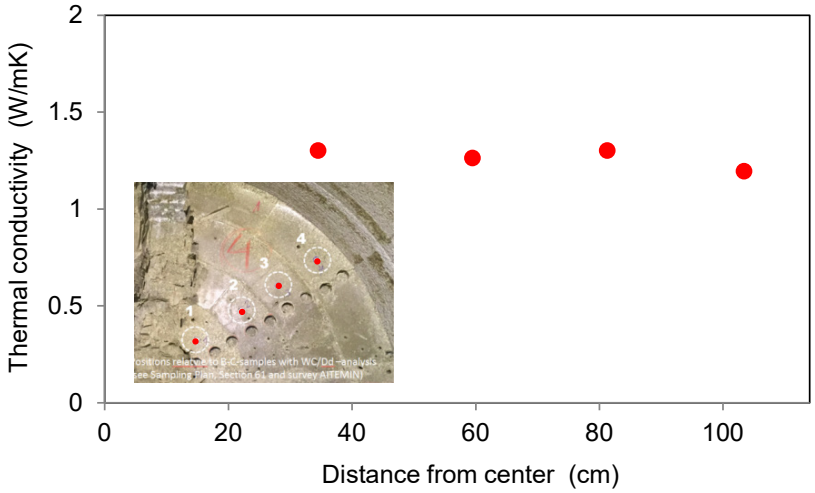


Fig. G-11: In-situ thermal conductivity as a function of radial distance (Section 61).
No measurement failure.

G.4.5 Summary of in-situ thermal conductivity measurements

All the in-situ measurement results (four sections, five layers) are summarised in Tab. G-3. The measured λ values for the hot sections are compared to those for the cold sections in Fig. G-12. The results show no clear spatial variations and no distinct difference between the two sets of data. In general, the λ values are somewhat constant in the radial direction with the mean of 1.28 W/mK and standard deviation of 0.06 W/mK.

Tab. G-3: Summary of the in-situ measurement results.

Section	Layer	point no.	distance from center (cm)	meas. date	K (W/mK)	T (˚C)	error*
46	45	1	101.5	6/25/2015	1.186	19.4	0.0022
		2	85.5		1.217	19.3	0.0011
		3	75.5		1.322	20.0	0.0077
		4	60.5			21.7	0.0349
		5	104.5		1.297	18.7	0.0068
		6	87.5		1.302	18.9	0.0051
		7	75.5			20.7	0.0405
		8	58.5			21.8	0.0563
53	29	1	60.5	7/14/2015	1.231	18.9	n/a
		2	81.5		1.260	18.7	n/a
		3	102.5			18.9	0.0115
58	13	1	15.7	7/27/2015	1.384	19.5	0.0088
		2	35.2		1.221	19.0	0.0037
		3	59.2		1.339	18.9	0.0058
		4	80.7		1.232	18.6	0.0031
		5	102.6		1.329	18.4	0.0061
58	9	1	0.2	7/28/2015	1.259	19.1	0.0042
		2	34.5		1.301	18.4	0.0045
		3	59.5		1.246	18.3	0.0030
		4	81.3			18.1	0.0168
		5	103.4		1.241	18.0	0.0051
		6	60.1		1.264	18.2	0.0044
		7	81.6		1.311	17.9	0.0036
		8	103.5		1.404	18.2	0.0078
		8	103.5		1.235	18.0	0.0028
61	4	1	34.5	7/30/2015	1.301	18.1	0.0049
		2	59.5		1.263	18.0	0.0038
		3	81.3		1.302	17.8	0.0046
		4	103.4		1.195	17.7	0.0035

* results wih error > 0.01 were discarded according to user's manual

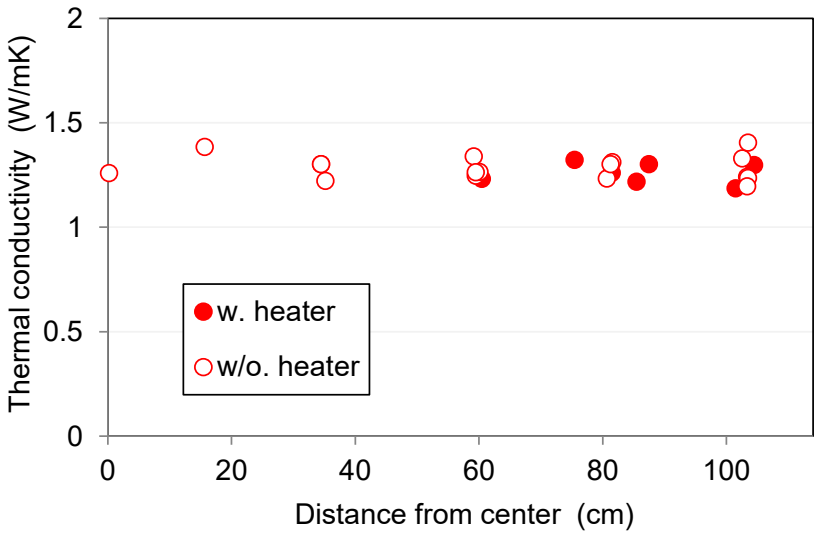


Fig. G-12: Comparison of in-situ thermal conductivity resuls in the hot and cold sections.

As shown in section G-6, the bentonite blocks were highly or fully saturated. The λ values (i.e. the mean of 1.28 W/mK with a S.D. of 0.06 W/mK) obtained in the in-situ measurements are consistent with the literature results (ENRESA 2002) for the same type of bentonite blocks as shown in Fig. G-13.

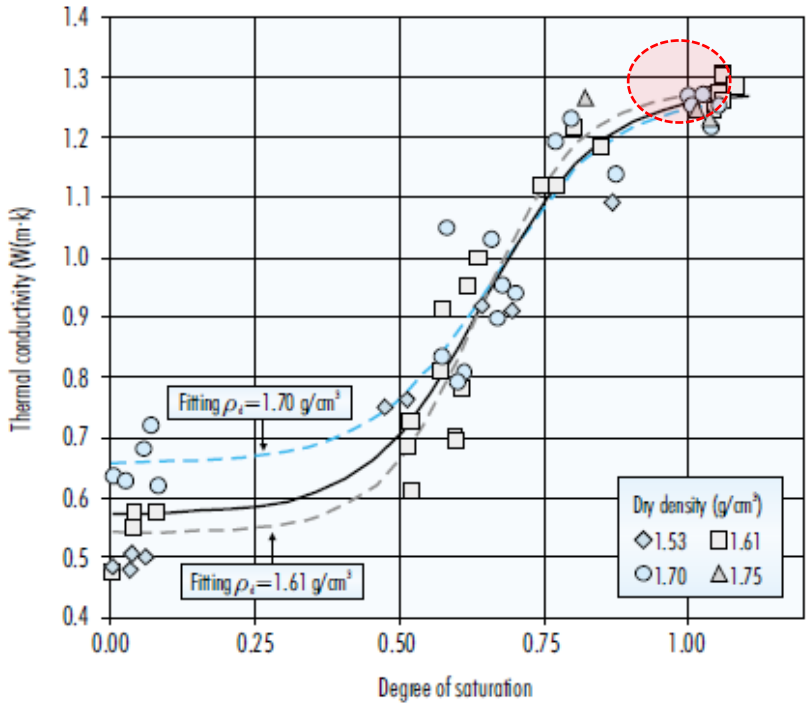


Fig. G-13: Thermal conductivity versus degree of saturation. (Figure taken from ENRESA 2002)

G.5 Comparison with laboratory-measured λ

In this section, the in-situ measured λ values are compared with those measured in the laboratory using the block samples collected from various sections (Villar et al., in prep., NAB 16-17).

The superficial thermal conductivity of the bentonite blocks was measured using a Kemtherm QTM-D3 system (Kyoto Electronics, 1987) based on the hot wire transient method. The plastic film around the blocks was removed only at the measurement position. The exposed block surface was smoothed with a scraper and brushed to remove any loose material. The thermal conductivity was generally measured on the surface of the block that faced the gallery entrance at two positions shown as rectangles in Fig. G-14. All measurements were performed at room temperature and details on the measurement are provided in Villar et al. (in prep., NAB 16-17).



Fig. G-14: Laboratory thermal conductivity measurement using Kemtherm QTM-D3 system (Photo from Villar et al., in prep., NAB 16-17).

The black heating wire probe is placed on the first measurement position (closer to wall) whereas the second position is marked as CT-2 (closer to center). The yellow equipment on the left is the relative humidity meter (not discussed).

The laboratory-measured λ values from Sections 36, 47, 53 and 59 (positions shown in Fig. G-3) are plotted in Fig. G-15 together with the in-situ results. The laboratory results scattered over a wider range (mostly between 1.1 and 1.3 W/mK) but showed no distinct spatial trend in the thermal conductivity, consistent with the in-situ results. The mean λ value was

1.17 W/mK and standard deviation of 0.08 W/mK. The wider scatter range could result possibly from the broad range in the dry density (Villar et al., in prep., NAB 16-17).

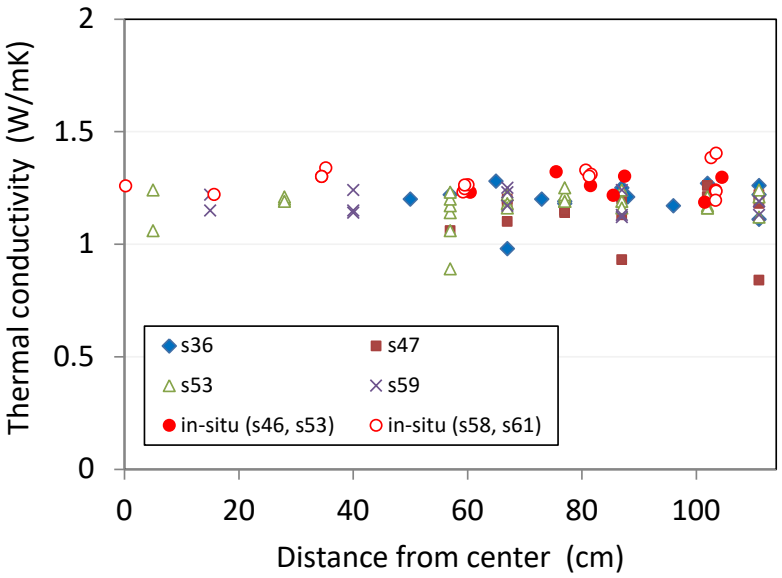


Fig. G-15: Comparison of the in-situ and laboratory mesaured thermal conductivity results. In-situ results lie around the high end of the laboratory results.

The comparison of the in-situ and laboratory thermal conductivity results indicated that the in-situ values lie at the high-end of the laboratory results range.

This slight difference is possibly due to the fact that the laboratory measurements were done 74 – 189 days after the blocks were collected whereas the in-situ measurements were done immediately after the surface appeared. According to Villar & Iglesias (2016, NAB 16-12) and Villar et al. (in prep., NAB 16-17), the dry density and water content measured in the laboratory were not significantly different from those measured on site. Nonetheless, the in-situ measurement performed directly on the section surfaces might reflect the thermal conductivity values of the blocks that are even less disturbed.

In addition, unlike the in-situ measurements, no thermal grease was used between the probe and the block surface (Fig. G-14) in the laboratory measurements. Any slight gaps (if any) could lead to underestimation of the thermal conductivity.

Finally, in the in-situ and laboratory measurements, two different tools were used. Although both are based on the transient method, the in-situ device requires insertion of the needle whereas the laboratory device is based on placing the probe on the smoothed surface of the block. The difference in the sampling volume of each device could also lead to a difference in the results.

Overall, the in-situ measurement results were consistent with the laboratory results as well as those in the literature (e.g. ENRESA 2002).

G.6 Water content and saturation (on-site sample results)

Thermal conductivity of bentonite is known to depend on water saturation and dry density. The dry density and degree of saturation from the sample analysis from the same or adjacent layers (Villar & Iglesias. 2016, NAB 16-12) are plotted below.

Fig. G-16 shows the results from Section 45 as a function of radial distance from the tunnel centre line. An opposite gradient is clearly seen. The saturation indicates that the bentonite was saturated near the rock wall and decreases down to 80 % toward the heater. On the other hand, the dry density takes the lowest value of about 1.5 Mg/m^3 near the wall and increases up to 1.7 Mg/m^3 toward the heater. As the water was provided from the wall, saturation started from the outer side which led to a swelling of the outer blocks and, in turn, to a compression of inner blocks. The heat from the heater prevented the inner blocks to reach full saturation that also contributed to inhibiting the swelling.

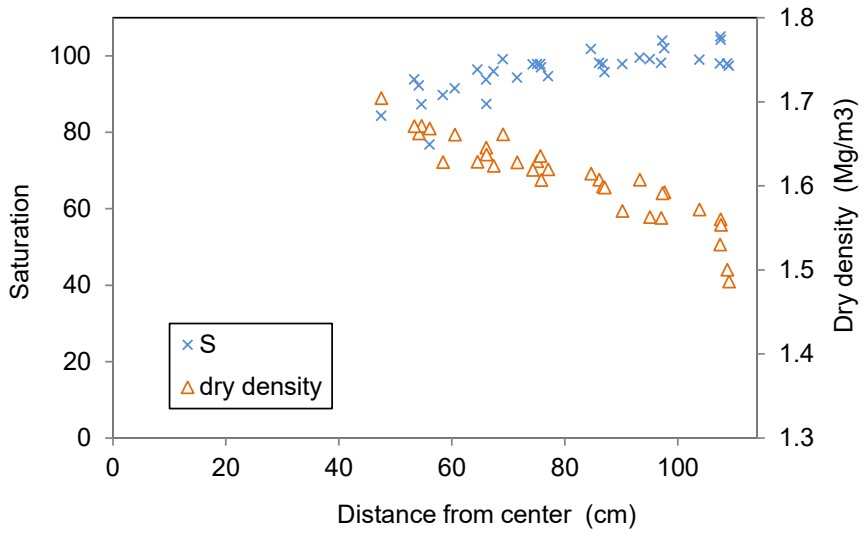


Fig. G-16: Dry density and saturation (S) as a function of radial distance.

The laboratory results are for samples taken from adjacent Section 45 (Villar et al., in prep.).

The saturation and dry density results from Section 52 (Villar & Iglesias 2016, NAB 16-12) are plotted in Fig. G-17 as a function of radial distance from the tunnel centre line. The saturation and dry density generally show a similar trend as Section 45 but with more scatter.

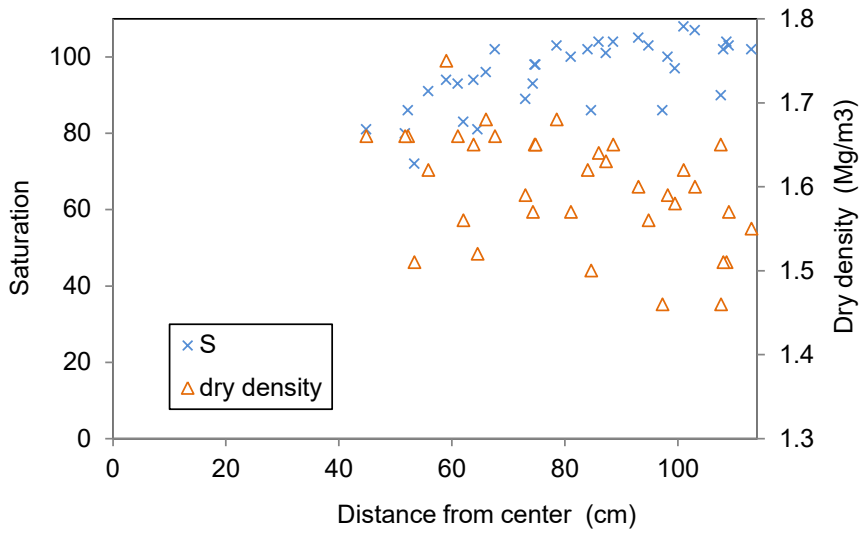


Fig. G-17: Dry density and saturation (S) as a function of radial distance.

The laboratory results are for samples taken from adjacent Section 52 (Villar et al., in prep.).

Fig. G-18 shows dry density and degree of saturation from Section 58. Unlike sections 45 and 52 (hot sections), the saturation indicates that the blocks were fully or nearly saturated everywhere. Dry density still shows a gradient with values as low as 1.5 Mg/m^3 only near the wall whereas the rest was constant at around 1.6 Mg/m^3.

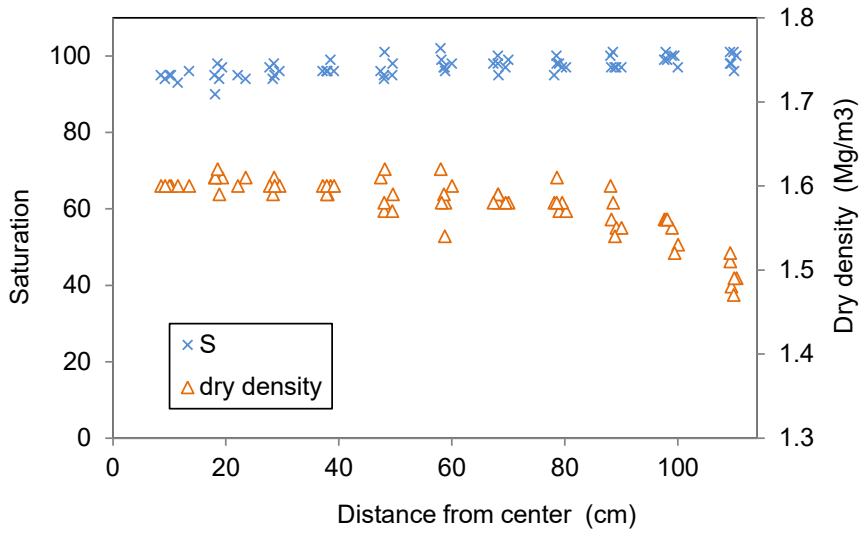


Fig. G-18: Dry density and saturation (S) as a function of radial distance.

The laboratory results are for samples taken from Section 58 (Villar et al., in prep.).

Fig. G-19 shows results for Section 61. As this section is sufficiently far from the heater, the saturation indicates that the blocks were uniformly saturated everywhere. Dry density scatters between 1.4 and 1.5 Mg/m^3 but there is no spatial variation.

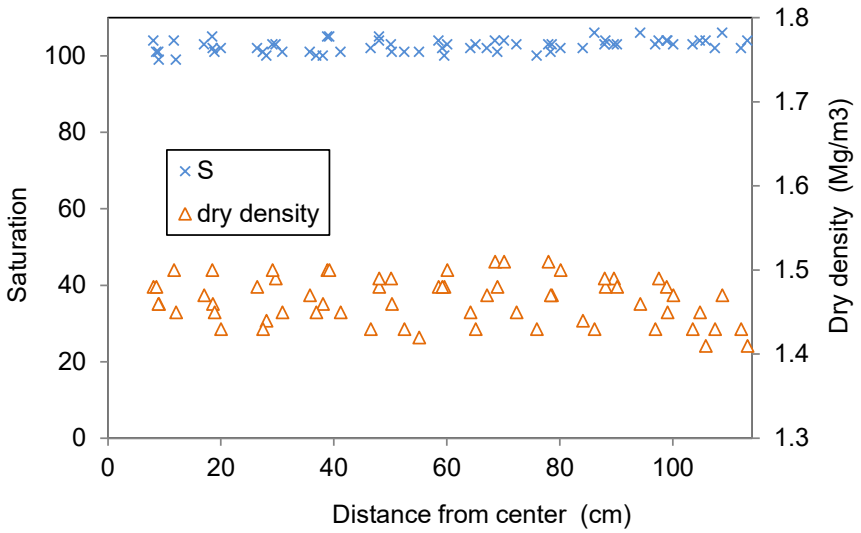


Fig. G-19: Dry density and saturation (S) as a function of radial distance.
The laboratory results are for samples taken from Section 61 (Villar et al., in prep.).

Saturation and dry density of the bentonite are the factors that strongly control thermal conductivity of the bentonite. These two factors, however, are competing processes that have opposite effects on the thermal conductivity. In the hot sections, both saturation and dry density showed large gradients each of which contributes to the thermal conductivity in an opposite manner. Their combined effect, however, on the thermal conductivity seemed to cancel each other. In the cold sections, smaller variations in the water content and dry density led to a constant thermal conductivity.

G.7 Concluding remarks

During the dismantling of FEBEX experiment at the Grimsel Test Site, a series of in-situ thermal conductivity measurements was performed at various sections with and without the heater.

A needle-based heat pulse sensor was inserted into the pilot holes drilled at various radial distances on the surface of the bentonite blocks. Thermal grease was used to ensure a good contact between the needle and the block. As the measurements were performed directly on the section surface in the FEBEX tunnel as soon as the surface of the measurement sections became available, the disturbance to the bentonite at the time of measurement was considered minimal.

The in-situ λ values ranged between 1.19 and 1.40 W/mK with a mean of 1.28 W/mK and standard deviation of 0.06 W/mK. The λ values were constant in the radial direction.

The in-situ λ values were compared with the laboratory results obtained separately by Villar et al. (in prep., NAB 16-17). *The laboratory λ values ranged between 0.84 and 1.28 W/mK with a*

mean of 1.17 W/mK and standard deviation of 0.08 W/mK. The laboratory results also showed a general trend of constant thermal conductivity in the radial direction.

The in-situ values lie at the high-end of the laboratory result range. Although the difference was very little, the possible cause is likely linked to a minimal disturbance in the block conditions for the in-situ measurements. Overall, the in-situ measurement results were consistent with the laboratory results and those in the literature.

G.8 Acknowledgments

Part of the in-situ thermal conductivity measurements was performed by Hansruedi Fisch of Nagra. The laboratory test results were provided by M.V. Villar of CIEMAT, Spain.

Appendix H: References

AITEMIN & INASMET (2003): "Characterization Department, "FEBEX Project Components: Corrosion Study", Final Report, Ref. 36.0045.0, 3 June 2003

AITEMIN (2014a): "Full Dismantling Test Plan (In Situ Experiment)", Dec. 2014.

AITEMIN (2014b): "Sensors Data Report, In Situ Experiment", Report Nº: 8 - FULL REPORT, 2014

Åkesson, M., Olsson, S., Dueck, A., Nilsson, U., Karnland O., Kiviranta L., Kumpulainen, S., Lindén, J. (2012): Temperature buffer test. Hydro-mechanical and chemical/ mineralogical characterizations, Swedish Nuclear Fuel and Waste Management Company (SKB), SKB P-12-06, Stockholm.

Arlinger, J., A. Bengtsson, J. Edlund, L. Eriksson, J. Johansson, S. Lydmark, L. Rabe and K. Pedersen (2013): Prototype repository - Microbes in the retrieved outer section. SKB Report P-13-16**,** 1-44

ASTM D5334 - 14 (2014): Standard Test Method for Determination of Thermal conductivity of Soil and Soft Rock by Thermal Needle Probe Procedure.

Barcena, I. & Garcia-Siñeriz. J.L. (2015): FEBEX-DP (GTS) Full Dismantling Test Plan R7. Nagra Arbeitsbericht NAB 15-14.

Bengtsson, A., Chukharkina, A., Eriksson, L., Hallbeck, B., Hallbeck L., Johansson J., Johansson, L. & Pedersen K. (2013): Development of a method for the study of H_2 gas emission in sealed compartments containing canister copper immersed in O_2-free water. SKB Technical Report TR 13-13. Swedish Nucclear Fuel and Waste management Co, Stockholm. pp 1

BGR (Kaufhold, S). (2014): Unpublished Data related to Mineralogy, Exchangeable Cations and Chemical Composition of MX80 bentonite, BGR, Aug 2014.

Buil, B., Gómez, P., Peña, J., Garralón, A., Turrero, M.J., Escribano, A., Sánchez, L., Durán, J.M. (2010): Modelling of bentonite–granite solutes transfer from an in situ full-scale experiment to simulate a deep geological repository (Grimsel Test Site, Switzerland). Applied Geochemistry, 25, 1797–1804.

Burgess, E.A., Wagner. I.D., Wiegel, J., (2008): Thermal environments and biodiversity. In: Physiology and biochemistry of extremophiles (Eds Charles Gerday and Nicolas) Glansdorff. Washington DC, 429 pp.

Carslaw, H.S. & J.C. Jaeger (1959): Conduction of Heat in Solids, 2nd Edition. Oxford, London.

CIEMAT (2012): FEBEX-e: Contribution of CIEMAT to the Test Plan for final dismantling. Technical Report CIEMAT/DMA/2G206/1/12

CIEMAT (2014): "FEBEX-e - Sampling and postmortem analyses - Contribution of Spanish groups: CIEMAT, CSIC, UAM, UPC", Technical Report CIEMAT/DMA/2G206/1/14, 2014.

Cross, M.M., Manning, D.A.C., Bottrell, S.H. & Worden, R.H. (2004): Thermochemical sulphate reduction (TSR): experimental determination of reaction kinetics and implications of the observed reaction rates for petroleum reservoirs. Organic Geochemistry 35, 393-404.

Decagon, Devices (2009): How to Reduce Contact Resistance Errors in Thermal Properties Measurements, Application Note.

Decagon Devices (2011): KD2 Pro Thermal Properties Analyzer Operator's Manual, Version 10 pp68.

Dupray, F., Francois, B. & Laloui, L. (2013): Analysis of the FEBEX Multi-barrier System Including Thermoplasticity of Unsaturated bentonite. International Journal for Numerical and Analytical Methods in Geomechanics, 37 (4), pp.399-422.

ENRESA (1995): Almacenamiento geológico profundo de residuos radiactivos de alta actividad (AGP). Diseños conceptuales genéricos. Publicación Técnica ENRESA 11/95. 105 pp. Madrid.

ENRESA (1998a): Publicacion Tecnica ENRESA 01/98, Madrid.

ENRESA (1998b): FEBEX. bentonite: origin, properties and fabrication of blocks. Publicación Técnica ENRESA 4/98. 146 pp. Madrid.

ENRESA (1998c): FEBEX: "Final Design And Installation of the "In Situ" Test at Grimsel". Publicación técnica 12/1998. Madrid, 1998.

ENRESA (2000): FEBEX Project. Full-scale engineered barriers experiment for a deep geological repository for high level radioactive waste in crystalline host rock. Final report. Publicación Técnica ENRESA 1/2000, Madrid, 354 pp.

ENRESA (2002): Thermo-hydro-mechanical characterisation of a bentonite from Cabo de Gata, A study applied to the use of bentonite as sealing material in high level radioactive waste repositories, Publicación Técnica 04/2002, 258 pp.

ENRESA (2003): "Dismantling of the heater 1 at the FEBEX "in situ" test: Description of operations". Publicación técnica 09/2003. Madrid.

ENRESA (2004): Febex Project Post-mortem Analysis: Corrosion Study. Enresa Report 08/2004, Enresa, Madrid.

ENRESA (2006a): "Full-scale Engineered Barriers Experiment", Updated Final Report 1994–2004, Publicación Técnica 05-0/2006. Madrid.

ENRESA (2006b): "FEBEX Project Final Addendum sensors data report. In situ experiment", Publicación técnica 05-5/2005. Madrid.

Fernández, A.M., Baeyens, B., Bradbury, M., Rivas, P. (2004): Analysis of the pore water chemical composition of a Spanish compacted bentonite used in an engineered barrier. Physics and Chemistry of the Earth, Vol. 29/1, pp. 105-118.

García-Siñeriz, J.L., Abós, H., Martínez, V. & De la Rosa, C. (2016): FEBEX-DP Dismantling of the heater 2 at the FEBEX "in situ" test. Nagra Arbeitsbericht NAB 16-11.

Gens, A., Sánchez, M., Do, L., Guimarães, N., Alonso, E.E., Lloret, A., Olivella, S., Villar, M.V. & Huertas, F. (2009): A Full-scale in Situ Heating Test for High-level Nuclear Waste Disposal: Observations, Analysis and Interpretation. Géotechnique 59 (4) (January): 377–399.

Giroud, N. (2014): "FEBEX - Assessment of Redox Conditions in Phase 2 before Dismantling". Nagra Arbeitsbericht NAB, 14-55.

Goldstein, T.P. & Aizenshtat, Z. (1994): "Thermochemical sulfate reduction a review." Journal of Thermal Analysis 42(1): 241-290.

Gómez-Espina, R. & Villar, M.V. (2010): Geochemical and mineralogical changes in compacted MX-80 bentonite submitted to heat and water gradients. Informes Técnicos CIEMAT 1199. Marzo 2010. Madrid, 33 pp.

Gómez-Espina, R. & Villar, M.V. (2013) : Modificaciones en la bentonita MX-80 compactada sometida a tratamiento termo-hidráulico. Informes Técnicos CIEMAT 1290. Madrid, 85 pp.

Gutiérrez-Rodrigo, V., Villar, M.V., Martín, P.L. & Romero, F.J. (2014) : Gas transport properties of compacted bentonite. In: Khalili, N., Russell, A. & Khoshghalb, A (eds.): Unsaturated Soils: Research & Applications. UNSAT2014, vol.2, 1735-1740.

Johnsson, A, Ödegaard-Jensen, A., Skarnemark, G. & Pedersen, K. (2009): Leaching of spent nuclear fuel in the presence of siderophores. Journal of radioanalytical and nuclear chemistry 279:619-626.

Kalinowski, B.E., Johnsson, A., Arlinger, J., Pedersen, K., Ödegaard-Jensen, A. & Edberg, F. (2006): Microbial mobilization of uranium from shale mine waste. Geomicrobilogy Journal **23**: 157-164.

Kim, J., Dong, H., Seabaugh, J., Newell, S.W. & Eberl D.D. (2004): Role of microbes in the smectite-to-illite reaction. Science 303, 830-832.

Kiviranta, L. & Kumpulainen, S. (2011): Quality Control and Characterization of bentonite Materials, Posiva Oy Workreport, WR 2011-84, Eurajoki.

Kluitenberg, G.J., Ham, J.M., & Bristow, K.L. (1993): Error analysis of the heat pulse method for measuring soil volumetric heat capacity, Soil Sci. Soc. Am. J., 57:1444-1451.

Kumpulainen, S. & Kiviranta, L. (2010): Mineralogical and Chemical Characterization of Various bentonite and Smectite-Rich Clay Materials, Posiva Oy Workreport, WR 2010-52, Eurajoki.

Kumpulainen, S. & Kiviranta, L. (2011): Mineralogical, Chemical and Physical Study of Potential Buffer and Backfill Materials from ABM Test Package 1, Posiva Oy Workreport, WR 2011-41, Eurajoki.

KYOTO ELECTRONICS Manufacturing Co. (1987): Kemtherm QTM-D3 Quick Thermal conductivity Meter Instruction Manual. Tokyo. 19 pp.

Lanyon, W. & Gaus, I. (2013): Main outcomes and review of the FEBEX In Situ Test (GTS) and Mock-Up after 15 years of operation". Nagra Arbeitsbericht NAB 13-096.

Madigan, M., Martinko, J., Stahl, D. & Clark, D. (2012): Brock Biology of microorganisms 13th ed. San Fransisco. 1150 pp.

Martin, P.L. (1999): Ensayo en maqueta: informe final. Instalación y operación. Versión 0. CIEMAT report. FEBEX report 70-IMA-M-9-4. Madrid.

Martinez, V. & García-Siñeriz, J.-L. (2015): FEBEX "in-situ" Test - Heating stoppage by the end of November 2014. AN 15-130.

Missana, T., Alonso, U., Albarran, N., García-Gutiérrez, M. & Cormenzana, J.L. (2011): "Analysis of colloids erosion from the bentonite barrier of a high level radioactive waste repository and implications in safety assessment", Phys. Chem. Earth, 36, 1607–1615.

Olsson, S., Jensen, V., Johannesson, L-E., Hansen, E., Karnland, O., Kumpulainen, S., Kiviranta, L., Svensson, D., Hansen, S. & Lindén, J. (2013): Prototype Repository. Hydro-mechanical, chemical and mineralogical characterization of the buffer and tunnel backfill material from the outer section of the Prototype Repository, Swedish Nuclear Fuel and Waste Management Company (SKB) Technical Report, SKB TR-13-21, Stockholm.

Pedersen K. (2010): Analysis of copper corrosion in compacted bentonite clay as a function of clay density and growth conditions for sulfate-reducing bacteria. Journal of Applied Microbiology 108, 1094-1104.

Pedersen, K., Nilsson, E., Arlinger, J., Hallbeck, L. & O'Neill, A. (2004): "Distribution, diversity and activity of microorganisms in the hyper-alkaline spring waters of Maqarin in Jordan." Extremophiles 8(2): 151-164.

Perdrial, J.N., Warr, L.N., Perdral, N., Lett, M.-C. & Elsass, F. (2009): Interaction between smectite and bacteria: Implications for bentonite as backfill material in the disposal of nuclear waste. Chemical Geology, 264: 281-294.

Sakaki, T, Kober, F. & Schläger, S. (in prep.): FEBEX-DP Post-mortem analysis: TDR. Nagra Arbeitsbericht NAB 16-21.

Smart, N.R., Rance, A.P., Reddy, B., Hallbeck, L., Pedersen, K. & Johansson, A.J. (2014): "In situ evaluation of model copper-cast iron canisters for spent nuclear fuel: a case of microbiologically influenced corrosion (MIC)." Corrosion Engineering, Science and Technology 49(6): 548-553.

Stroes-Gascoyne, S., Frutschi, M., Hamon, C., Bagnoud, A., Leupin, O. & Bernier-Latmani, R. (2013): MA experiment: Role of moisture, bentonite density and water activity on the development of microorganisms in the bentonite after its dismantling from the EB experiment. Mont Terri Technical Note. TN 2013-56.

Svemar, Ch., Johannesson, L-E, Grahm, P., Svensson, D., Kristensson, O., Lönnqvist, M. & Nilsson, U. (2016): Prototype Repository Opening and Retrieval of the outer section of the Prototype Repository at Äspö Hard Rock Laboratory. Summary Report SKB, TR-13-22.

Svensson, D., Dueck, A., Nilsson, U., Sandén, T., Lydmark, S., Jägevall, S. & Pedersen K. (2011): Alternative buffer material. Satus of the ongoing investigation of reference materials and test package 1. Technical report TR-11-06. Swedish Nuclear Fuel and Waste management Co, Stockholm. pp 1.

Tecnalia (2014): Proposal number: 043170 4/8 Corrosion Study of FEBEX-DP Components DRAFT Version: 02 (11/07/2014)

Villar, M.V. & Gómez-Espina, R. (2009): Report on thermo-hydro-mechanical laboratory tests performed by CIEMAT on FEBEX bentonite 2004-2008. Informes Técnicos CIEMAT 1178. Madrid, 67 pp. Agosto 2009.

Villar, M.V. & Lloret, A. (2004): Temperature influence on the mechanical behaviour of a compacted bentonite. In: Stephansson, O.; Hudson, J.A. & Jing, L. (eds.): Coupled thermo-hydro-mechanical-chemical processes in geo-systems. Fundamentals, modelling, experiments and applications. Geo-Engineering Book Series, vol.2. Elsevier, Amsterdam. 305-310.

Villar, M.V. & Lloret, A. (2008): Influence of dry density and water content on the swelling of a compacted bentonite. Applied Clay Science 39: 38-49.

Villar, M.V. & Iglesias, R.J. (2016): FEBEX-DP: onsite determinations report. Nagra Arbeitsbericht NAB 16-12.

Villar, M.V. (1997): Muestreo y caracterización de bloques para el ensayo en maqueta del Proyecto FEBEX. Informe Técnico, CIEMAT/IAE 54A15/7/97. Madrid, 7 pp.

Villar, M.V. (2002): Thermo-hydro-mechanical characterisation of a bentonite from Cabo de Gata. A study applied to the use of bentonite as sealing material in high level radioactive waste repositories. Publicación Técnica ENRESA 01/2002, Madrid, 258 pp.

Villar, M.V. (2005): MX-80 bentonite. Thermo-hydro-mechanical characterisation performed at CIEMAT in the context of the Prototype Project. Informes Técnicos CIEMAT 1053. CIEMAT, Madrid, 39 pp. Febrero 2005.

Villar, M.V. (2006): FEBEX Project Final report: Post-mortem bentonite analysis. ENRESA Publicacion tecnica 05-1/2006, CIEMAT, Madrid.

Villar, M.V. et al. (in preparation): FEBEX-DP Postmortem THM/THC Analysis Report. Nagra Arbeitsbericht NAB 16-17.

Villar, M.V., Gutiérrez-Rodrigo, V., Martín, P.L., Romero, F.J. & Barcala, J.M. (2013): Gas Transport in bentonite. Informes Técnicos CIEMAT 1301, Madrid, 63 pp.

Villar, M.V., Martín, P.L., Bárcena, I., García-Siñeriz, J.L., Gómez-Espina, R. & Lloret, A., (2012a): Long-term Experimental Evidences of Saturation of Compacted bentonite Under Repository Conditions. Engineering Geology 149-150 (November): pp.57–69.

Villar, M.V., Gómez-Espina, R. & Gutiérrez-Nebot, L. (2012b): Basal spacings of compacted bentonite. Applied Clay Science 65-66: 95-105.

Yumoto, I. (2007): Environmental and taxonomic biodiversities of Gram-positive alkaliphiles. In Physiology and biochemistry of extremophiles eds C Gerday and N Glansdorff 429 pp.